Source Term Models for Superheated Releases of Hazardous Materials

Thesis submitted for the Degree of Doctor of Philosophy
of the University of Wales Cardiff

by

Vincent Martin Cleary BEng (Hons)

September 2008

ProQuest LLC
789 East Eisenhower Parkway
P.O. Box 1346
Ann Arbor, MI 48106-1346

Abstract

Source terms models for superheated releases of hazardous liquefied chemicals such as LPG have been developed, governing both upstream and downstream conditions. Water was utilised as the model fluid, not least for reasons of safety, but also for its ability to be stored at conditions that ensure it is superheated on release to atmosphere.

Several studies have found that at low superheat jet break-up is analogous to mechanical break-up under sub-cooled conditions. Hence, a non-dimensionalised SMD correlation for sub-cooled liquid jets in the atomisation regime has been developed, based on data measured using a Phase Doppler Anemometry (PDA) system, for a broad range of initial conditions. Droplet SMD has been found to correlate with the nozzle aspect ratio and two non-dimensionalised groups i.e. the liquid Reynolds number and Weber number. An adaptation of the Rossin-Rammler distribution has been proposed for jets undergoing mechanical break-up.

Through a high-speed photographic study (1000fps), three distinctive break-up regimes of superheated jets have been identified. Mechanical break-up has been confirmed to dominate jet disintegration at low superheat. Criteria for transition between regimes have been established based on the liquid Jakob number and Weber number.

Using a PDA system, droplet SMD data has been produced for fully flashing jets at two sets of initial conditions and three axial downstream locations, with radial measurements performed at each position. Droplet SMD has been found to increase with nozzle diameter. An adaptation of the Rossin-Rammler distribution has been proposed for fully flashing jets.

The proposed correlation for sub-cooled break-up, the PDA data for superheated releases and the established transition criteria have been compiled to produce a complete SMD model governing transition from mechanical break-up to full flashing. The model has been validated against three previous studies of flashing jets.

An additional high speed photographic study (up to 50,000fps) of the upstream flow structure of superheated jets has been performed using Perspex nozzles. The downstream break-up regime has been found to depend on both the upstream bubble growth rate and concentration.

"They say that every dog has his day and today is woof day. That might sound crazy but I want to go and bark!"

Ian Holloway May 2004

Acknowledgements

Firstly, I must express my gratitude to Professor Phil Bowen, for presenting me with the opportunity to undertake this study and for all his help and support.

My thanks also go to Henk Witlox and Mike Harper at DNV for the financial support that I was generously afforded and for their considerable input throughout this study.

My thanks also go to the technicians in the workshop for their invaluable assistance with the practical aspects of this study. Particular thanks must go to Paul Malpas, Alan Griffiths and Malcolm Seabourne without whose encyclopaedic knowledge of all things mechanical, none of this would have been possible. Thanks also to Andrew Crayford and Peter Kay for all their help in this regard.

Thanks to all the members of the South Wales Celtic Supporters Club, especially Gerry, Dex and the clan, Ray, Craig, Tim and Andy. Cedwch y ffydd!

Thanks to all my friends, especially Sull, Mark, Michael, Nick, Gall, Damo, Shearer, Mark O'D, the boy Lockett, Ray, Alan, Rhys, Chris, Robin, Christophe, and Alex. It's been emotional!

Very special thanks go to my family, especially my sisters Rosemary and Colette. They blazed the trail, I simply followed.

My most heartfelt thanks go to my mum who has made me the man I am today. This is for you.

My final thoughts are for my dad. If I stood on this book, I'd nearly be as tall as him.

Table of Contents

List of Figures and Tables

Chapter 1 Introduction

Chapter 2 Literature Review

Chapter 3 Experimental Facilities and Procedure

Chapter 4 Elementary Characterisation of Superheated Jets

Chapter 5 Mechanical Break-Up

Chapter 6 Model Governing Transition to Flashing

Chapter 7 Upstream Flow Structure of Superheated Jets

Nomenclature

Symbol	Description	Units
b	constant	
C_{pl}	specific heat	$J\ kg^{-1}K^{-1}$
d_{10}	number averaged mean droplet diameter	m
d_0	nozzle diameter	m
d_p	droplet diameter	m
h	Planck's constant	$6.626x10^{-34}$ Js
H	Enthalpy	$J\ kg^{-1}$
H_{lg}	latent heat of vaporisation	$J\ kg^{-1}$
k	Boltzman's constant	$1.38x10^{-23}\ J\ K^{-1}$
k	thermal conductivity	$W\ m^{-1}K^{-1}$
J	nucleation rate	s^{-1}
Ja	Jakob number = $(\rho_l\ C_{pl}\ \Delta T_{sh}) / (\rho_v\ H_{lg})$	-
L	nozzle length	m
m	mass flow-rate	$kg\ s^{-1}$
M	molecular mass	kg
N	bubble number density	m^{-3}
N_0	liquid molecular density	m^{-3}
P	pressure	Nm^{-2}
$P(v)$	saturated vapour pressure	Nm^{-2}
ΔP_b	pressure difference between interior and exterior of bubble nucleus	Nm^{-2}
R	bubble radius	m
Re	Reynolds number = $(\rho_l\ u_j\ d_0) / \mu$	-
s	solid substrate	-
S	Supersaturation	-
SMD	Sauter Mean Diameter	m
t	time	s
t_d	delay time	s
$\bar{t}_d$	average delay time	s
T	Temperature	K
ΔT_{sh}	Superheat	K
u	velocity	ms^{-1}
$v(D)$	volume undersize function	-
We	Weber number $(\rho_l\ u_j^2\ d_0) / \sigma$	-

Greek letters

Symbol	Description	Units
α	thermal diffusivity	$m^2\ s^{-1}$
β	stable phase	-

Δ	difference	-
ε	void fraction	-
φ	metastable phase	-
η	mass fraction	-
η_n	efficiency of injector	-
η_R	rainout fraction	-
θ	angle	°
μ	dynamic viscosity	$N\ s\ m^{-2}$
ν	kinematic viscosity	$m^2\ s^{-1}$
ϕ	correction factor	-
ρ	density	$kg\ m^{-3}$
σ	surface tension	Nm^{-2}
τ	line tension of the three phase contact line	N
υ	specific volume	$m^3\ kg^{-1}$
$\Delta\Omega$	free energy of formation	J

Subscripts

Symbol	Description
0	initial conditions prior to atmospheric expansion
a	atmospheric
amb	ambient
as	adiabatic saturation
b	bubble
c	critical
coex	liquid/vapour coexistence
crit	critical
g	gas
inj	injection
l	liquid
p	droplet
sat	at saturated conditions
sh	superheated
st	stagnation
v	vapour

Superscripts

Symbol	Description
*	non-dimensionalised

Chapter 1 Introduction

1.1 Motivation

Today it is common practice to store and process various chemicals that exist as vapours at ambient temperature and pressure, as compressed liquids. For example, flammable gases are widely used in many industrial processes, due to both their good combustion properties (when mixed in adequate proportions with air) and by their ability to be easily transported and stored as liquid under pressure[1].

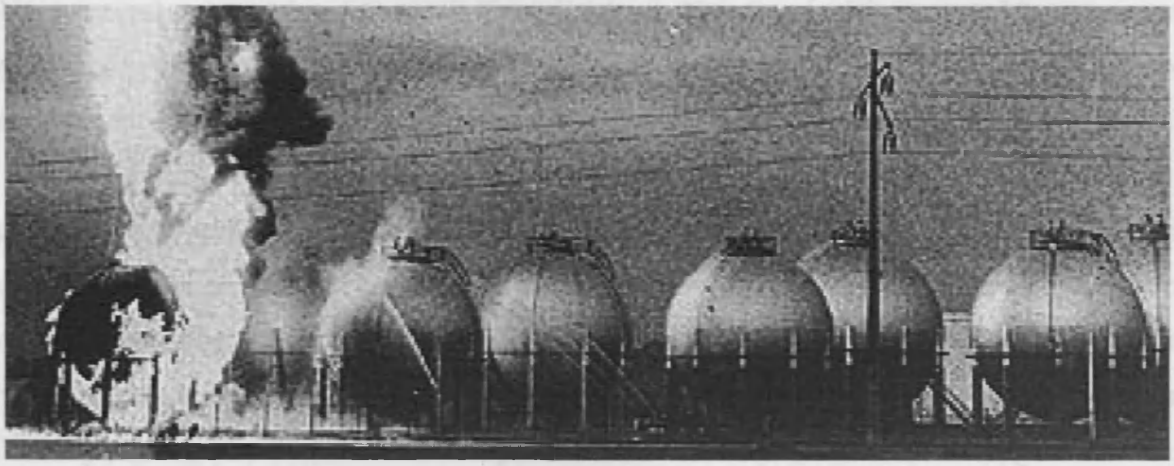

Figure 1.1 Escaping LPG ignites at Feyzin, France 1966.

Over the last 40 years more than 20 large scale incidents involving the sudden loss of containment of liquefied gases have been reported, including the failure of storage tanks, failure during the uploading and downloading of transportation lorries, traffic accidents during the transportation of liquid load or a combination of these scenarios. On 19 November 1984 a major fire and a series of catastrophic explosions occurred at the government owned and operated PEMEX LPG Terminal at San Juan Ixhuatepec, Mexico City. On that day, the plant was being filled from a refinery 400 km away when an 8-inch pipe between a sphere (LPG vessel) and a series of cylinders ruptured, causing a flashing release of LPG, which continued for about 5-10 minutes before the gas cloud, estimated at 200 m x 150 m x 2 m high, drifted to a flare stack and ignited. About fifteen minutes after the initial release the first BLEVE (boiling liquid expanding vapour explosion) occurred. For the next hour and a half there followed a series of BLEVEs as the LPG vessels violently exploded. As a consequence of these events some 500 individuals were killed and the terminal destroyed.[2] A similar event

took place at a refinery in Feyzin, France in 1966, which resulted in 18 fatalities and many more casualties. Figure 1.1 presents an image of the refinery fire at Feyzin, taken before the sphere eventually exploded, killing the men nearby.

As production from its North Sea gas field declines, the UK's dependence on gas imports is forecast to approach 46% by 2010[3]. Construction of the UK's largest LNG import terminal is currently underway at Milford Haven in South Wales. Due for completion next year, the site is expected to be importing up to 20% of the UK's natural gas in the form of LNG from Qatar by the end of 2007[4]. Plans are also under way to triple the capacity of the country's existing LNG terminal on the Isle of Grain in Kent, England. This terminal is expected to commence operations in late 2008, when it will account for 12% of the UK's annual gas demand[5]. These developments have refocused attention on the hazards associated with liquefied material.

When a liquid stored above the ambient saturation conditions is released to the atmosphere the liquid is described as 'superheated'. Rapid boiling of the resultant liquid jet occurs, producing two-phase flow. Under suitable conditions, dynamic expansion of vapour bubbles shatters the liquid stream to produce a finely atomised spray. This phenomenon, known as 'flashing', gives rise to potentially explosive and certainly hazardous heterogeneous two-phase clouds. In the example of LPG, the hazard is present in the potential for the cloud to ignite and explode; for other chemicals, it may be the toxicity of the cloud that defines the resultant hazard. Hence, it is necessary to understand the physical processes involved in large scale liquid releases at source, in order to quantify and ultimately mitigate the hazards associated with the loss of containment of liquefied chemicals of this kind.

When a liquid is released to the atmosphere below the ambient saturation conditions the liquid is described as 'sub-cooled'. There is a considerable body of evidence to show that at low superheat there is little qualitative difference between jet break-up under these conditions and sub-cooled releases. Break-up of the resultant jet is dominated by aerodynamic and surface tension forces at the liquid/air interface. This phenomenon, known as 'mechanical break-up', occurs when any random protrusion on the surface of a jet is subjected to a lower gas pressure over its crest than at its base.[6] The faster the jet relative to the surrounding atmosphere the more pronounced the effect. Eventually this protrusion may detach from the jet to form a droplet.

Whether a release occurs under sub-cooled or superheated conditions, rainout of larger droplets creates a spreading vaporising pool in the vicinity of the release orifice and determines the amount of material that remains airborne as the cloud disperses. A certain percentage of rained-out material will evaporate from the spreading pool and reattach itself to the dispersing cloud, potentially more dangerously as vapour. The liquid that remains on the ground presents its own hazard, as for example it can ignite to create a pool fire. For the purposes of accurate hazard quantification it is therefore necessary to be able to predict the behaviour of droplets in accidental releases of these kinds.

At Cardiff superheated jets are being investigated for a range of applications, including superheating for fuel injection, accidental release of superheated toxic chemicals and superheated water releases for explosion mitigation by fine water mists. Under suitable release conditions, superheat can induce very dynamic atomisation through bubble nucleation either within the jet upon release or upstream of the release orifice. However, conditions governing the mode - and hence the quality – of atomisation are currently ill-defined.

1.2 Physical Phenomenology

1.2.1 Thermodynamic Boundary Conditions

The scenario under consideration compromises a pressurised containment of a liquefied substance of any thermodynamic state. Figure 1.2 presents the two variations on this scenario that are considered within the remit of this thesis. Firstly the flashing liquid release and secondly the sub-cooled liquid release. In each case saturated conditions are represented by the blue curve such that crossing this boundary results in a change of phase. Point 1 represents the storage conditions of the substance, and point 2 the thermodynamic state of the substance upon release to atmosphere. In each scenario idealised isothermal conditions are envisaged so that only a sudden depressurisation is represented by the transition from point 1 to point 2. In a practical release scenario there may of course be some minor heat transfer, although generally speaking it should not be of sufficient significance to influence the nature of the resultant jet break-up process.

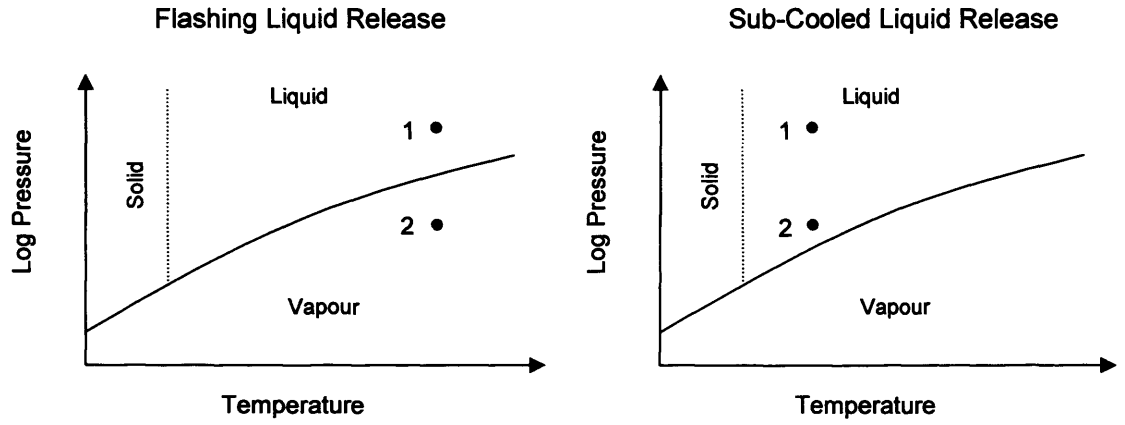

Figure 1.2 Thermodynamic conditions in relation to saturated conditions

The degree of superheat, ΔT_{sh}, of the contained liquid is given by Equation (1.1), where T_{st} is the stagnation temperature of the contained liquid (given by the temperature at point 1) and $T_{sat}(P_a)$ is the saturation temperature of the liquid at atmospheric pressure. If the saturation temperature at atmospheric conditions is less than the initial stagnation temperature of the liquid, then the release is defined as superheated. If the liquid is released into standard atmospheric conditions then this simply represents the degree by which the stagnation temperature exceeds its normal boiling point. At suitably high superheat one would expect to witness two-phase flashing atomisation of the resultant jet.

$$\Delta T_{sh} = T_{st} - T_{sat}(P_a) \qquad (1.1)$$

Where the degree of superheat is found to be negative, the liquid is said to be sub-cooled, and atomises as a single-phase homogenous jet which disintegrates through aerodynamic interaction and wave instabilities at the liquid surface[7]. The various mechanisms associated with jet break-up under these conditions are collectively termed 'mechanical' break-up. This type of jet break-up has received considerable attention in the literature, mainly at conditions of high pressure and small orifice sizes relevant to the automotive industry for direct injection engines[8,9,10].

Despite the fact that the behaviour of a liquid after a release depends heavily on the liquid itself, this study utilises water as the model fluid, not least for reasons of safety. This may initially seem unjustified but through reference to Figure 1.2, it is possible to highlight

important similarities between releases of superheated water and liquefied vapours. Both may be stored at elevated pressures under conditions that ensure their respective initial states are above the liquid/vapour transition curve. Essentially, as the initial upstream pressure is increased, then it may be observed that temperatures may be chosen for either fluid that will ensure that flashing conditions are encountered upon release to atmosphere i.e. such that the degree of superheat is positive.

1.2.2 Analogies with Other Two-Phase Industrial Processes

Effervescent atomisation utilises two-phase bubbly flow analogous to flashing jet releases, with the gaseous phase introduced mechanically under isothermal conditions. Upstream and downstream flow characteristics display similar properties and it seems plausible therefore that once two-phase flow has been established in superheated jets atomisation is controlled by physical processes such as the expansion and shattering of bubbles rather than any subsidiary thermodynamic influence.

Heat transfer processes in two-phase flows have a significant influence on the performance of heat exchangers. A study by Hewitt[11] provided a detailed characterisation of the various upstream flow structures as they change with increasing superheat. These changing flow regimes are consistent with those reported for effervescent atomisation, which reinforces the hypothesis that downstream atomisation processes are almost exclusively the result of bubble growth rates in the upstream flow. They also indirectly highlight the anticipated influence of geometric orifice characteristics on jet break-up as any bubble nucleation at the liquid/solid surface interface upstream of the exit orifice will be subject to the area available for this process to occur.

1.3 Overview of Current Understanding

There are various empirical correlations for mechanical break-up proposed in the literature, though most consider conditions outside the domain of interest for hazard analysis. Most atmospheric dispersion models currently utilise some form of the 'critical Weber number' criterion to estimate the maximum size of stable droplets from mechanical break-up and

flashing atomisation. However, there is little experimental verification that single droplet break-up criteria can be extrapolated for multi-droplet applications.

Flashing appears to be controlled by a transition superheat limit, allowing mechanical break-up mechanisms to dominate into the superheated region. However, studies of the criteria governing transition from mechanical break-up to flashing are limited. In order to develop towards a quantitative methodology, valid criteria governing transition between mechanical and flashing break-up need to be established.

Muralidhar *et al*[12] proposed a simple model that describes a transition point between mechanical break-up and flashing atomisation based on a critical superheat above which the rate of change of rainout falls sharply in accordance with a rapidly decreasing droplet size in the spray. However, beyond the initial transition superheat several further stages of transition are likely to exist until a final stage of atomisation is reached. For example, Park and Lee[13] identified three intermediary junctures of flashing. What is unclear is how rapid the evolution from the initial transition stage to the final transition stage occurs. It is necessary, therefore, to formulate a model governing jet break-up across the full spectrum of upstream conditions, including the establishment of valid criteria governing the various stages of transition from mechanical break-up to flashing atomisation.

While the long term aim must be to investigate jet break-up using flammable gases such as butane and propane directly, the immediate concern is to acquire a better understanding of the processes involved in atomisation without focusing on the physical properties of the fluid involved. Hence, at this stage predictions for other liquids will rely on the established non-dimensional variables adopted within the model, namely the Jakob and Weber numbers whilst it is understood that further work on other fluids will be required to validate this assumption.

1.4 Thesis Aim and Objectives

The aim of this thesis is to improve modelling approaches for superheated releases of hazardous material and add to existing understanding concerning the various phenomenologies involved. The objectives required to achieve this aim are outlined here.

- Perform a thorough review of the relevant literature concerning sub-cooled and superheated sprays and all other related subject areas to establish the cutting edge of current understanding (Chapter 2).

- Characterise rainout from flashing jet releases, highlighting potential empirical trends (Chapter 4).

- Develop an improved atomisation model for water jets undergoing mechanical break-up, which should be derived from empirical data acquired using the latest diagnostic techniques available in this field. Validation of the model should be performed through the comparison of the model predictions with available empirical datasets in the literature and models which are currently utilised or have been proposed previously (Chapter 5).

- Establish preliminary criteria governing the various stages of transition from mechanical break-up to flashing atomisation (Chapter 6).

- Undertake a detailed investigation of external droplet sizes and velocities in superheated jets and the effect of the primary input parameters on the downstream flow characteristics on sprays of this kind (Chapter 6).

- The successful completion of the objectives above should facilitate the aggregation of enough information to produce a complete model governing the release of pressurised liquids through simple orifices from mechanical break-up, through to flashing atomisation (Chapter 6).

- Explore in detail the nucleation and development of two-phase flow upstream of the exit orifice for superheated releases (Chapter 7)

Chapter 2 Literature Review

2.1 Introduction

In this chapter a thorough evaluation of the relevant literature is made, including a review of the various mechanisms of atomisation for both sub-cooled and superheated releases, an examination of relevant large scale studies and an in-depth analysis of empirical models which have been previously proposed. An appraisal of the various measurement techniques available for the study of liquid jets is also made.

2.2 Primary Input Parameters

Due to the complexity of the atomisation process several non-dimensional groups are commonly used to relate influential parameters for this problem. For the purposes of developing correlations with respect to mathematical rigour, this is clearly the most appropriate technique to pursue. However, before reviewing in detail the different atomisation processes, it is necessary to highlight the primary input parameters that influence the quality of atomisation for both mechanical break-up and flashing.

Atomisation studies usually quote the mean droplet size in terms of the SMD (Sauter Mean Diameter or D_{32}), which represents the droplet diameter for which the ratio of volume to surface area is identical to that of the whole spray. It is analogous to a moment of inertia so that it indicates around which central point of the frequency the volume distribution would rotate. It is in effect the centre of gravity of the distribution.[14] In terms of accidental release scenarios this is much more useful than a simple mean as it indicates the diameter of droplets which constitute the bulk of the spray. Several previous studies have relied on laser diffraction based techniques to measure particle size. Systems utilising this technique initially calculate a distribution based on volume terms. Hence, the SMD is reported in a prominent manner in the literature.

The mean droplet size of sub-cooled jets undergoing mechanical break-up has been universally shown to be a function of exit velocity, primarily due to the increase in turbulence in the jet as Reynolds number increases. Most published research has also shown the droplet size to be a function of the orifice diameter. The liquid properties also influence the

atomisation quality and for isothermal releases, density, viscosity and surface tension are the three most significant input parameters. The final most significant input parameter is the orifice aspect ratio, defined as L/d_0, where L is the length from the final orifice exit to the nearest upstream expansion within the orifice and d_0 is the diameter of the exit orifice.

The physical processes involved in flashing are not comparable with those involved in mechanical break-up. Hence, it is wrong to assume that the same primary input parameters have an effect of parallel significance. A more analogous situation is that presented by effervescent atomisation where break-up is a function of drive pressure but relatively independent of orifice size. Flashing is also less dependent upon the fluid properties than the mechanical break-up process; instead, the mean droplet size is a function of the superheat. However, atomisation should not be assumed to correlate with a thermodynamic quantity alone. A rainout study by the Centre for Chemical Process Safety (CCPS)[15] adopted this assumption at the outset, so that data from all releases is compared sequentially against one representative thermodynamic quantity. As a result, it is difficult to appraise the effect of any particular primary input parameter on the measured rainout.

2.3 Jet Break-Up

Various authors[16,17,18,19] have reported little or no discernible difference between jet releases under conditions of 'low' superheat and mechanical break-up. Moreover, other authors have reported different modes of flashing atomisation. Hence, in this section the different break-up phenomena are divided into appropriate sections and criteria governing transition between the various modes are highlighted where such correlations are available.

Generally, the key input parameter that determines the transition between the reported modes of flashing is the superheat. In addition the superheat is widely shown to be inversely proportional to the mean size of droplets produced via flashing atomisation, so that with regime change comes a reduction in the droplet SMD.

2.3.1 Mechanical Break-Up

Previous studies[20,21,22] have identified four primary modes of mechanical break-up determined by the exit velocity of a sub-cooled jet. As the exit velocity is systematically increased, the jet break-up mechanism transforms from Rayleigh-type instabilities[23], to shear induced atomisation, comprising first-wind and second-wind and finally full atomisation. These jet break-up mechanisms are presented in Figure 2.1.

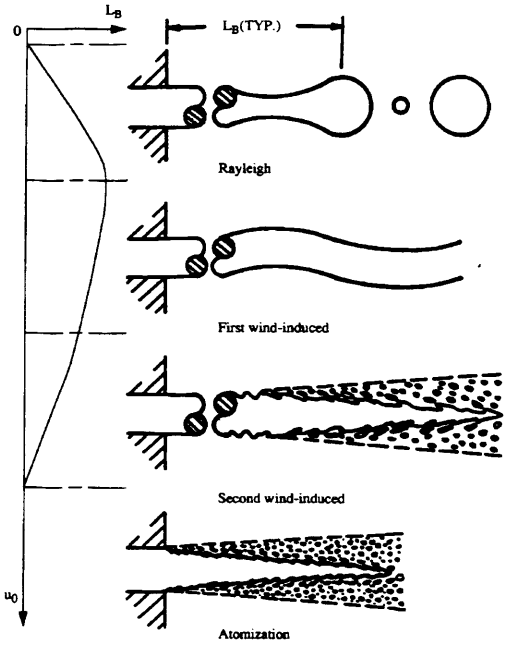

Figure 2.1 Mechanical Jet Break-Up Regimes[24]

Not shown in the figure, but prior to Rayleigh break-up, comes the drip regime, which involves the slow formation of large drops at the orifice exit which then fall as a single stream[25]. Rayleigh break-up is a surface tension effect, sometimes known as capillary break-up, which is manifested by the growth of axisymmetric oscillations of the jet surface and occurs many jet diameters from the orifice exit. It is characterised by a stream of drops of sizes greater than the orifice diameter. Nevertheless, the drip and Rayleigh break-up regimes do not present an increased hazard in the context of this study.

First-wind induced break-up is caused by an increase in the relative velocity between the jet and the ambient gas, which increases the surface tension effect and creates a static pressure

distribution across the jet. Break-up occurs many jet diameters downstream of the orifice exit and drop diameters are approximately the same size as the jet diameter.

Second-wind induced break-up is caused by the unstable growth of short-wavelength, small amplitude surface waves on the jet surface due to the relative motion of the jet and the ambient gas. One characteristic of this regime is a finite length along which insignificant atomisation occurs, followed by a diverging jet region containing droplets much smaller than the jet diameter.

The atomisation regime poses the most serious hazard in terms of accidental liquid-release scenarios. Atomisation begins with the formation of a conical jet close to the orifice exit with a cone angle that depends on the liquid velocity. This is followed by the entrainment of air and the division of the spray into concentric conical sprays. The velocity at the central axis is greater than at the edges of the spray, which results in the creation of radial velocities as the outer regions are decelerated by the central spray. Turbulence in the jet causes small oscillations in the liquid surface which lead to the formation of ligaments whose size and shape depend on the ratio of drag, surface tension forces and viscous forces. Ligaments then undergo further break-up due to the continued interaction of these forces to form droplets, which continues until a stable droplet size is achieved. So-called fully atomised sprays are characterised by a very small break-up length.

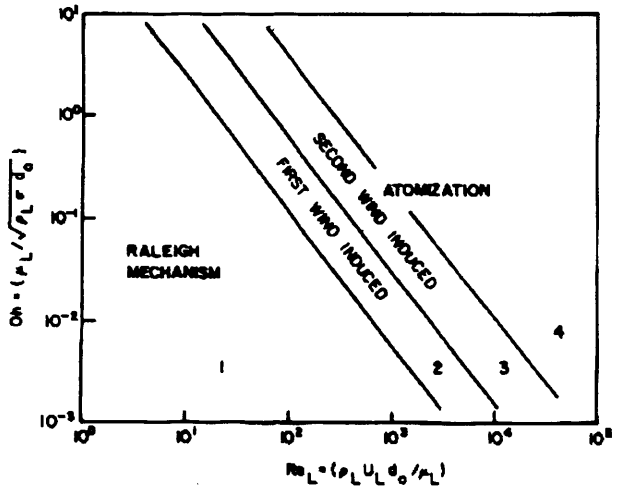

Figure 2.2 Classification of modes of disintegration[27]

The transition criteria between regimes are not yet universally defined. The most commonly quoted criteria for classifying jet disintegration are those proposed by Ohnesorge.[26] However, these criteria only apply to three stages of break-up. Lefebvre[22] highlighted the work carried out by Reitz[27], where he resolved some of the uncertainties surrounding the criteria proposed by Ohnesorge, using data based on diesel sprays obtained by himself and other workers, including Giffen and Muraszew[28] and Haenlein.[29] The criteria established by Reitz are presented in Figure 2.2.

2.3.1.1 Empirical Correlations in the Literature

Various empirical correlations for predicting droplet SMD have been previously proposed for mechanical break-up. These correlations are presented here in the order of their development.

Merrington and Richardson[30] developed their correlation based on experimental data from sprays produced by plain orifices of diameters in the range 0.8 – 8.0mm and for release pressures up to 25bar. Droplet diameters were measured from indentations made by droplets striking thin blotting paper placed in the flow field of the spray. Their correlation is presented by Equation (2.1).

$$SMD = 500\, d_0^{1.2}\left(\frac{\mu}{\rho}\right)^{0.2} u_j^{-1} \qquad (2.1)$$

Harmon's[31] correlation is a function of the density and dynamic viscosity of both the liquid and ambient gas, and is presented by Equation (2.2).

$$SMD = 3330\frac{d_0^{0.3}\mu_l^{0.07}\mu_g^{0.78}}{u_j^{0.55}\sigma^{0.15}\rho_l^{0.648}\rho_g^{0.052}} \qquad (2.2)$$

Tanasawa and Toyoda's[32] correlation is a function of the balance between inertial forces and surface tension forces at the liquid/gas interface and is given by Equation (2.3)

$$SMD = 47\cdot\frac{d_0}{u_j}\left(\frac{\sigma}{\rho_g}\right)^{0.25}\left[1+331\frac{\mu_l}{\sqrt{(\rho_l\sigma d_0)}}\right] \qquad (2.3)$$

Hiroyasu and Katoda[33] developed their correlation based on experimental data from sprays produced by diesel injectors, i.e. high pressure and small orifice diameter. Sprays were

released into an immersion chamber filled with liquid and droplet size measurements were made through the microscopic analysis of thousands of droplets in suspension. Their correlation is presented by Equation (2.4).

$$SMD = 2330\rho_g^{0.121}\Delta P^{-0.135}\left(u_j\frac{\pi d_0^2}{4}\right)^{0.131} \qquad (2.4)$$

Elkotb[34] proposed a correlation based on experimental data from sprays produced using a pintle-type diesel injector of diameters in the range 0.5 – 1.2mm and for release pressures in the range 75 – 180bar. Elkotb's correlation, presented by Equation (2.5), is a function of the injection velocity and liquid properties, but is independent of the orifice diameter.

$$SMD = 3.08\,\nu^{0.385}(\sigma\rho)^{0.737}\rho_g^{0.06}\Delta P^{-0.54} \qquad (2.5)$$

The correlation proposed by Tilton and Farley[35] is presented by Equation (2.6). Like the correlation proposed by Elkotb, it is a function of the jet velocity but is independent of the orifice diameter.

$$SMD = \frac{0.585}{u_j}\sqrt{\frac{\sigma}{\rho_l}} \qquad (2.6)$$

In all cases, the referenced correlations are dimensional and there are very few, if any, non-dimensional correlations previously proposed in the literature. The reliability of a dimensional correlation is subject to the coherence of the units on each side of the equation. Based on this criterion, several of the referenced correlations must be treated with caution as the coherence of the units is open to question. For example, the units in the correlation proposed by Tilton and Farley in Equation (2.6) clearly do not balance. Nevertheless, it is worth highlighting consistencies between correlations in terms of the proposed influence of the primary input parameters on the resultant droplet size.

Each of the referenced correlations indicates that the SMD is inversely proportional to the gauge pressure, ΔP (where $\Delta P = P_0 - P_a$). Tilton and Farley[34] and Elkotb[35] both present correlations that are independent of the orifice diameter, d_0. However, of those correlations that do include the orifice diameter, each one indicates that it is positively correlated with the droplet SMD. Table 2.1 provides a summary of the range of exponents of orifice diameter and release pressure given by previously proposed correlations in the literature.

Table 2.1 Range of Exponents for Primary Input Parameters with Respect to SMD

Input Parameter	Range of exponent with respect to SMD
d_0	0.262 – 1.2
ΔP	-0.07 – -0.69

When a liquid flows through an orifice of a given length, the pressure at the exit is slightly less than at the inlet. Friction losses contribute to the pressure drop, which are usually represented mathematically as the discharge coefficient, C_D. This dimensionless nozzle characteristic can significantly affect the velocity profile and break-up of the liquid jet. The exact nature of this influence is as yet poorly understood, although it is generally held that a decrease in the discharge coefficient will lead to an increase in the atomisation quality, i.e. a decrease in the droplet SMD. A previous study [36] conducted at Cardiff University has shown that the discharge coefficient is significantly influenced by the nozzle aspect ratio (L/d_0), but again the exact nature of this influence is somewhat ambiguous as they are reported to demonstrate a non-linear, "wavy" relationship.

Of the referenced correlations none include the nozzle aspect ratio as an operative input parameter. This may be because the actual relevance of aspect ratio to the break-up process is still a matter of debate. Some authors[37,38] report that the discharge coefficient is not significantly affected by the aspect ratio whereas Ramamurti *et al*[39] report that the discharge coefficient decreases with increase in aspect ratio and Reynolds number. Work by the same authors[40] has qualified this conclusion with the postscript that it is only applicable to attached, non-cavitating flows. Dumont *et al*[41] report that by increasing the aspect ratio and keeping the same Reynolds and Ohnesorge numbers, atomisation is improved. This assertion is based on empirical data produced by MacCarthy[42]. However, the lack of a significant body of experimental data in this area clearly requires attention.

2.3.1.2 Atmospheric Dispersion Models

Various authors[43,44,45,46] have proposed a range of critical Weber numbers for determining the maximum stable droplet diameter of individual droplets breaking up in a gas flow stream, see Equation (2.7).

$$We_{crit} = \frac{\rho_a u_0^{\,2} d_p}{\sigma_l} = 7.2 - 22 \qquad (2.7)$$

In addition, various atmospheric dispersion models[47,48,49,50] currently adopt the critical Weber number criterion to estimate the maximum size of stable droplets produced by mechanical break-up in sub-cooled jets. However, the Weber number is independent of orifice size and the exponent of release pressure is outside the range of experimentally determined values presented in the literature. Hence, it is not clear whether this approach is appropriate for this application. In addition, there seems to be little experimental verification of the hypothesis that the single droplet break-up criterion can be extrapolated to quantify the mean of a large collection of droplets in the example of a liquid jet. Furthermore, a previous study[51] in the related field of spray impingement initially utilised a summation of single droplet impingement studies for modelling purposes, but concluded that this approach is in fact inappropriate.

Reitz and Diwakar[52] proposed a so-called 'blob model' for mechanical break-up whereby the atomisation process as a whole is subdivided into primary atomisation, where large droplets are sheared from the jet surface, followed by aerodynamic break-up of the primary droplets into secondary spray. The primary spray is modelled by imposing an axisymmetric disturbance onto the steady jet. This wave-like disturbance is then fed into the conservation equations to derive a dispersion equation for the frequency of the instabilities. This equation may be solved to derive the wavelength associated with the most likely surface wave, which in turn is linearly related to the size of droplets created from parent 'blobs' of larger size. The rate of change of parent droplets is inversely related to the break-up time. Reitz[53] later developed this model further to apply to automotive applications.

Various authors[34,54] suggest that spray distributions from simple orifices can be adequately represented using the simple Rossin-Rammler distribution function[55]. Elkotb's[34] version of this distribution function is presented in Equation (2.8).

$$1 - v(d_p) = e^{-0.422\left(\frac{d_p}{SMD}\right)^{5.32}} \qquad (2.8)$$

Here, the function $v(d_p)$ represents the fraction of the total volume of the spray contained in droplets of size less than d_p, and provides a useful first approximation for atmospheric dispersion releases. One advantage of presenting data using this distribution function is that if one selects a critical droplet size above which all liquid released will rain out, the percentage of the volume of spray that rains out can be immediately determined from the graph.

2.3.2 Low Superheat

The earliest studies of flashing jets were limited to relatively low degrees of superheat[16,18,56,57,58]. Under these conditions the effect of upstream bubble nucleation has been shown either to be negligible so that mechanical break-up prevails or restricted to the external break-up mode where bubbles are generated downstream of the nozzle exit.

Muralidhar *et al*[12] suggest that flashing atomisation appears to be limited by a transition superheat limit, which allows mechanical break-up mechanisms to dominate into the superheated region. This idea is represented schematically by Figure 2.3, which forms the basis for a simple model based on the relationship between liquid 'capture' (rainout) and degree of superheat. It is necessary at this stage to modify the terminology used by Muralidhar *et al*, so that 'transition' superheat now replaces 'critical' superheat as this word has specific connotations with respect to phase change and may be unnecessarily confusing.

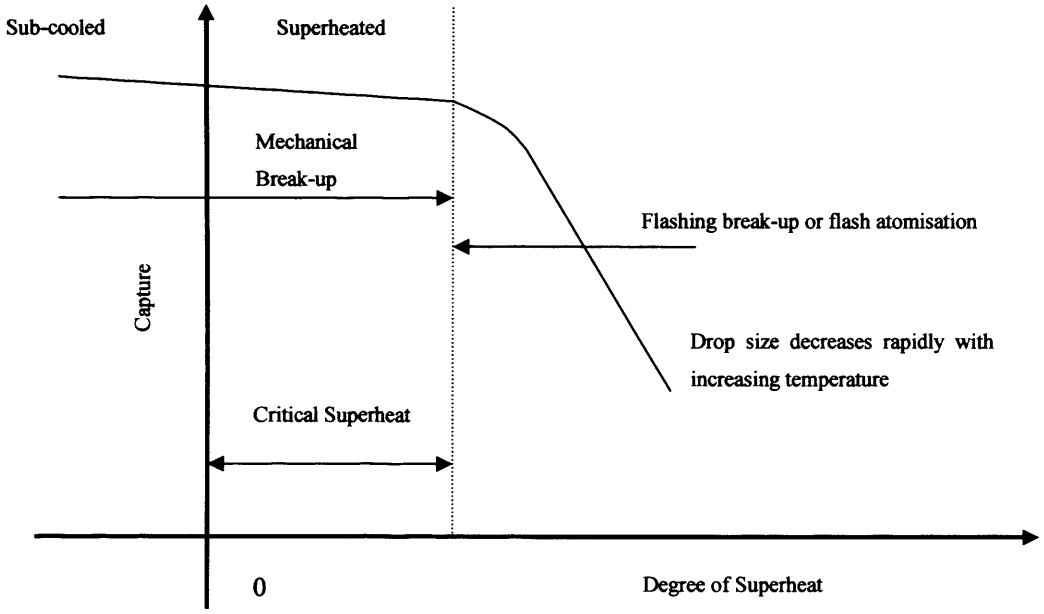

Figure 2.3 Schematic of flashing and non-flashing regions in relation to rainout (Muralidhar et al[12])

In the same study, Muralidhar *et al* also performed small scale Hydrogen Fluoride/additive release experiments at vapour pressures above 1bar. The authors argue strongly that their releases did not show any signs of flashing but that their model predictions for sub-cooled

break-up were in agreement with their rainout data for these superheated releases. In addition, Aquino *et al*[59] report that flashing atomisation is analogous to the spray pattern of multi-component jets for most regions except that of low superheat. Although multi-component jets are complicated by some complex aerosol chemistry, this strongly indicates that mechanical break-up is the dominant mode of atomisation at conditions of low superheat.

Johnson and Woodward[15] measured the rainout from superheated releases of a range of materials, and retro-calculated droplet diameters based on the rainout fraction of the total volume of released liquid. Although the justification for this technique is not certain, the data appears to indicate that a transitional superheat exists at which point a strong correlation between superheat and droplet size begins. Lantzy *et al*[60] describe experiments carried out using monomethylamine to investigate the effect of storage temperature on the atomisation of accidental releases and conclude that flashing atomisation can be avoided if the monomethylamine is stored at less than 10°C superheat.

In order to develop towards a quantitative methodology, valid criteria governing transition between mechanical break-up and flashing atomisation need to be established. Kitamura *et al*[61] propose a transitional correlation using superheated water and ethanol flowing through 'long' nozzles ($50 < L/d_0 < 115$) and flashing into an evacuated chamber, which is presented by Equation (2.9)

$$Ja\,\phi = 100\,We^{-\frac{1}{7}} \qquad (2.9)$$

where,

$$\phi = \left\{1 - e^{\left[-2300\left(\frac{\rho_v}{\rho_l}\right)\right]}\right\}$$

Here, *Ja* is the Jakob number and *We* is the vapour Weber number, as presented by Equations (2.10) and (2.11)respectively.

$$Ja = \frac{\rho_l C_{pl} \Delta T_{sh}}{\rho_v H_{fg}} \qquad (2.10)$$

$$We = \frac{\rho_v u_j^{\,2} d_0}{\sigma} \qquad (2.11)$$

This correlation is claimed to govern transition to 'complete' flashing, where ϕ is a function of the ratio of vapour to liquid density, ρ_v is the vapour density at ambient conditions and ρ_L is the liquid density at upstream conditions. It compares favourably with earlier data produced by Brown and York[16], who observed the minimum superheat for flashing at atmospheric pressure.

2.3.3 'External' Flashing Atomisation

At slightly higher degrees of superheat the mechanical process no longer dominates. As the liquid jet leaves the orifice it exists as a metastable liquid above its normal boiling point. After an initial 'idle' period during which the inception of bubble nucleation occurs, the jet shatters due to homogenous bubble nucleation and the subsequent rapid formation of vapour within the jet. The nominal droplet size depends on the ratio of surface tension and expansion forces in the flashing stream. Oza and Sinnamon[62] refer to this type of atomisation as the 'external' mode.

Lienhard and Day[56] developed a general formula for calculating the 'idle time' as a function of superheat (expressed in terms of vapour pressure). This is useful in terms of calculating the break-up length although it does not give any indication of resultant droplet sizes. Tilton and Farley[35] developed upon this work, initially using this equation to determine the break-up mechanism as a function of the break-up length, at which point they applied one of three proposed expressions to calculate the initial droplet size in either the capillary regime, the aerodynamic regime (mechanical break-up) or the flashing regime, which is represented by Equation (2.12). The authors consider that droplets initially formed by one of the three break-up mechanisms may be unstable and disintegrate further. In order to deal with this they adopt the critical Weber number approach to determine the maximum stable droplet size.

$$SMD = 5\times10^{-4}\left(\frac{2\sigma}{\rho_g u_0^{\,2}}\right) \qquad (2.12)$$

Razzaghi[63] developed an external flashing model for water jets at high pressure (>100bar) and high superheat (>475K upstream temperature). The model presumes that droplets are sheared from the jet before the vapour generation takes place within spherical bubbles. The critical Weber number approach is utilised to estimate the primary droplet size, which is then

extended to develop a log-normal distribution of droplet sizes. Secondary droplets originate from the shattering of bubbles within primary droplets and tertiary droplets originate from the shattering of bubbles within secondary droplets. The number of tertiary droplets is estimated to vary from 1-10 per bubble burst; mass conservation then yields the droplet size. At low superheat mechanical break-up is said to dominate and superheat only serves to enhance droplet surface evaporation. Although the model is theoretical it is claimed to be based on available empirical correlations and experimental data and reference is made to the experimental observation of single bubble formation inside flashing butane droplets[64].

Zeng and Lee[65] developed upon the so-called 'blob' model first proposed by Reitz and Diwakar[52] for mechanical break-up to include the effects of expanding bubbles due to flashing. Interestingly this model assumes that aerodynamic forces dominate the regime of low superheat. This model has been implemented into a modified version of multi-dimensional CFD code, i.e. KIVA-3V code.

2.3.4 'Internal' Flashing

This mode of atomisation is the most catastrophic and is characterised by finely atomised droplets, which result in low or zero rainout. It is thought to have strong phenomenological links with effervescent atomisation, where studies of both internal flashing[13] and effervescent atomisation[66,67] have indicated that a change in the internal flow regime is accompanied by a corresponding transition in the external mode of atomisation. Hence, the internal flashing mode can itself be divided into various sub-sections. Figure 2.4 summarises the findings of a systematic photographic study, which demonstrates the dependence of the external spray formation on the internal flow structure. Studies of effervescent atomisation[68,69,70,71,72,73] have also indicated that break-up is a function of drive pressure but relatively independent of orifice size. It is not clear whether this is reflected in internally flashing releases, but it provides a platform from which one can begin to assimilate the physical processes involved in this break-up phenomenon.

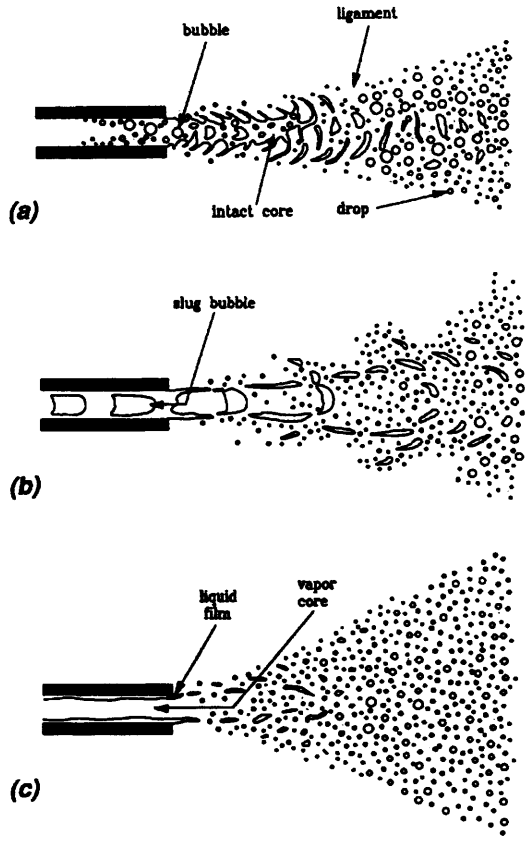

Figure 2.4 Dependence of spray characteristics on upstream flow conditions (Park and Lee[13])

The 'bubbly flow' regime occurs at conditions of low superheat, but still high enough to induce internal bubble nucleation, with bubbles forming close to the orifice exit. When this bubbly mixture is ejected from the nozzle, a significant liquid 'core' remains intact, despite the presence of bubbles in the flow stream, with bubbles bursting into fine drops at the surface. 'Slug' flow occurs when nucleation and growth of bubbles becomes sufficiently active for bubbles to collide and coalesce. Downstream, the slug bubbles burst into ligaments and then disintegrate into small drops. The length of the liquid core is greatly reduced. 'Annular' flow occurs when nucleation and growth of bubbles is so high that a liquid film forms at the nozzle wall and vapour flows at a much higher velocity along the core region. Upon release the jet is completely shattered into small droplets.

Park and Lee point out that in addition to conditions of high superheat, the injection pressure and nozzle length are both critical to the inception of slug flow and annular flow. Lower release pressure implies lower flow rate, which implies longer residence time for the fluid

inside the nozzle. In the same way, a longer nozzle also implies a longer residence time for the fluid. Hence, if either condition is met, there is more time for bubble growth and the void fraction at the nozzle exit increases. Therefore, it is suggested that the key upstream input parameters that determine the downstream characteristics of a superheated release are the void fraction, flow regime, nozzle geometry and discharge pressure.

2.3.4.1 Flow Regimes in Pipes and Tubes under Superheated Conditions

The primary motivation for previous studies of nucleating or boiling flows in pipes has been the importance of such flows in heat exchangers within the nuclear industry. For example, Jones and co-workers[74,75] developed a series of simple one dimensional numerical models for both heterogeneous nucleation[74] and mixed nucleation[75]. Figure 2.5 presents a summary of a study by Hewitt[11] of the internal flow of superheated liquids in pipes, which compares very well with the flow characteristics of 'internal flashing' displayed in Figure 2.4. Hence, it is reasonable to assume that there are significant parallels between the two processes and that the results presented in are indicative of the various stages of flow development that one would expect to occur upstream of the exit orifice prior to release to atmosphere.

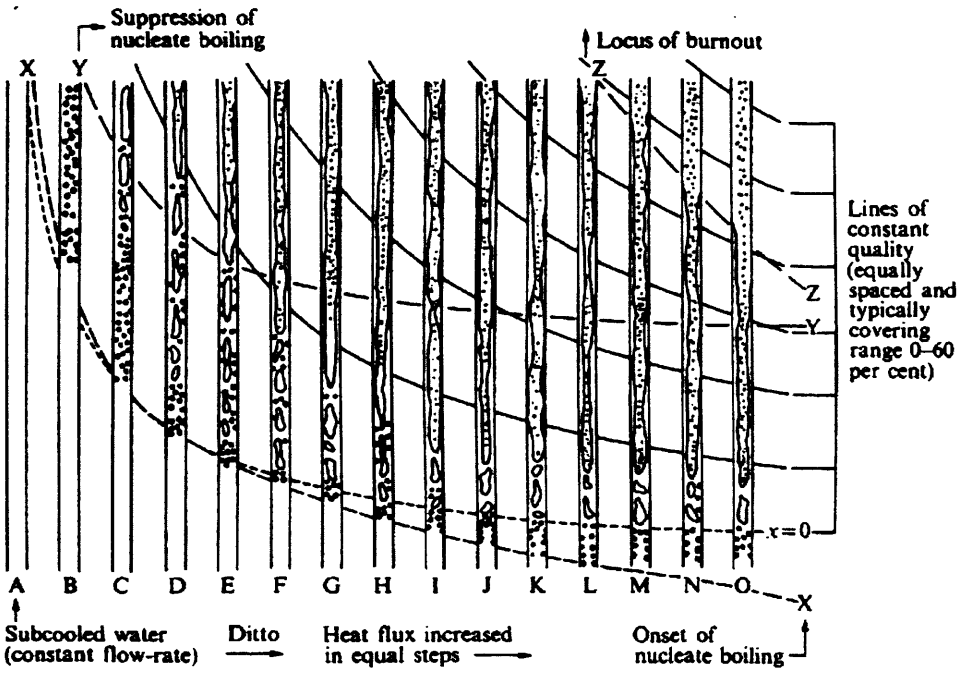

Figure 2.5 Schematic of variation of two-phase flow with increasing heat flux (Hewitt)[11]

Saha *et al*[76] adopted a semi-empirical approach to the development of two-phase flashing regimes along a pipe. Each of flow regimes presented in Figure 2.4 were considered and simplified modelling was introduced at each stage. The void fractions corresponding to transition between bubbly flow, bubbly-slug flow and annular/annular-mist flow were assumed to be 0.3, 0.8 and 0.95 respectively. The classical critical bubble radius for the existence of a stable bubble nucleus (also known as the Laplace equation) was adopted by the authors and presented by Equation (2.13).

$$R_c = \frac{2\sigma}{P(v) - P_l} \qquad (2.13)$$

The limiting conditions for the inception of bubble growth were then established as the critical bubble radius and the bubble number density at the flashing inception point. The bubble number density was incorporated as part of the model, but varied to obtain optimum fits with void fraction data against which the model was validated. All further nucleation downstream was neglected on the basis that bubble growth rate is a strong function of development time. An equivalent radius was presumed for non-spherical bubbles and a simplified model for the relative velocity between the bubbles and the liquid employed. The void fraction was utilised as the correlating parameter for the thermodynamic aspects of atomisation and predictions for the void fraction were determined as a function of axial distance from the throat and compared against experimental data taken in a vertical convergent-divergent nozzle. Reasonably good agreement of the void fraction was observed subject to the aforementioned varying of the bubble number density at inception.

Ishtii and Mashima[77] provided a physical explanation for the limiting void fraction ($\varepsilon = 0.3$) for bubbly flow, in that this is the limiting condition before spherical bubbles begin to touch. The authors developed a model for the bubbly and bubbly-slug regimes, based on the same limiting void fractions utilised by Saha *et al*[76], by integrating previously developed models for heterogeneous and homogenous flow respectively.

The model predictions were compared against various sources of data in the literature for convergent-divergent nozzles and it was shown that a model based purely on bubbly-flow only compared well against the experimental data up to void fractions of about 0.35. Thereafter, the models representing other flow regimes diverged such that discrepancies in the region of 15% between models were identified for void fractions of about 0.6. The model,

including bubbly, bubbly-slug, transitional and dispersed flows, demonstrated excellent agreement with experimental data, with errors in void fraction typically within 5% at a particular axial distance from the throat of the injector.

Fujimoto *et al*[78] incorporated an expression for the bubble number density in their model for characterising downstream atomisation for the application of automotive fuel injection. Their approach was consistent with that of Saha *et al*, in that the primary input variables were used to determine the secondary input variables of void fraction and pressure at the orifice, which were then used to correlate downstream atomisation characteristics. The bubble number density, N, was proposed as an empirical function of the superheat and is presented by Equation (2.14).

$$N = 5.757x10^{12} e^{\left(\frac{-5.279}{\Delta T_{sh}}\right)} \qquad (2.14)$$

Their model, for the formation of droplets in a flashing spray, released through a pintle–type injector is presented in Figure 2.6. Predictions were provided for superheated n-pentane and n-hexane. Due to the nature of the model only mono-disperse droplets are predicted so results were compared with the arithmetic mean from a limited data set, where reasonable agreement was observed.

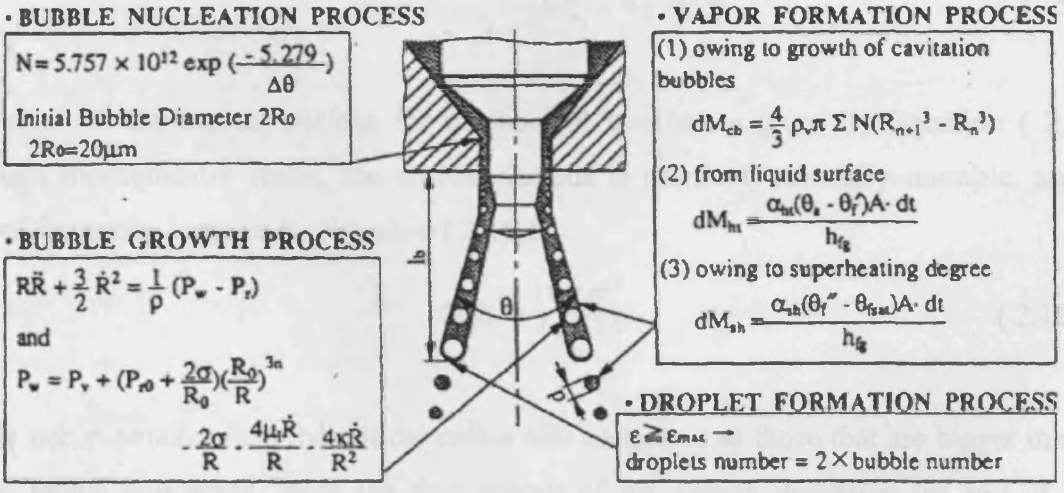

Figure 2.6 Phenomenological model of flash boiling spray (Fujimoto et al)[78]

2.3.4.2 Bubble Nucleation in Superheated Liquids

From studies of the flow of superheated liquids in pipes it is now well established that two-phase flow is induced via two mechanisms: homogenous nucleation as a result of molecular processes throughout the body of the fluid and heterogeneous nucleation at the liquid/solid surface interface.

Homogenous nucleation occurs when thermal fluctuations in a bulk liquid cause clusters of molecules to take on higher than macroscopic average energies. If the superheat is high enough these molecules can take on 'vapour-like' energies and form a stable vapour nucleus. Volmer and Weber[79] and Becker and Döring[80] developed the classical nucleation theory for homogenous nucleation in the first half of the 20th century. The classical theory assumes that a cluster can be represented as a droplet whose properties are the same as those of the bulk liquid. This is known as the capillarity approximation. The free energy of formation for a droplet of radius R is given by the sum of the energy associated with the formation of a volume $4/3\pi R^3$ of the thermodynamically stable phase and the energy required to sustain a liquid/gas interface of area $4\pi R^2$ and is presented by Equation (2.15), where ΔP_b is the pressure difference between the interior and exterior of the nucleus, balanced by the surface tension σ of the interfacial boundary.

$$\Delta\Omega = -\frac{4\pi R^3}{3}\left|\Delta P_b\right| + 4\pi R^2\sigma \qquad (2.15)$$

The radius of the critical nucleus for mechanical stability is given by Equation (2.13). Although mechanically stable, the critical nucleus is thermodynamically unstable, and the work of formation is given by Equation (2.16)

$$\Delta\Omega_c = \frac{16\pi\sigma^3}{\left(\Delta P_b^{\,2}\right)} \qquad (2.16)$$

Bubble nuclei smaller than the critical radius will collapse and those that are bigger than the critical radius will grow, since the free energy of the system decreases for any of these processes. The work of formation acts as the barrier energy of nucleation and the classical homogenous nucleation rate J_c is given by Equation (2.17) where k_B is the Boltzman's constant and T is the temperature of the liquid.

$$J_c = J_0 e^{\left(\frac{-\Delta\Omega_c}{k_B T}\right)} \qquad (2.17)$$

The pre-exponential factor J_0 depends upon the particular kinetics of cluster formation of the system[81]. A statistical mechanics approach by Blander and Koltz[82] and Skirpov and Pavlov[83] yielded a value for J_0 as presented by Equation (2.18) where h is Planck's constant and N_0 is the liquid molecular density.

$$J_0 = \frac{kT}{h} N_0 \qquad (2.18)$$

Iwamatsu[84] presents an approximation for J_0 as presented by Equation (2.19) where ρ_l is the density of the liquid, ρ_g is the density of the vapour and M is the molecular mass.

$$J_0 \approx \frac{\rho_g^{\,2}}{\rho_l} \sqrt{\left(\frac{2\sigma}{\pi M}\right)} \qquad (2.19)$$

If the liquid is assumed to be incompressible and the vapour to be ideal, then the pressure difference can be written as a function of the supersaturation S, see Equation (2.20). The supersaturation $S = P_g/P_{coex}$, where P_g is the pressure of the supersaturated vapour and P_{coex} is the pressure at the liquid/vapour coexistence.

$$\Delta P_b = \rho_l k_B T \ln(S) \qquad (2.20)$$

However, the classical nucleation theory has been criticised for assuming that the properties of any critical nucleus are homogenous, independent of size and identical to those of a macroscopic liquid droplet in equilibrium with its vapour.[85] The classical nucleation theory has also been criticised for predicting a finite barrier of formation as the spinodal line is approached[86], whereas in practice, beyond the spinodal, there is no barrier to nucleation and the new phase appears spontaneously through a dynamic process called spinodal decomposition. Oxtoby and Evans[87] proposed a non-classical nucleation theory based on the density functional theory, which does not resort to the capillarity approximation. In this theory, the free energy of the system depends on the value of the density of the particles at every position throughout the fluid. Hence the free energy is a 'functional' of the density. In its first approximation the free energy functional is given as the sum of the local entropy of the system and the energy of attraction between particles, which leads to thermodynamic relationships that determine all the thermodynamic properties of the system. To its credit, the

density functional theory predicts that the free energy of formation goes to zero at the spinodal line. In addition, Laaksonen *et al*[88] and Oxtoby[89] have demonstrated that the theory provides good agreement with experimental data.

Delale[90] reports that in spite of the advances in understanding provided by the density functional theory, it is difficult to implement in flows with boiling or cavitation. For this reason, the author presents a reworking of the classical nucleation theory, which he demonstrates provides good agreement with experimental data.

Heterogeneous nucleation is induced on the surface of a foreign body, such as the wall of the container or a small solid particle, or by the presence of a single molecule or ion impurity.[85] Container surfaces provide sites for nucleation in the form cracks or cavities. The interaction between the fluid particles and the foreign body lowers the barrier to nucleation and the critical nuclei form at a much faster pace.[91] Using a classical approach to model the process of nucleation occurring on a solid substrate, *s*, the critical nucleus may be visualised as a cap-shaped aggregate of the stable phase β, surrounded by the metastable phase φ, as demonstrated by Figure 2.7.

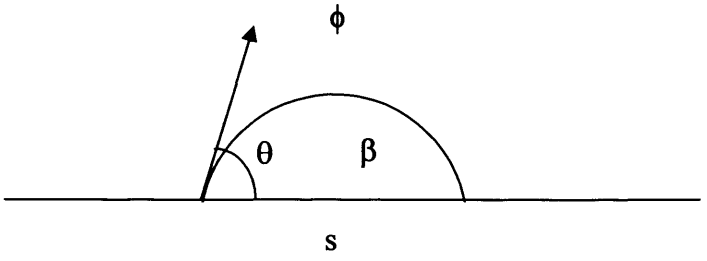

Figure 2.7 Schematic representation of a droplet on a planar surface

The work of formation of the critical nucleus is given by Equation (2.21), where τ is the line tension of the three-phase contact line of length $2\pi R\sin\theta$ and $f(\theta_c)$ is given by Equation (2.22), with θ_c given by Equation (2.23).

$$\Delta\Omega_c = \frac{16\pi\sigma_{\phi\beta}^{\ 3} f(\theta_c)}{3\Delta P^2} + \frac{2\pi\tau\sin\theta_c\sigma_{\phi\beta}}{\Delta P} \qquad (2.21)$$

$$f(\theta_c) = \frac{(2+\cos\theta_c)(1-\cos\theta_c)^2}{4} \qquad (2.22)$$

$$\sigma_{\beta s} - \sigma_{\phi s} + \sigma_{\phi\beta}\cos\theta_c + \frac{\tau}{(R\sin\theta_c)} = 0 \qquad (2.23)$$

Kolev[92] highlighted that boiling flow and flashing flow are essentially driven by the same physics and it has been well established that the rate of heat transfer associated with boiling systems is strongly dependent on the nucleation site density[93]. However, only a small fraction of all cavities become effective sites for vapour nucleation[94]. Various authors[95,96,97] have attempted to predict the nucleation site density in boiling systems using a variety of techniques. With the exception of specially prepared surfaces these have met with little success. As a whole, experimental and theoretical research into heterogeneous nucleation is in its infancy[85] and clearly requires particular attention in this field.

2.3.4.3 Bubble Growth in Superheated Liquids

Numerous studies have been made on the thermodynamics of bubble growth in superheated liquids. The earliest and perhaps the simplest description for bubble growth is given by the Rayleigh equation[98], presented by Equation (2.24).

$$\frac{dR}{dt} = \left[\frac{2}{3}\left(\frac{P(v)-P_l}{\rho_l}\right)\right]^{0.5} \qquad (2.24)$$

Equation (2.25) is derived from Scriven's analysis of motionless bubble growth[99], where the constant C is $(2\pi/3)^{0.5}$. Plesset and Zwick[100] also present this value for C, while Forster and Zuber[101] propose a value of $\pi^{0.5}$ in their study.

$$R = C\,Ja[\alpha(t-t_0)]^{0.5} \qquad (2.25)$$

Studies by Mikic *et al*[102] and Miyataka and Tanaka[103,104] have shown that bubble growth in superheated liquids can be divided into three consecutive stages. During the first stage of growth, surface tension is dominant, impeding growth for a certain delay period. Once the bubble reaches a given size, e.g. doubles its diameter, bubble growth is controlled by the difference between the vapour pressure inside the nozzle and the exterior pressure, balanced

by the inertia of the surrounding liquid; i.e. inertial growth. As the bubble grows further, the wall temperature consequently drops, causing an increased temperature difference between the surrounding liquid and the bubble wall. Hence, the final stage of growth is controlled by the rate of energy transfer from the liquid to the liquid-vapour interface to produce vapour and maintain the pressure; i.e. thermal growth. Mikic et al developed a complete model for spherical bubble growth model presented by Equations (2.26) - (2.30), where *Ja* is the Jacob number, α_l is the thermal diffusivity and b is a constant that depends on whether the bubble develops near a surface or an infinite medium.

$$R^* = \frac{2}{3}\left[(t^*+1)^{\frac{3}{2}} - t^{*\frac{3}{2}} - 1\right] \qquad (2.26)$$

$$R^* = \frac{RA}{B^2} \qquad (2.27)$$

$$t^* = \frac{tA^2}{B^2} \qquad (2.28)$$

$$A = \left[\left(\frac{b\Delta T}{T_{sat}\rho_l}\right)H_{lg}\rho_g\right]^{0.5} \qquad (2.29)$$

$$B = \left[\left(\frac{12}{\pi}\right)Ja\alpha_l\right]^{0.5} \qquad (2.30)$$

This model does not account for the formation of the critical bubble radius. Hence, Miyatake and Tanaka developed an experimentally validated model based on Mikic *et al*'s solution which covers the entire bubble life span.

Lee and Merte[105] conducted a numerical study of bubble growth in a uniformly superheated liquid. They investigated the problem of coupling the Rayleigh equation with the conversation of energy equation for the liquid temperature profile in a growing boundary layer surrounding the bubble. Their numerical results were found to represent their experimental data very well for a range of liquid pressures and superheats. However, Chang and Lee[106] report that the computational cost of their approach is too high for practical spray simulations.

2.3.4.4 Global Droplet-Size Correlations for Flashing Atomisation

A droplet size correlation for superheated jets was first proposed by Brown and York[16] (1962), where the liquids investigated were water and Freon at release pressures of between 5-10bar. High-speed silhouette photography was used to determine the sizes and axial velocity components of droplets in the spray. The mean droplet size (d_{10}) was proposed to be linearly proportional to the temperature and inversely proportional to the Weber number, see Equation (2.31). Although not dimensionally correct, this correlation represents the influence of both thermodynamics and fluid dynamics. They also reported that the mass fraction of flashed liquid at the exit orifice compared favourably with the air to liquid ratio required for effervescent nozzles.

$$d_{10} = \frac{[1840 - 5.18T(°F)]}{We} \qquad (2.31)$$

Sher and Elata[57] proposed that the droplet size produced during flash atomisation is linearly proportional to liquid surface tension and inversely proportional to the degree of superheat. Their model is based on nuclei generation and a bubble bursting mechanism. However, there are some problems with applying the final correlation proposed for droplet size with any generality. For example, the authors claim that the source of vapour nuclei was a valve within their injection mechanism (specific to aerosol deodorant containers). Without this, nuclei were not generated, although the parameter representing the volume density of vapour nuclei could presumably be modified for a more general case. Furthermore, the analysis was undertaken for binary mixtures (toluene and Freon 22) so it is not clear how this would differ for single component liquids.

Soloman *et al*[107] advocate the subdivision of the release conditions based on the transition from mechanical break-up to flashing. They cited four equations recommended in the literature which represent these stages of transition[108,109,110]. When fluid flashes in the injector orifice they claim the flow is analogous to a 'pre-filming type air-blast injector', for which the correlation proposed by Lefebvre[110] is suggested, see Equation (2.32), where η_n is the efficiency of the injector. Droplet SMDs measured using a Malvern Particle Size Analyzer were found to be approximately correlated by this equation.

$$\frac{\eta_n SMD}{\left[1+\left(\frac{m_l}{m_v}\right)\right]} = 0.073\left[\frac{\sigma_l}{\left(\rho_v u_v^{\,2}\right)}\right]^{0.6}\left(\frac{\rho_l}{\rho_v}\right)^{0.1} d_0^{\,0.4} + 6x10^{-4}\left[\frac{u_l^{\,2} d_0}{\sigma_l \rho_v}\right]^{0.5} \qquad (2.32)$$

Senda *et al*[111] presented data for flashing n-Pentane and n-Hexane jets at pressures of less than 10bar. Droplet size distributions were measured using micrograph photography. Flashing was achieved by reducing the chamber pressure. Mechanical break-up was found to dominate under sub-cooled conditions, producing typical droplet sizes of several hundred microns. When slightly supersaturated conditions were encountered, there was a marked increase in SMD. The authors claim that this was due to the contracting spray, however, a contracting spray in this scenario seems to be counter intuitive as conventionally cone-angle increases with a decrease in ambient pressure. Clearly this requires further investigation. Further reduction in the chamber pressure was accompanied by a sharp decrease in droplet SMD associated with flashing atomisation. Flashing jets were observed to be far more uniform than sub-cooled jets undergoing mechanical break-up, with uniformity reported along radial profiles also.

Park and Lee[13] also reported increasing uniformity in the radial droplet size distribution with increasing superheat for flashing jets, while the mean droplet SMD decreased with increasing superheat, consistent with all previous studies. Droplet SMD was observed to decrease exponentially with increasing dimensionless superheat (ΔT_{sh}*), where ΔT_{sh}* is given by Equation (2.33).

$$\Delta T_{sh}^{*} = \frac{T_{inj} - T_{sat}(P_l)}{T_{sat}(P_{inj}) - T_{sat}(P_l)} \qquad (2.33)$$

In their review published in the CCPS book, Johnson and Woodward[15] reference a number of those correlations already mentioned as well as the correlation of Crowe and Comfort[112], presented here by Equation (2.34).

$$d_p = 4.6\left[\frac{\sigma k_l d_0}{u_0 \rho_l C_{pl} \Delta P}\right]^{\frac{1}{3}} \qquad (2.34)$$

Nagai *et al*[113] developed a series of correlations which change form according to the nozzle aspect ratio. The influence of superheat – via the dimensionless superheat, ΔT_{sh}* - was also

considered, as well as the orifice diameter. The influence of injection pressure was accounted for in the dimensionless superheat, which included a term for the saturated temperature. The absolute maximum droplet size measured in the spray was found to be a multiple of the SMD and a multiplication factor in the range 2.0-2.6, which is higher than the 1.8 quoted by Elkotb[34] with reference to mechanical break-up. Droplet size distributions were also given some consideration, and the data was represented by a Nukiyama-Tanasawa distribution. The proposed correlation take the following form;

When $L/d_0 < 7$ and $0.55 < \Delta T_{sh}^* < 1.0$

$$SMD = 36.8(\Delta T_{sh}^*)^{-2.58} microns \qquad (2.35)$$

When $L/d_0 > 7.8$ and $0 < \Delta T_{sh}^* \leq 0.55$

$$SMD = 70.4\left[-1+0.14\left(\frac{L}{d_0}\right)\right]^{-0.22} d_0^{0.72}(\Delta T_{sh}^*)^{-0.38} microns \qquad (2.36)$$

When $L/d_0 > 7.8$ and $0.55 < \Delta T_{sh}^* \leq 1.0$

$$SMD = 39.1\left[-1+0.14\left(\frac{L}{d_0}\right)\right]^{-0.22} d_0^{0.72}(\Delta T_{sh}^*)^{-1.33} microns \qquad (2.37)$$

Particle sizing was undertaken using an intrusive impactor methodology with post-analysis, and hence, the data may require reappraisal using laser diagnostic techniques. In addition, the correlations proposed were specifically for brass nozzles, though the authors provide data and note differences in atomisation quality with change in nozzle material due to surface roughness influencing the number of nucleation sites.

2.3.5 Rainout

Rainout is defined as the mass of liquid that is lost from the airborne mass due to droplet impact and subsequent retention on the ground. Similar considerations are made in engine studies under the so-called process of impingement, but due to the decrease in appropriate length-scale by several orders of magnitude between the buoyancy-dominated atmospheric dispersion problem and the momentum driven engine environment, little further useful

comparison can be made. In atmospheric dispersion studies, the low settling velocities of typical clouds means that no secondary spray will result from droplets reaching the ground, although it is likely that some of the liquid may re-evaporate and rejoin the spray potentially more dangerously as vapour.

Atomisation due to mechanical break-up results in a narrow characteristic cone angle and large mean droplet sizes in the order of hundreds of microns. Hence almost all the released material will rainout, creating a spreading pool of considerable mass over a relatively small area in the vicinity of the exit orifice. By contrast, flashing releases produce sprays with wide cone angles and much smaller droplet sizes. As a result, a typical fully flashing release of a volatile substance is likely to give rise to a dew-like coating on the ground rather than a pool, which one would imagine could evaporate very quickly for highly volatile liquids.

A considerable body of work has been undertaken by The Finnish Meteorological Institute[114,115,116] in collaboration with the University of Helsinki concerning the fate of freely falling single and binary droplets under varying initial conditions. For liquids with a boiling point considerably lower than atmospheric temperature (e.g. LPG or LNG) atomising via the internal flashing mode, rainout seems unlikely under atmospheric conditions.

Vesala *et al*[116] proposed a detailed numerical model and a simplified analysis for the fate of freely falling droplets. The authors compared critical droplet sizes for the full numerical solution with the explicit equation from the reduced analysis for releases of high volatility (ammonia) and low volatility (water) aerosols. The difference in model results was found to vary with concentration and release height, with the error between the two methods at its minimum for lower concentrations and release heights. A height of 1m and a concentration of 10 droplets/cm^3 appeared to represent the upper limits of these parameters, for which the critical droplet sizes for water and ammonia were found to be 47μm and 107μm respectively, using the full numerical scheme. The simplified analytical equation derived by the authors was in error by 8% and 12% respectively.

To date, validated correlations for predicting rainout efficiency during a release of superheated liquid have been relatively scarce. Kletz[117] suggested that the rainout fraction, η_R, can be approximated by Equation (2.38)

$$\eta_R = 1 - 2\left[\frac{C_{pl}}{h_{lg}}(T_0 - T_{sat})\right] \tag{2.38}$$

De Vaull and King[118] adopted a simple empirical approach to the problem of predicting the mass rainout fraction from a superheated release, with the explicit intention of avoiding the numerical complexity of previously developed numerical fluid models. Their correlation is based on the adiabatic saturation temperature T_{as} rather than the saturation temperature T_{sat}, where the adiabatic saturation temperature is the minimum temperature reached by an equilibrium droplet-air mixture as the droplets dry out. Liquids were divided into categories of non-volatile and volatile where volatile liquids were defined by Equation (2.39).

$$\frac{T_{amb} - T_{as}}{T_{amb}} \geq 0.14 \tag{2.39}$$

Equations (2.40) - (2.42) present the proposed correlations for volatile liquids

$$\frac{\eta_R}{\eta_R^*} = 1 - \left[\frac{1}{0.145} C_{pl} \frac{(T_0 - T_{sat})}{L}\right] \quad if \quad C_{pl}\frac{(T_0 - T_{sat})}{H_{lg}} < 0.145 \tag{2.40}$$

$$\frac{\eta_R}{\eta_R^*} = 0 \qquad if \quad C_{pl}\frac{(T_0 - T_{sat})}{h_{lg}} \geq 0.145 \tag{2.41}$$

where

$$\eta_R^* = 1 - 2.33\left[\frac{(T_{amb} - T_{as})}{T_{amb}}\right] \tag{2.42}$$

Equation (2.43) presents the proposed correlation for non-volatile liquids

$$\eta_R = 1 - \frac{C_{pl}}{h_{lg}}(T_0 - T_{as}) \tag{2.43}$$

2.4 Previous Large-Scale Studies

In this section, various large scale studies, which have considered the theme of this study are reviewed, with reference made to the experimental methodology employed, with a brief summary of the main conclusions of each study. These include a programme of work undertaken by the Health and Safety Laboratory[119,120,121], an EU initiative under the so-called

STEP programme, undertaken by CEA-Grenoble[1,122] and more recent studies undertaken by the Von Karman Institute[123,124,125].

2.4.1 CCPS Experiments and RELEASE Model

Johnson and Woodward[15] reviewed a number of literature studies and collated a series of large-scale experimental programmes started in the 1980s with the aim of proposing a validated model for predicting rainout from flashing jet releases. They measured the rainout fraction from flashing jets under various initial conditions and reverse calculated droplet sizes to fit the data using the Unified Dispersion Model (UDM)[126,127]. These 'experimental' droplet sizes were correlated against a number of differing parameters, of which, the partial expansion energy was found to correlate best. Hence, they propose a correlation for the droplet size (SMD) as a function of the partial expansion energy E_p, as presented by Equation (2.44).

$$SMD = 0.833x10^{-3} - 0.0734x10^{-3} \ln\left(E_p\right) \qquad (2.44)$$

Where the partial expansion energy is given by Equation (2.45).

$$E_p = \begin{cases} -\Delta H - \left[P(v)T_{st} - P_a\right] + \left[P_{st} - P(v)T_{st}\right]\upsilon_{st}, & P_a < P(v)T_{st} \\ \left(P_{st} - P_a\right)\upsilon_{st}, & P_a \geq P(v)T_{st} \end{cases} \qquad (2.45)$$

Where ΔH is the change in enthalpy from stagnation to final post expansion conditions, P_{st} is the stagnation pressure, T_{st} is the stagnation temperature, υ_{st} is the stagnation specific volume, P_a is the atmospheric pressure and $P(v)$ is the saturated vapour pressure. The two cases essentially correspond to superheated and sub-cooled conditions.

However, the final model that they recommend (RELEASE) selects the minimum droplet size from the flashing correlation, presented by Equation (2.45) and a critical Weber number correlation, presented by Equation (2.46) where u_f is the post expansion velocity and the critical Weber number is taken to be 12.5 in line with recommendations made by Brown and York[16], Heinze[44] and the TNO Yellow Book[128].

$$SMD = \frac{\sigma_l We_{crit}}{u_f^{\,2} \rho_a} \qquad (2.46)$$

Adopting the post expansion velocity as the characteristic velocity in this critical Weber number correlation accounts for the influence of two-phase flow in the prediction of droplet SMD. However, the correlation still relies on the competition between inertial and surface tension forces. Moreover, utilising their model, the authors show that mechanical break-up always dominates at superheated conditions, which is highly inconsistent with experimental evidence in the literature. In addition, the reverse calculation method utilised to derive their correlation for flashing break-up is clearly subject to both the accuracy of the Unified Dispersion Model and the accuracy of the rainout data, which in this case is known to have inherent deficiencies.

2.4.2 EEC Programme: STEP

The synopsis of the STEP programme presented by Hervieu and Veneau identified high purity (99.5%) liquid propane as the fluid utilised, which was released into atmospheric conditions. The propane was stored under saturated conditions, so superheat would have varied as a function of storage pressure. Measurements were performed utilising a PDA system. However, due to the very high droplet concentration, it was necessary to prevent incident and scattered light from attenuation through the implementation of intrusive protection cylinders in the jet. The authors tentatively claim that shielding the spray was likely to have caused a 20% and 40% underestimation of droplet size and velocity respectively. However, the authors claim that no result could be expected without such protection.

Droplet SMD was shown to be inversely proportional to release pressure and positively correlated with the nozzle diameter. The droplet SMD also decreased with increasing axial downstream distance. As a whole, the results indicate that very little if any rainout should be expected from an 11bar release based on the sizes of droplets alone. In all cases a characteristic bell-shaped jet was observed, which seems to be a universal characteristic of flashing jets. Moreover the diameter of the jet increased significantly with storage pressure (pressure and superheat). The results of the study are summarised in Tables 2.2 and 2.3. Blanks indicate that the spray density precluded measurements being made.

Table 2.2. STEP on axis measurements for a 2mm nozzle diameter

Pressure (bar)	5			11			17		
z (mm)	30	60	95	30	60	95	30	60	95
SMD (μm)	49.5	38.5	35.8	-	30.2	25.2	-	26.6	23.7

Table 2.3. STEP on axis measurements for a 5mm nozzle diameter

Pressure (bar)	5			11			17		
z (mm)	30	60	95	30	60	95	30	60	95
SMD (μm)	-	48.5	52.8	-	31.2	27.0	-	-	23.7

2.4.3 HSL Experiments

The series of papers published by Allen[119,120,121] represent several years of experimental study undertaken by the UK Health and Safety Laboratories as part of a CEC joint-industry project on a rig specifically developed for characterisation of two-phase flashing releases. Again LPG was considered as the test fluid.

Only one set of initial conditions was investigated where the mean release temperature was 16°C and the mean mass flow-rate was 0.0951kg/s at saturated conditions. Results were presented for one nozzle of diameter 4mm and aspect ratio 10. A non-intrusive laser based diffraction particle sizer was used to measure droplet sizes. However, due to high obscuration rates and vignetting effects caused by the high density of the spray, considerable post-processing of the data was required. LDA measurements provided particle velocity measurements and LIF was developed towards quantification of jet temperature. Before manipulation, the data presented three characteristic particle size peaks. Post-processing, useful size information was provided subject to the appropriateness of the manipulation process, where the data was reduced to a bimodal distribution and the majority of droplet diameters were found to be less than 32μm. Data was subsequently presented in relative size bands where repeatability of the analysis technique was demonstrated. However, the authors recommended that the data at any point should not be considered in absolute terms, but rather in terms of identifying general trends and overall size distributions.

2.4.4 Von Karman Institute Experiments

Yildiz *et al*[123,124,125] used a refrigerant material known as R134-A, which corresponds to 1,1,1,2-tetrafluoroethane[129]. Externally pressurised nitrogen was used to control pressure within the storage vessel, which was considered a reasonable experimental approach, although an ideal system would eliminate the potential for dissolved gases to influence the process. Measurements were made using PDA without encountering the necessity to utilise intrusive protection cylinders.

In an initial study[123], results from one set of initial conditions were presented for a 1mm nozzle diameter at 187mm downstream of the nozzle outlet. The nozzle length was not given in the paper but is assumed to be sufficiently small that it can be taken as zero. The release temperature was 23°C, which corresponds to a superheat of 49°C, and the release pressure was between 7.0-7.5bar. Global SMD values of 80-100μm are estimated from the spatially distributed SMD values quoted in the paper.

In a follow-up study[124,125], results from a series of initial conditions were presented for 1mm and 2mm orifice diameters at downstream locations of 110mm, 220mm and 440mm. The effect of superheat on droplet diameter was investigated for liquid temperatures in the range 20-28°C (46-54°C superheat) for release pressures of 7.9-8.3bar and 12-14bar. The authors present linear correlations which relate the log of the droplet diameter with the log of the Jakob number for particular release pressures. However, the data appears to indicate that a more general expression could be achieved by correlating droplet diameter with Jakob number irrespective of release pressure, where droplet SMD decreases relatively linearly from 158μm to 30μm for increasing Jakob numbers in the range 0.318 – 0.365 (presumed superheat in the range 46-54°C)

The effect of drive pressure on droplet diameter was investigated by producing three datasets at three fixed liquid temperatures of 20°C, 24°C and 28°C for release pressures of 8bar, 12bar and 14bar. At 20°C (46°C superheat) increasing the pressure from 8bar to 12bar caused the droplet SMD to decrease from 158μm to 130μm, but at higher superheats the effect of increasing pressure was negligible.

The effect of orifice diameter on the droplet diameter was investigated for two orifice diameters of 1mm and 2mm. For low superheat, the mean droplet sizes show that larger nozzles lead to slightly larger mean diameters, but when superheat increases, the nozzle diameter does not have an effect on the droplet size. This is consistent with observations in the literature where aerodynamic processes dominate break-up at low superheat. In general however, the authors claim that nozzle diameter has almost no effect on droplet size compared to the effect of superheat.

The effect of orifice aspect ratio (L/d_0) on droplet diameter was investigated for a 2mm nozzle diameter with aspect ratios of 0, 2, and 7 at downstream locations of 220mm and 440mm. Increasing the nozzle aspect ratio results in smaller droplets compared to the sharp-edged orifice. At 220mm downstream, $L/d_0 = 7$ generates larger droplets than $L/d_0 = 2$, probably because of incomplete detachment of the spray from the nozzle wall leading to incomplete atomisation, but at 440mm downstream the effect on droplet size is negligible, where evaporation and rainout between 220mm and 440mm cause the droplet diameters to converge.

In summary, the authors report that liquid superheat plays the most dominant role on the droplet SMD, regardless of drive pressure, orifice diameter, aspect ratio or axial location.

2.5 Measurement Techniques

In this section a comprehensive review of the diagnostic technology applied to the application of liquid jets is made, from the earliest studies right up to current cutting edge techniques.

2.5.1 Sample Collection

Before the introduction of laser-based techniques, sample collection and post-analysis were the only methods available to derive droplet size distributions. They are still of use today in hostile environments where the use of laser-based techniques would not be possible or appropriate. A typical example is the magnesium-oxide powdered slide utilised by Sher and Elata[57] for characterising sprays from pressurised aerosol canisters. The slide is exposed to

the two-phase flow for a very short period of time before being mechanically covered again to protect the data. Droplets in the flow impinging on the plate leave imprints which are subsequently analysed manually (more recently with the aid of image analysis software) to determine droplet sizes.

Another variant is the method of freezing the droplets in a wax or similar material, e.g. silicon oil, used by Peters *et al*[19], ready for post-analysis. However due to the uncertainty and wide range of inaccuracies inherent in these techniques, they have been superseded by laser-based methods.

2.5.2 Laser-based Diffraction

A considerable advantage of laser-based techniques is their non-intrusive nature, their data acquisition rates and speed of processing. For example, fuel injectors can now be characterised on a transient basis, despite the fact that they typically deliver fuel over millisecond time periods with droplet speeds exceeding $100ms^{-1}$ and droplet sizes in the range 1-100μm.[130]

To date, atomisation and spray research has principally relied on a laser-diffraction based technique, the commercial version of which is marketed primarily by Malvern Instruments, UK. The basic principle of this technique was first reported by Swithenbank *et al*[131] and relies on the fact that the angle of diffraction of incident monochromatic light on a spherical particle is inversely proportional to the particle size. Using Fraunhofer theory, this angular variation can be calibrated and with the aid of a Fourier-Transform lens, the optical system allows a spatially resolved temporal measurement of spray distribution along a line of sight.

Considerable work was undertaken by the UK Nuclear Industry in the 1980s, which considered the transportation of radioactive nuclei via airborne aerosols, for which in-house particle-sizing techniques were developed. Bates *et al*[66] described the development of a robust particle sizing analyser for field work, utilising a mixed Doppler-intensity sizing strategy for characterising superheated water jets through sharp-edged orifices at pressures from 19-160 bar and temperatures from 110-312°C. Limited optical access was achieved at

the higher pressures (>30bar) and superheats, which was attributed to the density of the spray coupled with the low-powered laser utilised (5mW).

Solomon *et al*[107] utilised the diffraction methodology in the form of the Malvern Particle Analyser. Most subsequent experimental sizing investigations for flashing jets have utilised the Malvern instruments, often with compensating formulae to accommodate the dense sprays encountered. For example, Park and Lee[13] utilised the obscuration compensation formula advocated by Dodge[132]. Allen[120] utilised a modified Malvern system to characterise flashing propane releases through a 4mm final orifice ($L/d_0 = 10$). Considerable modification of the Malvern based system was required to undertake measurements and as previously highlighted, it was necessary to account for the harsh optical environment through additional post-processing of the data. Obscuration levels of over 90% were reported, whereas ideal conditions are between 11-30%. Even after analysis, it is noted that accurate droplet size distribution measurements were not possible and only qualitative descriptions of the variation of the droplet size were feasible.

2.5.3 Phase Doppler Anemometry

The basis of Phase Doppler anemometry (PDA) was first reported by Durst and Zaré[133] in 1975. Systems relying on the same basic principle but with optimised electronics and post-processors are now marketed by companies such as Aerometrics, Biral and DANTEC. PDA is essentially an extension of laser Doppler anemometry (LDA), but whereas LDA is only capable of measuring particle velocities, PDA is capable of simultaneously measuring both particle size and velocity. Measurements are made based on phase Doppler interferometric theory, whereby light from two incident laser beams is scattered by particles entering the measurement volume, which is defined by the intersection of the two beams. The superposition of the scattered waves creates a Doppler burst with a specific frequency that is proportional to the velocity of the particle. Receiving optics placed at a specific off-axis location project the scattered light onto multiple photo-detectors. The phase shift between signals from different detectors is directly proportional to the particle diameter.

Allen[121] characterised the velocity profile across transverse downstream axial locations using a two-component TSI LDA system powered by a 4 Watt continuous wave Argon-Ion Laser.

Again difficulties due to harsh spray environment were reported, but after some post-processing, valid velocity data profiles across the axial centreline and several lateral profiles at various axial locations were presented. Consistency with data from other pressure-liquefied studies was established, in particular the Gaussian velocity profile, which is consistent with LDA data generated for effervescent atomisation (Panchagnula and Sojka, 1999)[67].

The EU-funded STEP[1] programme and the Von Karmen Institute[123] study both utilised PDA as the primary diagnostic technique. The former set out with the aim of addressing the problem considered in this body of work, namely the example of a large-scale blow-down of a release of LPG. Whilst the experimental programme appears to have been undertaken in a rigorous manner, the density of the spray, particularly for larger-scale releases, proved problematic. As previously mentioned protection cylinders were required to prevent incident and scattered light from attenuation. Without these it is claimed that PDA measurements would not have been possible. However, in the latter study reported that measurements were made using PDA without encountering the necessity to utilise intrusive protection cylinders.

2.6 Summary

The hazard generated by accidental releases of volatile liquids is generally considered to be the quantity of matter that remains airborne. Hence, the magnitude of the hazard is inversely related to the quality of the spray, which is essentially defined by the size of the droplets generated.

Atomisation is fundamentally divided into two categories: mechanical break-up and flashing. Mechanical break-up is considered to be independent of the thermodynamic condition of the jet, whereas for flashing, thermodynamics is the dominant input parameter.

It is widely accepted that mechanical break-up is comprised of four separate sub-divisions. Of these, only second-wind induced and atomisation represent increased hazards in the context of this study. Numerous studies, utilising a variety of appropriate laser diagnostic techniques, have shown that the break-up is governed by the orifice size, the exit velocity and the fluid properties. Other parameters such as the nozzle aspect ratio, surface roughness and orifice shape are also known to be influential. Various correlations have been proposed to describe

droplet sizes produced by sprays in these regimes, with proposed exponents for nozzle diameter and release pressure ranging from 0.262 – 1.2 and -0.07 - -0.69 respectively. The effect of the nozzle aspect ratio is a matter of ongoing debate and the lack of a significant body of experimental data in this area clearly requires attention.

Most atmospheric dispersion models currently utilise the critical Weber number criterion derived from single droplet studies, to determine droplet sizes in sprays undergoing mechanical break-up. Critical Weber numbers, representing the ratio of inertia forces to surface tension forces, vary between ten and twenty. However, the single droplet Weber number criterion does not reflect the body of empirical data in the literature, as it is independent of orifice size and its scaling with release velocity is inconsistent with the range published via empirical correlations. Hence, this methodology for characterising droplet sizes in releases undergoing mechanical break-up is considered inappropriate.

There is a considerable body of evidence to show that at low superheat there is little qualitative difference between jet break-up under these conditions and sub-cooled releases. However, this has not been proven on a quantitative basis and is therefore an area that needs to be addressed. Nevertheless it is generally accepted that flashing appears to be controlled by a transition superheat limit, allowing mechanical break-up mechanisms to dominate into the superheated region. Studies of the criteria governing transition from mechanical break-up to flashing are limited, with Kitamura's experimentally validated transition criteria representing the current standard for studies in this field.

Beyond the superheat limit for mechanical break-up there are several modes of what is generally termed flashing; the distinction being whether vapour production first commences upstream or downstream of the exit orifice. 'External' flashing is characterised by an initial 'idle' period, where the liquid jet leaves the orifice as a metastable liquid above its normal boiling point before the inception of bubble nucleation occurs. The jet then shatters further downstream due to homogenous bubble nucleation and the subsequent rapid formation of vapour within the jet. 'Internal' flashing is the most catastrophic mode of atomisation and is characterised by finely atomised droplets, which result in low or zero rainout. It is thought to have strong phenomenological links with effervescent atomisation, where studies of both internal flashing and effervescent atomisation have indicated that a change in the internal flow regime is accompanied by a corresponding transition in the external mode of

atomisation. Hence, the internal flashing mode can itself be divided into various sub-sections. Currently, there is no simple methodology available for predicting transition between these different modes in terms of the downstream spray characteristics.

In terms of quantifying flashing atomisation, at the very least, the characteristic droplet sizes should be less than those predicted for mechanical break-up. Most of the qualitative descriptions reported for flashing sprays are fully consistent with published work on effervescent sprays. There is considerable potential for model development and validation if this consistency could be extended to justify quantitative equivalence. The particular properties that have shown commonality, albeit compared with the limited data available for flashing jets, include: independence of orifice size, dependency on drive pressure, uniformity of mean droplet size across transverse sections and Gaussian transverse velocity profiles.

Current atmospheric dispersion models governing flashing atomisation either attempt some variation of the critical Weber number approach, or are based on correlations derived from retro-calcualtions, using a dispersion code to derive initial droplet sizes. At a qualitative level, the modified critical Weber number approach shows both an independence of orifice diameter and inverse dependence on drive pressure. However, it is felt that this is likely to be coincidental. The 'reverse' modelling approach, aside from its weakness in terms of scientific rigour already mentioned, is further hindered by the fact that data is presented where both dynamic and thermodynamic parameters vary. Hence, it is not possible to immediately determine whether the indicated droplet sizes correlate well with a thermodynamic parameter since the pressure effects, possible orifice size effects and liquid properties will also have influenced the data. In summary, neither approach is felt to suitably address the problem.

The mean droplet size in flashing sprays is consistently reported to be inversely proportional to superheat. However, there is disagreement over the actual form of this relationship. Hence, it is probably most appropriate at this stage to rely on the limited data sets available in the literature to provide approximations for droplet sizes in medium-scale flashing releases. However, this is clearly an area which requires significant attention.

In addition to mean droplet size, the distribution of droplets produced in a spray will influence downstream rainout. Two established functions have been recommended in various papers to represent sprays from flashing releases, namely the Rossin-Rammler and log-

normal distributions. The log-normal distribution is adopted by most atmospheric dispersion codes currently available, however, the development of an optimal representation of the droplet size distribution still requires attention.

The primary variables that that require quantification in flashing jet atomisation studies are; droplet size distributions and mean droplet size, velocity components and mean velocities, relative phase distribution and jet temperature. Ideally all the diagnostics are required on a spatially resolved basis. With this specification, the most appropriate diagnostic techniques currently available are PDA (simultaneous droplet size and velocity components), LDA (droplet velocity components). However, the environment within a flashing jet is extremely harsh for any diagnostic technique, and hence even the most appropriate techniques will encounter some difficulties and limitations. Empirical correlations can only be as accurate as the data available to validate them, and this in turn depends on which droplet sizing technology is used for data generation. Nevertheless, it is felt that the PDA methodology is the most appropriate for characterising flashing sprays, primarily due to its suitability for measuring relatively dense sprays.

Chapter 3 Experimental Facilities and Procedure

3.1 Introduction

In this section the experimental facilities and procedures utilised in the investigation of mechanical break-up, transition between break-up phenomena and flashing atomisation are detailed, and the where appropriate, the principles behind each measuring technique are highlighted and explained.

3.2 Rig Design

3.2.1 Nozzles

Sharp-edged brass nozzles were manufactured in-house, with care taken to avoid the formation of aberrations or inaccuracies on the nozzle inlet as recent work[134] has indicated that these influence the internal flow characteristics and may significantly alter the atomisation process. The nozzles utilised for both sub-cooled and superheated releases are presented in Figure 3.1.

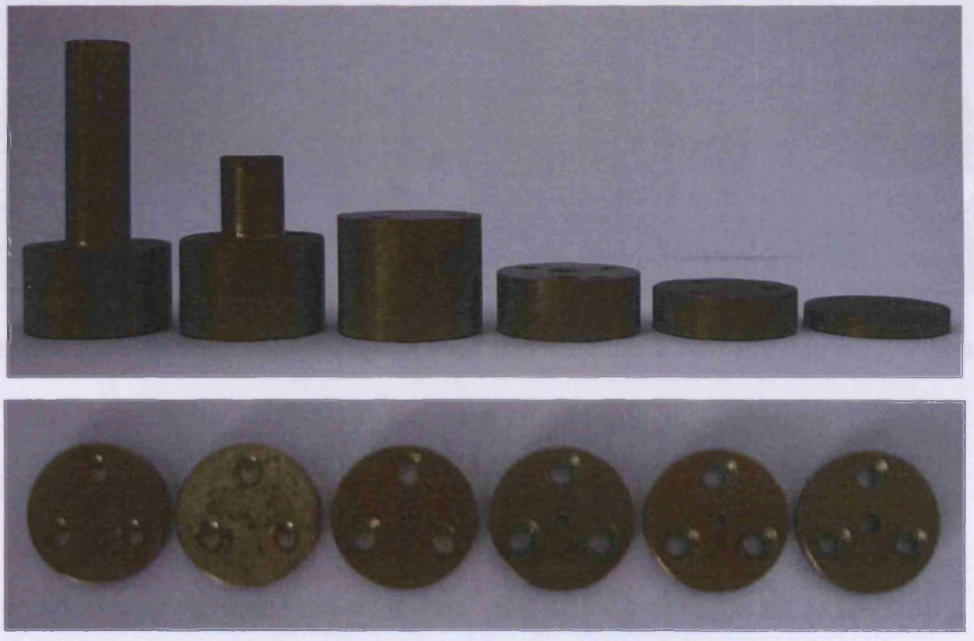

Figure 3.1 Brass sharp-edged nozzles utilised for sub-cooled and superheated releases.

The first image presents nozzles with a constant orifice diameter of 1mm and nozzle lengths of 50, 30, 20, 10, 7 and 3.5mm respectively. The second image presents nozzles with a constant nozzle length of 3.5mm and orifice diameters of 0.5, 0.75, 1, 2, 3 and 4mm respectively. The orifice geometry is defined to be consistent with that defined in standard atomisation and jet break-up literature[17,135].

Nozzles were attached to a stainless steel adaptor using three countersunk screw caps in the face of each nozzle. A seal was achieved with a small rubber o-ring at the nozzle/adaptor interface. For superheated releases the adaptor was modified so that temperature and pressure in the nozzle could be monitored. The adaptor was fitted with a pressure transducer and a thermocouple 15mm upstream of the orifice inlet, and is presented in Figure 3.2. Here (A) is the thermocouple, (B) the main body of the adaptor (which was the original part of the adaptor which existed for investigating sub-cooled releases), and (C) is a pressure gauge which was used for calibrating the data acquisition system and monitoring the pressure at the nozzle during releases. The data acquisition system utilised during superheated releases was capable of recording temperature and pressure at a rate of 1000Hz.

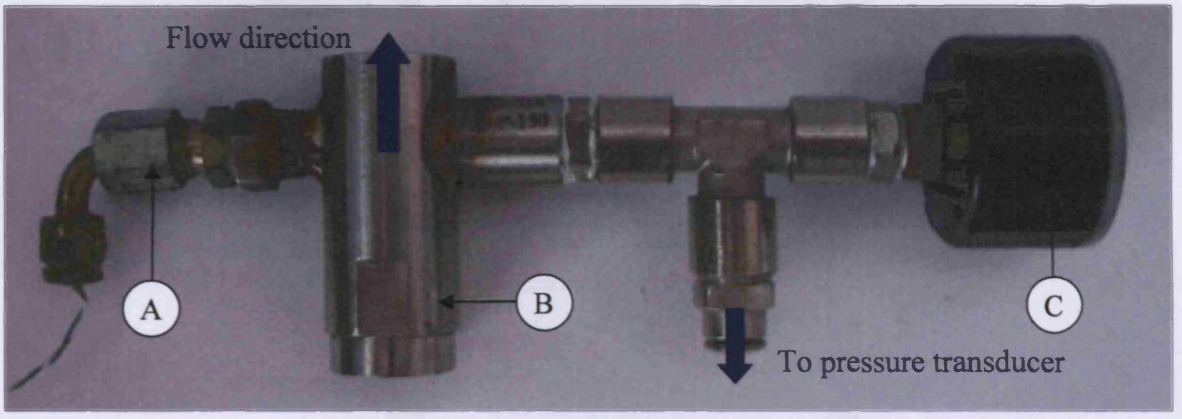

Figure 3.2 Stainless-steel adaptor with thermocouple and pressure transducer

3.2.2 Sub-Cooled Rig

The sub-cooled spray rig consisted of a steel tank of base dimensions 1x1m with a working capacity of 200 litres, and a vertical nozzle position approximately 1.5m above the base of the tank, so as to negate any gravitational effects on the spray. Water was circulated using a

Lowara SV224 centrifugal vertical pump. A pressure gauge and a pressure relief valve were located downstream of the pump to facilitate pressure regulation of the discharge line. The pressurised flow was then directed to the nozzle inlet via a reinforced flexible pipe. The whole tank was encased in polythene sheeting, with laser optical access to the spray being facilitated by openings in the front and adjacent side of the sheeting. Figure 3.3 presents the arrangement of the sub-cooled rig including the positioning of the PDA transmitting and receiving optics. An orthogonal over-head view of the set-up is also presented.

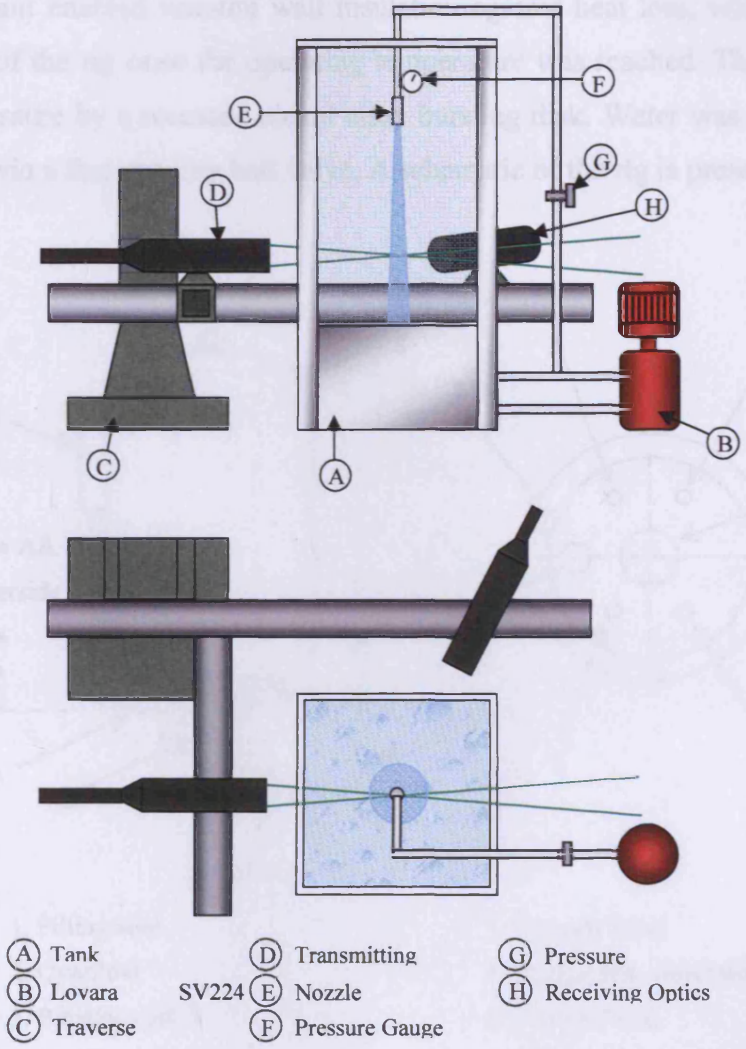

Figure 3.3 Sub-cooled rig with positioning of PDA transmitting and receiving optics

3.2.3 Superheated Atomiser

The superheated spray rig consisted of a sealed pressure vessel with a working capacity of approximately 33 litres. A helical-shaped electrical incoloy heating element was used to heat the water inside the tank. Pressure was created through the expansion of the water (i.e. conditions within the vessel were initially saturated) and hence the flowrate was a function of the water temperature and the orifice geometry. Nozzles were attached to the rig via a conduit elbow at the base of the tank, so that releases were directed parallel to the ground, thereby making gravitational influences on the droplet distribution unavoidable. The double-skinned design of the unit enabled vacuum wall insulation against heat loss, which in turn enabled prolonged use of the rig once the operating temperature was reached. The rig was protected against overpressure by a recessed nickel alloy bursting disk. Water was discharged through the exit orifice via a fast opening ball valve. A schematic of the rig is presented in Figure 3.4.

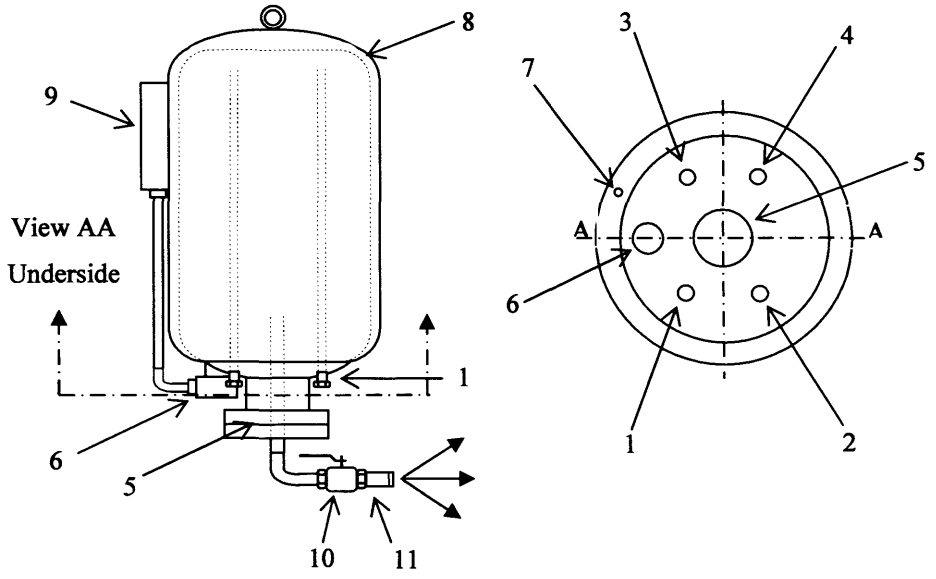

1. Filling vent
2. Overflow
3. Bursting disk
4. Auxiliary filling vent
7. Vacuum bleed
8. Double skin vessel wall
9. Control Panel
10. Ball valve

Figure 3.4 Schematic of superheated atomiser

The design of the superheated rig incorporated a collar and flange at the base of the tank for attaching conduits of varying diameter to the main vessel. As a consequence of this design, a cold 'slug' of water remained inside the collar, which did not reach the temperature of the water in the upper part of the tank after heating. Therefore, at the beginning of each release, as superheated water from the upper region of the tank flowed through the exit conduit, a temperature gradient was created, which generated considerable heat loss in the system between the tank and exit orifice. Hence, the temperature of the jet at the exit orifice was transient during the initial stages after the start of a release. As the jet temperature increased, the jet break-up mechanism changed accordingly. After a period of time the jet temperature became relatively stable; generally in the region of 20-30°C below the initial stagnation temperature, depending on the orifice geometry and the stagnation temperature itself.

3.3 Measuring Techniques

3.3.1 Rainout Collection

Although admittedly crude, the technique used for measuring rainout was effective in providing data where up to now there has been a dearth of information. While various patternators and designs were initially considered, a simple 6m x 4m steel frame aligned with the release direction, covered by two 5m x 4m tarpaulin sheets was found to be the simplest and most effective solution to the problem. Steel dead-weights were used to hold the sheets in place.

Figure 3.5 demonstrates an example of a release using this set-up for a 4mm orifice diameter and a stagnation temperature of 160°C. For a given set of initial conditions the rig was left to fully discharge, and the volume of water in the collection rig was measured manually using a 3 gallon (13.64 litre) bucket. Given sufficient due care and consideration, this was an easier task to undertake than one might anticipate, with minimal liquid loss encountered at any stage. A small amount of water remained within the release containment vessel, which was also measured and recorded. The rainout fraction was then given by Equation (3.1), where V_R is the volume of discharged water, V_T is the total volume of water in the rig prior to a release and V_U is the volume of un-discharged water.

$$\eta_R = \frac{V_R}{V_T - V_U} \qquad (3.1)$$

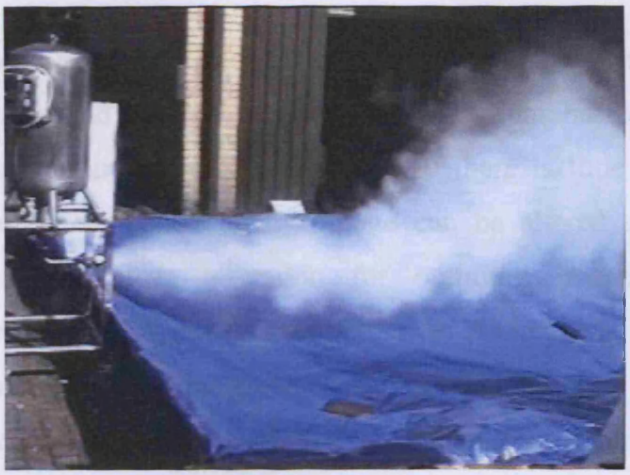

Figure 3.5 Experimental set-up for measuring rainout fraction

3.3.2 Geometric Spray Characterisation

This analysis technique was developed within the context of this study as a means of investigating the potential for characterising flashing jets at an intrinsically basic level. As previously mentioned, a characteristic particular to the superheated rig was the transient nature of the temperature at the exit orifice during the initial stages of a release. This corresponded to an increase in both the jet width and the bulk plume density until the system approached a relatively stable condition. This mirrored the findings of the STEP programme presented by Hervieu and Veneau, where the jet width was found to increase with superheat. Hence, it was suggested that characterising the jet width could be used as a simple and inexpensive method of characterising flashing atomisation.

Digital images of the jet were taken at regular intervals after the inception of a release. Jet widths were then derived through detailed image-by-image analysis. The images were examined using the software package 'Corel Photo-Paint', which incorporates various image analysis techniques. Measurements of the jet width were made possible by the combination of precise pixel-by-pixel spray-edge location and the implementation of a scale factor. The scale factor was determined from the analysis of a ruled grid at a fixed radial location off-set from

the jet during each release. Where the exact position of the jet boundary was found to be vague or ambiguous i.e. at low flow rates, the software also facilitated image enhancement, through the application of various colour filters.

The 'Bit Planes' filter is a powerful tool for analysing gradients in images. It reduces the image to basic red, green and blue colour components and emphasizes tonal changes. For example, certain areas appear as solid blocks because there is little change in tone. The saturation of each colour component in the image can be altered allowing the user the optimum combination of colour saturation for optimum image enhancement. The 'Psychedelic' filter, see Figure 3.6, changes the colours in the image to bright electric colours such as orange, hot pink, cyan and lime green. The effect on the image is startling and allows the unambiguous determination of the location of the jet boundary in almost all cases.

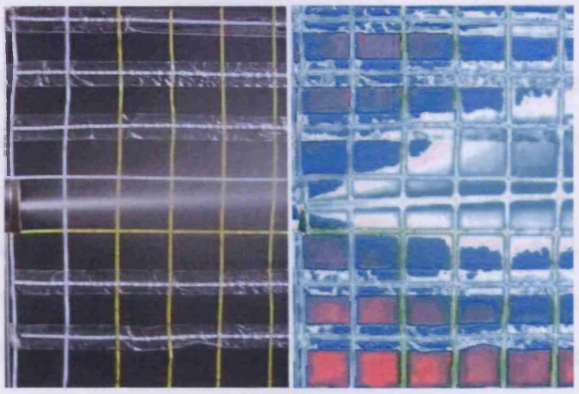

Figure 3.6 Image enhancement using the psychedelic filter

Nozzle diameters in excess of 2mm generated high flow-rates, which reduced the transient 'warm-up' period, which in turn reduced the available window for taking images of the spray. It was not possible to produce fully flashing sprays at stagnation temperatures below 180°C using nozzles smaller then 2mm in diameter, which was the maximum operating temperature of the superheated rig. Hence, it was only possible to conduct geometric spray characterisation using a 2mm nozzle diameter.

3.3.3 High-Speed Backlit Shadowography

This technique was essentially an extension of that utilised for geometric spray characterisation. However, in this case a 1000W backlight was used to illuminate the spray in order to define the flow structures in the spray with greater clarity. In addition, sophisticated high-speed camera equipment was utilised to record short films of the spray at very high frame-rates, which were then analysed on a frame-by-frame basis. Two variations on this technique were employed; firstly, for the investigation of the transition between downstream break-up regimes and secondly to analyse the internal flow structures upstream of the nozzle outlet using transparent nozzles.

3.3.3.1 Transition between Downstream Break-Up Regimes

This technique also utilised the transient nature of the temperature at the exit orifice during the initial stages of a release. By combining high-speed shadowography with a thermocouple and pressure transducer located close to the nozzle exit, it was possible to couple the observed break-up characteristics with the jet temperature and release pressure and subsequently pinpoint the exact conditions at which transition between break-up regimes was occurring. Figure 3.7 illustrates the experimental facilities for investigating the transition between break-up regimes

Backlit shadowgraphs of superheated jets were taken using a NAC 1000 high speed video camera and a VCR, which recorded images at 1000 fps. Jets were backlit using a 1000 W spotlight focused at the plane of the jet's centreline. An efficient extract system was used to prevent droplet recirculation. As previously mentioned it was not possible to produce fully flashing sprays using a 1mm nozzle diameter at stagnation temperatures below 180°C. As a result this was the only release condition for which images were taken using this nozzle diameter. Table 3.1 summarises the full-set of initial conditions for which images were recorded.

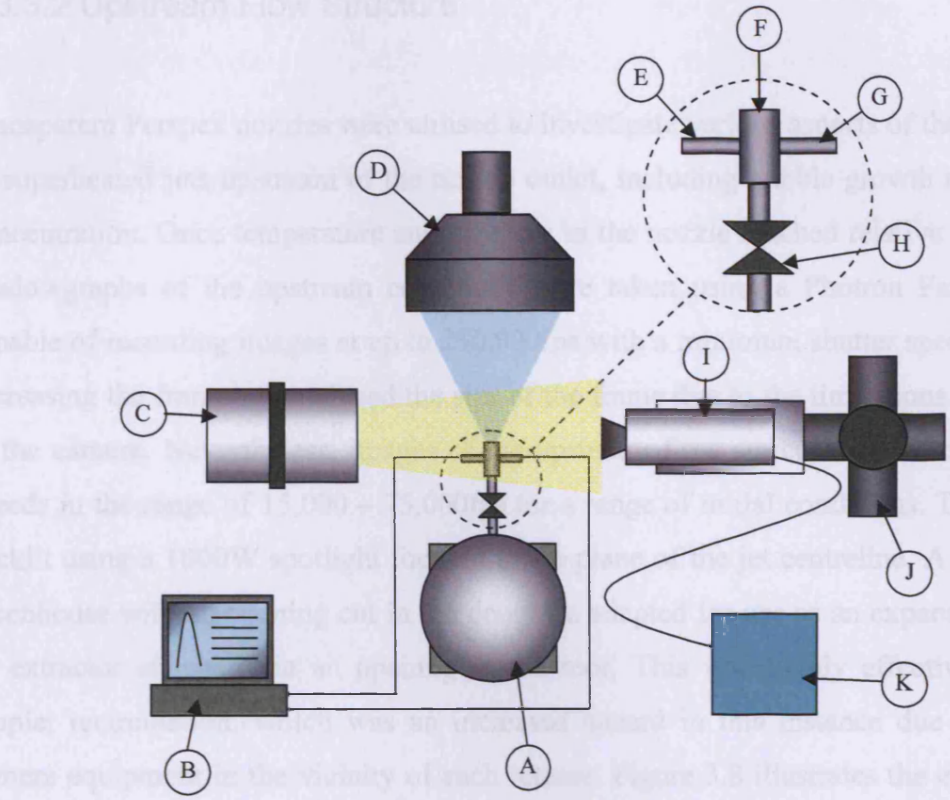

A Superheated atomiser
B Data acquisition processor
C 1000W spotlight
D Extractor
E Thermocouple
F Nozzle adaptor
G Pressure transducer
H Ball valve
I NAC1000 High Speed Camera
J Tripod
K VCR

Figure 3.7 Experimental apparatus for investigating transition to flashing

Table 3.1 Experimental programme for investigating transition to flashing

Stagnation Temperature (°C)	Nozzle Diameter (mm)	Aspect Ratio (L/d_0)
130		
140	4	0.85
150	3	1.13
160	2	1.70
170		
180	1	3.40

3.3.3.2 Upstream Flow Structure

Transparent Perspex nozzles were utilised to investigate various aspects of the flow structures of superheated jets upstream of the nozzle outlet, including bubble growth rates and bubble concentration. Once temperature and pressure in the nozzle reached relative stability, backlit shadowgraphs of the upstream conditions were taken using a Photron Fastcam-APX RS, capable of recording images at up to 250,000fps with a minimum shutter speed of 0.000005s. Increasing the frame-rate reduced the size of the frame due to the limitations of the processor in the camera. Nevertheless, images of the upstream flow structure were recorded at frame speeds in the range of 15,000 – 75,000fps for a range of initial conditions. The nozzles were backlit using a 1000W spotlight focused at the plane of the jet centreline. A common plastic greenhouse with an opening cut in the door was adapted for use as an expansion vessel, with an extractor attached via an opening in the roof. This was highly effective at preventing droplet recirculation, which was an increased hazard in this instance due to the sensitive camera equipment in the vicinity of each release. Figure 3.8 illustrates the experimental set-up for investigating the flow structure upstream of the exit orifice.

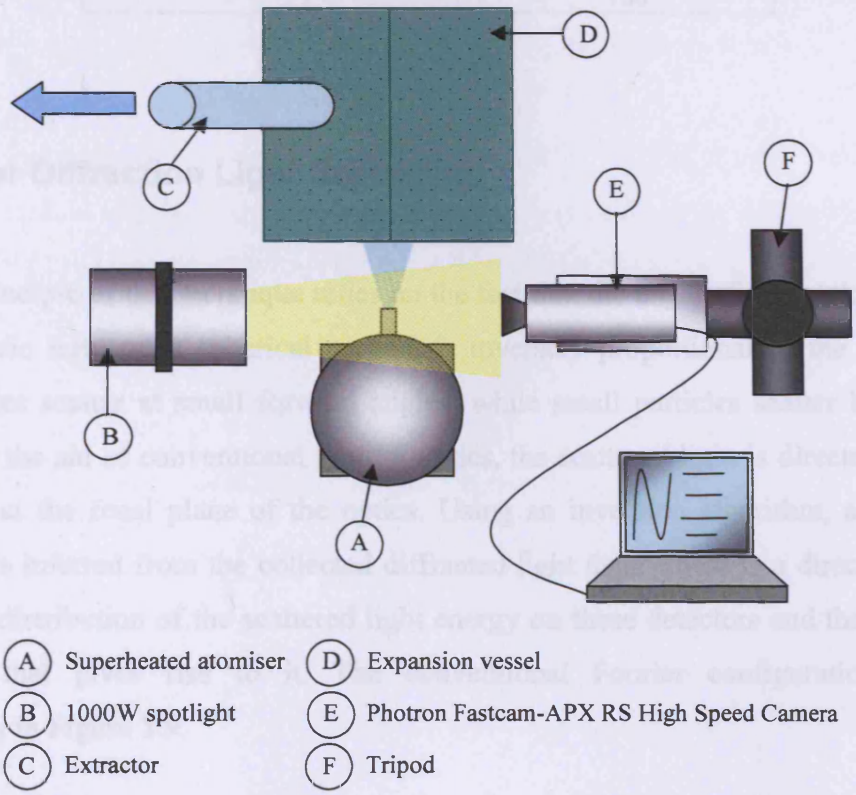

Figure 3.8 Experimental apparatus for investigating upstream flow structures

Bubble growth rates and bubble frequency were derived via the same detailed frame-by-frame analysis procedure outlined for geometric spray characterisation. Measurements of the jet width were made possible by the combination of precise pixel-by-pixel spray-edge location and the implementation of a scale factor, derived from the dimensions of the nozzle. Table 3.2 presents the full programme of initial conditions for which tests were performed.

Table 3.2 Experimental programme for investigating upstream flow structure

Nozzle Diameter (mm)	Aspect Ratio	Stagnation Temperature (°C)
1	3.4	140 150 160 170
	10 20 30	140
2	1.7	150 160 170 180
2	3.5	140 150 160 170 180

3.3.4 Laser Diffraction Light Scattering

The basic principle of this technique relies on the fact that the angle of diffraction of incident monochromatic light on a spherical particle is inversely proportional to the particle size. Large particles scatter at small forward angles, while small particles scatter light at wider angles. With the aid of conventional Fourier optics, the scattered light is directed to an array of detectors at the focal plane of the optics. Using an inversion algorithm, a particle size distribution is inferred from the collected diffracted light data. There is a direct relationship between the distribution of the scattered light energy on these detectors and the particle size distribution that gives rise to it. The conventional Fourier configuration is shown schematically in Figure 3.9.

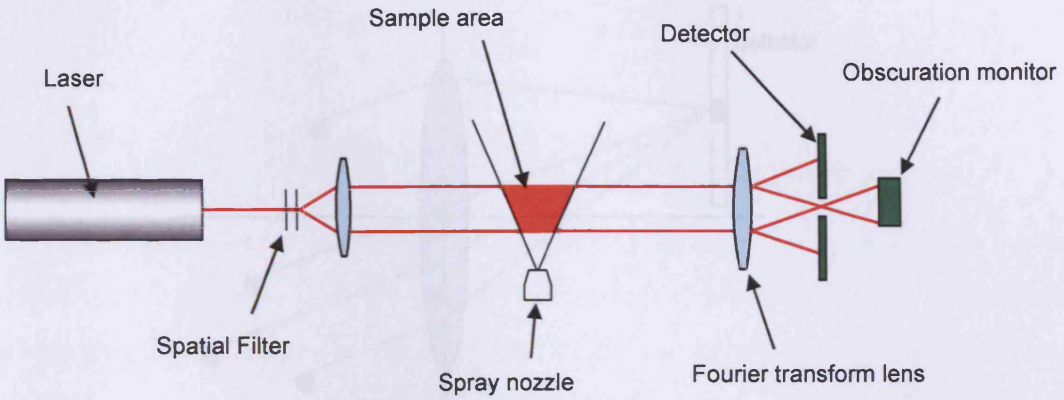

Figure 3.9 Conventional Fourier optical configuration

The light from a low power Helium-Neon (He-Ne) laser is used to form a collimated, monochromatic light beam. Both the light scattered by particles traversing the beam and the un-scattered remainder are incident on the receiving lens. This operates as a Fourier transform lens forming the far-field diffraction pattern of the scattered light at its focal plane where a solid state detector gathers the scattered light over a range of angles. The un-scattered light passes through a small aperture in the detector and on to an obscuration monitor, which measures the total laser power passing through the system.

Figure 3.10 illustrates the working principle of the Fourier transform lens. Particles of equal size scatter light at equal angles so that wherever a particle is in the analyser beam its diffraction pattern is stationary at any distance from the lens and centred on its optical axis. This facilitates the analysis of moving particles within sprays as it does not matter that a particle is moving through the analyser beam; its diffraction pattern remains stationary and centred on the optical axis of the lens. No practically encountered sample velocities are high enough to cause significant deviation from this characteristic.

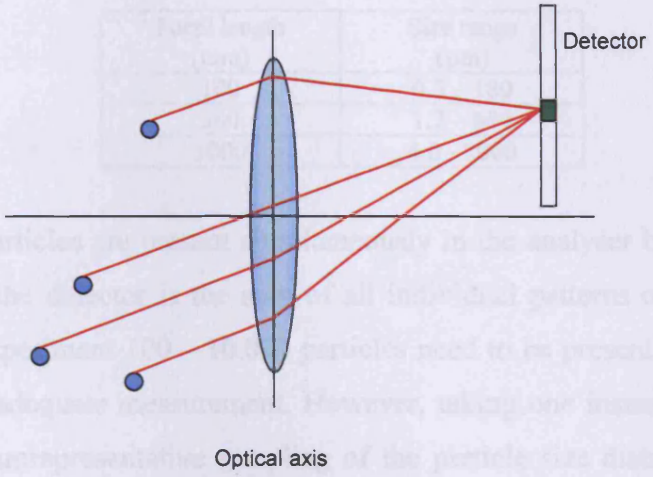

Figure 3.10 Properties of the Fourier transform lens

Un-scattered light received by the obscuration monitor determines the sample volume concentration. The concentration range over which reliable measurements are possible is expressed in terms of obscuration and is demonstrated in Table 3.3.

Table 3.3 Obscuration range for reliable measurements

Obscuration level (%)	Measurement suitabiltity
0 – 5	Too low
6 – 10	Low, but usable
11 – 30	Ideal
31 – 50	High, but usable
51 – 100	Too high

If the obscuration is too low then there are not enough samples to ensure valid, accurate measurements. However, if the obscuration is too high, then 'multiple scattering' is likely to occur. This effect occurs when incident light is diffracted and re-diffracted due to the high density of particles in the spray. This creates artificially high scattering angles, which in turn leads to artificially small particle sizes being outputted by the system. Calibration equations have been proposed to allow post-processing of measured data in dense sprays to obtain more accurate estimates[136].

Table 3.4 Standard range lenses for Long Bed Mastersizer X

Focal length (mm)	Size range (μm)
100	0.5 – 180
300	1.2 – 600
1000	4.0 - 2000

In practice many particles are present simultaneously in the analyser beam and the scattered light measured on the detector is the sum of all individual patterns overlaid on the central axis. In a typical experiment 100 – 10,000 particles need to be present simultaneously in the beam to obtain an adequate measurement. However, taking one instantaneous measurement creates the risk of unrepresentative sampling of the particle size distribution in the sample material. By making many measurements of the detector readings (*sweeps*) and averaging over many such sweeps of the detector it is possible to build up an integral light scattering characteristic which is fully representative of the average particle size distribution based on millions of individual particles.

One error associated with diffraction-based techniques is the phenomenon known as 'vignetting'. Vignetting occurs when diffraction angles of the smallest droplets pass outside the diameter of the collection lens. This effect can be minimised by selecting appropriate measuring distances. For larger scale applications this often means shielding sections of the spray which introduces an obvious compromise in terms of obtrusiveness. Alternatively, a larger than standard collection lens may be applied[137] to ensure that droplets are measured from even the widest collection angles. This needs to be considered when investigating flashing jets as it is well known that flashing produces dense sprays with wide cone-angles.

3.3.4.1 Laser Diffraction Facilities at ENEL Ricerca, Livorno Italy

During the course of this study, the opportunity arose to make use of the experimental facilities at ENEL Ricerca based in Livorno, Italy, as part of an EU funded TMR (Training for Mobility of Researchers) programme 'Euroflam'. Jet atomisation was performed using the superheated atomiser, which was incorporated into the existing apparatus in operation at ENEL. This consisted of an expansion vessel for containing the spray, a Malvern Mastersizer X, intrusive protection cylinders and a traverse for mounting and controlling the position of the nozzle. A schematic of the facilities available is presented by Figure 3.11.

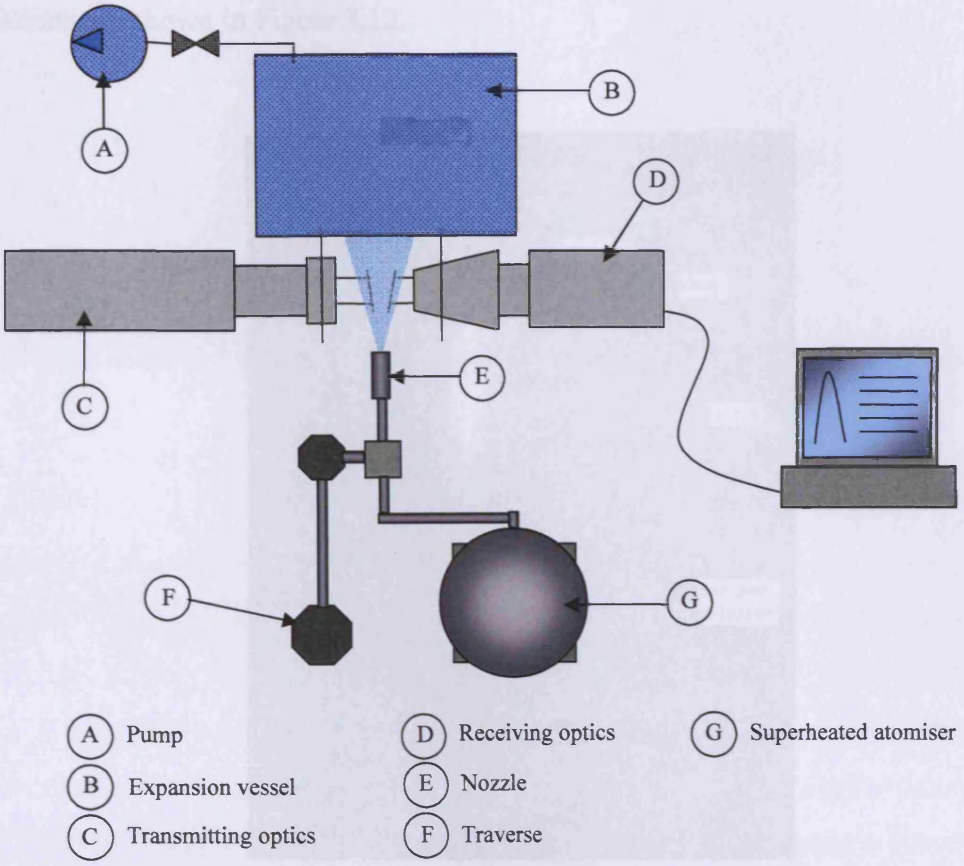

Figure 3.11 Modification of facilities at ENEL for use with the superheated atomiser

The Malvern Mastersizer X comprises a Helium-Neon (He-Ne) laser (λ=0.63μm), which has good stability properties and good signal to noise properties compared with higher wavelength laser diodes.[138] The receiving optics consist of a slice of photosensitive silicon with a discrete number of detectors. The instrument relies on the Fraunhofer approximation, which assumes firstly that the particles being measured are much larger than the wavelength of light employed (ISO13320 defines this as being greater than forty wavelengths i.e. 25μm when a He-Ne laser is used), secondly that all sizes of particle scatter with equal efficiencies, and finally that the particle is opaque and transmits no light.

In order to accommodate the atomiser with the Malvern Masterisizer X, the nozzle/atomiser was fitted to the exit pipe on the heating rig via a flexible length of piping. The nozzle was then attached to a traverse with the use of a clamp. This enabled measurements to be made at

pre-defined multiple axial and radial locations, using increments of 10mm. These modifications are shown in Figure 3.12.

Figure 3.12 Rig modifications for integration with spray measuring equipment

The expansion vessel, used to contain the two-phase jet during a release, was fitted to a pump, which extracted the water/vapour droplets to prevent recirculation. In order to prevent attenuation of incident and scattered light intrusive protection cylinders were implemented in the jet. These cylinders were held in place via perspex windows positioned at the entrance of the expansion vessel. Metal disks were fitted to the ends of the protection cylinders in order to deflect droplets away from the measurement area. Figure 3.13 shows the position of the expansion vessel in relation to the rig, and the beam protectors fitted at its entrance.

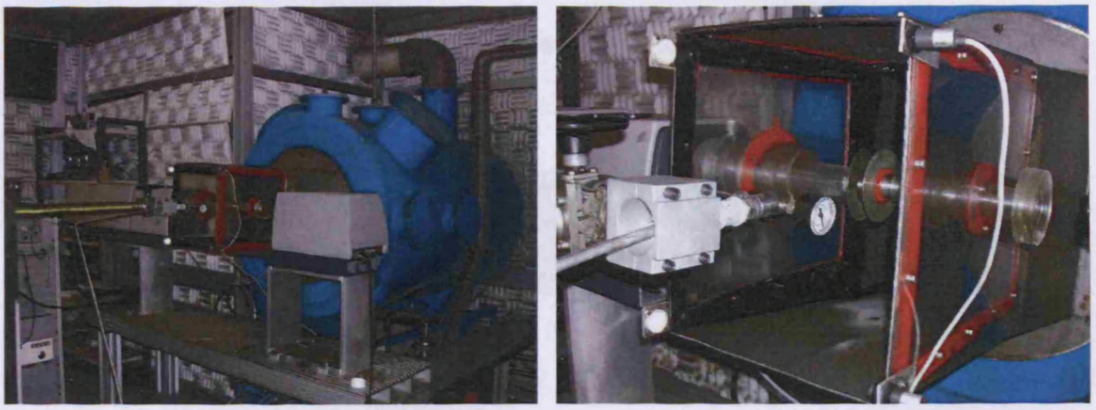

Figure 3.13 Expansion vessel and beam protection cylinders

Unfortunately the work undertaken at this research facility was limited by time and facility functionality. Although originally protected against overpressure by a 12bar bursting disk, due to failure of the disk during preliminary safety tests and the difficulty faced with replacing it, it was only possible to fit the atomiser with an 8bar safety valve. This limited the maximum operating stagnation temperature inside the rig to 150°C. Furthermore, owing to time constraints, it was only possible to perform tests using a 2mm nozzle diameter and an initial tank stagnation temperature of 140°C, giving a nozzle temperature of approximately 125°C. At this temperature the jet was observed to be in transition from mechanical break-up to flashing atomisation. Droplet size measurements were taken at three axial locations; 350mm, 400mm and 450mm, and varying radial locations at each downstream position. Radial measurements were performed at increments of 10mm in both positive and negative directions, taking the spray centreline as the origin.

3.3.5 Phase Doppler Anemometry (PDA)

3.3.5.1 Principles of PDA

When two coherent laser beams intersect they interfere in the volume of their intersection, forming interference fringes. If intersection occurs at the waist of each beam, the wave fronts are nearly plane and consequently the interference fringes are parallel, see Figure 3.14.

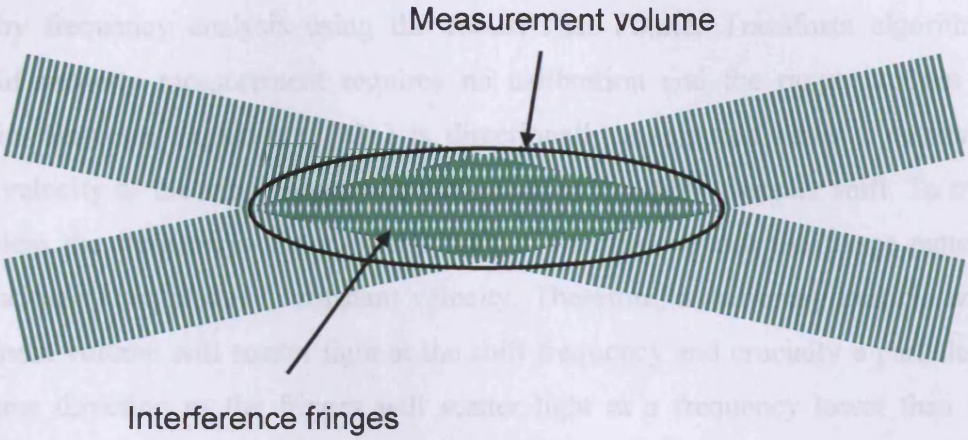

Figure 3.14 Interference fringes created by intersecting coherent light sources

Light scattered by a particle traversing the measurement volume consists of two components, corresponding to each beam. Both components have a Doppler shift corresponding to the velocity of the particle; however, the shift also depends on the direction of the beam. Since the two beams are at an angle, the two components of scattered light have different Doppler shifts. If the intersection of the two beams takes place away from the beam waist, the plane wave approximation no longer holds and the distance between fringes is position dependent. This means that two particles crossing the intersection volume at the same velocity but at different positions will give rise to Doppler bursts of different frequency. Intersecting the beams at their waists counteracts this problem and ensures that there is a uniform velocity-frequency relationship over the entire measurement volume.

The fringe distance d_f is defined by the wavelength of the laser light and the angle between the beams, and is defined by Equation (3.2)

$$d_f = \frac{\lambda}{2\sin\left(\frac{\vartheta}{2}\right)} \qquad (3.2)$$

The velocity is calculated from the Doppler frequency and the fringe distance, as defined by Equation (3.3)

$$u = d_f f_D = \frac{\lambda}{2\sin\left(\frac{\vartheta}{2}\right)} f_D \qquad (3.3)$$

Doppler bursts are filtered and amplified in the signal processor, which determines f_D for each particle by frequency analysis using the robust Fast Fourier Transform algorithm. This method of velocity measurement requires no calibration and the range is from zero to supersonic. However Equation (3.3) is directionally ambiguous since a positive and a negative velocity of the same magnitude will result in the same Doppler shift. To overcome this problem the frequency of one of the beams is shifted so that the fringe pattern is no longer stationary but moves at constant velocity. Therefore, a stationary particle within the measurement volume will scatter light at the shift frequency and crucially a particle moving in the same direction as the fringes will scatter light at a frequency lower than the shift frequency, whilst the signal from a droplet moving in the opposite direction will be of a higher frequency, as demonstrated by Figure 3.15.

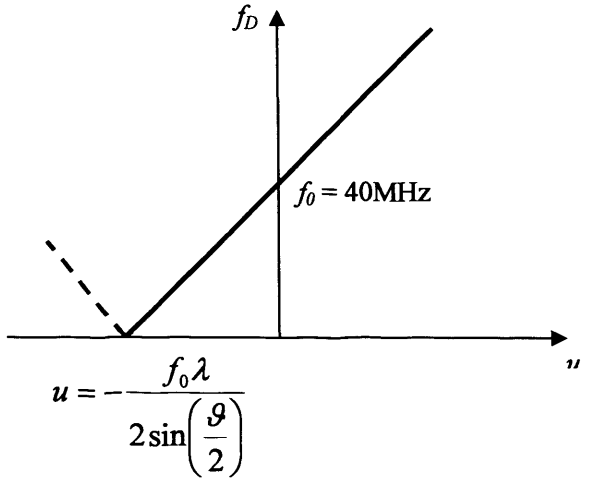

Figure 3.15 Velocity-frequency relationship with frequency shift

Figure 3.15 also shows that the higher the shift frequency the greater the velocity range it is possible to measure. In the DANTEC LDA and PDA equipment at Cardiff University a shift frequency of 40MHz is used. This shift is achieved using a Bragg cell, which also doubles as a beam splitter dividing the light intensity equally between the two beams and is illustrated by Figure 3.16.

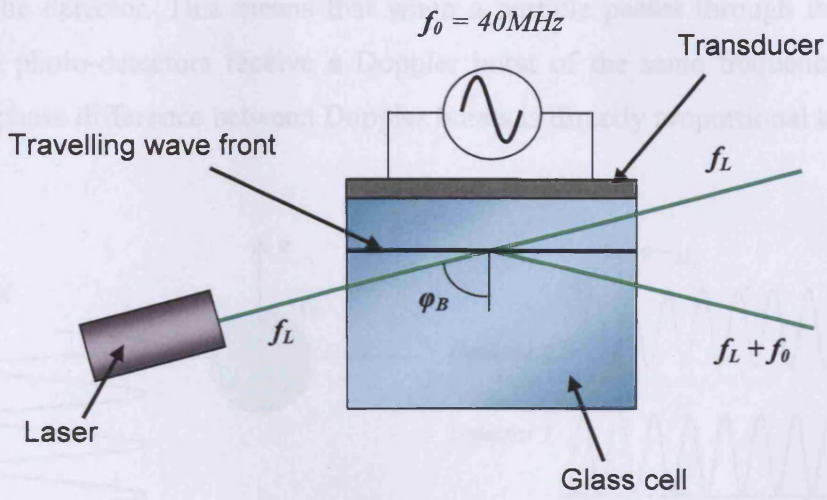

Figure 3.16 The Bragg cell

The Bragg cell consists of a block of glass with an electro-mechanical transducer (piezo crystal) attached to one side, which is driven by an oscillator to produce acoustical waves propagating through the block. The opposite side of the block is shaped to minimise reflection of the acoustic wave. The incident light beam hits a series of travelling wave fronts which act as a thick diffraction grating. Interference of the scattered light causes intensity maxima to be emitted in a series of directions. By adjusting the tilt angle of the Bragg cell and the acoustic signal intensity, the intensity balance between the direct beam and the first order of diffraction can be set.

In order to measure two velocity components, two extra beams can be added to the transmitting optics in a plane perpendicular to the first beams. This is achieved by transmitting the beam pairs orthogonally, with all the beams intersecting in a common measurement volume. In order to separate the beam components, different wavelengths are used. The dominant wavelengths of the Argon-ion laser are 514.5 and 488nm, which correspond to green and blue light respectively. Green is used in the primary flow axis i.e. vertical for a spray injected downwards, and blue is used for either radial or tangential velocity measurement, depending on the orientation of the spray relative to the transmitting optics.

In order to extend the principles of LDA to size measurement, a second photo-detector is added to the receiving optics. The optical path length of scattered light changes with the

position of the detector. This means that when a particle passes through the measurement volume both photo-detectors receive a Doppler burst of the same frequency, but different phases. The phase difference between Doppler bursts is directly proportional to the size of the particle.

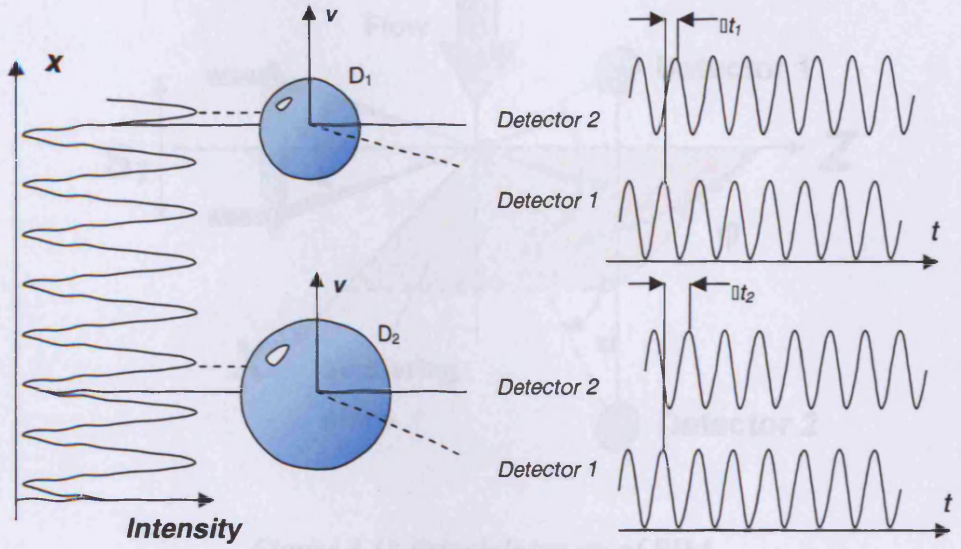

Figure 3.17 Increasing phase difference with increasing particle diameter

Figure 3.17 illustrates a small particle with diameter D_1 and a larger with diameter D_2. If Δt is the time lag separating the wave fronts reaching two detectors, the corresponding phase difference is given by Equation (3.4).

$$\Phi_{12} = 2\pi f.\Delta t \qquad (3.4)$$

The phase of a Doppler burst received at detector i is expressed as:

$$\Phi_i = \pi \frac{n_i}{\lambda} d_p \cdot \beta_i \qquad (3.5)$$

where n_i is the refractive index of the scattering medium, λ is the laser wavelength, d_p is the particle diameter and β_i is the geometrical factor.

The geometrical factor depends on the three angles θ, φ_i and ψ_i. The angle of intersection between the two incident beams (θ), is determined by the beam separation (S_t) and the focal length of the front lens (F_t). The scattering angle (φ) and the elevation angle (ψ) define the

direction towards the centroid of the photo detector from the measurement volume as indicated by Figure 3.18.

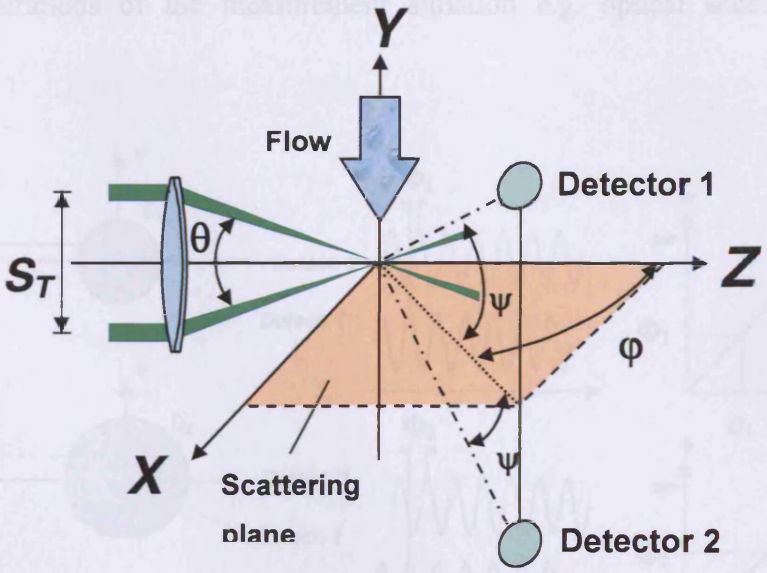

Figure 3.18 Principle set-up of PDA

For reflection, the geometrical factor can be expressed as,

$$\beta_i = \sqrt{2} \cdot \left\{ \frac{\sqrt{\left(1 + \sin\frac{\vartheta}{2}\sin\varphi_i \sin\psi_i - \cos\frac{\vartheta}{2}\cos\varphi_i\right)}}{\sqrt{\left(1 - \sin\frac{\vartheta}{2}\sin\varphi_i \sin\psi_i - \cos\frac{\vartheta}{2}\cos\varphi_i\right)}} - \right\} \qquad (3.6)$$

and for a first order refraction,

$$\beta_i = 2\left[\sqrt{1 + n_{rel}^{\,2} - \sqrt{2}\cdot n_{rel}\cdot\sqrt{f_{i+}}} - \sqrt{1 + n_{rel}^{\,2} - \sqrt{2}\cdot n_{rel}\cdot\sqrt{f_{i-}}}\right] \qquad (3.7)$$

n_{rel} = particle refractive index / medium refractive index and $f_{i\pm}$ is given by Equation (3.8)

$$f_{i\pm} = 1 \pm \sin\frac{\vartheta}{2}\sin\varphi_i \sin\psi_i + \cos\frac{\vartheta}{2}\cos\varphi_i \qquad (3.8)$$

Higher refraction orders cannot be expressed as a correlation of first order, but must be solved numerically or iteratively. As it is shown from the above correlations, the geometrical factor and hence the sensitivity and range of the PDA can be altered by changing any of the angles θ, φ_i and ψ_i. In practice, there are some restrictions in the selection of the geometrical

optical parameters. For instance, the selection of scattering angle (φ), is quite restricted, either to ensure a specific scattering mode or a sufficient signal-to-noise ratio, or from practical considerations of the measurement situation e.g. optical access and working distance.

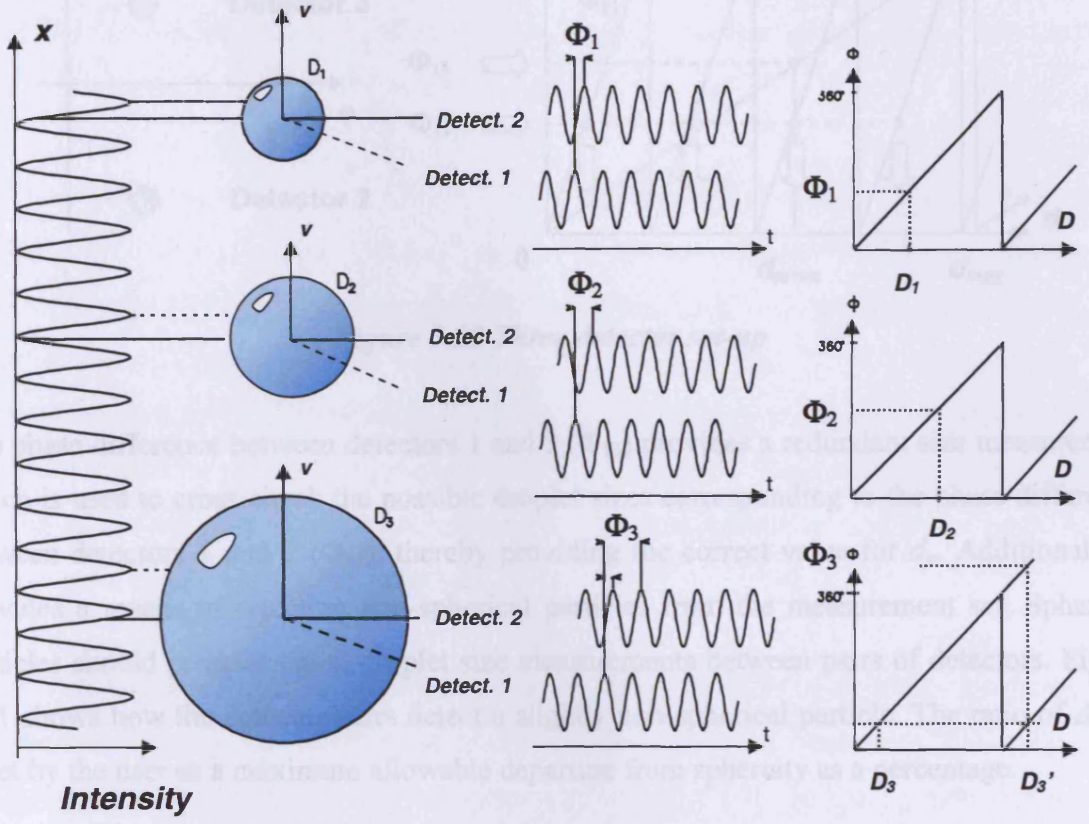

Figure 3.19 2π ambiguity in two-detector systems

The maximum particle size that can be unambiguously measured with two detectors is limited by a phase shift of Φ_{12} = 360°. This is illustrated by Figure 3.19 where the phase difference for the largest particle falls outside this range. Therefore there is no way of knowing whether the droplet diameter is D_3 or D_3' from measuring the phase difference between the Doppler bursts received by the two detectors. This is because it is not possible to discriminate between a phase difference of Φ and $\Phi \pm 2n\pi$, where n = 1,2,3,... This is known as the 2π ambiguity. Reducing the distance between detectors can increase the particle size range, this however also reduces the measurement resolution. To overcome this problem, a third photo-detector is added to the receiving optics. The detectors arr arranged asymmetrically with two placed relatively distant for high resolution and the other two placed close together to extend the working range of the system. The overall effect provides both a

large measurement size range (Φ_{13}) and high measurement resolution (Φ_{12}), as shown in Figure 3.20.

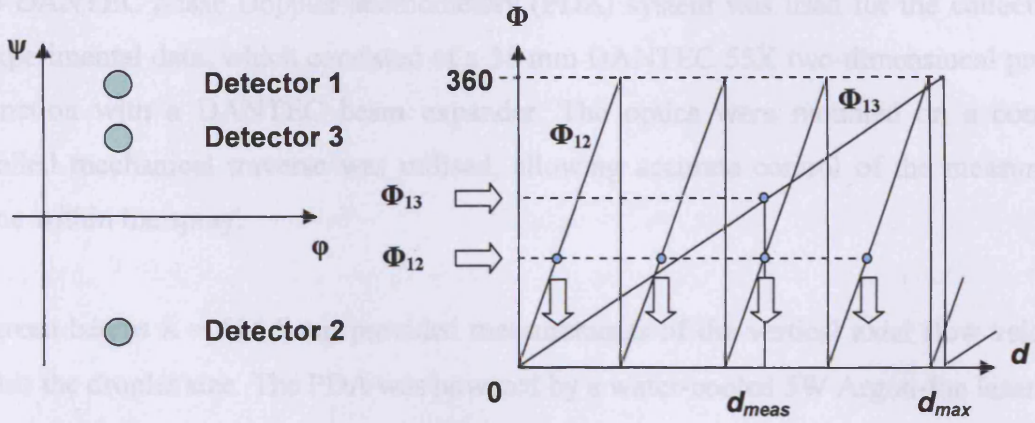

Figure 3.20 Three detector set-up

The phase difference between detectors 1 and 3 (Φ_{13}) provides a redundant size measurement which is used to cross check the possible droplet sizes corresponding to the phase difference between detectors 1 and 2 (Φ_{12}), thereby providing the correct value for d_p. Additionally it provides a means of rejecting non-spherical particles from the measurement set. Spherical particles should produce equal droplet size measurements between pairs of detectors. Figure 3.21 shows how the detector pairs detect a slightly non-spherical particle. The ratio of $\Delta d/d_p$ is set by the user as a maximum allowable departure from sphercity as a percentage.

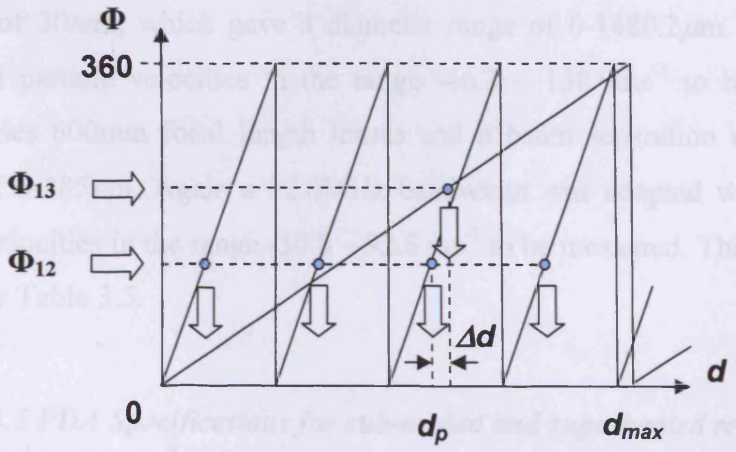

Figure 3.21 Particle sphericty detection

3.3.5.2 PDA Specifications

A 1D DANTEC phase Doppler anemometery (PDA) system was used for the collection of the experimental data, which consisted of a 38 mm DANTEC 55X two-dimensional probe in conjunction with a DANTEC beam expander. The optics were mounted on a computer controlled mechanical traverse was utilised, allowing accurate control of the measurement volume within the spray.

The green beams λ = 514.5 nm provided measurements of the vertical axial flow velocities and also the droplet size. The PDA was powered by a water-cooled 5W Argon-Ion laser and a collection angle of 72 degrees from forward scatter was used as determined by the refractive index of water. The power source was used together with a DANTEC 60X40 transmitter box, which incorporated the Bragg cell. The scattered light was collected, via the DANTEC integrated receiving optics, for processing using a DANTEC co-variance particle analyser and the associated Sizeware software package. All data collection and movements of the traverse were controlled via the software.

A range of optical configurations were appraised before the final system was specified. This was necessary due to the broad range of droplet sizes produced by some of the sprays. The optimum optical set-up for sub-cooled releases consisted of 600mm focal length lenses and a beam separation of 20mm, which gave a diameter range of 0-1480.2μm. A bandwidth of 12.0MHz enabled particle velocities in the range -46.3 – 138.9ms^{-1} to be measured. For superheated releases 600mm focal length lenses and a beam separation of 30mm gave a diameter range of 0-385μm. Again a 12.0MHz bandwidth was adopted which in this case enabled particle velocities in the range -30.8 – 92.6 ms^{-1} to be measured. These specifications are summarised by Table 3.5.

Table 3.5 PDA Specifications for sub-cooled and superheated releases

Thermodynamic Conditions	Beam Separation (mm)	Focal Length (mm)	Bandwidth (MHz)	Diameter Range (μm)	Velocity Range (ms^{-1})
Sub-Cooled	20	600	12.0	0-1480.2	-46.3-138.9
Superheated	30	600	12.0	0-385.0	-30.8-92.6

3.3.5.3 Measurement Programme for Sub-Cooled Releases

In preliminary tests it was observed that the droplet SMD was sensitive to downstream distance from the orifice. However, to include this effect in a final correlation would require the inclusion of an upper cut-off point beyond which the effect should be ignored, as one intuitively understands that the jet disintegration cannot continue indefinitely. Findings from automotive injector studies of simple atomisers usually quote that the jet is fully developed after some 75-100 nozzle diameters downstream, though these will be for considerably higher pressures and for jets in the 'atomisation' break-up regime. Releases considered in this study invariably fall into the 'second-wind' break-up regime. This means that for an appreciable distance downstream the jet does not break-up at all, but in fact remains intact as a 'pencil' jet. Hence, fully developed sprays will not be established until further downstream than distances quoted for automotive sprays i.e. several hundred nozzle diameters. Therefore a compromise is required between the atmospheric dispersion modelling approach of a fully developed spray existing immediately downstream and the reality of a finite break-up length preceding the fully developed spray. In the course of this study post-expansion data was taken at 500mm downstream of the exit orifice, beyond which point it was assumed that dynamic jet break-up was complete. This is also found to be consistent with previous data produced by Buchlin *et al*[54].

Due to the increased flow rate developed by the 2.0mm nozzle diameter, the maximum pressure at which it was possible to operate was 20bar. This defined the upper cut off point at which tests were conducted for this orifice size. For all other nozzles 24bar was the maximum operating pressure. This pressure range was considered to encompass 'low' to 'medium' release pressures in the context of similar work done in this field.

In terms of modelling practical release scenarios, if, for example, a release occurs from an aperture in a large vessel, then the length may be considered as the thickness of the vessel wall, which for large scale hazards, is likely to result in a relatively 'small' aspect ratio. By contrast, in the event of scenario such as shearing of a long pipe containing pressurised liquid, then the length may be considered as 'large' in the context of jet break-up. Therefore, nozzle aspect ratios were selected to represent this broad range of practical release scenarios.

Table 3.6 summarises the programme of experimental work carried out for the investigation of sub-cooled jets.

Table 3.6 Experimental programme for sub-cooled releases

Gauge Pressure (bar)	Nozzle Diameter (mm)	Aspect Ratio (L/d_0)
$4 \leq P \leq 20$ @ 2bar increments	2.00	1.7
		3.5
$4 \leq P \leq 24$ @ 2bar increments	1.00	3.4
		7.0
		10.0
		20.0
		30.0
		50.0
	0.75	4.53
		9.33

3.3.5.4 Measurement Programme for Superheated Releases

High spray densities produced by nozzles with diameters in excess of 1mm and lengths in excess of 3.4mm prevented sufficient spray penetration by the laser used for droplet diameter and velocity measurement. As a result, this limited the experimental programme only to those nozzles of characteristic geometries presented in Table 3.7. Using these nozzles it was not possible to produce fully flashing sprays at stagnation temperatures (temperatures inside the tank) below 180°C, which was the maximum operating temperature of the superheated rig. For this reason it was only possible to conduct PDA particle sizing for one set of upstream conditions.

Table 3.7 Experimental programme for superheated releases

Stagnation Temperature (°C)	Downstream Distance (mm)	Nozzle Diameter (mm)	Aspect Ratio (L/d_0)
180	250	0.75	4.53
	500 750	1.00	3.40

Figure 3.22 shows how the transmitting and receiving optics were arranged around the nozzle of the superheated atomiser and the measurement volume in a superheated spray. Releases were carried out to atmosphere through a hole cut in a sheet of polythene, stretched between the hanger doors of a well ventilated laboratory. This method was found to be more than suitable for preventing recirculation of the spray.

Figure 3.22 PDA set-up for superheated atomiser

3.3.5.5 Measurement Procedure

For both sub-cooled and superheated sprays, PDA data was taken at regular horizontal increments through the spray in the plane of the central axis. At each radial location the PDA system recorded 15,000 'validated' samples. A time window of 75 seconds terminated data collection if the specified number of bursts had not been reached during sub-cooled releases and 45 seconds during superheated releases. The difference between the two was due to the difference in spray quality and hence data collection rates. However, due to the high flow rates produced by both sprays under investigation, the time-out function was rarely required.

Due to the poor atomisation quality for low-pressure sub-cooled release conditions, validation rates were relatively low. Typical validation rates for sub-cooled sprays ranged from 20-40% at low pressure i.e. 4bar, and 60-90% at high pressure i.e. 24bar. However validation rates for flashing releases were typically in the range 70-95%. Validation rates varied inversely with spray density throughout the spray cross-section, i.e. validation rates were at their highest at the edge of the spray where the spray density was at its minimum, and vice versa. The poor quality of the spray for sub-cooled conditions also presented challenges in terms of data truncation. These issues were minimised by the adopted optical configuration, where the system functioned at its maximum operating range. However it is never possible to be completely confident that truncation has been eliminated for low-quality subcooled jets. However, by inspection of the data, it was possible to almost completely eliminate data

truncation for superheated releases, as each measured sample was less than 200 μm, almost half the upper diameter size afforded by the associated optical set-up.

The necessity to represent the distribution as a whole by a single number requires that measurements taken at these radial locations be transformed to 'global' measurements. Because of the non-uniformity of the droplet concentration through the spray and the fact that a fixed number of samples were collected at each point, it was not possible to take a mean in order to provide this single number. Doing so would bias the 'global' measurements towards those results taken at radial locations towards the edge of the spray, where the droplet concentration was at its lowest. This problem was not envisioned when the experimental programme was first formulated. In order to simplify the procedure of globalising radial droplet distributions, future studies should always adopt a fixed time window rather than a fixed sample number approach, as this method inherently takes droplet concentration or flux into account. Instead a comprehensive approach was adopted for the globalisation of the local measurements. The global size and velocity are defined in similar ways and are both numerically expressed as demonstrated by Equation (3.9) and (3.10)

$$Global\ SMD = \frac{\sum_{i=1}^{n}\left(SMD_r \cdot Flux \cdot Abs.Val\right)_i}{\sum_{i=1}^{n}\left(Flux \cdot Abs.Val\right)_i} \qquad (3.9)$$

$$Global\ Velocity = \frac{\sum_{i=1}^{n}\left(\bar{u}_d \cdot Flux \cdot Abs.Val\right)_i}{\sum_{i=1}^{n}\left(Flux \cdot Abs.Val\right)_i} \qquad (3.10)$$

where SMD_r is the measured droplet size and $\bar{u}_d$ is the mean droplet velocity at each radial location respectively. *Flux* is the volumetric flow rate per unit area and *Abs.Val* (absolute validation rate) is the number of spherical samples validated by the PDA system as a percentage of the total number of attempted samples. Radial values are normalised by the absolute validation rate so that proportionately each global measurement is based on the same number of samples. However, this approach relies on the assumption that the samples rejected by the PDA system have the same distribution characteristics as those accepted.

Few previous correlations for these types of release conditions have been generated utilising data with spatial resolution. Early non-optical studies utilising droplet impact type methods invariably considered one spray position, typically the centreline. First optical techniques utilised laser diffraction technology where measurements are implicitly spatially-averaged.

3.4 Summary

This programme relies on a broad range of advanced optical diagnostic techniques, experimental rigs and facilities. The functionality, technical background and limitations of all facilities have been highlighted and explained in this chapter, the implications of which will require referencing in the course of data analysis in the following chapters.

Chapter 4 Elementary Characterisation of Superheated Jets

4.1 Introduction

In this chapter the results from a photographic study of superheated jets is presented and the downstream jet width is established as a means for characterising the transition from mechanical break-up to flashing. The effect of superheat and orifice size on rainout fraction is also investigated. Superheat is demonstrated to be inversely proportional to the rainout fraction, and although the results are limited, the effect of nozzle diameter on rainout fraction is found to be negligible. Rainout data is compared to the data presented by Johnson and Woodward[15], and the rainout correlation proposed by DeVaull and King[118] is evaluated in light of the both datasets. The findings are summarised by Cleary *et al*[139].

4.2 Preliminary Experiments

Prior to pursuing the study objectives, it was necessary to investigate the performance of the superheated rig during a release. This was undertaken for a number of reasons; the first was to ascertain the time taken for the vessel to empty under its full range of initial conditions, as this defined the data collection window for the various measurement techniques applied in this study. Secondly, as previously made clear in Chapter 2, the temperature of the jet at the exit orifice was transient during the initial stages of a release, causing the jet break-up mechanism to change accordingly. It was therefore necessary to determine the significance of this effect for the full range of conditions investigated. Figure 4.1 illustrates the evolution of temperature and pressure during a release for which the nozzle diameter was 2mm and the tank stagnation temperature was 170°C.

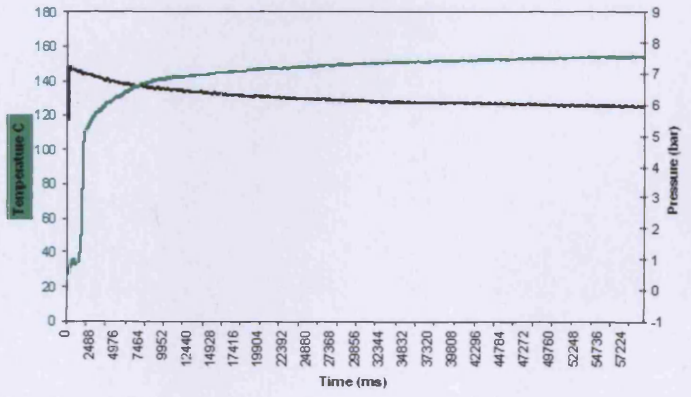

Figure 4.1 Transient nature of temperature and pressure during a release.

The shapes of the curves in Figure 4.1 are representative of a distinctive development of the temperature and pressure in the nozzle during a release and are a result of the atomiser design. The rate of increase of the jet temperature steadily declines until it achieves relative stability. The tank is of a fixed volume and pressure is provided by the expansion of the water as it is heated. Hence, the pressure falls as the tank empties, as does the rate of pressure loss, until the pressure also reaches relative stability. Increasing the stagnation temperature increases the pressure in the tank, which in turn increases the flow-rate. Therefore, increasing the initial stagnation temperature reduces the discharge time. Increasing the nozzle diameter has the same effect. As the flow-rate increases, the time taken for the system to reach relative stability decreases. Hence the period during which pressure and temperature are transient was determined by the stagnation temperature and nozzle diameter. Figure 4.2 presents the transitional break-up period for a release at 170°C stagnation temperature but with a 4mm nozzle diameter. Comparing Figure 4.2 with Figure 4.1 it can clearly be seen that the time taken to reach relative stability is greatly reduced.

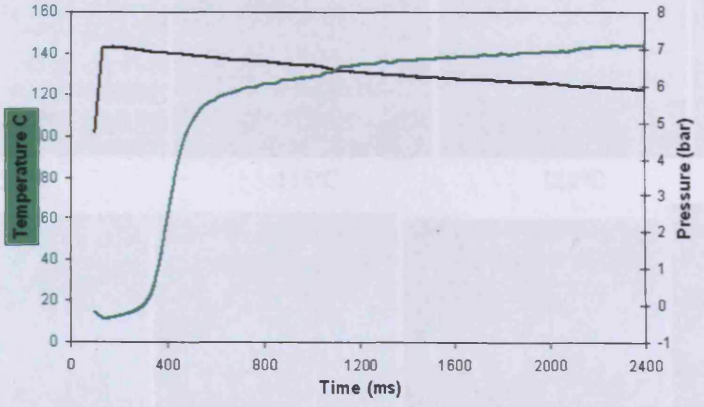

Figure 4.2 Orifice data for a 4mm nozzle diameter at 170 °C stagnation temperature.

4.3 Geometric Spray Characterisation

The time taken for the release conditions to stabilise was determined for stagnation temperatures in the range 130°C to 180°C at 10°C increments for a 2mm nozzle diameter. Digital images of each release were taken at regular intervals determined by the length of the 'warm-up' period. Pressure and temperature in the nozzle were recorded at the moment each image was taken. Since the drive (stagnation) pressure was determined by the stagnation temperature, each data set is classified by the average pressure during a release in order to avoid confusion between jet temperature and stagnation temperature. Jet widths were measured at distances of 50mm and 100mm downstream of the exit orifice and plotted against jet temperature. Figure 4.3 shows examples of the images of the jet which were taken at 3.1bar, 5.2bar and 8.3bar respectively.

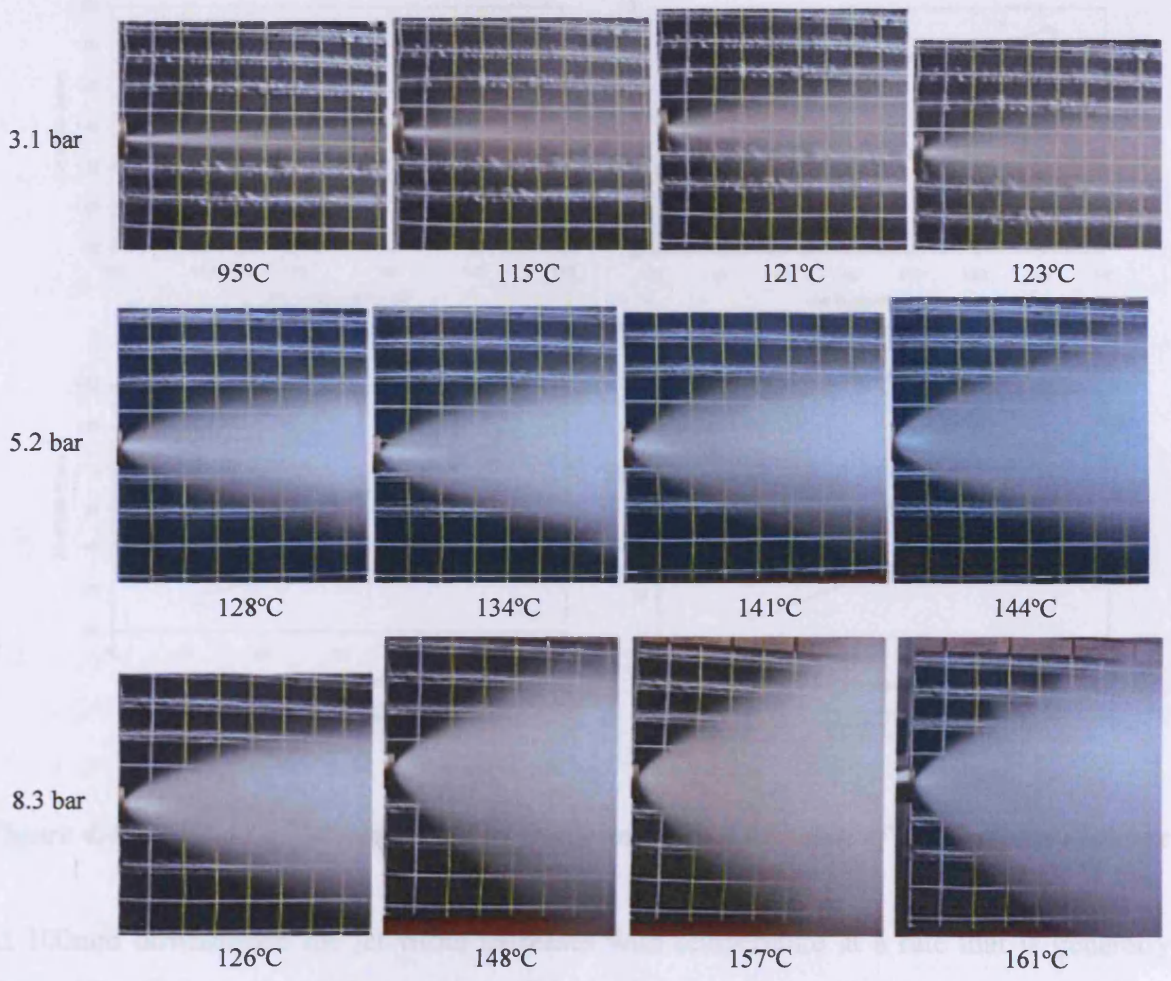

Figure 4.3 Superheated jet development at 3.1bar, 5.2bar and 8.3bar

4.3.1 Spray Geometry Results

Figure 4.4 displays the relationship between jet width and jet temperature as a function of the downstream distance, for the full range of initial conditions at which releases were performed. In each case it can be seen that the relationship is quasi-linear.

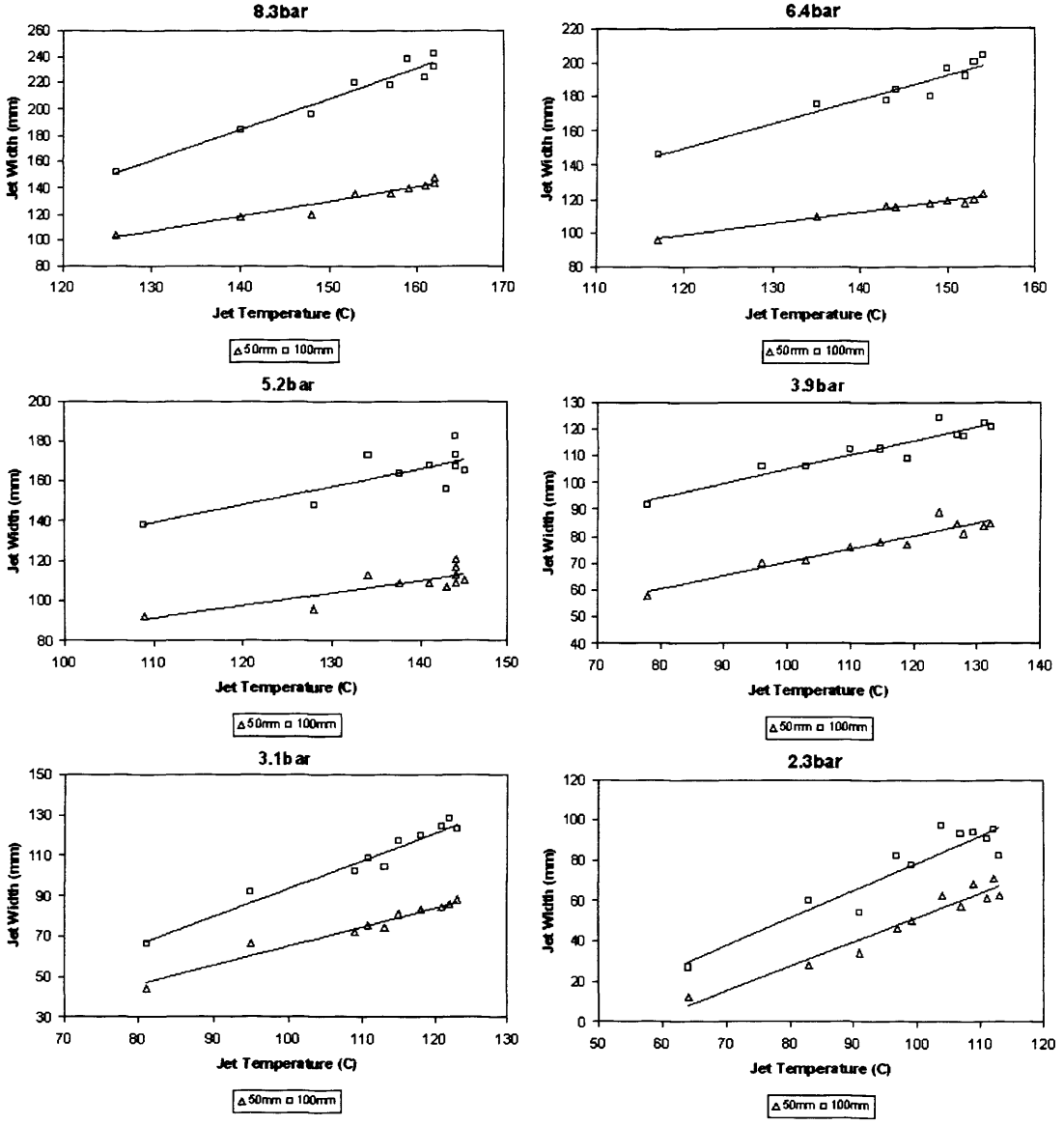

Figure 4.4 Variation of jet width with jet temperature as a function of downstream distance

At 100mm downstream the jet width increases with temperature at a rate that is generally higher than that at 50mm downstream. This is due to the fact that the jet expands in a scissors-like manner, with the fulcrum at the exit orifice. In general, the amount by which the expansion is greater is proportional to the release pressure.

At 8.3bar and 6.4bar, (180°C and 170°C stagnation temperature respectively), flashing was the dominant break-up mechanism. However, at jet temperatures below 150°C a small liquid core existed at the exit orifice before gradually diminishing at temperatures above 150°C, where the bulk plume density appeared to become homogenised.

At 5.2bar (160°C stagnation temperature), again flashing was the dominant break-up mechanism. However, a small liquid core was observed to exist at the exit orifice, which diminished as the temperature increased, but never fully disappeared.

At 3.9bar (150°C stagnation temperature), external atomisation initially dominated jet break-up with a characteristic liquid core existing at the orifice throughout the release, only abating at jet temperatures above 120°C, where flashing became dominant.

At 3.1bar (140°C stagnation temperature), jet break-up was initially dominated by second-wind induced break-up, which was gradually replaced by external atomisation and finally the early stages of flashing. A significant liquid core was present throughout the release and only diminished at jet temperatures above 120°C.

At 2.3bar (130°C stagnation temperature) the jet did not flash during this release. Instead, second-wind induced break-up was gradually replaced by external atomisation at jet temperatures above 110°C.

4.3.2 Discussion of Spray Geometry Results

For every set of initial conditions, the temperature of the jet at the exit orifice was directly proportional to the jet width, at both downstream locations. Figure 4.5 compares the rate at which the jet width increases with jet temperature between data sets at both 50mm and 100mm downstream of the exit orifice.

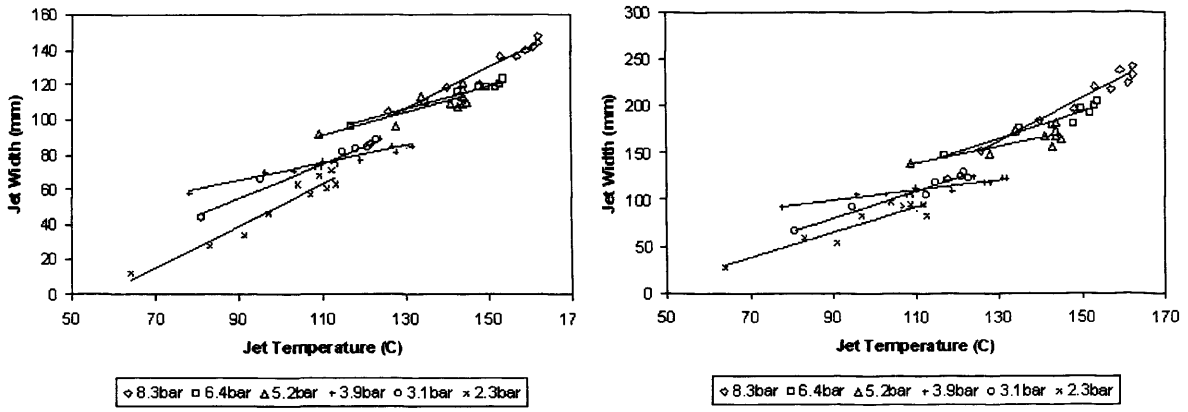

Figure 4.5 Variation of jet width with jet temperature at 50mm and 100mm downstream of the exit orifice

In both cases it initially appears that the data sets combine to produce an overall linear trend. However, the rate at which jet width changes with jet temperature varies between data sets. This can be explained by the fact that as the stagnation temperature, and therefore the jet temperature, gradually increased, the jet break-up mechanism developed accordingly. As second-wind induced break-up develops into external atomisation there is a rapid development of the typical wide angled jet associated with this break-up mechanism. This is reflected in the strong influence of increasing jet temperature on the jet width at low stagnation temperatures. Once external atomisation begins to stabilise, the rate of change of jet width gradually decreases. As conditions become conducive to flashing there is a further increase in the rate of change of jet width with temperature as rapid bubble bursting shatters the jet to produce the characteristic wide-angled cone of flashing atomisation.

In addition, the datasets are shifted upwards as the release pressure at the exit orifice increases. As highlighted previously, the pressure in the tank was a function of the stagnation temperature, since the pressure was generated by the expansion of water.

Figure 4.6 shows how the pressure increased with stagnation temperature. Although the pressure is transient during a release, after an initial period of rapid decline, it reaches a level of relative stability, so that the total pressure drop is not felt to be sufficient to significantly affect the change in the jet break-up mechanism during a release. However, the increase in the pressure brought on by the increase in stagnation temperature is felt to be significant enough to create the shift between data sets demonstrated by Figure 4.6

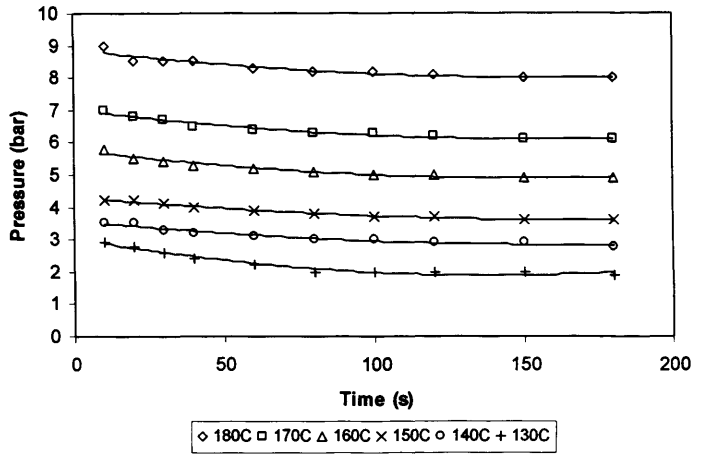

Figure 4.6 Pressure drop during the initial stages of release

Figure 4.7 demonstrates how the rate of change of jet width changes with increasing jet temperature. The jet temperature is taken as the average jet temperature recorded at the nozzle during a release. At both downstream locations the resultant curves produce parabolas with their minima located at a jet temperature of about 120°C. The mechanisms that dominate break-up at 120°C are external atomisation and to a lesser extent second-wind induced break-up. The mechanism that dominates break-up at stagnation temperatures above 120°C is flashing. It is proposed therefore that the minima demonstrated by Figure 4.7 represent the transition from mechanical break-up to flashing atomisation.

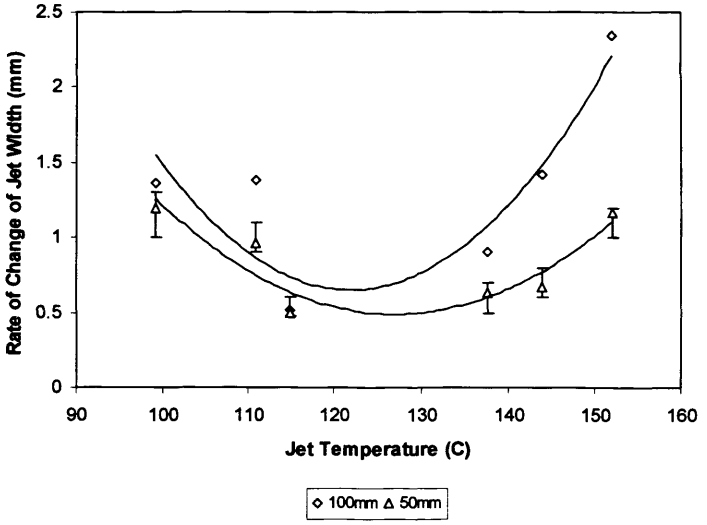

Figure 4.7 Rate of change of change of jet width with increasing jet temperature

The parabolae in Figure 4.7 are characteristic of the differential of an inflection curve. If there was a way to eliminate the step increases in pressure between datasets, it is reasonable to assume that the results presented in Figure 4.5 would then display all the characteristics of an inflection curve, as it would negate the apparent shift between datasets. The point of inflection would then represent the point of transition to flashing. By integrating the equations of the parabolas in Figure 4.7 it is possible to do this, the results of which are demonstrated in Figure 4.8.

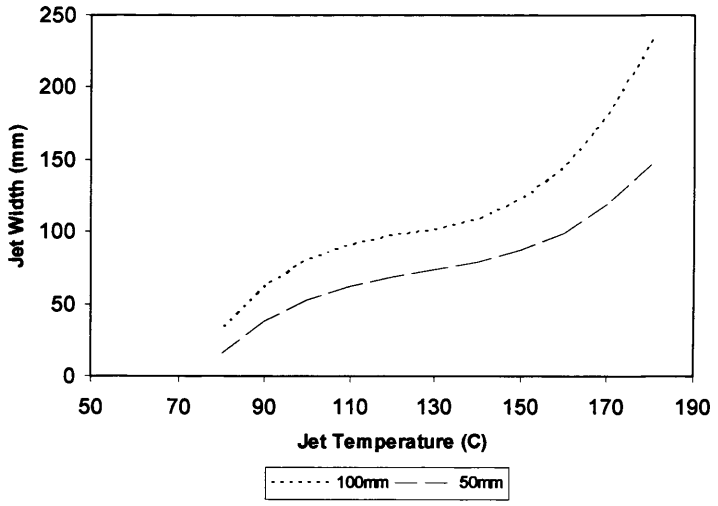

Figure 4.8 Proposed relationship between jet width and temperature

Figure 4.8 accurately reflects the break-up mechanisms occurring in the jet as observed during releases across the full range of initial conditions. The point of inflection occurs between 120°C and 130°C, which is where the transition from mechanical break-up to flashing atomisation occured. The steep increase in the curve before this point is representative of the transition between second-wind induced break-up and external atomisation, characterised by the gradual disintegration of the liquid core and the development of a wide angled jet. The curve gradually flattens as the external atomisation mode approaches its upper limit. The succession of flashing over external atomisation is then marked by a gradual increase in the jet width as internal and external bubble nucleation begins to completely shatter the liquid core, creating the characteristic wide angled cone. The gradual nature of this change is significant as it implies that the boundaries between break-up regimes are not strictly defined but are in fact more blurred. The shape of the curves suggests

that the jet will increase infinitely with temperature; however, it is more likely that the jet width will approach an upper limit. Nevertheless, this is in an area for future investigation.

As mentioned previously, it is proposed that the incremental rise in pressure caused by the increase in stagnation temperature causes the datasets to become offset. This suggests that the effect of the increase in pressure is uniform for each data point in a given dataset, so that pressure is also proportional to jet width. It is hypothesised that the increased flow rate generated by the increased pressure leads to an increase in the rate of bubble nucleation. In effect it exacerbates the effects of superheat on jet break-up. In summary, while the degree of superheat is directly responsible for causing the transition to flashing in liquid jets, the pressure determines the extent to which it occurs.

There were a number of potential sources of error associated with performing superheated releases in this way, the first being the fact that tests were performed outdoors. While care was taken to ensure the location of the rig was well sheltered, the ambient conditions varied between releases and were unfortunately not recorded. Therefore, the effect of air temperature, humidity, and cross-winds on the jet width remains unknown. Although it is not anticipated that the effect would be large enough to significantly influence the results, it is recommended that for future work, ambient conditions should be recorded and their effect on flashing be quantified.

Another potential source of error was the position of the 50mm grid and the digital camera relative to the jet. The ideal position for the grid would have been in the plane of the exit orifice. This of course was not possible as it would have upset the natural formation of the jet; instead it was positioned behind the jet relative to the camera. Measurements were fundamentally based on the equivalence of the grid rulings and the jet dimensions. However, due to the difference in perspective the absolute measurements of the jet width were subject to error. Nevertheless, this error was constant for all releases, so that while the trends observed should still be upheld, the measurements cited cannot be used as accurate guides to the widths of flashing jets under the conditions investigated.

During each release, once the jet temperature and break-up mechanism, had stabilised, natural fluctuations in the jet width not caused by a changing break-up mechanism were observed. These fluctuations are represented by clusters of data points at temperatures at the

far end of the measured range in Figure 4.7. These fluctuations were a result of what can be described as a rhythmical pulsing of the jet during a release. In order to reduce the uncertainty caused by these fluctuations, it is recommended that for future studies, the average jet width should be taken from several images instead of just one. In spite of this, these fluctuations do not detract from the conclusions stated above since the findings of this study are qualitative and not quantitative.

4.4 Rainout

Rainout tests were carried out in two phases. Phase one involved investigating the influence of jet temperature, using a fixed nozzle diameter of 4mm. Phase two consisted of investigating the effect of varying the nozzle diameter, keeping a fixed stagnation temperature of 160°C. The tests consisted of elevated horizontal releases 0.57m above ground level. The influences of release orientation and elevation on water capture were not investigated. Figure 4.9 demonstrates the experimental set-up employed for investigating rainout.

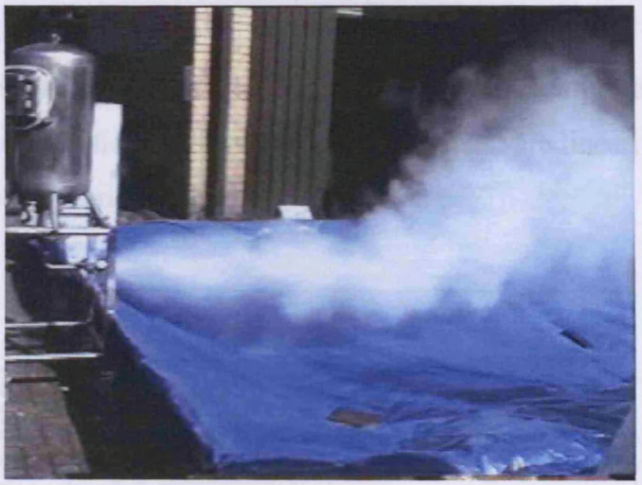

Figure 4.9 Release at 160°C stagnation temperature through a 4mm nozzle

Figure 4.10 shows that for a fixed nozzle diameter of 4mm, the rainout fraction is inversely proportional to superheat. However, the exact nature of the relationship is fairly ambiguous as it could be argued that there is a point of inflection at approximately 40°C superheat. Nevertheless, in the absence of additional data, it is difficult to say categorically whether this

is indeed the case. An indication of the exact nature of the relationship can be taken from the superheat at which no rainout is predicted, which can be found by extrapolating both linear and polynomial curves. If the relationship is linear, the predicted superheat at which there is no rainout is 160°C (absolute jet temperature 260°C). If a point of inflection exists, the predicted superheat at which there is no rainout is 86°C (absolute jet temperature 186°C). Johnson and Woodward[15] show that superheated water at 120°C jet temperature still generates a significant rainout fraction. Hence, the relationship is more likely to be linear.

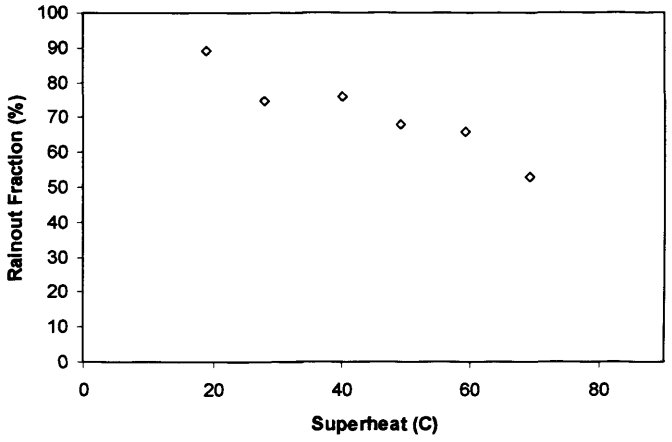

Figure 4.10 Variation of rainout fraction with jet temperature

Figure 4.11 shows how the recorded data compares with the data produced by Johnson and Woodward. Each data set indicates that rainout and superheat are linearly related. Hence, it is likely that this is in fact the true nature of this relationship.

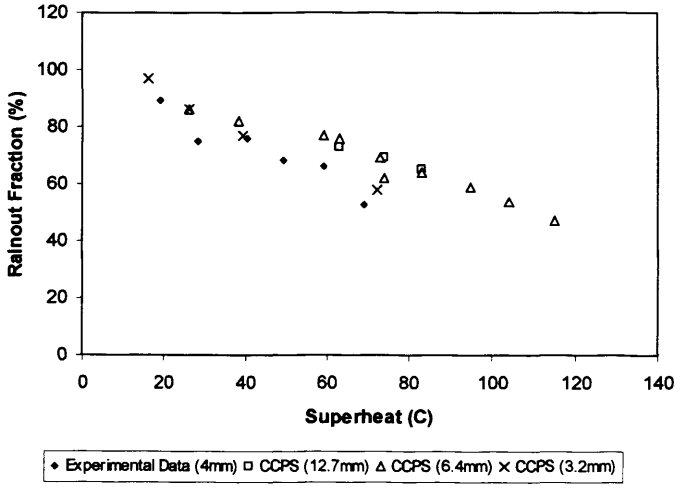

Figure 4.11 Comparison of recorded data with CCPS data[15]

The CCPS data[15] for a 3.2mm nozzle diameter demonstrates a slightly higher rainout fraction than the 4mm nozzle diameter used in this study. This discrepancy could be explained by the differing atmospheric conditions under which each test was conducted. While the CCPS data was carried out inside an air-conditioned greenhouse-type structure where the atmospheric conditions were regulated, the tests performed here were conducted outdoors and were therefore subject to the prevailing weather conditions. Although wind speeds were light, varying from 0.5-2ms^{-1}, it was observed that very light gusts were capable of directing the plume away from the water collection rig during a release. Taking this into account the two datasets display a certain level of agreement, which is significant because the conditions under which releases were performed differed appreciably. As a condition of the tests carried out by Johnson and Woodward (although no dimensions are provided) the length of piping from the storage tank to the exit orifice was kept as short as possible in order to minimise flashing prior to release to the atmosphere. This is in contrast to the superheated atomiser used in this study where the corresponding pipe-length was approximately 0.6m. In addition, all the tests conducted in the CCPS study involved horizontal releases approximately 1.22m above ground level. This is more than twice the height of the exit orifice of the superheated atomiser used here. One would intuitively expect closer proximity to ground level to increase the rainout fraction. In contrast the 4mm orifice produced less rainout than any nozzle utilised during the CCPS study, including the 3.2mm orifice. Nevertheless, the results suggest that orifice diameter, height of the nozzle above ground level, and pipe length prior to the exit orifice have little or no significant effect on the rainout fraction from the release of a superheated flashing jet. Instead the primary input parameter appears to be the temperature of the jet at the exit orifice.

Figure 4.12 presents the rainout data for varying orifice diameter at constant stagnation temperature. However, it is difficult to evaluate the influence of nozzle diameter on the rainout fraction in this case because the break-up mechanism was not consistent across the range of initial conditions investigated. In contrast to the 2mm and 4mm nozzle diameters, it was not possible to generate a fully flashing spray at 160°C stagnation temperature using a 1mm nozzle diameter. This was because the flow-rate through a 1mm nozzle diameter was not high enough for heat losses in the system to be replaced at a rate comparable with the flow-rate through a 2mm or 4mm orifice diameter. As a result, the temperature at the exit orifice was approximately 15°C lower than when a 2mm or 4mm nozzle diameter was attached to the rig. As discussed later in Chapter 6, once a jet becomes superheated, there are

various stages of transition to full flashing which are dependent on the degree of superheat. In the case of a 1mm nozzle diameter, the temperature was not high enough to generate a fully flashing spray.

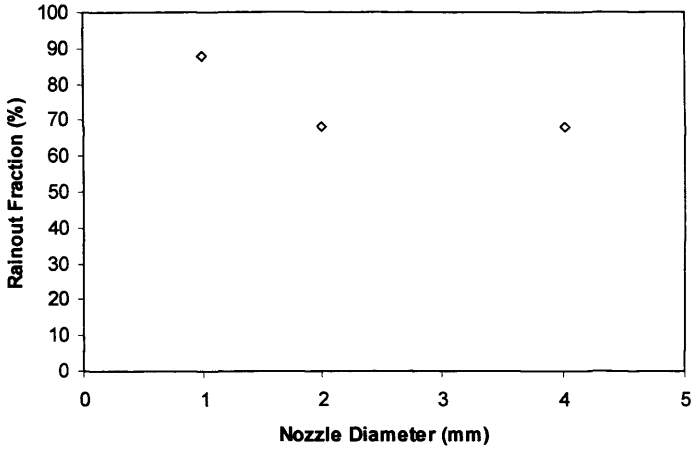

Figure 4.12 Variation of rainout fraction with nozzle diameter

Although the data is clearly limited, once flashing conditions were established (i.e. using 2mm and 4mm nozzle diameters) the effect of nozzle diameter on rainout appears to be negligible, which is consistent with the CCPS data[15] and the few previous rainout studies in the literature[49,117]. This being the case, the data indicates qualitatively how the transition to full flashing reduces the rainout fraction from a release of superheated liquid.

Figure 4.13 compares the available datasets with the correlation proposed by De Vaull and King[118] for non-volatile liquids, which is based on a simple empirical approach to predicting rainout. The correlation over-predicts the rainout fraction measured in this study, but compares particularly well with the CCPS data. Significantly the predicted rainout is independent of orifice size, as indicated by the results of this study. It is tentatively suggested therefore that the correlation is a useful tool for providing an estimate, possible conservative, of the rainout fraction from releases of superheated liquids, particularly for its relative simplicity.

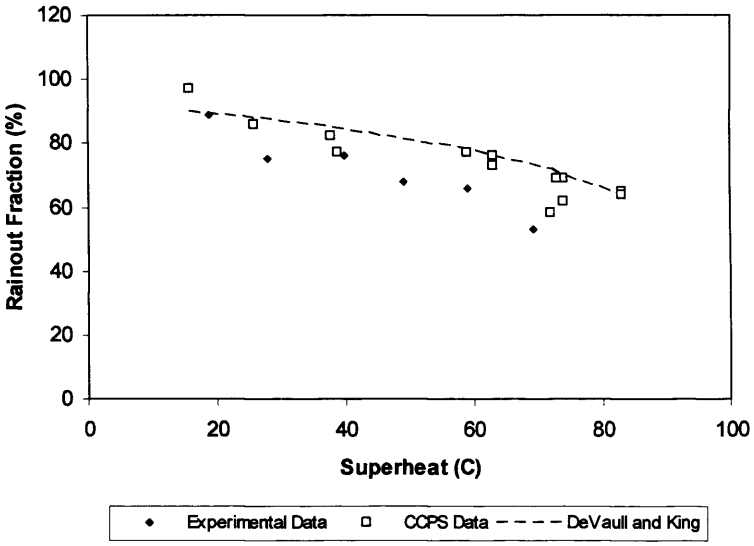

Figure 4.13 Comparison of data with De Vaull and King's rainout correlation

4.5 Summary

Analysis of the spray jet-width has been proposed as a simple and unobtrusive method of characterising the transition from mechanical break-up to flashing for superheated sprays. A point of inflection in the relationship between the jet superheat and jet width characterises the point of transition, which is found to exist between 20-30°C superheat for a 2mm x 3.4mm nozzle.

Rainout fraction has been demonstrated to be inversely proportional to the degree of superheat. It is tentatively suggested that the orifice size, height of the orifice above ground level and the length of piping prior to the orifice inlet have minimal influence on the resultant rainout associated with a release of superheated liquids.

The correlation proposed by De Vaull and King[118] for non-volatile liquids is suggested as a useful tool for providing an estimate of the rainout fraction from releases of non-volatile superheated liqiuids.

4.6 Future Work

The upper cut-off limit at which the jet width ceases to significantly increase requires investigation. In addition, the use of the jet width as a method of jet characterisation requires validation for a more comprehensive range of initial conditions, with particular reference to the orifice dimensions.

It is necessary to develop towards an improved experimental methodology for the investigation of rainout fraction. The possible effects of variable ambient conditions need to be included, and a more accurate method of rainout collection implemented. The current data requires validation and the precise nature of the influence of superheat on the collected rainout fraction requires investigation. The pressure head inside the atomiser was generated by the expansion of liquid as it was heated. Hence it was not possible to de-couple the pressure and temperature using this rig. It is necessary therefore to design and develop a rig capable of de-coupling these two input parameters so that their influence on the rainout fraction can be better understood.

A feasibility study of the possibility of safely measuring rainout from large scale controlled releases of a range of hazardous materials should be conducted, and the results implemented in order to understand the effect of the fluid properties on the rainout fraction.

Chapter 5 Mechanical Break-Up

5.1 Introduction

In this section the data from sub-cooled releases are analysed and processed to produce a correlation for determining the non-dimensionalised droplet SMD (Sauter Mean Diameter) for mechanical break-up. The accuracy of the correlation in reproducing the original dataset is discussed for SMD predictions, and some sample graphs are compiled for a range of release scenarios, comparing predictions from four previously proposed models. A correlation for determining the droplet size distribution is also proposed as a development upon the Rosin-Rammler[140] approach adopted by Elkotb[34].

5.2 Jet Break-Up Regime

The established break-up regimes for mechanical break-up of liquid jets are presented in Figure 5.1[22,27]. Transition between jet break-up regimes is given in terms of (a) jet injection velocity and (b) Ohnsorge number and Reynolds number.

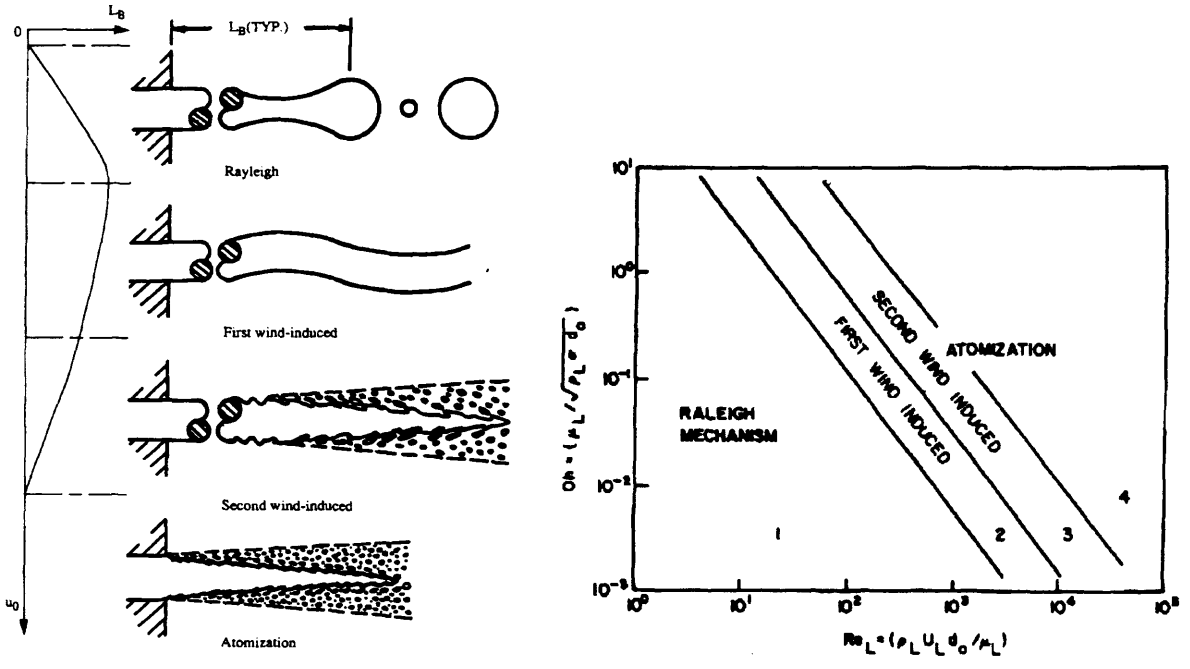

Figure 5.1 Jet break-up regimes and transition criteria between regimes[22,27]

Figure 5.2 presents Re-Oh plots for the full range of release pressures and orifices of length 3.4 and 7.0mm respectively. The data indicates that break-up fell into the 'atomisation' regime in almost every case. This corresponds to observations made during the acquisition of the experimental data, where a liquid core existed immediately downstream of the orifice exit, the length of which diminished with increasing release pressure. Despite the fact that a liquid core is now believed to exist even for very high-pressurised engine sprays[33], at low pressure the atomisation quality was relatively poor, where the break-up was almost borderline second-wind induced. In terms of modelling droplet sizes in sub-cooled sprays, regimes below second wind induced break-up do not produce droplets small enough to remain airborne over a significant distance. In these cases it can be assumed that a large proportion of the released liquid will rainout, depending on the rate of vaporisation.

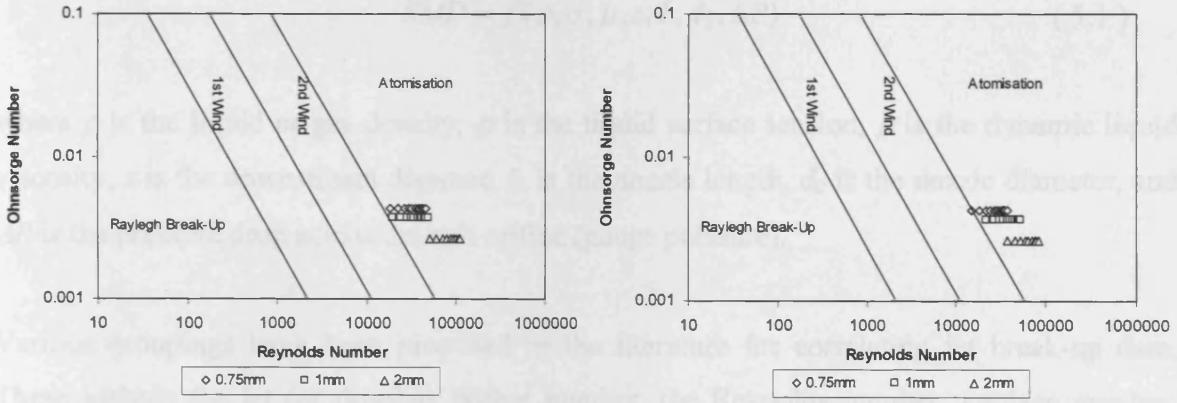

Figure 5.2 Break-up regime of the tested nozzles with length L = 3.4mm and 7mm respectively

5.3 SMD Correlation for Mechanical Break-Up

The process of non-dimensionalisation ensures dimensionally balanced equations. The process also has several other advantageous features; appropriate dimensionless groupings provide an insight into the relative effects of different process parameters and provides a method of scaling, so that the effect of liquid material can be determined. Hence, for mathematical rigour, ease of presentation and extrapolation to cases outside the domain of the current data-set, the proposed correlation is presented in a non-dimensionalised format.

In all experiments water was utilised as the model fluid, and thus the influence of liquid characteristics are not explicitly appraised in this programme. However, the dimensionless groups utilised include fluid properties, thereby facilitating similarity scaling. This technique must be used therefore in the absence of validation data to provide predictions for fluids other than water. Nevertheless, future studies of the effect of variation of fluid properties remain necessary, in order to justify the validity of this approach.

5.3.1 Derivation of SMD Correlation

Taking both 'primary' and 'secondary' parameters into account, the SMD can be expressed in a general form:

$$SMD = f(\rho, \sigma, \mu, z, L, d_0, \Delta P) \qquad (5.1)$$

where ρ is the liquid or gas density, σ is the liquid surface tension, μ is the dynamic liquid viscosity, z is the downstream distance, L is the nozzle length, d_0 is the nozzle diameter, and ΔP is the pressure drop across the exit orifice (gauge pressure).

Various groupings have been proposed in the literature for correlating jet break-up data. These include the jet (or droplet) Weber number, the Reynolds number, Laplace number, Ohnsorge number, Capillarity number, etc. Here, the most common combination of correlation groupings is adopted, namely the liquid Weber number, the liquid Reynolds number and the aspect ratio, which is an additional grouping for characterisation of the nozzle geometry (L/d_0). By applying dimensionless analysis, Equation (5.1) can be quoted in non-dimensional form in the following format:

$$\frac{SMD}{d} = C \cdot \left(\frac{L}{d}\right)^a \mathrm{Re}^b We^c \qquad (5.2)$$

where C is a constant (absorbing the outstanding liquid dimensionless groups of viscosity and density ratios here), *Re* is the Reynolds's number, defined by Equation (5.3), and *We* is the Weber number, defined by Equation (5.4). The Reynolds number represents the ratio of inertia forces to viscous forces, while the Weber number represents the ratio of inertia forces to surface tension forces. Here ρ_l is the liquid density, ρ_v is the vapour or ambient density and u_j is the jet velocity.

$$\mathrm{Re} = \frac{\rho_l \cdot u_j \cdot d_0}{\mu} \qquad (5.3)$$

$$We = \frac{\rho_l \cdot u_j^{\,2} \cdot d_0}{\sigma} \qquad (5.4)$$

The power indices *a*, *b* and *c* are determined by the experimental data via a two-stage process; first the non-dimensionalised SMD is plotted against the primary physical input parameters, i.e. L/d_0, ΔP, and d_0, on a logarithmic scale. This determines power law proportionalities between these factors. The indices taken from these power law proportionalities are then used to generate simultaneous equations, which yield the required indices, *a*, *b* and *c*.

5.3.1.1 Aspect Ratio

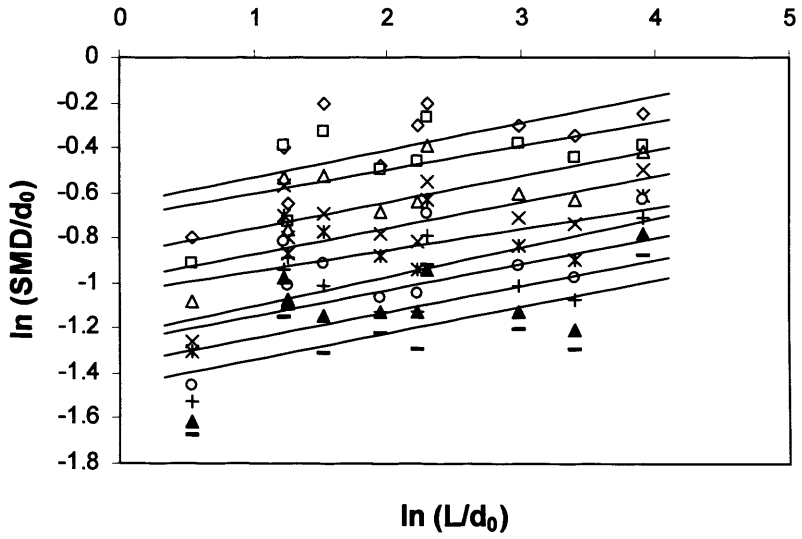

Figure 5.3 Effect of nozzle aspect ratio on the dimensionless SMD

From the data presented in Figure 5.3 an average trend-line can be applied to the entire data set, which produces the following equation

$$\ln\left(\frac{SMD}{d_0}\right) = 0.114\ln\left(\frac{L}{d_0}\right) - 1.0626 \qquad (5.5)$$

This is manipulated to produce the following power law proportionality

$$\frac{SMD}{d_0} = 0.346\left(\frac{L}{d_0}\right)^{0.114} \qquad (5.6)$$

5.3.1.2 Release Pressure

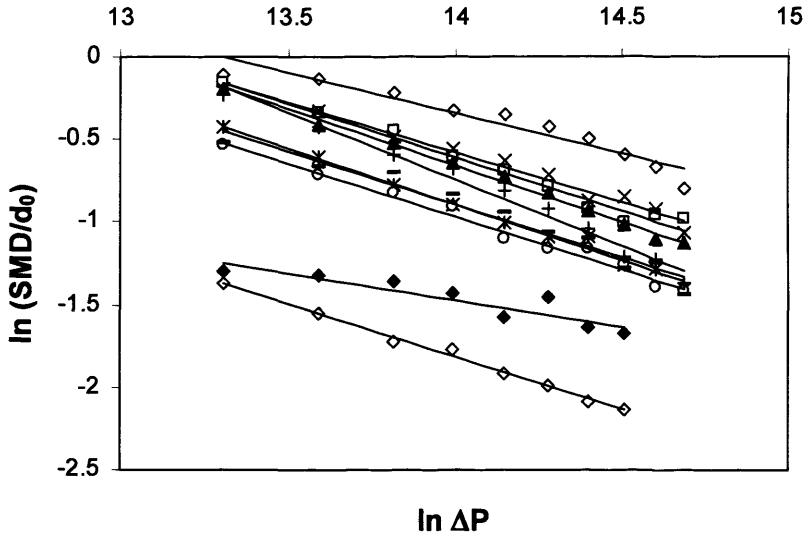

Figure 5.4 Effect of release pressure (gauge) on the dimensionless SMD

From the data presented in Figure 5.4 an average trend-line can be applied to the entire data set, which produces the following equation;

$$\ln\left(\frac{SMD}{d_0}\right) = -0.54\ln(\Delta P) + 6.694 \qquad (5.7)$$

This is manipulated to produce the following power law proportionality

$$\frac{SMD}{d_0} = 807.3\Delta P^{-0.54} \qquad (5.8)$$

5.3.1.3 Nozzle Diameter

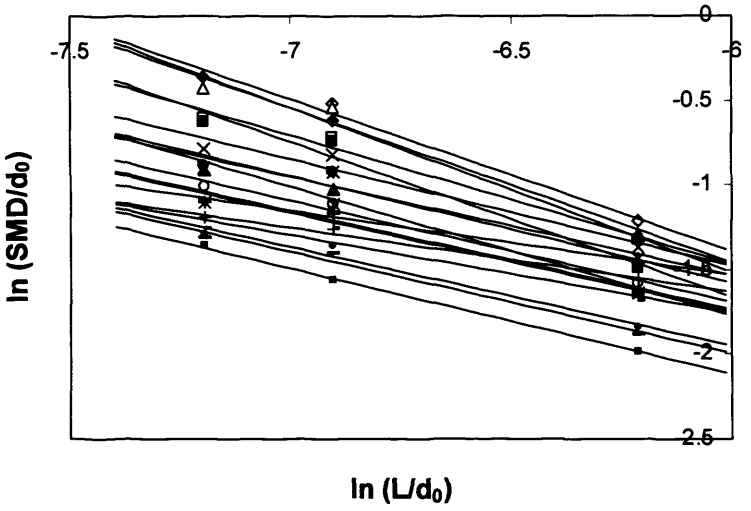

Figure 5.5 Effect of nozzle diameter on the dimensionless SMD

From the data presented in Figure 5.5 an average trend-line can be applied to the entire data set, which produces the following equation;

$$\ln\left(\frac{SMD}{d_0}\right) = -0.661\ln(d_0) - 5.627 \qquad (5.9)$$

This is manipulated to produce the following power law proportionality

$$\frac{SMD}{d_0} = 0.004 d_0^{-0.66} \qquad (5.10)$$

5.3.1.4 Final Correlation

By substituting the indices derived from the relationships between the non-dimensionalised SMD and the various input parameters into Equation (5.2) the correlation obtains the general form presented in Equation (5.11).

$$\frac{SMD}{d_0} = C\left(\frac{L}{d_0}\right)^{0.114} \mathrm{Re}^b We^c \qquad (5.11)$$

Through the application of simultaneous equations it is possible to deduce the remaining indices *b* and *c*.

Matching of indices in terms of u_j [by substituting Equations (5.3),(5.4) and (5.8) into Equation (5.11)] gives;

$$b + 2c = -1.08 \qquad (5.12)$$

Matching of indices in terms of d_0 [by substituting Equations (5.3),(5.4) and (5.10) into Equation (5.11)] gives;

$$-0.114 + b + c = -0.661 \qquad (5.13)$$

The above equations can easily be solved for b and c to give b = -0.014 and c = -0.533. Hence, Equation (5.11) obtains the form:

$$\frac{SMD}{d_0} = C\left(\frac{L}{d_0}\right)^{0.114} \mathrm{Re}^{-0.014} We^{-0.533} \qquad (5.14)$$

The co-efficient *C* is essentially the average correction factor between the non-dimensionalised SMD given by Equation (5.14) in its current form and the measured data. The value of *C* is found to be 64.73, hence the final form of the correlation is given by Equation (5.15)

$$\frac{SMD}{d_0} = 64.73\left(\frac{L}{d_0}\right)^{0.114} \mathrm{Re}^{-0.014} We^{-0.533} \qquad (5.15)$$

5.3.2 Effect of Primary Input Parameters on SMD Correlation

The effects of the various input parameters on the droplet SMD are demonstrated by Equations (5.16),(5.17) and (5.18)

$$SMD \propto d_0^{0.34} \qquad (5.16)$$

$$SMD \propto \Delta P^{-0.54} \qquad (5.17)$$

$$SMD \propto \left(\frac{L}{d_0}\right)^{0.114} \qquad (5.18)$$

Table 5.1 Influence of primary input parameters on previously and currently proposed correlations

Investigators	Exponent of Orifice Diameter (d_0)	Exponent of Release Pressure (ΔP)
Merrington &Richardson[30]	1.2	-0.5
Harmon[31]	0.3	-0.275
Tanasawa & Toyoda[32]	0.5	-0.5
Hiroyasu & Takoda[33]	0.262	-0.07
Elkotb[34]	Independent	-0.54
Tilton & Farley[35]	Independent	-0.5
Proposed Correlation (5.15)	0.34	-0.54

A broad range of correlations have been previously proposed in the literature for essentially plain orifice atomisers. For the purposes of validating the submitted correlation, the derived exponents of the primary input parameters have been compared with those presented in those previously established equations. The large majority have been derived outside the range of interest of the current study (i.e. higher pressures and smaller orifice sizes), and have used a variety of orifice characteristics and diagnostic techniques to measure mean droplet size. All these factors are likely to have contributed to the range of exponents for primary parameters expressed previously. The results of the comparisons have been summarised in Table 5.1. This table includes the dependence of each correlation on the orifice diameter d_0 and the release pressure ΔP. Exponents have been compared based on three criteria: (i) intuition; (ii) proximity to range of previous exponents; (iii) quantitative agreement with selected correlations. No suitable correlations have been found to compare the effect of aspect ratio for plain orifice atomisers, so it is not possible to provide a quantitative comparison for the effect of this parameter.

In accordance with established droplet break-up theory one would expect droplet SMD to increase with increasing orifice diameter. This theory is supported by the inclusion of a positive exponent of orifice diameter in every example where it has been incorporated as an explicit factor in the correlation. Moreover the proposed exponent of the power-law is within range of those quoted by other researchers, albeit for different release conditions. For example, Harmon[31] quotes an exponent of 0.3, and Hiroyasu *et al*[33] quote 0.26 for an incomplete spray.

Similarly the influence of release pressure demonstrated by each of the given correlations is also intuitively reasonable, as one would expect droplet SMD to be inversely proportional to the release pressure. This is expressed with the inclusion of a negative exponent for this particular input parameter. Furthermore the proposed exponent is consistent with several of the researchers in the literature; Merrington and Richardson[30], Tanasawa and Toyoda[32] and Tilton and Farley[35], who all quote the exponent as -0.5, and Elkotb[34], who quotes an exponent of -0.54, which is identical to that submitted here.

The influence of aspect ratio on SMD as presented in Equation (5.18) is found to be relatively strong and positive. Here the exponent of aspect ratio is found to be 0.114. In effect this represents an 8.2% increase in the size of the global droplet SMD for a two-fold increase in the nozzle aspect ratio. This is fairly consistent with the observed effect of doubling the nozzle length for a fixed diameter, where the spray cone angle was observed to narrow and the spray quality was observed to decrease significantly. One would make the comparison with the phenomenon of 'rifling' where increasing the barrel length of a shot-gun, narrows the trajectory of the shot and improves the accuracy of the weapon over longer distances. Hence the proposed influence seems plausible and again is qualitatively consistent with general atomisation understanding. However, the effect of nozzle aspect ratio is still a matter of some debate and ongoing research. Far from the trend being linear, the relationship between droplet SMD and nozzle aspect ratio takes on a complicated form, which fluctuates in a way which at first glance appears to be random but on further inspection does have some order. This also reflects recent findings from work undertaken at Cardiff University[141] where a 'wavy' relationship was found to exist between aspect ratio and discharge coefficient.

Figure 5.6 presents the relationship between the dimensionless droplet SMD and the and discharge coefficient, where it can be seen that although droplet SMD decreases with increasing pressure, the form of the relationship between droplet SMD and nozzle aspect ratio is almost identical in the three examples presented, despite its apparently haphazard complexion.

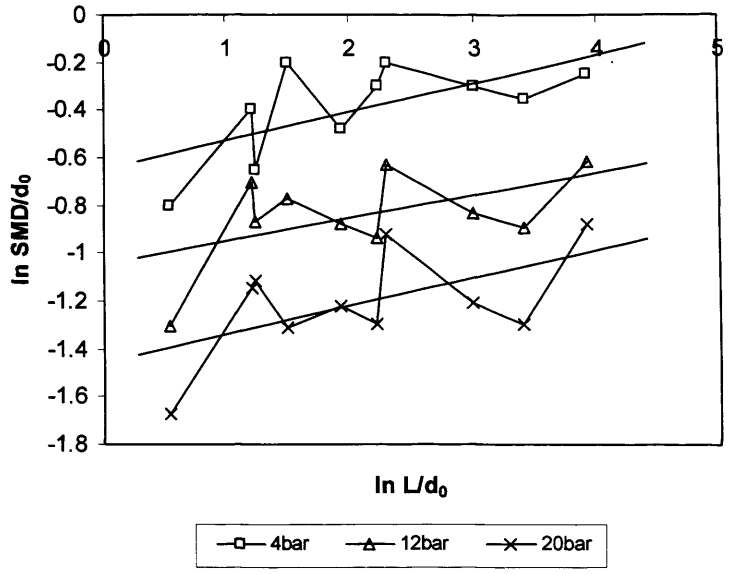

Figure 5.6 'Wavy' relationship between nozzle aspect ratio and droplet SMD

It is likely that irregularities in the surface finish of the nozzle and aberrations on the nozzle inlet and outlet contributed to this 'wavy' relationship, particularly since the nozzles were made of brass, which is a relatively soft metal. Such imperfections could have arisen at the manufacturing stage or as a result of general wear and tear during testing. However, it is difficult to classify imperfections of this nature in a way that would permit the systematic analysis of their effect on the droplet SMD. For this reason it is not possible to make a recommendation on how one should incorporate these factors in the overall correlation at this stage. Therefore, for the sake of simplicity and for its inclusion in more general atmospheric modelling, a linear relationship has been superimposed over the observed 'waviness' for the full range of aspect ratios included in the experimental programme, so that it is possible to derive a coherent correlation from the data. However this is a phenomenon that clearly requires further investigation to be understood fully.

For scenarios where the aspect ratio in a practical release is outside the range considered here it is recommended that the minimum and maximum values of the range included here be adopted as the lower and upper cut-off limits respectively, i.e. a lower cut-off limit of 1.7 and an upper cut-off limit of 50. It is reasonable to assume that a lower cut-off exists because a sharp-edged orifice ($L/d_0 = 0$) produces a spray with a finite SMD. Given the relatively weak

dependence of L/d_0 indicated in the correlation, this means that for L/d_0 an order of magnitude less than the lower cut off limit, the maximum error in SMD prediction is 30%.

Similarly there is physical justification for adopting an upper cut-off limit as one would expect the influence of aspect ratio on downstream spray conditions to eventually diminish. For an aspect ratio an order of magnitude higher than the upper limit the maximum error in SMD is also 30%.

5.4 Extension of SMD Correlation to Other Materials

The correlation proposed in Equation (5.15) has been derived from an experimental programme using water as the test fluid. In terms of validated predictions for releases of other hazardous materials further work is required to assess the influence of fluid parameters and possibly modify the correlation accordingly. As an interim measure, the effect of liquid parameters may be considered using scaling criteria, under the assumptions that appropriate non-dimensionalised groups are chosen, and that a sufficient number of groups have been utilised to fully describe the process. For atomisation and liquid jet break-up, the three primary parameters usually considered are the density, shear viscosity and surface tension of the liquid. In this section the proposed correlation is assessed accordingly in the context of non-dimensional analysis (similarity scaling) and undergoes a logical qualitative assessment

In the proposed correlation the exponent of surface tension is +0.533, as introduced via the Weber number. Qualitatively, this has the anticipated effect, in that an increase in surface tension should increase the mean size of the droplets due to the heightened influence of liquid retention forces. Quantitatively, this is similar to the correlation of Tilton and Farley[35], who propose an exponent of +0.5. Other correlations typically quote surface tension exponents in the range 0.25-0.75, thus the surface tension exponent appears to be credible and does not therefore require further amendment.

The proposed correlation provides an exponent of liquid shear viscosity of +0.014, introduced via the Reynolds number. Again qualitatively, this is sensible, in that for an increase in liquid viscosity one would expect a decrease in the atomisation quality i.e. larger mean droplet sizes. Tilton and Farley[35] do not include viscosity in their correlation -

mathematically an exponent of zero - and Harmon[31] proposes an exponent of 0.07, indicating a positive but weak influence, consistent with the current prediction. Exponents for other correlations vary widely, although there is a certain degree of consistency with some previous studies, which tends to indicate that the influence of liquid viscosity derived from the similarity scaling approach demonstrated here retains some credibility. Hence, no further modification of the correlation is required at this stage.

The exponent of liquid density in the proposed correlation is -0.547, and is introduced by both the Reynolds number and the Weber number. Most previous correlations express negative exponents, and hence the proposed correlation is qualitatively consistent in this respect. Both correlations provided by Tilton and Farley[35] (-0.5) and Hiroyasu *et al*[33] for 'complete jets' (-0.54) provide correlations very similar to that proposed here. Though other correlations in the literature propose different liquid density exponents, this does not provide a strong case for introducing an extra non-dimensionalised grouping at this stage.

5.5 SMD Statistics and Correlation Limitations

In order to evaluate the accuracy of the method adopted to derive the correlation from the experimental data, the measured data has been plotted against the data predicted by the correlation for equivalent conditions, presented in Figure 5.7.

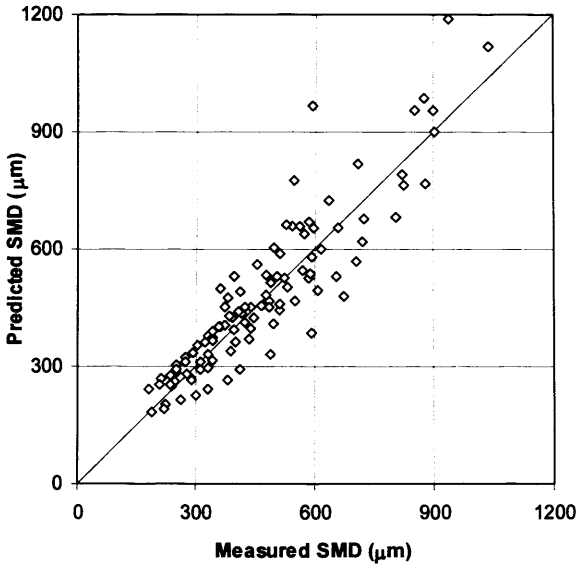

Figure 5.7 Accuracy of proposed correlation

The disparity between prediction and experimental data, while relatively low, is the overhead of adopting a more generalised coefficient for the correlation. If instead coefficients found to correspond to each nozzle are utilised - hence eliminating the parameters which introduce the most non-linearity - it is possible to generate a more accurate technique for predicting mean droplet size, albeit at the expense of generality. Figure 5.8 demonstrates the improved accuracy it is possible to achieve using this method

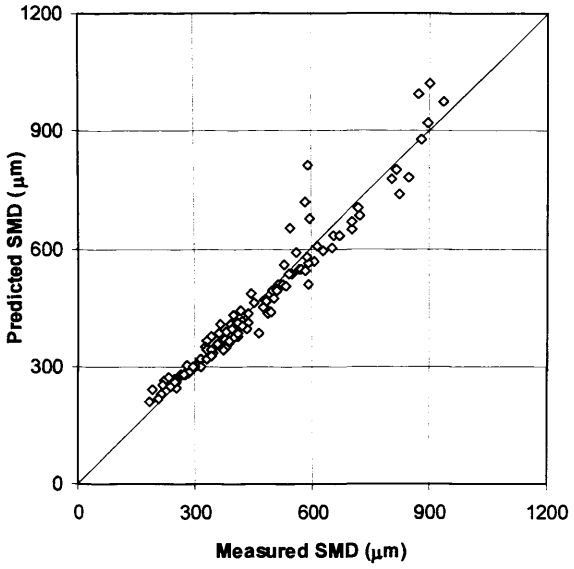

Figure 5.8 Accuracy of nozzle-specific correlations

The mean relative error of the SMD droplet size diameter, $\Delta_{rel}(SMD)$ indicates how well the correlation is able to predict the measured data, and is defined by Equation (5.19).

$$\Delta_{rel}(SMD) = \frac{1}{N}\sum_{i=1}^{N}\frac{\left|(SMD)_i^{measured} - (SMD)_i^{predicted}\right|}{(SMD)_i^{predicted}} \qquad (5.19)$$

The more effective the correlation, the closer the relative error will be to zero. The standard deviation provides an indication of the scatter of data away from the mean, and is defined by Equation (5.20).

$$\sigma_n = \sqrt{\frac{1}{N}\sum_{i=1}^{N}(x_i - \bar{x})^2}$$

where, $$x_i = \left|\frac{(SMD)_i^{measured}}{(SMD)_i^{predicted}}\right| \quad and \quad \bar{x} = \frac{1}{N}\sum_{i=1}^{N} x_i \qquad (5.20)$$

As defined by basic statistical theory, one positive or negative standard deviation away from the mean accounts for approximately 68 percent of the data. Two standard deviations away from the mean accounts for approximately 95 percent of the data. The mean relative error and the standard deviation (σ_n) of the data have been calculated and are displayed in Table 5.2. In spite of the correlation's sensitivity to the irregular influence of nozzle aspect ratio, given the range over which the proposed correlation predicts droplet SMDs, the relatively low figures indicate that the correlation represents the data very effectively.

Table 5.2 Errors associated with the predicted data with respect to the measured data

Correlation	Mean Relative Error	σ_n
Proposed	0.135	0.172
Nozzle-Specific	0.065	0.083

Under conditions similar to diesel injection (> 10^8 Pa), SMD values less than 20 microns are predicted by the proposed correlation, which is consistent with data from automotive diesel sprays[34]. This offers a degree of confidence, albeit limited, in using the correlation to extrapolate to conditions outside the current dataset.

5.6 Comparison with Previous Models

In this section, the proposed correlation for SMD is compared against previous models utilised for atmospheric dispersion modelling. The previous models considered include those proposed by Lefebvre[22], Elkotb[34], Tilton and Farley[35] and that contained in the TNO Yellow Book[128], which is a publication by a Dutch government agency known as the 'Committee for the Prevention of Disasters', which would be an equivalent of the Health and Safety Executive in Britain.

Lefebvre[22] provides an expression for the maximum droplet diameter D_{max} in terms of a critical Weber number, $We_{crit(SMD)}$. Analysis of the 'typical' droplet size distribution produced by diesel-type injectors (Elkotb[34]) indicates that D_{max} is approximately 1.8 times the SMD. Under these assumptions, the following correlation is derived for the SMD:

$$SMD = \frac{D_{\max}}{1.8} = \frac{\sigma We_{crit}(\max)}{1.8 u_j^{\,2} \rho_a} = \frac{\sigma We_{crit}(SMD)}{u_j^{\,2} \rho_a} \qquad (5.21)$$

$$\text{where} \quad We_{crit}(SMD) = \frac{We_{crit}(\max)}{1.8} = \frac{8}{C_{drag}} \times \frac{1}{1.8}$$

Johnson and Woodward[15] quote values of critical Weber number in the range 12-22 and the TNO Yellow Book[128] quotes values in the range 10-20 with a recommended value of 15; see also Brown and York (1962)[16] and Heinze (1955)[44].

The correlation proposed by Elkotb is reproduced here, having originally been presented in Equation (2.5).

$$SMD = 3.08\left(\frac{\mu}{\rho_l}\right)^{0.385} (\sigma \rho_l)^{0.737} \rho_a^{\,0.06} \Delta P^{-0.54} \qquad (2.5)$$

The correlation proposed by Tilton and Farley is reproduced here, having originally been presented in Equation (2.6).

$$SMD = \frac{0.585}{u_j}\left(\frac{\sigma}{\rho_l}\right)^{0.5} \qquad (2.6)$$

The TNO Yellow Book[128] recommends the initial droplet-size calculation method based on the work by Appleton[50] and presented by Wheatley[49], given by Equation (5.22).

$$SMD = 1.89 d_0 \sqrt{1 + 3\frac{We_L^{\,0.5}}{\mathrm{Re}_L}}, \; if \left\{ We < 10^6 \,\mathrm{Re}^{-0.45} \; and \; T_0 < 1.11 T_c^{boil} \right.$$

$$= \frac{\sigma_L We_{crit}(SMD)}{u_f^{\,2} \rho_a} \qquad ,else \qquad (5.22)$$

T_0 is the exit temperature at the orifice, T_c^{boil} is the boiling point at ambient conditions, u_f the post-expansion velocity, d_0 the nozzle diameter, and with all material properties evaluated at the post-expansion temperature T_f. Note that the second part of the model is equivalent to the critical Weber number approach recommended by Lefebvre[22]. Figure 5.9 presents a comparison between SMD predictions using the proposed correlation and the 4 correlations referenced. It presents the influence of velocity at the orifice against predicted SMD, for the specific cases of two nozzles of orifice diameter 1mm but with differing aspect ratios of 1 and

10. In each case the data is calculated at ambient conditions i.e. 20°C. The assumptions are made that pressure at the orifice is assumed to be equal to ambient, and that post-expansion velocity u_f equals the pre-expansion jet velocity u_j.

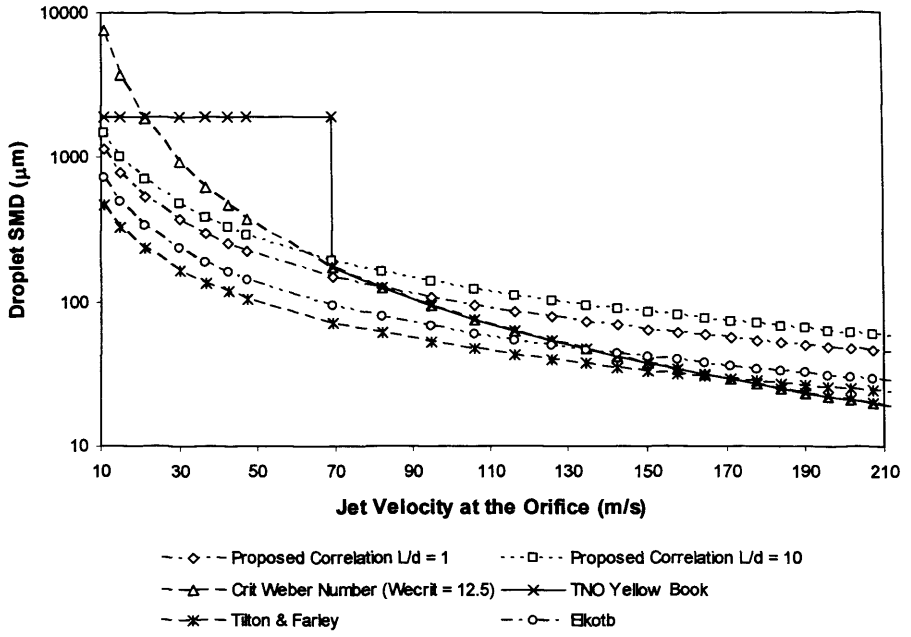

Figure 5.9 Comparison of previously proposed models with newly proposed correlation

Along the experimental range (velocities below 50 m/s or stagnation pressure below 24 bar), the proposed correlation results in lower SMD predictions than both the TNO Yellow Book and the critical Weber number approach, and in higher SMD predictions than the Elkotb and Tilton and Farley correlations. At velocities higher than those encountered within the scope of the experimental programme undertaken, the proposed correlation predicts larger droplet SMDs than each of those referenced. It is worth noting that the rate of decrease of droplet SMD with jet velocity is very similar for the proposed correlation and the Elkotb and Tilton & Farley correlations. This is because each correlation incorporates either explicitly or indirectly a similar exponent of release pressure, as previously demonstrated in Table 5.1.

At this stage, ut is necessary to highlight the fact that none of the previously proposed correlations are able to account for varying nozzle length or orifice diameter (except, up to a limited degree, the TNO correlation). This fact is manifested in the observation that while the predictions based on the other correlations are rigid, irrespective of the nozzle characteristics, the newly proposed correlation is much more flexible and therefore demonstrates a marked

difference between predicted data sets based on the varying nozzle characteristics. Despite this, data predicted by the proposed correlation appears to reflective the collective trends of several models already proposed in the literature regarding sub-cooled mechanical break-up.

It is also worth noting that no previously proposed model has been validated with data from modern laser diagnostic technology. Only the correlations proposed in this study have been produced via this method. Furthermore the correlation proposed by Elkotb was not considered for use at low pressures and relatively large orifice sizes; on the contrary, it was developed for use with releases in excess of 180bar, which is outside the range of interest utilised here. Intriguingly however, the pressure exponents of Elkotb's correlation and the newly proposed one are identical. There are few applicable recent data sets suitable for validation, but one that is relevant; that proposed by Buchlin and St Georges[54] also indicates similar pressure dependence. Their experimental pressure exponent of –0.37 is not far from the –0.54 presented here. Moreover, the Buchlin and St Georges dataset generally shows similar agreement with the current correlation for very low pressure releases (less than 8bar), i.e. droplet SMDs of 700μm and above.

Figure 5.10 provides a comparison of the influence of variation in orifice size for the newly and previously proposed correlations, in the case of a 20 m/s and 40 m/s jet velocity at the nozzle. In each case the nozzle aspect ratio is 5, kept constant so that solely the effect of changing nozzle diameter can be observed. Notice that none of the previously proposed models predict any variation in droplet size as orifice size systematically increases. The TNO correlation purports an exponent of orifice diameter of 1, i.e. doubling the orifice diameter will double the droplet diameter, which is intuitively highly unlikely. An increase in diameter from 1mm to 10mm (as demonstrated by Figure 5.10) would result in a tenfold increase in the droplet SMD, thereby far exceeding the scale presented. For this reason this correlation is omitted from the figure.

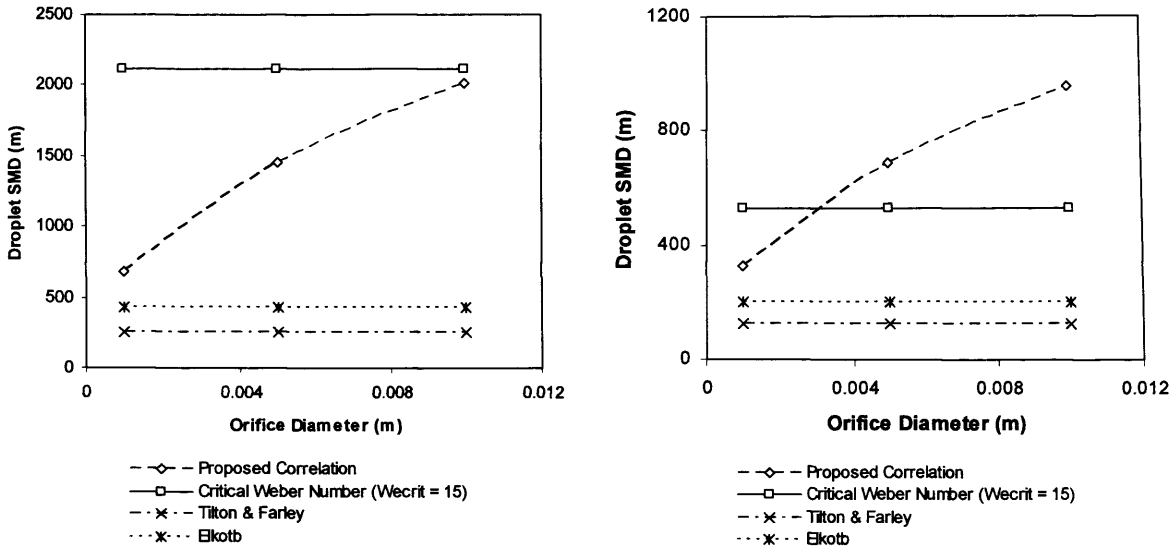

(a) 20ms^{-1} *(b) 40ms^{-1}*

Figure 5.10 Effect of variation in orifice diameter on SMD predictions

5.7 Droplet-Size Distribution

Figure 5.11 presents three examples of droplet size distributions, representing release pressures of 4, 14 and 24bar respectively. At 4bar it is evident that significant data truncation occurred due to the poor atomisation quality of the spray, as typified by the low validation rates achieved at these conditions, explained later in detail. At 14bar and 24bar there is still evidence of data truncation although not to the same extent as at very low pressure. Due to the shape of the distributions at medium and medium-high pressure, there are grounds for suggesting that the distribution was in fact bi-modal. This would signify that a significant body of liquid was contained in droplets with SMDs in excess of 1500μm. However, research carried out by DANTEC[142], who manufacture the laser equipment utilised, has shown that standard 1D PDA systems are prone to a particular kind of error known as the trajectory effect Depending on the trajectory of a particle, scattered light detected by the receiving optics is either dominated by refraction or reflection due to the Gaussian intensity profile of the laser beams across the measurement volume. As a result, light from an unwanted scattering mode is sometimes detected by the receiving optics. This effect is enhanced for large transparent particles, which reflects the application presented here. As a result the measured droplet SMD can be as much as 50% in excess of the actual droplet size. The

overall effect is the measurement of so-called phantom droplets at the upper size range limit, which produces the effect displayed in Figure 5.11. By using an updated Dual PDA 2D system, it is possible to almost completely eliminate this error.

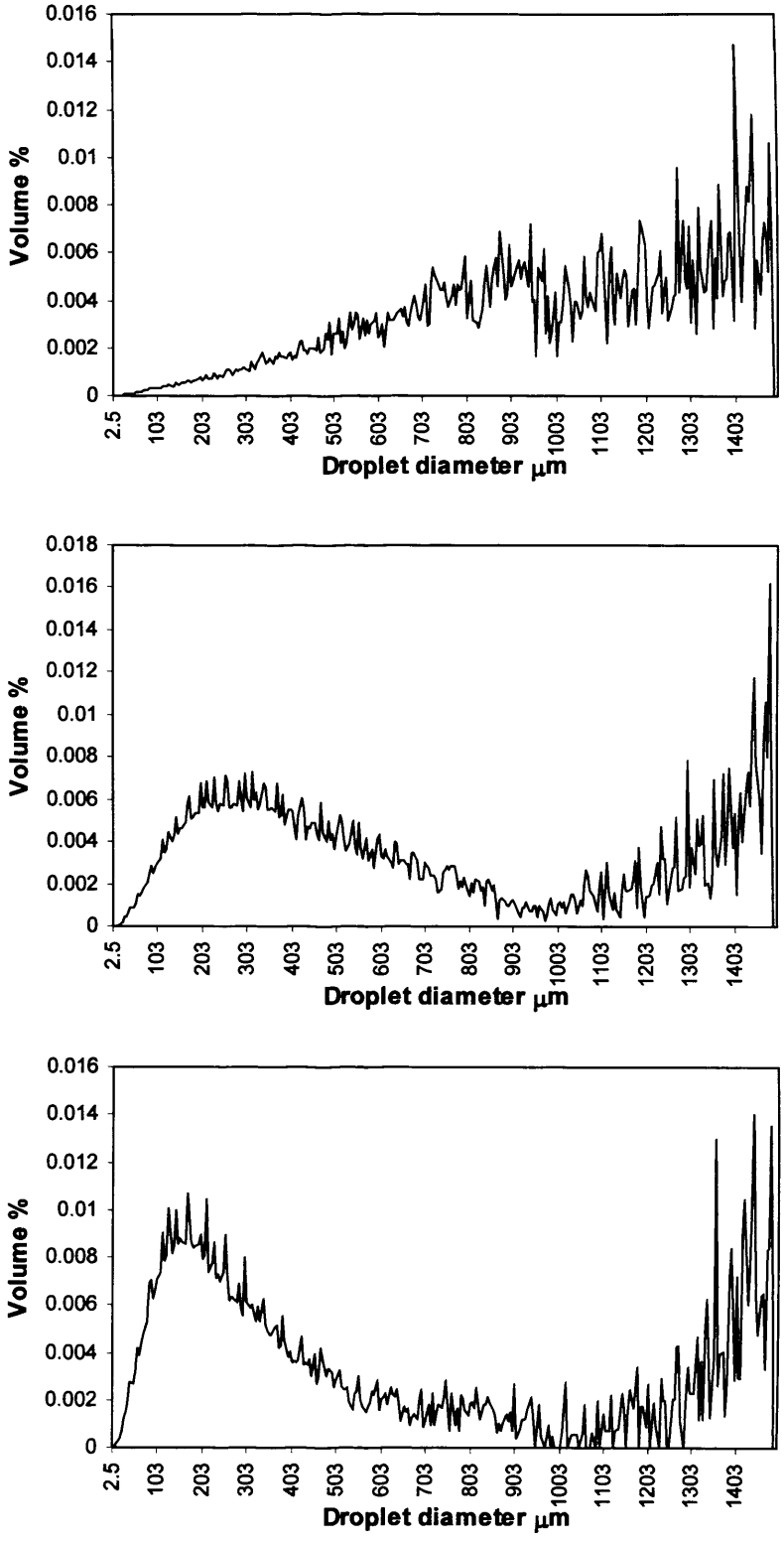

Figure 5.11 Droplet size distributions for 4, 14 and 24bar respectively

Figure 5.12 shows the results from the DANTEC study, where the presence of large droplets at the upper size range limit has been eliminated through the use of a 2D system. In spite of this, it is still likely that data truncation occurred to a certain extent as a result of the poor quality of the spray. The effect of data truncation was minimised by the adopted optical configuration, which ensured that the system was functioning at its maximum operating range. However, it is never possible to be completely confident that truncation has been eliminated for low-quality sub-cooled jets, particularly at low release pressures. As a result it is impossible to know with certainty what percentage of the measured droplets found to have diameters in excess of 1mm were actually present in the spray, and what percentage showed up due to the so-called trajectory effect. Nevertheless, it is felt that the level of truncation indicated by Figure 5.11 is largely due to the errors associated with the 1D system, and does not indicate a bi-modal droplet size distribution. However, this requires further investigation.

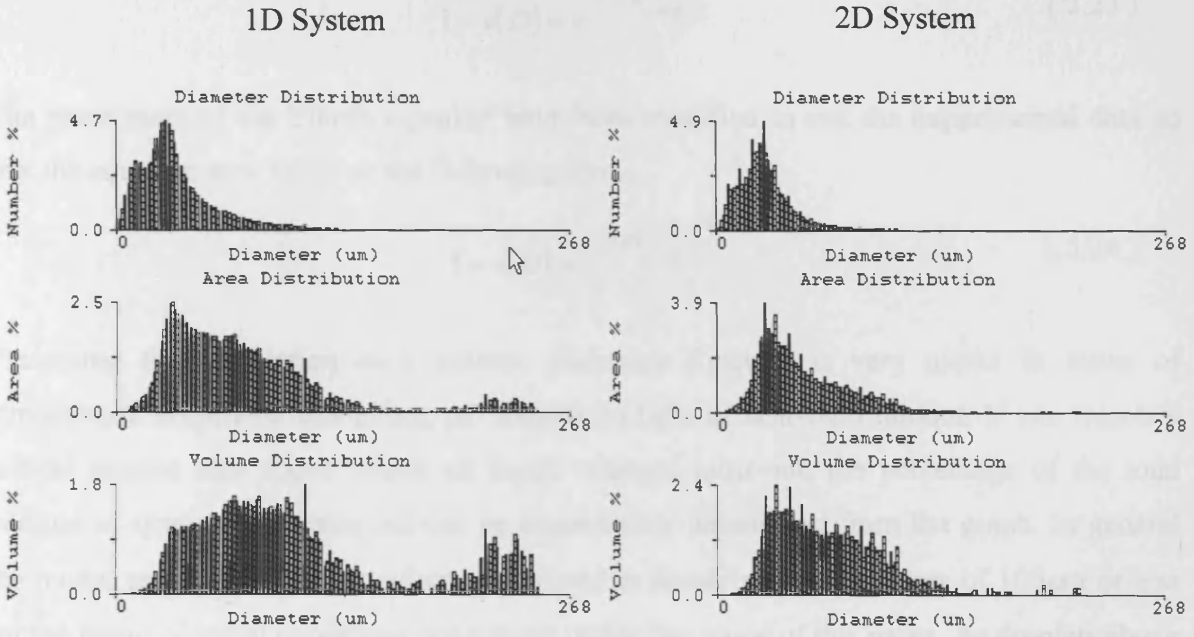

Figure 5.12 Improved accuracy of 2D system[142]

The poor atomisation quality for low-pressure sub-cooled release conditions also presented problems in terms of the validation rates. Typical validation rates for sub-cooled sprays ranged from 20-40% at low pressure i.e. 4bar, and 60-90% at high pressure i.e. 24bar. Validation rates varied inversely with spray density throughout the spray cross-section, i.e. validation rates were at their highest at the edge of the spray where the spray density was at its minimum, and vice versa.

The proposed droplet size correlation given by Equation (5.15) is presented in terms of the droplet SMD and is therefore susceptible to biasing by the presence of large droplets in the spray. For this reason it is likely that the measured droplet SMDs, and consequently, the predicted droplet SMDs are slightly over-evaluated. Nevertheless, its favourable comparison with previous droplet size correlations indicates that while errors were inherent in the measurement process, they do not preclude the use of the correlation as a tool for modelling releases of pressurised, sub-cooled, liquid jets to the atmosphere.

In spite of the low validation rates and the so-called trajectory effect, a correlation for droplet-size distribution has been developed in the spirit of the work done by Elkobt[34], based on the common Rosin-Rammler size distribution. Elkobt presents this correlation as a volume undersize function [v(D)], as presented by Equation (5.23).

$$1 - v(D) = e^{-0.422\left(\frac{D}{SMD}\right)^{5.32}} \qquad (5.23)$$

The parameters of the Elkotb equation have been modified to suit the experimental data so that the equation now takes on the following form.

$$1 - v(D) = e^{-1.34\left(\frac{D}{SMD}\right)^{0.5}} \qquad (5.24)$$

Presenting the correlation as a volume undersize function is very useful in terms of atmospheric dispersion modelling, particularly in light of near-field rainout. If one selects a critical droplet size above which all liquid released rains-out, the percentage of the total volume of spray which rains out can be immediately determined from the graph. In general the model predicts negligible volume contained in droplets with diameters of 100μm or less for the range of initial conditions considered within the scope of this paper. As droplets above 100μm will rainout, for 'low' to 'medium' release pressures the model predicts that most of the released material will rainout and contribute to pool formation rather than a potentially hazardous cloud.

Figure 5.13 shows how the proposed distribution correlation compares with the recorded data for three examples of individual data sets, which represent release pressures of 4, 14 and 24bar respectively, which are considered to be low, medium and medium-high in terms of practical release scenarios.

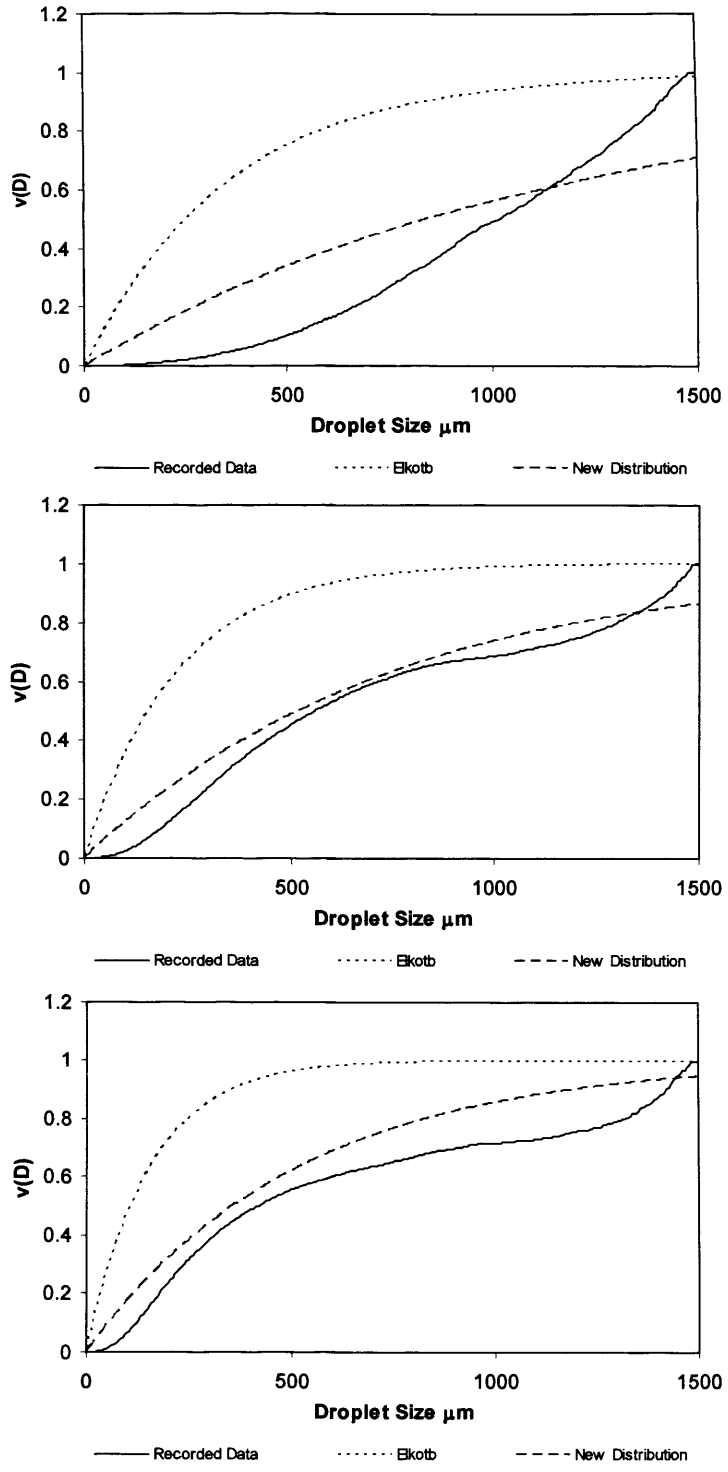

Figure 5.13 Comparison of droplet size distributions for 4, 14 and 24bar respectively

As mentioned previously, the droplet size distribution at 4bar was highly irregular. This was due to the poor atomisation quality of the spray at low pressures, leading to significant ligament formation, non-spherical droplets, and considerable data truncation for the adopted optical configuration. The implication is that the poor atomisation quality of sub-cooled sprays at low pressures (4-8bar) precludes the *accurate* application of droplet size distribution correlations. However, the data indicates that the volume of liquid contained in droplets with diameters less that 100μm is negligible for releases at low pressures and as a result it can be assumed that almost all of the released liquid will rain-out under these conditions.

For medium and medium-high release pressures the proposed correlation represents the data comparatively well, and presents a significant improvement on the version of the correlation proposed by Elkotb.

5.8 Summary

A non-dimensionalised SMD correlation for break-up of sub-cooled sprays has been developed based on PDA data for isothermal water jets in the atomisation regime. The accuracy of the correlation in reproducing the original dataset has been discussed, with predicted results representing a mean relative absolute error of 0.135, and a standard deviation of 0.172 from this error. Sample graphs have been compiled for a range of release scenarios, comparing predictions from 4 different previous models, developed outside the range of parameters investigated here. The proposed correlation compares favourably with previously proposed models, demonstrating good agreement for exponents of d_0 and ΔP. Under conditions similar to diesel injection (> 10^8 Pa), SMD values less than 20 microns are predicted by the proposed correlation, which is consistent with data from automotive diesel sprays, providing confidence in using the correlation to extrapolate to conditions outside the current dataset.

Similarity scaling has been performed in terms of the liquid density, shear viscosity and surface tension, in order to evaluate the applicability of the correlation to fluids other than water. The exponents of the primary parameters inherent in the proposed correlation are intuitively sensible and demonstrate good agreement with previously proposed correlations

developed outside the domain of this study, which supports the interim use of the correlation in its current form until data from releases of materials other than water becomes available.

At low pressure, the PDA data is subject to truncation errors as a result of the poor atomisation quality of sprays under these conditions (< 8bar). The system utilised represented technology at the cutting edge of current diagnostic techniques, which operated at the limit of its capability at all times. Data truncation was therefore an inevitable consequence of the application investigated. Nevertheless the favourable comparison of the proposed correlation with previous droplet size correlations and moreover, with the dataset for low pressure releases (less than 8bar) presented by Buchlin and St.Georges[54], indicates that while errors associated with the measurement process were not insignificant, they do not preclude the use of the correlation as a tool for modelling sub-cooled releases of sub-cooled liquid jets to the atmosphere. On the contrary, it would appear that it is more appropriate than any previously proposed correlation currently available.

A correlation for the droplet size distribution has been proposed based on the common Rossin-Rammler distribution. The proposed correlation demonstrates good agreement with the recorded data and represents a significant improvement on previously proposed droplet distributions.

5.9 Future Work

The following recommendations are made concerning future work resulting from the findings of this programme:

The dataset requires validation through the use of a Dual PDA 2D system with particular reference to the impact of the so-called 'trajectory effect'. The development of non-intrusive diagnostic technologies capable of measuring droplet sizes outside the range of the system utilised in the course of this study should be monitored so that the influence of data truncation on the recorded data can be assessed and eliminated when and where such technologies arise. The extension of the proposed correlation to conditions outside the current dataset requires justification. Droplet sizes in sub-cooled releases at pressures above 24bar, and therefore in

the 'atomisation' break-up regime should be investigated. The proposed lower and upper cut-off limits for nozzle aspect ratio also require validation.

The influence of fluid properties on the proposed correlation requires assessment, in order to justify its application to fluids other than water. Hence, it is necessary to design and conduct an experimental programme capable of investigating releases of potentially toxic or flammable liquids in a safe and controlled manner.

A more complete understanding of the impact of the nozzle aspect ratio on droplet SMD is required. In addition the impact of realistic surface aberrations, and material of manufacture, on spray characteristics compared with the 'idealised', carefully manufactured orifices utilised in this study requires appraisal.

Chapter 6 Model Governing Transition to Flashing

6.1 Introduction

In this chapter the results from a quantitative experimental methodology for identifying the transition from mechanical break-up to full flashing are presented. Three distinctive stages of transition are identified. Two equations governing the beginning and end of transition are developed and recommended for phenomenological modelling purposes.

PDA data produced from a quantitative study of flashing jets are presented and discussed. These results are combined with the established transition criteria and the droplet-size correlation for mechanical break-up presented in Chapter 5 to produce a complete model governing the transition from mechanical break-up to full flashing for pressurised releases of liquid jets through simple orifices.

6.2 Transition between Downstream Break-Up Regimes

Backlit shadowgraphs of superheated jets were taken during the initial stages after a release when pressure and temperature were most transient, using a NAC 1000 high speed video camera and a VCR, which recorded images at a rate of 1000fps. Pressure and temperature were monitored using a thermocouple and pressure transducer connected to a high-speed data acquisition system which recorded data at 1000Hz. Hence, by synchronising the data acquisition system with the video camera, it was possible to determine the exact release conditions in each frame. Images were analysed on a frame-by-frame basis in order to determine the conditions at which transition from mechanical break-up to flashing occurred for a range of nozzle diameters.

An example of the evolution of the jet break-mechanism is demonstrated in Figure 6.1. In the images presented, the release pressure was approximately 3.5bar and the nozzle diameter was 4mm (aspect ratio 0.85). At 0°C superheat break-up was dominated by mechanical processes. At 5°C bubbles could be seen forming in the jet, causing the jet to swell. At 10°C bubbles began bursting at the surface of the jet, causing minor ligament formation. Large bubbles were observed within the spray. At 15°C the liquid core began to disintegrate, with extensive

ligament formation at the edges of the spray. At 17.5°C a wide angled jet developed with rapid bubble growth almost causing the complete disintegration of the core.

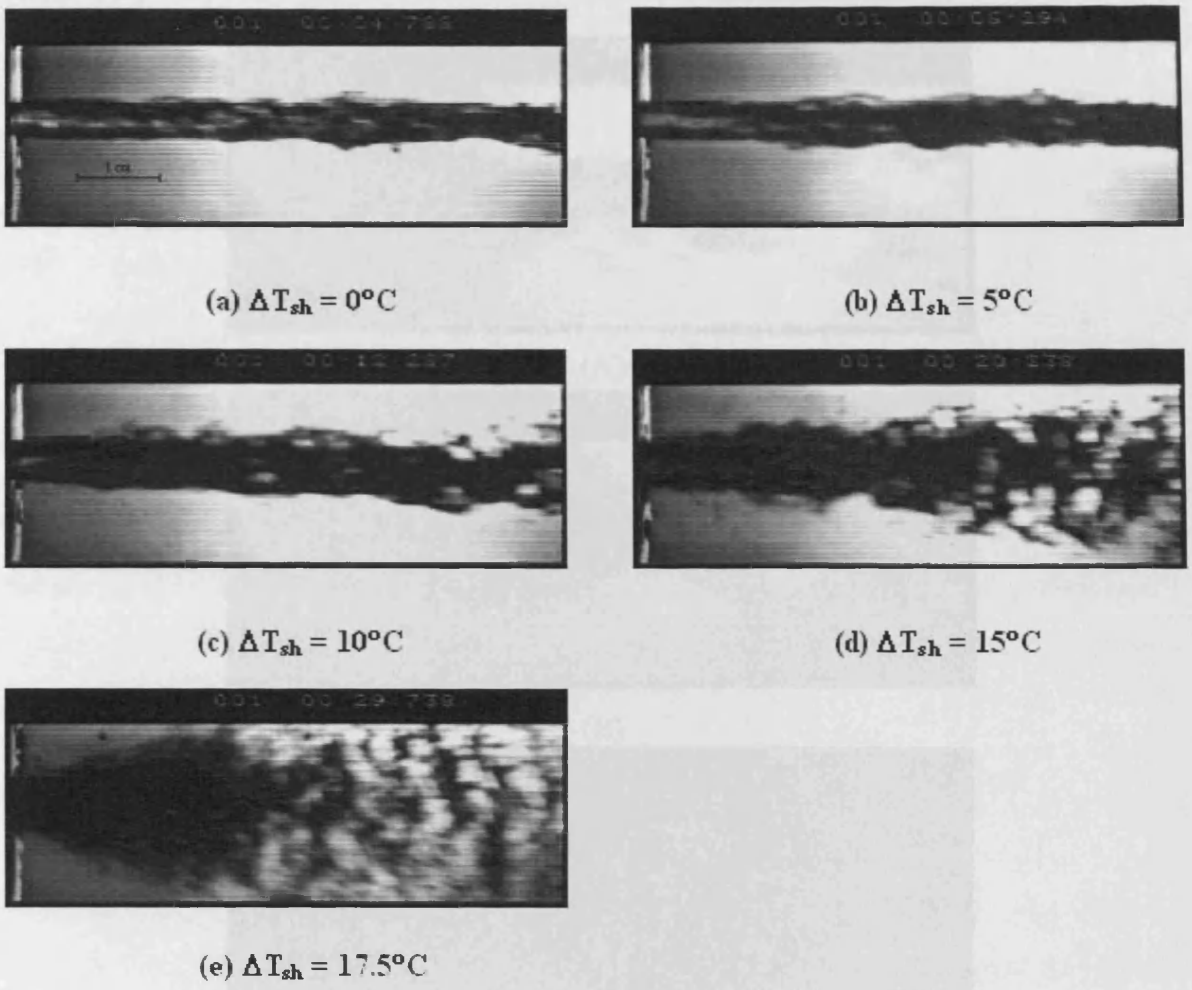

(a) $\Delta T_{sh} = 0°C$ (b) $\Delta T_{sh} = 5°C$

(c) $\Delta T_{sh} = 10°C$ (d) $\Delta T_{sh} = 15°C$

(e) $\Delta T_{sh} = 17.5°C$

Figure 6.1 Evolution of jet break-up with increasing temperature

6.2.1 Establishment of Jet Break-Up Transition Regimes

Three distinct stages of transition have been identified and are presented in Figure 6.2, where the nozzle diameter in each image was 2mm. Condition A is defined as the point at which downstream bubble growth replaces mechanical break-up as the dominant break-up mechanism. Bubbles were observed to shatter near the edge of the jet leaving a significant liquid core of finite length immediately downstream of the exit orifice, beyond which disintegration of the jet created a distinctive wide-angled spray. This regime also corresponds to the image in Figure 6.1(d). Figure 6.1(b) and Figure 6.1(c) present evidence of bubble

bursting in the jet at lower temperatures than that of transition condition A. However, aerodynamic processes were still dominant.

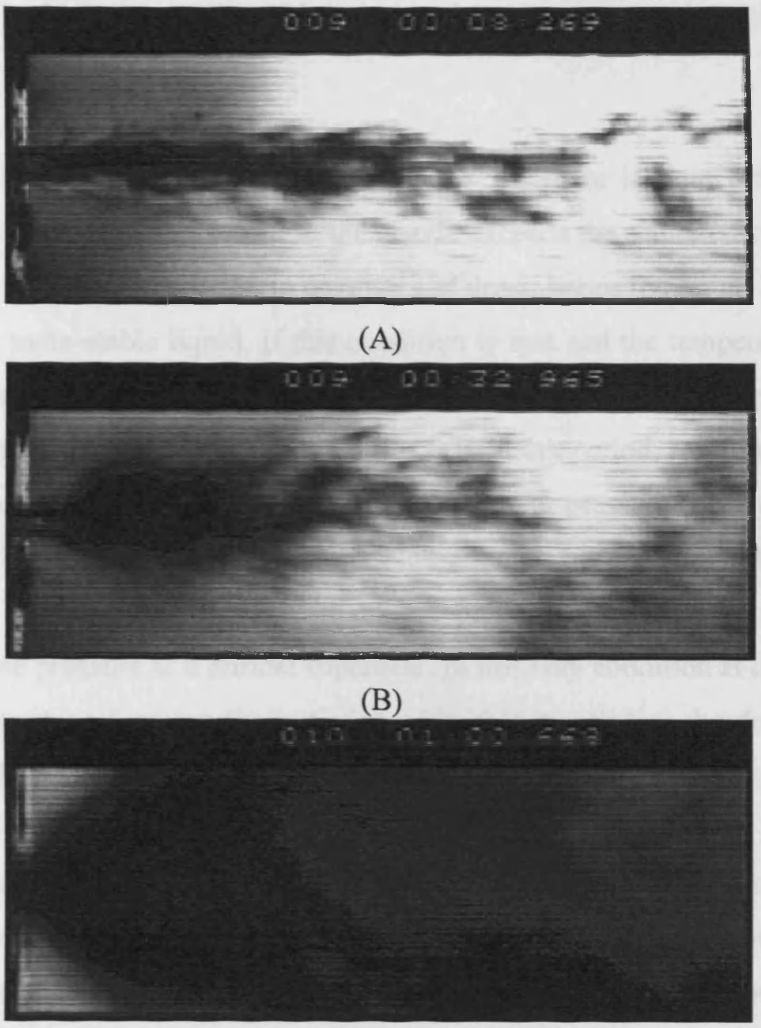

(A)

(B)

(C)

Figure 6.2 Stages of transition between break-up regimes

Condition B is characterised by an unbroken liquid core immediately downstream of the nozzle outlet, which exists as a single-phase meta-stable liquid above its normal boiling point. The liquid core completely disintegrates at a distance between 0.5 – 3 nozzle diameters downstream due to the rapid growth of bubbles nucleating in the jet. Kitamura *et al*[61] define a critical superheat for flashing based on this transition regime.

Condition C represents transition to full flashing and can be defined as the upper limit of development for a superheated jet. It is characterised by a barrel shaped spray, with violent

jet disintegration at the nozzle with no delay time for bubble growth, i.e. the liquid leaves the exit orifice as a two-phase jet. This indicates that annular flow occurs upstream of the nozzle outlet, caused by the high growth rate of multiple bubble nuclei generated by heterogeneous processes at the liquid/nozzle wall interface and molecular processes throughout the body of the fluid.

In terms of the physical processes occurring in the jet, there is little difference between conditions B and C. When the pressure in the nozzle exceeds the saturated vapour pressure it is impossible for stable bubble nuclei to develop and grow, hence the liquid leaves the nozzle as a single phase meta-stable liquid. If this condition is met and the temperature of the jet is sufficient, bubbles nucleate in the jet on release to atmosphere, which rapidly expand and cause the complete disintegration of the jet after a brief delay period, resulting in an unbroken liquid core immediately downstream. If the saturated vapour pressure is above the pressure in the nozzle, and the bubble nucleation rate is high enough, upstream bubble growth creates annular flow in the nozzle. For a given release pressure, the saturated vapour pressure exceeds the release pressure at a critical superheat. In this way condition B can be considered as an intermediate stage between the initiation of bubble bursting as the dominant break-up mechanism and the onset of complete flashing.

The conditions which govern transition between break-up phenomena can be defined in terms of a relatively simple relationship between the Jakob number and Weber number, presented in Figure 6.3. The Jakob number, presented by Equation (6.1), represents the non-dimensionalised superheat and the Weber number represents the ratio of inertia forces to surface tension forces.

$$Ja = \frac{\rho_l C_{pl} \Delta T_{sh}}{\rho_g H_{lg}} \qquad (6.1)$$

Included in Figure 6.3 are the experimental critical superheats for flashing observed by Kitamura *et al*[61], where water was the test fluid. These data are represented by comparatively high Jakob numbers and comparatively low Weber numbers because the tests were performed by spraying into an evacuated chamber, where the pressure ranged from 2.73 – 4.93 x10^3 Pa. Hence, the gas/vapour density in the chamber was between 100 – 200 times less than the gas/vapour density at atmospheric pressure. Jakob number is inversely proportional to the gas

density while Weber number is proportional to the gas density and hence these dimensionless numbers take on these very high and very low respective values.

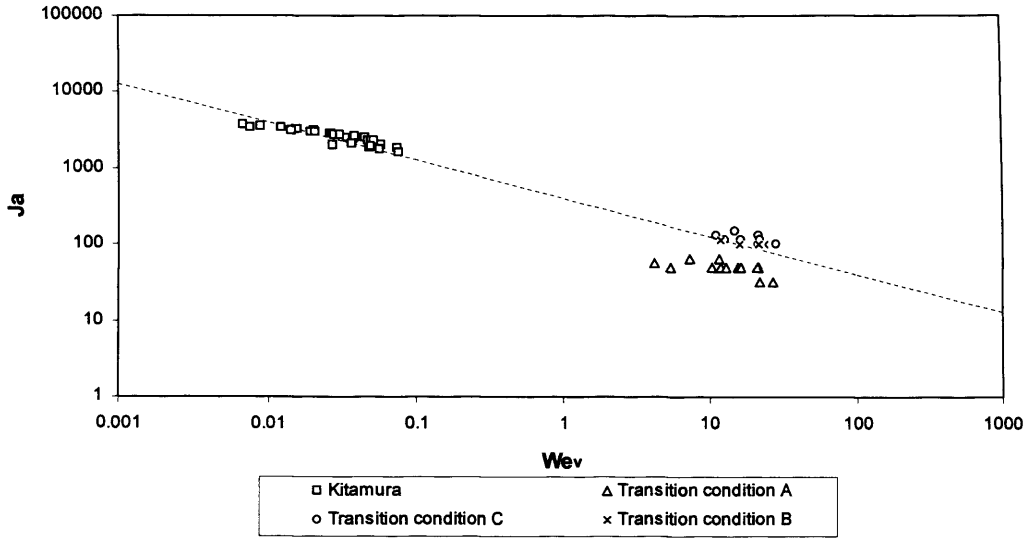

Figure 6.3 Critical Jakob number for flashing as a function of vapour Weber number

The data for transition to condition B agree extremely well with the critical superheat for flashing as defined by Kitamura *et al*[61]. This relationship is expressed in Equation (6.2).

$$Ja = 400We_v^{-0.5} \qquad (6.2)$$

6.2.2 Extension of transition criteria to other liquids

Flashing phenomena are controlled by bubble growth rates in superheated liquids[16,18,56]. Equation (2.25), reproduced here, is derived from Scriven's theory for motionless bubble growth[99], where the constant C is $(2\pi/3)^{0.5}$. Plesset and Zwick[100] also present this value for C, while Forster and Zuber[101] propose a value of $\pi^{0.5}$ in their analysis.

$$R = C\,Ja\left[\alpha(t-t_0)\right]^{0.5} \qquad (2.25)$$

Kitamura *et al*[61] compared the theoretical growth rates obtained using Equation (2.25) with various experimental datasets in the literature[58,143,144,145,146]. They found that while those experimental growth rates are in good agreement with Equation (2.25) at low superheats, those at high superheats are over-predicted by this formula. Hence, they present a reworking

of Equation (2.25)in the form of Equation (6.3), where ϕ is a correction factor, corresponding to the ratio of experimental to theoretical growth rates.

$$R = \phi Ja\left[\pi\alpha\left(\frac{x - x_0}{u_l}\right)\right]^{0.5} \qquad (6.3)$$

Kitamura *et al* go on to present ϕ as a function of the ratio of vapour to liquid density for a range of datasets including their own dataset for water, Hooper and Abdelmessih's dataset for water, Cole and Shuman's dataset for water, methanol and pentane, and Suzuki and Yamamoto's dataset for water. Kitamura *et al* show that all the data can be correlated by a single function as presented by Equation (6.4).

$$\phi = 1 - e^{-2300\left(\frac{\rho_v}{\rho_L}\right)} \qquad (6.4)$$

By modifying the Jakob number with the liquid to vapour density ratio, Kitamura *et* al demonstrate that the transition to flashing as defined by their own data for water and ethanol, and Brown and York's[16] data for water and Freon-11 can be described by one expression, presented in Equation (6.5).

$$Ja\phi = 100We^{-\frac{1}{7}} \qquad (6.5)$$

Presenting the correction factor ϕ in terms of a density ratio permits similarity scaling for use of the transition criterion with other liquids. In addition, Kitamura *et al*[61] show that this expression is representative of a range of liquids. Figure 6.4 presents Equation (6.5) with respect to the measured data and Kitamura's dataset for water.

Figure 6.4 also demonstrates that condition A and C can be correlated by variations on the critical superheat for condition B, as defined by Equation (6.5). The correlations governing transition to conditions A and C are presented by Equations (6.6) and (6.7) respectively.

$$Ja\phi = 55We_v^{-\frac{1}{7}} \qquad (6.6)$$

$$Ja\phi = 150We_v^{-\frac{1}{7}} \qquad (6.7)$$

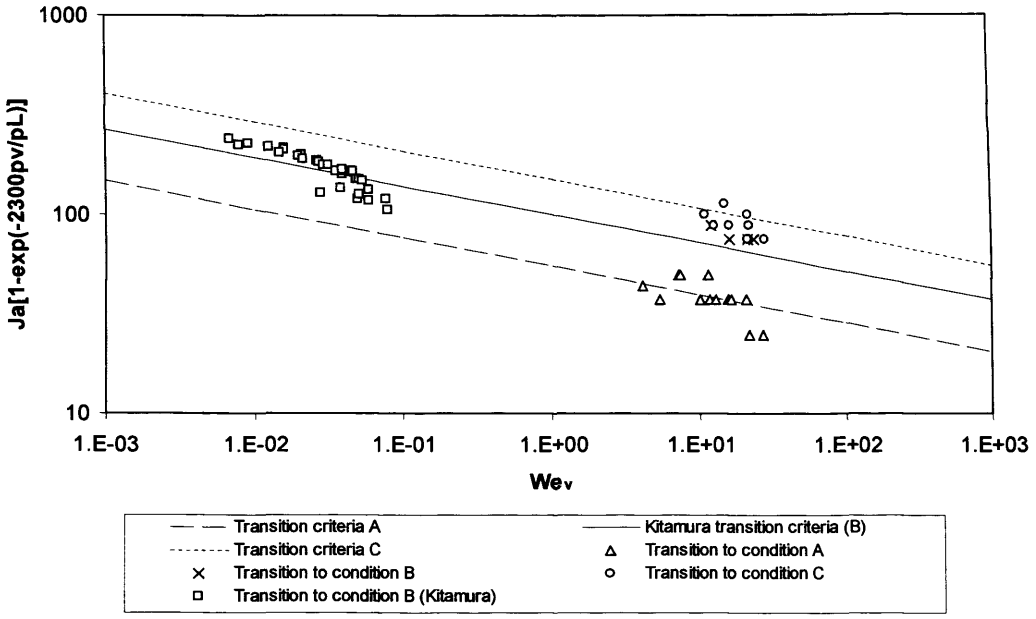

Figure 6.4 Critical Jakob number for three identified stages of transition

The scattering of data can be attributed in part to the difficulty encountered in identifying the exact conditions at which transition occurred. Equations (6.6) and (6.7) define precise conditions for the transition between break-up regimes, however, as determined by the results of the geometric characterisation in Chapter 5, the reality is that evolution of the break-up mechanism is a more gradual process. At the transition boundaries it was not unusual for the jet to display two break-up regimes in consecutive frames. For this reason, these transition criteria should be interpreted as guidelines rather than definitive points of reference.

The proximity of the data sets representing conditions B and C in Figure 6.4 confirms that the two processes are closely related. However, the exact nature of the differences in the upstream flow structure requires investigation. The relative impact of each process on the downstream droplet SMD also needs to be understood as it may confirm the assertion of Kitamura *et al* that condition B represents transition to full flashing, and would therefore necessitate the declassification of condition C as a separate break-up regime.

6.3 Laser Based Droplet Sizing

Droplet sizing of superheated jets was conducted using two laser-based techniques. The first of these is based on the principle of laser light scattering, and was performed using a Malvern Mastersizer X, composed of a Helium-Neon (He-Ne) laser with a conventional Fourier optical configuration. The second technique relies on Doppler interferometric theory, and was performed using a 1D DANTEC phase Doppler anemometry (PDA) system.

6.3.1 Laser Light Scattering

Laser light scattering relies on the fact that the diffraction angle of incident light scattered by a particle in a mono-chromatic beam is inversely proportional to the size of the particle. Droplet size measurements were taken at three axial locations of 350mm, 400mm and 450mm downstream. Radial measurements were performed at increments of 10mm in both positive and negative directions, taking the spray centreline as the origin. Tests were performed using a 2mm orifice diameter (1.7 aspect ratio) at one initial stagnation temperature (140 °C), which produced an average release temperature of 125 °C. At these conditions the jet was observed to be in transition from mechanical break-up to full flashing.

Figure 6.5 presents the measured droplet SMDs and corresponding obscuration rates at each downstream location where measurements were taken. For data validation purposes, 11-30% obscuration is considered ideal, 30-50% is considered high but useable and +50% is considered too high. According to these criteria 76% of the data is considered unreliable, while the remaining 24% is close to the upper limit for useable data. In addition the obscuration profile mirrors the diameter profile at each downstream location, which indicates that the two properties are not mutually exclusive. Hence, the data as a whole is considered unreliable.

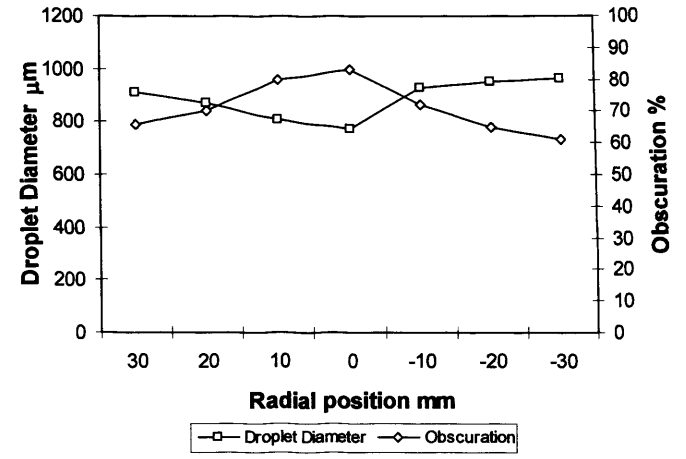

z = 350mm

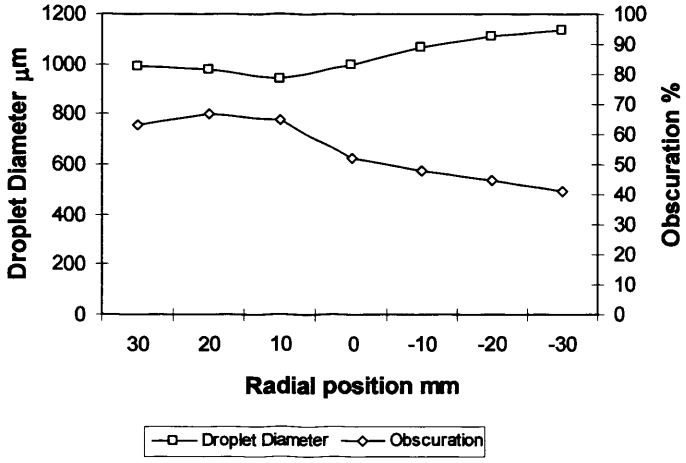

z = 400mm

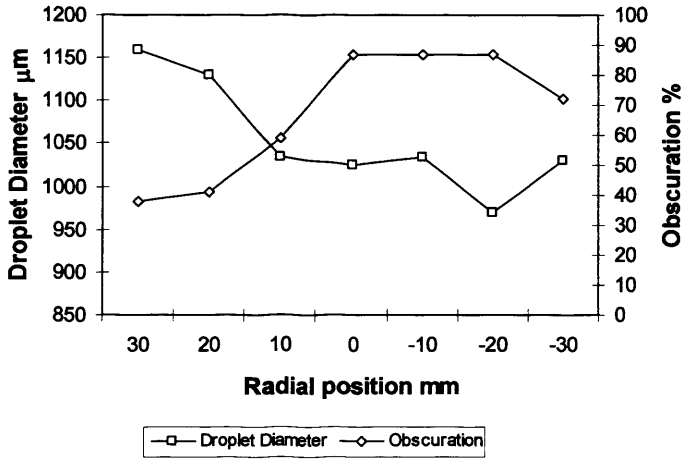

z = 450mm

Figure 6.5 Droplet diameter and obscuration at 350, 400 and 450mm downstream

A study undertaken by the HSL[119,120,121] which utilised the same diffraction technology to analyse droplet diameters in flashing sprays of LPG also encountered problems with laser obscuration. Post-processing of the data was performed in order to counteract the associated errors. However, in this instance the data is considered well beyond the range of applicability of corrective calibration equations. Hence, the only useful conclusion that can be drawn from the data is confirmation of the unsuitability of traditional diffraction technology for the environment of flashing sprays. Recent technological developments concerning this methodology have been aimed at alleviating this restriction for dense spray characterisation, though these have not been appraised within the scope of this study.

6.3.2 Phase Doppler Anemometry

Doppler interferometric theory relies on the fact that the phase shift between signals from light scattered by a particle entering the intersection (measurement volume) of two incident laser beams is directly proportional to the particle diameter. Droplet size measurements were taken at three axial locations of 250mm, 500mm and 750mm downstream. Radial measurements were performed at 11 sample points in the spray in both positive and negative directions, from one edge to the other, taking the spray centreline as the origin. Tests were performed using two orifice diameters of 1mm and 0.75mm (3.4 and 4.53 aspect ratio respectively) at one initial stagnation temperature (180 °C), which produced an average release temperature of 155 °C. At these conditions the jet was observed to be fully flashing, i.e. analogous to condition C-type flashing.

Droplet sizing was conducted once fully flashing conditions were established and the jet temperature and pressure had reached relative stability. The PDA system was set-up to record 15,000 samples with a 45 second timeout facility. Although release conditions were continually changing, once fully flashing conditions were established, jet temperature and release pressure could only be expected to vary by a maximum of 0.1°C and 0.05bar respectively during a 45 second period. For the purposes of dispersion modelling it was therefore assumed that conditions were stable during droplet sizing.

Results have been collated to produce 'cherry plots', which illustrate the distribution of droplet SMDs and axial components of velocity in the spray. These diagrams are presented

by Figure 6.6 and Figure 6.7 in two parts; the first part displays the measured droplet diameters in terms of a colour code, which corresponds to the scale given on the right of each figure. The droplets are also scaled so that the size of each circle is proportional to the measured droplet SMD. The mean axial velocity of particles at each sample point is presented as a velocity vector. The scale for these vectors is presented in the top left corner of each figure. The second part of each figure utilises a function of Matlab, which interpolates the data between each sample point to give an estimated droplet size distribution throughout the whole spray. At 750mm downstream, the width of the spray produced by the 1mm orifice diameter exceeded the operating parameters of the PDA rig. Hence, it was not possible to take droplet data in the outer region spray at this axial location. As a result, data from the edge of the spray is missing.

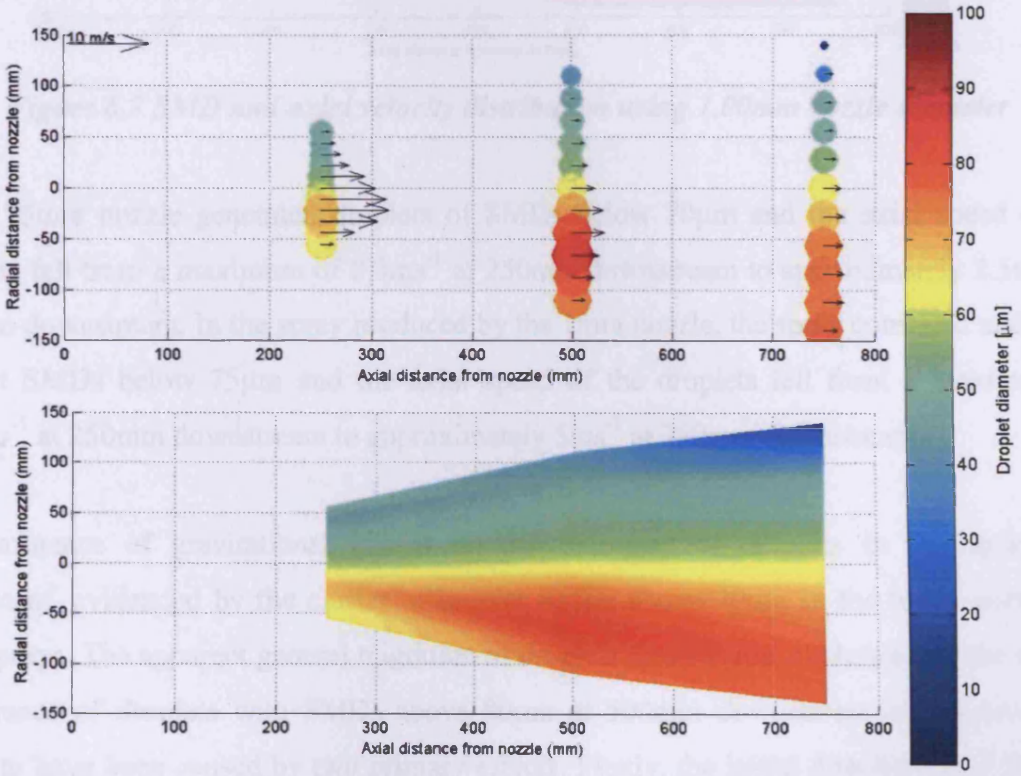

Figure 6.6 SMD and axial velocity distribution using 0.75mm nozzle diameter

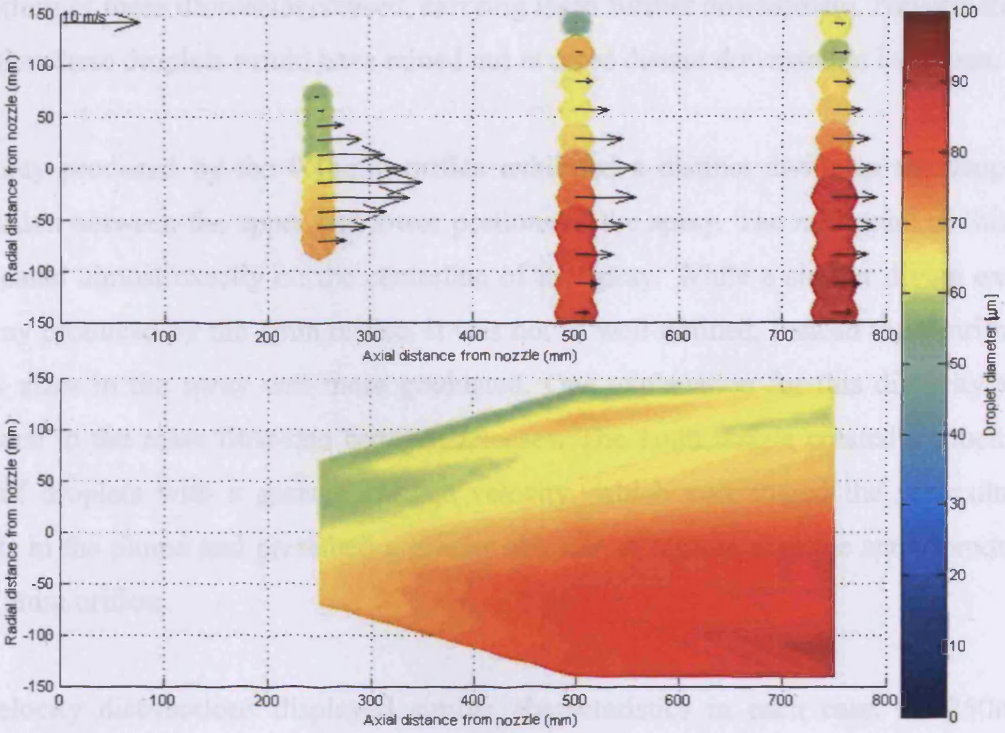

Figure 6.7 SMD and axial velocity distribution using 1.00mm nozzle diameter

The 0.75mm nozzle generated droplets of SMDs below 70μm and the axial speed of the droplets fell from a maximum of 8.3ms^{-1} at 250mm downstream to approximately 2.5ms^{-1} at 750mm downstream. In the spray produced by the 1mm nozzle, the spray consisted mainly of droplet SMDs below 75μm and the axial speed of the droplets fell from a maximum of 13.6ms^{-1} at 250mm downstream to approximately 5ms^{-1} at 750mm downstream.

The influence of gravitational effects on the trajectory of droplets in the spray was significant, evidenced by the cluster of droplet SMDs above 70μm in the lower portion of both sprays. The apparent general migration of droplets downwards, evidenced by the sudden appearance of droplets with SMDs above 80μm at 500mm downstream of the nozzle, is likely to have been caused by two primary effects. Firstly, the initial distribution of droplets within the spray separate so that the larger droplets rain out more quickly, whereas the smaller droplets are carried away with the plume. Secondly, it is possible that coalescence may be occurring due to the density of the spray. In the case of the 0.75mm nozzle diameter most of these droplets rained out at 750mm downstream. In the case of the 1.00mm nozzle diameter, the increase in orifice size created larger droplets with higher velocities. Hence the

momentum of these droplets increased, carrying them further downstream. Nevertheless, it is likely that these droplets would have rained out at more distant downstream locations.

The spray produced by the 0.75mm orifice exhibited a distinct divide in the droplet size distribution between the upper and lower portions of the spray. The mid-point of this divide was located almost exactly on the centreline of the spray. While a similar divide existed in the spray produced by the 1mm orifice, it was not as well-defined. Instead the distribution of droplet sizes in the spray was more graduated. One explanation for this disparity was the difference in the mass flow-rate between releases. The 1mm nozzle created a much denser spray of droplets with a greater average velocity, which encouraged the recirculation of droplets in the plume and presented a greater obstacle to rainout than the spray produced by the 0.75mm orifice.

The velocity distributions displayed similar characteristics in each case. At 250mm the velocity was shifted towards the lower region of the spray. This was due to the relative influence of aerodynamic drag on droplet trajectory with respect to droplet diameter, since this portion of the spray also contained the larger droplets. At each downstream location the average droplet velocity was approximately proportional to droplet SMD. As the droplets progressed further downstream the velocity reduced and the velocity profile flattened. The spray produced by the 1mm orifice contained droplets with higher average velocities than the 0.75mm orifice due to the increase in momentum through the larger exit orifice.

Table 6.1 displays the global SMDs of droplets in the sprays produced by both nozzles, where the data indicates that the droplet SMD increased with downstream distance.

Table 6.1 Measured global droplet SMD

Nozzle Diameter (mm)	Aspect ratio (L/d_0)	Downstream Distance (mm)	Global SMD (μm)	Standard Deviation
0.75	4.53	250	59.5	10.0
0.75	4.53	500	71.0	17.0
0.75	4.53	750	68.9	22.6
1.00	3.40	250	62.8	4.8
1.00	3.40	500	71.0	9.3
1.00	3.40	750	79.0	10.8

In the spray generated by the 0.75mm orifice, the SMD peaked at 500mm downstream due to the rainout of larger droplets at 750mm downstream. Significantly the increase in nozzle

diameter corresponded to an increase in droplet SMD. This is in accordance with both accepted theory and the findings from the study of sub-cooled jets presented in Chapter 4.

The standard deviation provides an indication of the scatter of data away from the mean. One positive or negative standard deviation from the mean accounts for approximately 68 percent of the data. Two standard deviations from the mean accounts for approximately 95 percent of the data. Close to the nozzle, the droplet size distribution in a spray is dictated by the release conditions. As droplets progress further downstream aerodynamic influences, coalescence and rainout dominate. Hence the scatter increased with downstream distance. As a result, for the purposes of atmospheric dispersion modelling, post-expansion data was taken at 250mm downstream, at which point it was assumed that dynamic jet break-up was complete and the effect of coalescence and rainout was least significant.

Smaller droplets in a spray contribute to a very small percentage of the total volume of released liquid. Hence, the SMD is not significantly influenced by these droplets. However, it is these droplets that remain airborne and disperse in the atmosphere, which in the case of flammable or toxic chemicals will form the principle hazard associated with an accidental release. The standard deviation can be used as means of indicating the total volume of the spray contained in these smaller droplets. Figure 6.8 and Figure 6.9 present the validation rates of the recorded data at each spatial location where measurements were taken. The high percentages attained are indicative of a good set-up and a well atomised spray. Lower validation rates were attained using the 1.00mm orifice due to the increase in the density of the spray. Nevertheless, the validation rates are still predominantly in the high 80-90% region. The sphericity approached 100% in all cases, which is also indicative of a good setup and reliable data.

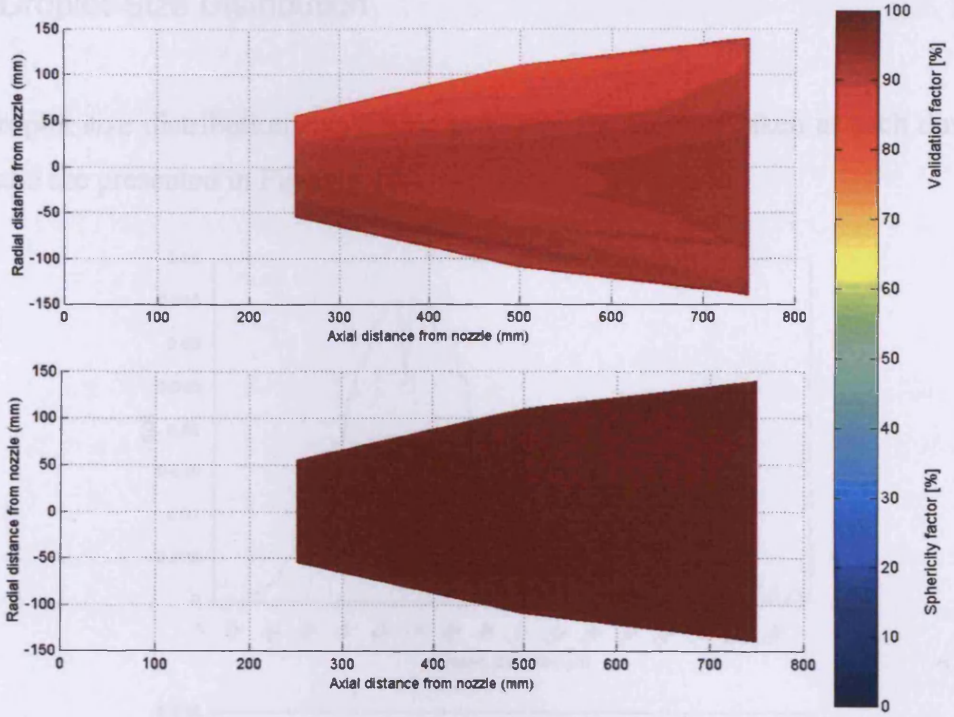

Figure 6.8 Validation rates associated with results from the 0.75mm nozzle

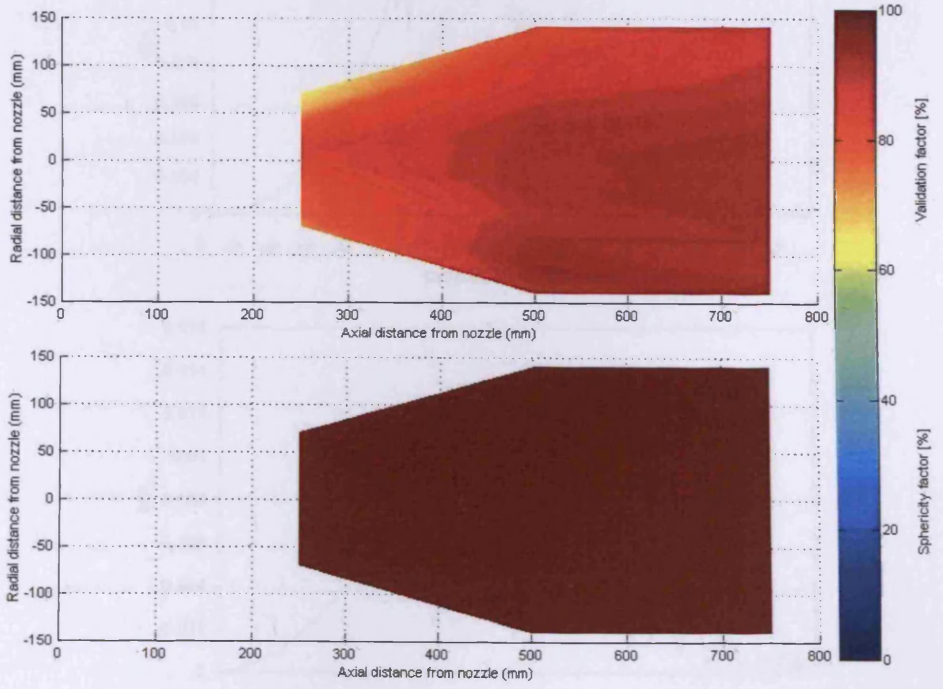

Figure 6.9 Validation rates associated with results from the 1.00mm nozzle

6.3.2.1 Droplet-Size Distribution

Global droplet size distributions have been produced for the data taken at each downstream location and are presented in Figure 6.10.

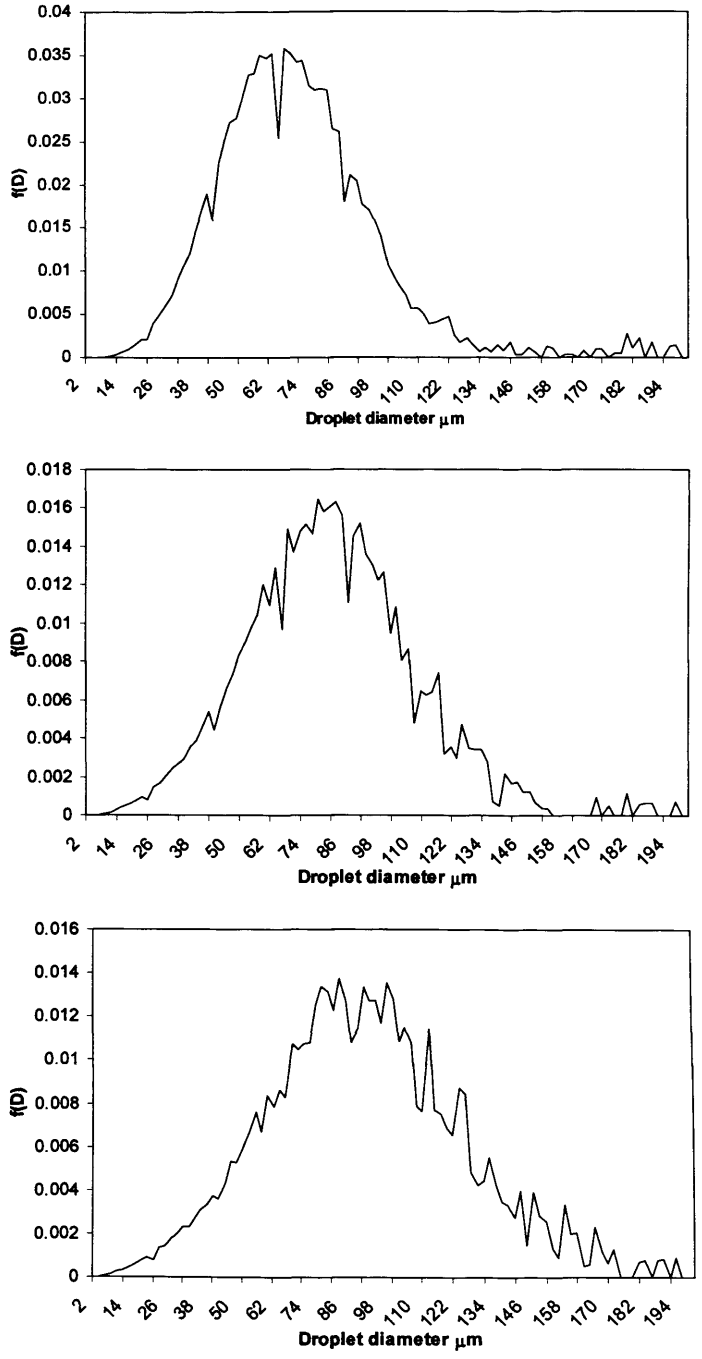

Figure 6.10 Droplet size distributions using 1mm nozzle diameter, at 250, 500 and 750mm downstream.

At 250mm and 500mm downstream, the distributions demonstrate relatively symmetrical Gaussian profiles. At 750mm downstream, the distribution is slightly less well defined, owing to the fact that as mentioned it was not possible to traverse the whole spray at this location, hence there are some points missing from this dataset. It is possible to observe how the droplet SMD increases with downstream distance in the above figures, as the peak of each distribution profile shifts towards the right.

Figure 6.11 presents the volume undersize distribution for the experimental data produced using the 1mm nozzle at 250mm downstream. Also included is the log-normal distribution recommended in the literature[15], presented by Equation (6.8), Elkotb's[34] version of the Rossin-Rammler distribution, and a modified version of this equation based on the experimental data, presented by Equation (6.9).

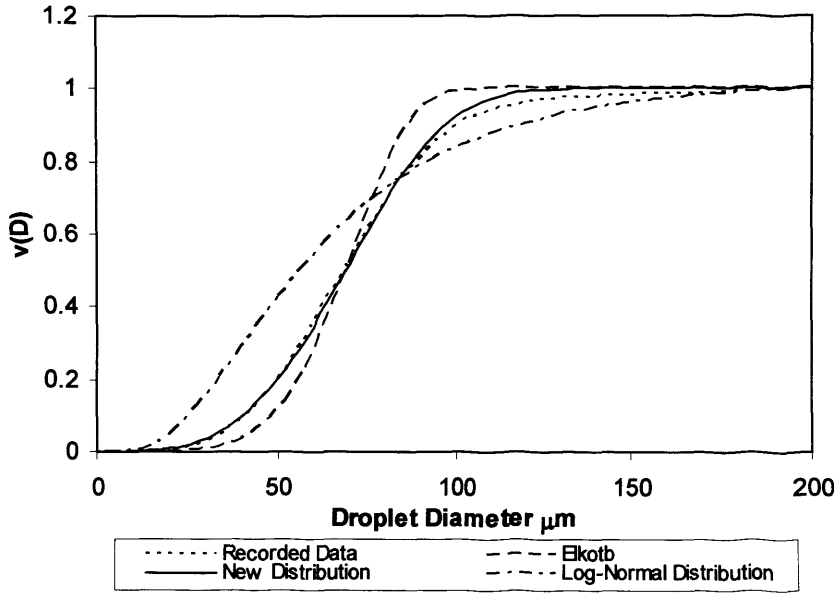

Figure 6.11 Fully flashing volume undersize distribution (Nozzle =1mm, SMD=62.8μm)

$$f(d_p) = \frac{p(t = d_p / d_{pm})}{d_p}, \text{ with } p(t) = \frac{1}{(2\pi)^{0.5} \ln(\sigma_G)} \exp\left[-0.5\left(\frac{\ln t}{\ln(\sigma_G)}\right)\right]^2 \qquad (6.8)$$

$$1 - v(D) = e^{-0.5\left(\frac{D}{SMD}\right)^{3.5}} \qquad (6.9)$$

The form of the modified Rossin-Rammler distribution clearly represents the recorded data most accurately of the three correlations presented. Hence, this distribution equation is proposed for modelling of droplet sizes in fully flashing sprays.

6.4 Complete SMD model for transition to flashing

The proposed SMD correlation for sub-cooled sprays, the established criteria for transition from mechanical break-up to full flashing, and the PDA data for fully flashing sprays have been combined to produce a complete SMD model governing transition from mechanical break-up to full flashing, based on Muralidhar's[12] simple model for liquid 'capture' outlined in Chapter 2. The results are summarised by Witlox *et al*[147,148] and Cleary *et al*[149,150].

A linear relationship is assumed to exist between superheat and droplet SMD during the intermediary stage of transition, which begins with the end of mechanical break-up and intercepts the measured droplet SMDs for full flashing at 250mm downstream. It is difficult to obtain high quality atomisation with droplet SMDs of 30μm or less, even with dynamic processes such as those which occur during superheated releases[22]. For this reason, the linear relationship is extrapolated until a droplet SMD of 30μm is achieved, after which point it is assumed that droplet size decreases slowly at a nominal rate of 1μm for every 10°C increase in superheat.

Figure 6.12 and Figure 6.13 present the model diagrammatically for a release at 10bar (gauge) through a 0.75mm and 1mm nozzle respectively. Transition conditions A and C outlined in section 6.1.3 are represented by red, vertical dashed lines. In order to extend the model to the full range of possible initial conditions it is recommended at this stage of development that the ratio of droplet SMD at the first stage of transition to the final stage of transition, here taken to be 5, be adopted for all potential release scenarios.

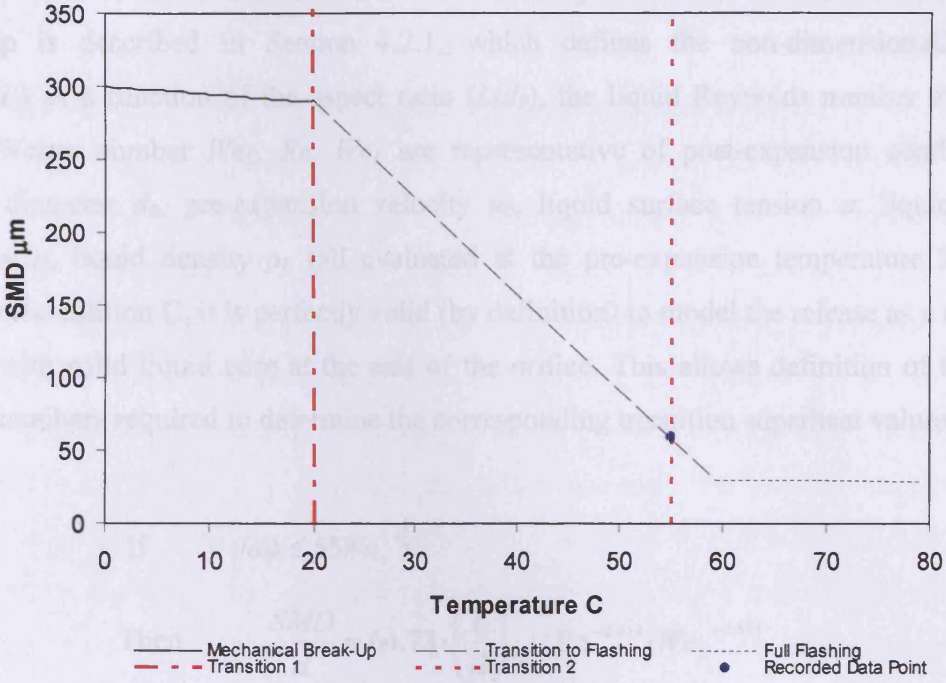

Figure 6.12 Transition from mechanical break-up to full flashing (10 bar gauge; 0.75mm nozzle)

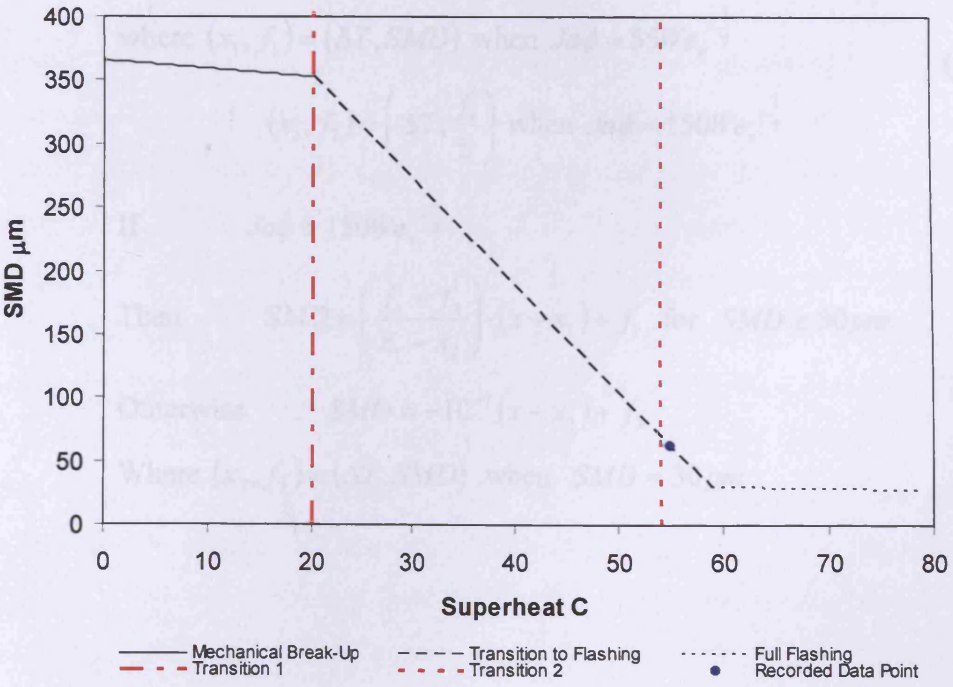

Figure 6.13 Transition from mechanical break-up to full flashing (10 bar gauge; 1.00mm nozzle)

Equation (6.10) summarises the model in its entirety. The SMD correlation for mechanical break-up is described in Section 4.2.1, which defines the non-dimensionalised SMD (SMD/d_0) as a function of the aspect ratio (L/d_0), the liquid Reynolds number Re, and the liquid Weber number We_L. Re, We_L are representative of post-expansion conditions, i.e. nozzle diameter d_0, pre-expansion velocity u_0, liquid surface tension σ, liquid dynamic viscosity μ, liquid density ρ_L (all evaluated at the pre-expansion temperature T_0). Up to transition condition C, it is perfectly valid (by definition) to model the release as a metastable liquid, with solid liquid core at the exit of the orifice. This allows definition of the critical Weber numbers required to determine the corresponding transition superheat values.

$$
\begin{aligned}
&\text{If} \quad Ja\phi \le 55We_v^{-\frac{1}{7}} \\
&\text{Then} \quad \frac{SMD}{d} = 64.73 \cdot \left(\frac{L}{d}\right)^{0.114} \mathrm{Re}^{-0.014} \cdot We_L^{-0.533} \\
&\text{If} \quad 55We_v^{-\frac{1}{7}} < Ja\phi \le 150We_v^{-\frac{1}{7}} \\
&\text{Then} \quad SMD = \left(\frac{f_1 - f_2}{x_1 - x_2}\right) \cdot (x - x_1) + f_1 \\
&\text{where } (x_1, f_1) = (\Delta T, SMD) \text{ when } Ja\phi = 55We_v^{-\frac{1}{7}} \\
&\qquad (x_2, f_2) = \left(\Delta T, \frac{f_1}{5}\right) \text{ when } Ja\phi = 150We_v^{-\frac{1}{7}} \\
&\text{If} \quad Ja\phi > 150We_v^{-\frac{1}{7}} \\
&\text{Then} \quad SMD = \left(\frac{f_1 - f_2}{x_1 - x_2}\right) \cdot (x - x_1) + f_1 \quad \text{for} \quad SMD \ge 30\mu m \\
&\text{Otherwise} \quad SMD = -10^{-7}(x - x_3) + f_3 \\
&\text{Where } (x_3, f_3) = (\Delta T, SMD) \text{ when } SMD = 30\mu m
\end{aligned}
\qquad (6.10)
$$

6.4.1 Validation of Proposed Model

Det Norske Veritas Ltd (DNV) is a risk management company that has developed a number of specialised software packages for design, strength assessment, risk analysis, asset life cycle management and knowledge based engineering. In early 2000, DNV released Version 6.0 of their consequence modelling package PHAST, which includes models for the discharge of hazardous chemicals to atmosphere, including the discharge model DISC and the atmospheric expansion model ATEX. In PHAST 6.0, ATEX calculates the initial droplet size using the model proposed by Johnson and Woodward[15] in the CCPS book, which is explored in section 2.4.1. Essentially, the model assumes two possible mechanisms for droplet formation, i.e. mechanical break-up or flashing, and then selects the droplet diameter calculated by the mechanism that gives the smallest value. DNV has recently implemented the model proposed in the previous section into Modelling Development Environment (MDE) spreadsheets which are methods/procedures used to develop its mathematical consequence and risk models, of which DISC and ATEX form a part. Users of PHAST have been provided with these spreadsheets and the model is planned to be made available in a new version of PHAST in the near future.

In this section the results of a series of validation studies are presented where the droplet diameters predicted by the version of ATEX in PHAST Version 6.0 (the CCPS correlation) and the version of ATEX updated using the MDE spreadsheets (the proposed correlation) are compared with experimental data from a range of studies including the STEP programme[1], a study by the Von Karman Institute (VKI)[123] and experiments performed by both the Ecole des Mines and INERIS as reported by Touil *et al*[151]. Comparisons are also made with the correlation recommended in the TNO Yellow Book[128], i.e. the method for initial droplet-size calculation based on the work by Appleton[50] and presented by Wheatley[49], previously highlighted in section 5.6 by Equation (5.22). An additional comparison is made between the droplet SMD predicted by the proposed model and data from the HSL experiments[119,120,121]. The results of these validation studies are summarised by Witlox *et al*[152,153].

The liquid used in the STEP experiments was 99.5% propane and 0.5% butane, but was modelled as 100% propane. The authors used intrusive 'protection cylinders' in the spray,

causing an estimated 20% under evaluation of droplet size, which is taken in to account here. Results are presented for only one set of release conditions, for which the most experimental data was available, i.e. a 5mm orifice diameter and 11bar initial pressure. Under these conditions the authors report a rapid pressure drop from 10barg to 9.5barg between 1 and 6 seconds after start of release. Hence, the storage pressure is taken as the average pressure during this period, i.e. 10.75bar (absolute). The observed flow rate was approximately 0.2kgs^{-1}, from which the jet velocity at the orifice has been determined. The value of L/d_0 is assumed to be sufficiently small as to be modelled as zero. Figure 6.14 presents the validation of the ATEX SMD correlations against the STEP experiment. The CCPS flashing correlation over-predicts the droplet SMD. However, in ATEX, the CCPS correlation selects the droplet diameter calculated by the mechanism that gives the smallest value. Hence, the outputted droplet size is given by the CCPS mechanical break-up correlation, which under-predicts the droplet SMD. The TNO Yellow Book correlation grossly over-predicts the droplet SMD. The proposed correlation provides close agreement with the experimental data point.

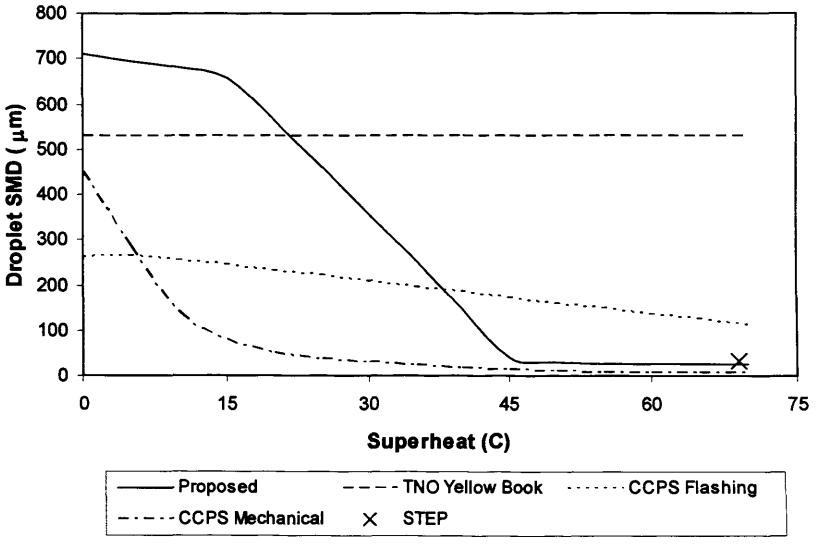

Figure 6.14 Validation of ATEX SMD correlations against STEP experiment

In the VKI experiments, the liquid used was the refrigerant R134-A, which corresponds to 1,1,1,2-tetrafluoroethane[154] (CAS ID 811972). The global SMD quoted has been estimated from the spatially distributed SMD values quoted in the paper. The storage pressure was 8.25bar and the orifice diameter was 1mm, but again, the value of L/d_0 is assumed to be sufficiently small as to be modelled as zero. Figure 6.15 presents the validation of the ATEX SMD correlations against the VKI experiment. Again, the CCPS flashing correlation over-

predicts the droplet SMD, but again the outputted droplet size is given by the CCPS mechanical break-up correlation, as this mechanism provides the smallest droplet diameter of the two. However, as before, the CCPS mechanical break-up correlation under-predicts the measured droplet SMD. As in the case of the STEP experiment, the TNO Yellow Book correlation grossly over-predicts the droplet SMD. The proposed correlation under-predicts the experimental data point but provides the closest agreement of the three correlations.

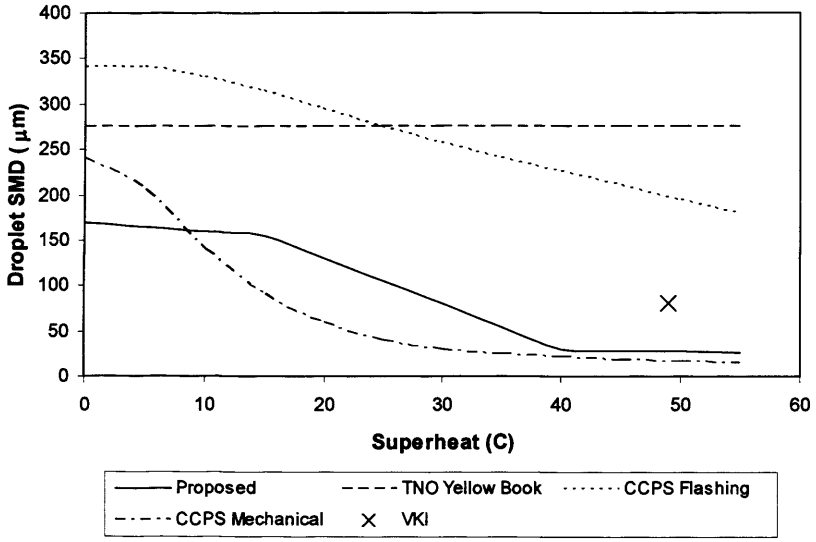

Figure 6.15 Validation of ATEX correlations against VKI experiment

In the Ecole des Mines experiments the liquid used was water. The results from two experiments are presented where the storage pressure was 9.2bar and 11.4bar and the storage temperature was 164°C and 167°C respectively. In both cases the orifice diameter was 2mm and again, the value of L/d_0 is assumed to be sufficiently small as to be modelled as zero. A PDA set-up with a droplet diameter range of 0-600μm was used to generate the droplet data. For the purposes of distinguishing between these two sets of initial conditions, the experiments are labelled EdM1 and EdM2. In each case two alternative points are given for the experimental data; the first (smallest) is for D<150μm and the second (largest) is for the entire droplet population including 150<D<600μm. This is because the droplet size distributions exhibited a peak in the range 0-150μm, consistent with data produced through this study and others in the literature, as well as a secondary peak in the range 150<D<325μm, not previously reported. Additional 'residual' droplets were also detected in the range 325<D<600μm, which despite their low number, constitute a large fraction of the liquid mass since the mass is proportional to D^3. The authors claim that this is evidence for

bi-modal droplet break-up, i.e. different portions of the spray are subject to different break-up mechanisms; one portion of the spray undergoes flashing while the other portion is still subject to mechanical break-up. This bi-modal droplet size distribution was not detected in the course of this study, despite a PDA set-up with a droplet diameter range of 0-385μm being used. Hence, this phenomenon requires further investigation. Quoting two droplet SMDs in this way means that data can be compared on a like-for-like basis, while consideration can be made for the possibility of a bi-modal distribution while remaining non-committal on the actual existence of this trend. Figure 6.16 and Figure 6.17 present the validation of the ATEX correlations against the Ecole des Mines experiments.

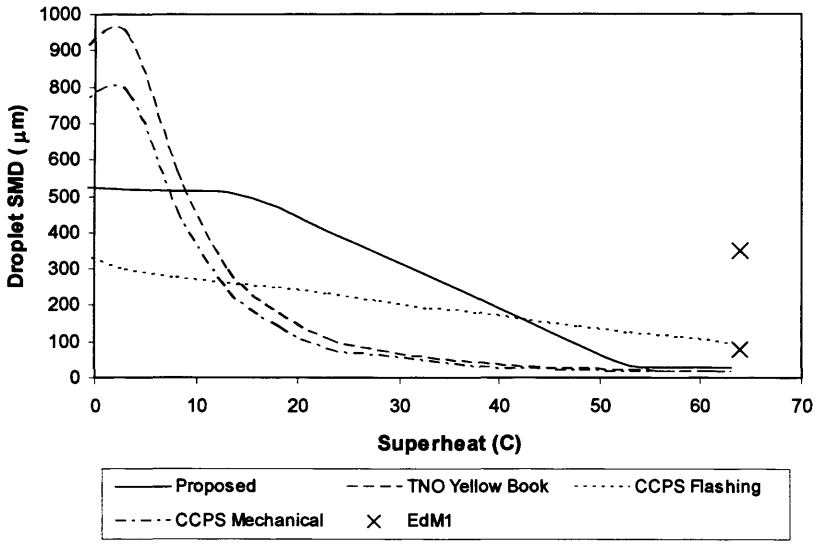

Figure 6.16 Validation of ATEX correlations against experiment EdM1

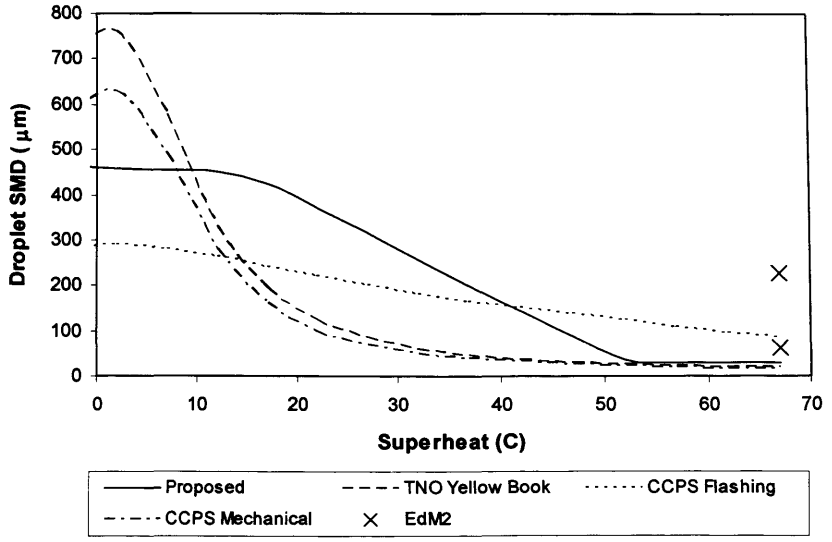

Figure 6.17 Validation of ATEX correlations against experiment EdM2

In both cases, the CCPS flashing correlation over-predicts the droplet SMD for D<150μm. The CCPS mechanical break-up correlation under-predicts the droplet SMD and, being the lower of the two, is the outputted droplet size. The TNO Yellow Book correlation also under-predicts the droplet SMD. The proposed correlation under-predicts the experimental data point but provides the closest agreement of the three correlations. In both cases each correlation grossly under-predicts the droplet SMD for 0<D<600μm. However, this is to be expected given the detection of a significant proportion of droplets with diameters in the range 150<D<600μm not normally associated with flashing jets.

In the INERIS experiment the liquid used was butane. The storage pressure was relatively low at 3 bar and the orifice diameter was 5mm. Figure 6.18 presents the validation of the ATEX correlations against the INERIS experiment. The CCPS flashing correlation over-predicts the droplet SMD, but the outputted droplet size is given by the CCPS mechanical break-up correlation, as this mechanism provides the smallest droplet diameter of the two. In this instance the CCPS mechanical break-up correlation provides reasonably good agreement with the measured droplet SMD, as does the TNO Yellow Book correlation. However, the proposed correlation greatly over-predicts the experimental data.

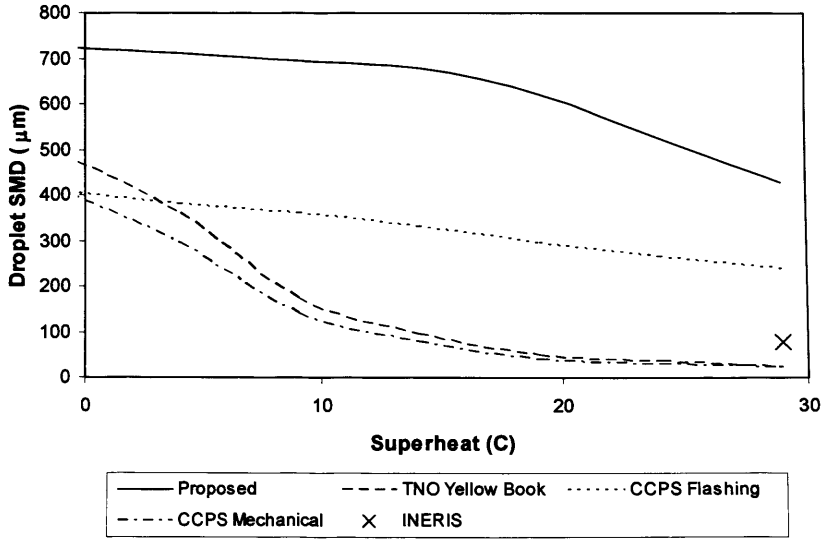

Figure 6.18 Validation of the ATEX correlations against INERIS experiment

In the HSL experiments a Malvern Mastersizer X was used to generate droplet size data. However, problems were encountered in terms of obscuration, with the system operating

outside its usual range of applicability. The author makes use of calibration equations in post-processing of the data to provide quantitative analysis and hence it is necessary to regard the data with a degree of caution. The data is effectively presented in terms of a droplet size distribution, and hence the global SMD has had to be derived assuming the form of the droplet size distribution proposed in this study. In this instance neither PHAST 6.0 nor the updated MDE spreadsheets have been used to predict the droplet SMD, but the droplet SMD predicted by the proposed correlation has been calculated for comparison with the data. Table 6.2 presents the data as part of a summary of the validation studies detailed in this section.

Table 6.2 Summary of validation studies for the proposed model and models included in PHAST 6.0 against experimental data in the literature

Experiment	STEP	VKI	E des M	E des M	INERIS	HSL
Experimental Conditions						
Material	Propane	R134-A	Water	Water	Butane	Propane
Storage pressure (bar)	10.75	8.25	9.2	11.4	3	7.5
Storage temperature (C)	27.1	23	164	167	23.85	16
Orifice diameter (mm)	5	1	2	2	5	4
Aspect Ratio (L/d_0)	0	0	0	0	0	10
Flow-rate (kg/s)	0.2	-	0.08	0.09	-	-
Measurements						
Downstream location (mm)	95	187	200	200	200	500
Measured SMD (μm)	32.4	80-100	79	61	80	50
Model Predictions						
TNO Yellow Book (μm)	531	286	888	694	487	-
Yellow Book (isentropic) (μm)	4.6	15.1	15.2	13.8	36	-
CCPS flashing (μm)	97.2	197	97.9	90.6	264	-
CCPS mechanical break-up (μm)	3.8	12.6	12.7	11.5	30	-
Proposed (μm)	26.3	28.7	28.8	28.2	522	29.6

The proposed model is based on PDA data taken at 250mm downstream of the exit orifice. This was considered to be sufficiently far downstream for jet break-up to be complete, and that spray density would not limit optical access of the laser. As flashing jets break-up considerably earlier than those undergoing mechanical break-up, well-established sprays exist considerably closer to the exit orifice. The only data-set which was produced at an axial location significantly upstream of the point at which the model was developed was the STEP data, which itself was limited by flow field obstructions used to mitigate the dense-spray issue. The VKI, Ecole des Mines and INERIS datasets were obtained within a similar downstream region and are therefore comparable with the conditions under which the model was developed. The HSL data was taken at twice the downstream distance at which data was collected in the course of this study. Hence, the downstream distances utilised in obtaining

the VKI, Ecole des Mines and INERIS datasets are considered a good compromise given the experimental limitations, and hence provide the most suitable comparisons with the proposed model.

Ironically the proposed model under-predicts the data produced by the VKI and the Ecole des Mines, over-predicts the INERIS data and provides close agreement with the STEP data. There is reasonable agreement with the HSL experiments, although as previously stated, it is necessary to treat this data set with a degree of caution. In most cases the proposed correlation provides the closest agreement with the experimental data, although this is partly because the CCPS book erroneously advises to take the minimum of the droplet sizes derived from the mechanical break-up and flashing correlations. This assumption consistently results in the under-prediction of droplet sizes. It also incorrectly describes the effect of increasing superheat; in the sub-cooled region the minimum SMD is frequently given by the flashing correlation while in the superheated region the minimum SMD is frequently predicted by the mechanical break-up correlation. This demonstrates the need for appropriate transition criteria as included in the proposed correlation. Nevertheless, the validation studies indicate, particularly in the case of the INERIS butane experiment, that the accuracy of the new correlation could potentially be improved by modifying the form of the correlation between transition points. This would require significantly more droplet size measurements at various degrees of superheat.

Overall, the level of agreement obtained with the referenced datasets provides sufficient evidence to justify the approach to extending the model to other fluids outlined in Section 6.4. However, the necessity to further improve the accuracy of the correlation through the measurement of droplet SMDs in sprays produced by a wide range of materials is clearly a matter of high priority for future studies. Nevertheless, in the meantime, it is felt that the proposed model provides a better characterisation of droplet SMDs in liquid releases undergoing flashing atomisation than those proposed previously.

6.5 Summary

A quantitative experimental methodology for identifying transition from mechanical break-up to full flashing has been designed and implemented, allowing comparison of transition data

with the correlation previously proposed by Kitamura *et al.* The current dataset has been demonstrated to be consistent with the correlation advocated by Kitamura *et al*, based on the Weber number and Jakob number, modified by a correction factor derived from the difference between theoretical and measured bubble growth rates in superheated jets. Hence, it is proposed that this correlation is adopted until a broader dataset for a range of materials becomes available.

Three distinctive stages of transition have been identified for the break-up of superheated jets from the mechanical regime to full flashing. Two equations governing the starting point and end point of transition have been produced and recommended for modelling purposes.

Traditionally laser diffraction based techniques have been shown to be inadequate for investigating large-scale pressurised releases of superheated jets; it is not possible to comment on recent developments for dense spray measurements. Although calibration equations exist, the obscuration rates associated with recorded data precluded the application of these equations to the current dataset. Consistent with the recommendations of the literature review, PDA has been shown to be currently the most suitable optical technique for characterisation of flashing jets.

PDA data for fully flashing sprays at two release conditions have been presented and discussed. Close to the orifice exit, the release conditions dominate the droplet size distribution, while aerodynamic influences, coalescence and rainout begin to take over as droplets move further downstream. Hence, post-expansion data was taken at 250mm downstream, at which point it was assumed that dynamic jet break-up was complete and the effect of coalescence and rainout was least significant.

A correlation for the droplet size distribution has been proposed based on the common Rossin-Rammler distribution. The proposed correlation demonstrates good agreement with the recorded data and represents a significant improvement on previously proposed droplet distributions.

The SMD correlation for mechanical break-up proposed in chapter 4, the established transition criteria and the PDA data have been combined to produce an SMD model governing complete transition from mechanical break-up to full flashing, based on

Muralidhar's simple model for liquid 'capture', outlined in Chapter 2. In the absence of data, a linear relationship has been assumed to exist between droplet SMD and superheat during the intermediary stage of transition.

The model has been validated against experimental data from a range of studies. Since the model was developed based on data generated using water as the model fluid, the lack of data for different materials is considered the most significant deficiency at this stage of understanding. Hence, although it provides an improvement on previously proposed models for superheated releases, there is still considerable research and development required to appraise, consolidate and develop some of the assumptions and modelling approaches adopted in this study. Nevertheless, the level of agreement between the model and experimental data in the literature provides confidence in extending the model for use with fluids other than water until a more comprehensive dataset becomes available.

6.6 Future Work

Given the current structure and relative simplicity of the SMD model for superheated sprays, the main priority for future work should be to provide data representative of conditions between the departure from mechanical break-up and fully flashing conditions

This experimental programme was restricted in terms of scale of release, due to the density of the spray for larger orifice sizes (Reynolds numbers). Further work should aim to utilise new developments in droplet size diagnostics, specifically focussed on dense-spray applications, which allow the measurement of releases for high mass flow-rates to the undertaken.

It is unlikely that a discontinuous linear correlation between the various modes of breakup is appropriate. Methods and models for characterising non-linear effects should be considered. For example, a two-phase model would be more appropriate after fully flashing conditions have been attained, and the presumed 'slow' linear decay of droplet size with superheat after the SMD has reached 30um requires appraisal. In addition the influence of orifice characteristics on droplet SMD in superheated jets needs to be investigated further.

Subject to constraints of the measurement technique, the feasibility of measuring the effect of superheat on droplet SMD in one complete sweep from sub-cooled to fully flashing sprays should be appraised. This would facilitate the direct comparison of the actual correlation function with that presumed (discontinuous linear function) in this study.

The development of a superheated rig capable of decoupling release pressure from the internal stagnation temperature is necessary for a more comprehensive evaluation of the impact of these input variables on the resultant spray characteristics.
This study has only considered water and, as with the results achieved for sub-cooled releases, a similarity scaling approach has been utilised to allow predictions of other materials in lieu of data. Hence, the influence of variation in fluid properties on the proposed correlation needs to be assessed. This could have the affect of modifying the correlation, or require the introduction of additional dimensionless groups.

Whilst the focus of this work has been to develop simplified, semi-empirical models, more detailed modelling approaches for two-phase atomisation would also be beneficial and complementary to this study.

Chapter 7 Upstream Flow Structure of Superheated Jets

7.1 Introduction

In this chapter the results from a high-speed photographic study of the upstream flow structure of superheated jets are presented for a range of orifice geometries and release conditions where the nozzle material was Perspex.

Upstream conditions are categorised in terms of the bubble growth rate (given as the average measured growth rate), delay time and concentration. The Rayleigh equation[98] for bubble growth is found to adequately represent the data and two non-dimensionalised equations governing the delay time and bubble concentration are recommended for modelling purposes. A simple model for determining the downstream break-up regime is presented in terms of the upstream bubble growth rate and bubble concentration.

Backlit shadowgraphs of the upstream flow structure were taken using a Photron Fastcam-APX RS high-speed camera, which was used to record images at a range of frame rates between 3,000 and 75,000fps. Due to the high frame rates and short filming time, conditions were assumed to be constant between frames. Nevertheless, pressure and temperature were monitored at 1000Hz. In some cases, for various reasons, including calibration of the image intensifier, complexities in the upstream flow structure and poor illumination, the recorded image quality required additional post-processing to facilitate edge detection of bubbles in the flow. The software programme Corel Photo-Paint was used for this purpose, which includes various colour transform special effects. Figure 7.1 demonstrates two examples of image enhancement associated with this software, where the first image is the original frame.

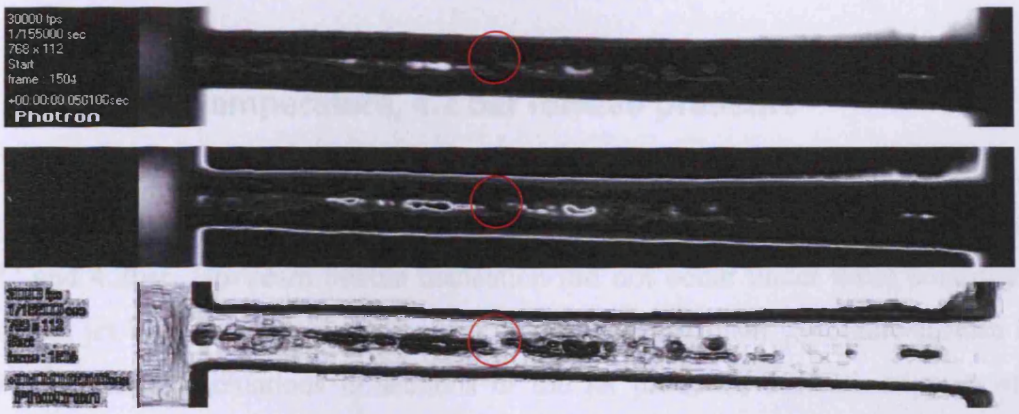

Figure 7.1 Image enhancement filters available with Corel Photo-Paint

The first example has been enhanced using the 'solarise' effect which transforms colors in an image by reversing image tones. The second example has been enhanced using the 'edge-detect' function, which detects the edges in an image and converts them to lines on a single-color background. This effect can be customised by specifying the intensity of the outline and the background colour.

7.2 1mm x 3.4mm Orifice

Due to inaccuracies in the manufacturing process of the 1mm x 3.4mm orifice, the diameter of the outlet was slightly bigger than the inlet. When measuring the droplet diameters a scale factor was applied to the images based on the diameter of the nozzle, which was a 'known' dimension. For this purpose it was assumed that the inlet, being the narrowest section of the nozzle, was equal to 1mm in diameter.

The irregularity of the nozzle dimensions exacerbated cavitation effects inside the nozzle, evidenced by upstream surface structures which were similar to those observed downstream of the orifice exit. Combined with surface imperfections on the nozzle walls, this made it difficult at times to track bubbles and differentiate between those flow structures which were attributable to the temperature of the jet and those which were caused by inconsistencies in the nozzle geometry. In addition the circular shape of the outer diameter of the nozzle magnified the upstream conditions so that the cavitation effect was exaggerated. Hence it was impossible to determine the extent to which cavitation was occurring. Nevertheless, the full range of recorded results is presented here.

7.2.1 116.2°C jet temperature, 4.2 bar release pressure

Figure 7.2 presents the upstream and downstream flow characteristics of a superheated jet at 116.2°C and 4.2bar. Upstream bubble nucleation did not occur under these conditions, and downstream jet break-up was dominated by mechanical processes. Sporadic surface boiling caused by thermal fluctuations in sections of the jet produced surface stripping of small quantities of liquid, although the effect of this phenomenon on the overall break-up mechanism was insignificant.

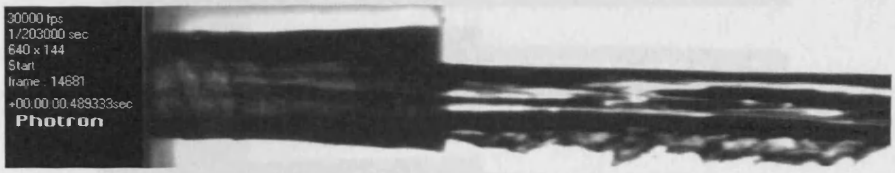

Figure 7.2 Internal and external flow conditions at 116.2°C and 4.2bar

7.2.2 121.3°C jet temperature, 4.9 bar release pressure

Figure 7.3 presents the upstream and downstream flow characteristics of a superheated jet at 121.3°C and 4.9bar. No upstream bubble nucleation was observed under these conditions and downstream jet break-up was dominated by mechanical processes. Downstream bubble nucleation occurred in intermittent bursts, as a result of thermal fluctuations in sections of the jet, which were of sufficient temperature to initiate stable bubble nucleation. However, due to the very low bubble frequency at these conditions the effect of this phenomenon on the overall break-up mechanism was insignificant.

Figure 7.3 Internal and external flow conditions at 121.3°C and 4.9bar

7.2.3 129.4°C jet temperature, 5.3 bar release pressure

Figure 7.4 presents footage taken at 50,000fps of an example of upstream bubble growth and subsequent downstream shattering at 129.4°C and 5.3bar. The upstream bubble frequency was 0.66kHz, which corresponded to a bubble concentration of 1.079×10^7 bubbles/m^3. Nevertheless, the downstream jet break-up was still dominated by mechanical processes. The bubble growth rate was 3.98 ms^{-1}, which was relatively high with respect to bubble growth rates measured across the range of conditions investigated. Downstream shattering of these bubbles produced fine localised atomisation.

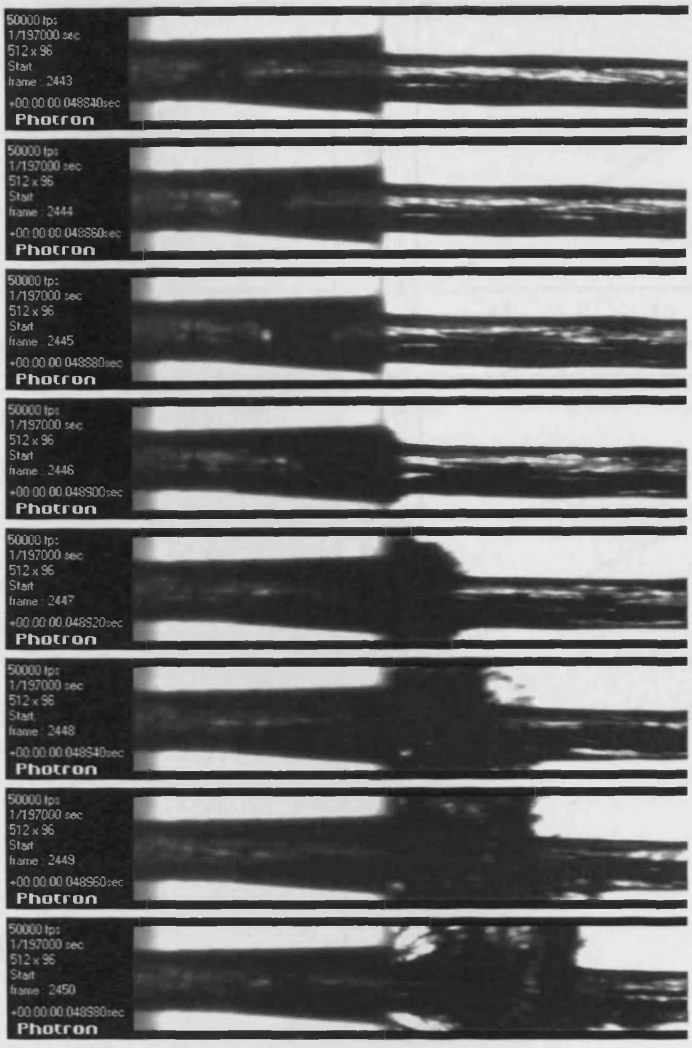

Figure 7.4 Bubble growth inside 1x3.4mm nozzle at 129.4°C and 5.3bar

Figure 7.5 presents the bubble growth rates measured inside the 1x3.4mm nozzle at 129.4°C and 5.3bar. In each case, the relationship between the bubble radius and the downstream distance from the nozzle inlet was linear. Since the flow velocity was constant, this indicates that the bubble radius increased linearly with time. The point at which the trendline intercepts the x-axis corresponds to the delay length for the inception of bubble growth. From this length it is possible to derive the corresponding delay time t_d, which was fairly consistent in each case. The average delay time was 2.6×10^{-6}s (0.06mm in terms of the delay length). The bubble growth rate varied from 2.4 – 5.6ms^{-1} between cases.

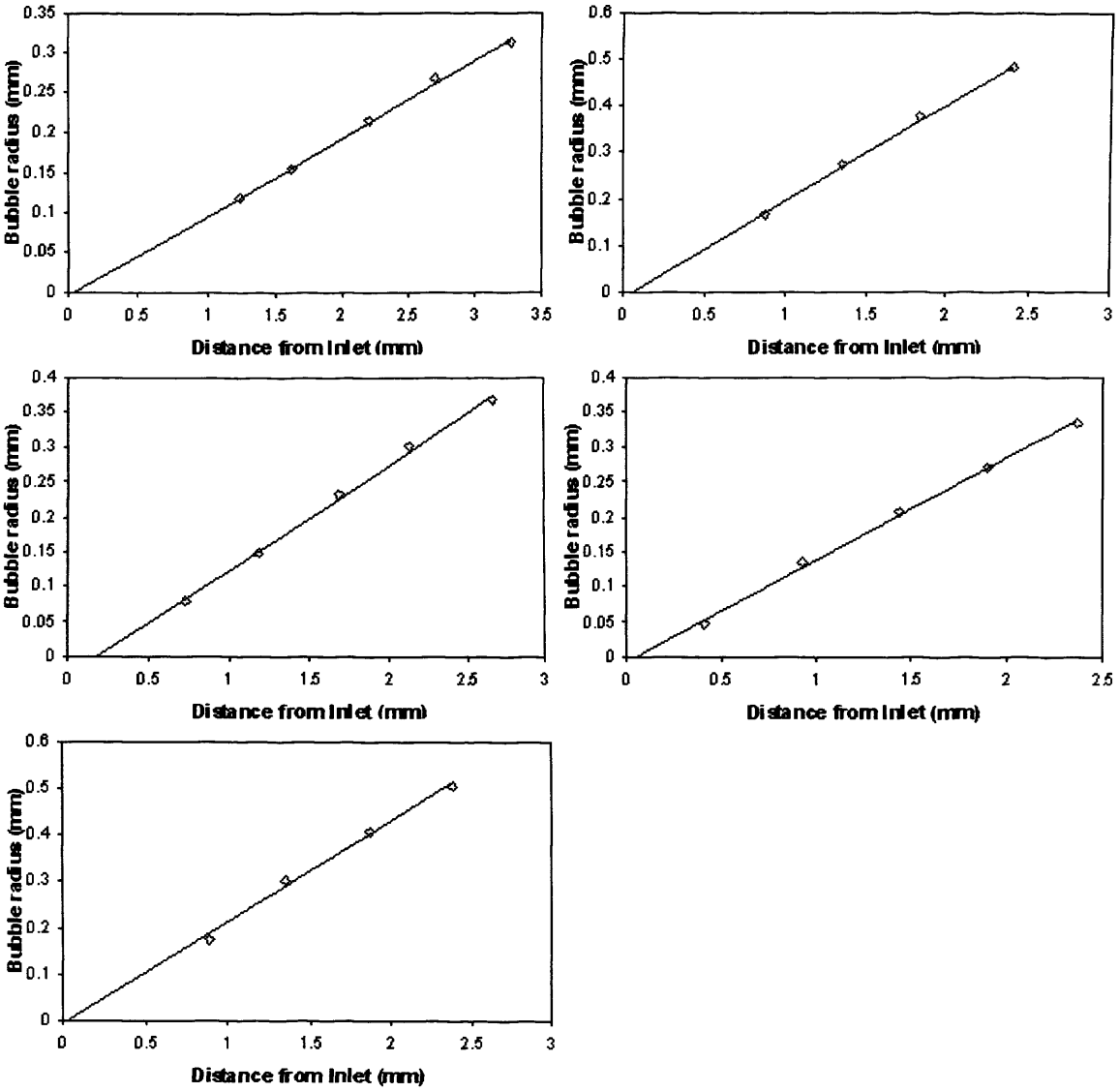

Figure 7.5 Bubble growth rates inside 1mm x 3.4mm nozzle at 129.4°C and 5.3bar

The variation in bubble growth rate can be explained in part by the deviation from sphericity of the bubbles measured. Bubble diameters were measured in the horizontal and vertical planes and an average taken from both measurements. Bubbles were selected for measurement based on their sphericity, however in some cases the irregular development of the bubble shape was likely to have caused errors the measured growth rate. Nevertheless, some variation should be expected due to fluctuations in the process of bubble nucleation at the molecular level.

7.2.4 135.0°C jet temperature, 7.5 bar release pressure

Figure 7.6 presents the upstream and downstream flow characteristics of a superheated jet at 135.0°C and 7.5bar. The downstream conditions exhibited characteristics of the first stage of transition to flashing. Bursting of relatively small bubbles at the surface of the jet created finely atomised droplets which seemed to constitute the early stages of a dispersed spray. Nevertheless the core of the jet remained unbroken and retained the majority of the liquid mass, with localised bursting of relatively large droplets creating intermittent gaps. Upstream bubble nucleation did not occur, since the pressure in the nozzle exceeded the saturated vapour pressure, thereby preventing the development of stable bubble nuclei.

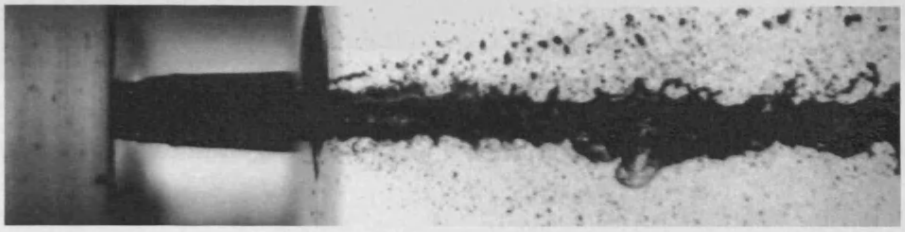

Figure 7.6. Internal and external flow conditions at 135.0°C and 7.5bar

7.3 1mm x 10mm Orifice

7.3.1 116.2°C jet temperature, 4.2 bar release pressure

Figure 7.7 resents footage taken at 50,000fps of an example of bubble development inside the 1mm x 10mm nozzle at 122.8°C and 2.8bar. Despite the relatively low liquid temperature, the upstream bubble frequency was 18.2kHz, which corresponded to a bubble concentration of 1.86×10^9 bubbles/m^3. The bubble growth rate was $0.81 ms^{-1}$ and the downstream break-up displayed characteristics of an intermediate transition regime, between the departure from mechanical break-up and full flashing. Although the jet temperature was relatively low, the release pressure exceeded the saturated vapour pressure inside the nozzle, creating conditions conducive to stable bubble nucleation. In addition surface imperfections on the nozzle wall appeared to provide important additional nucleation sites for vapour bubbles to form.

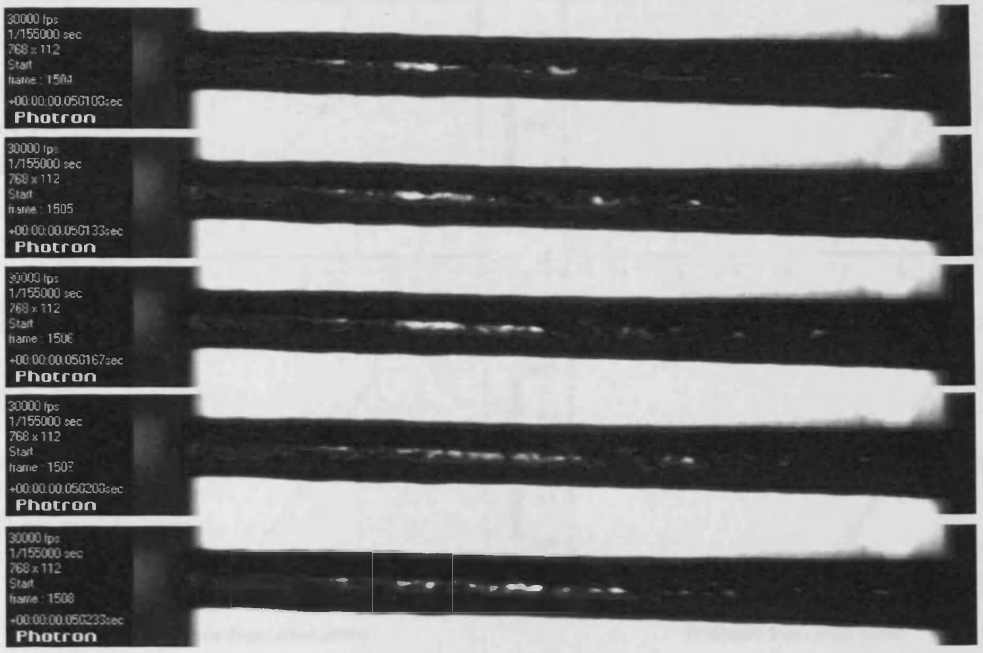

Figure 7.7 Bubble growth inside 1x10mm nozzle at 122.8°C and 2.8bar

Figure 7.8 presents the downstream flow at conditions of 124.0°C and 2.4bar. Once bubble nucleation occurred, bubbles expanded at a rate determined by the temperature and pressure in the nozzle. The length of the orifice increased the dwell time for bubble growth, thus bubbles collided with each other and coalesced inside the nozzle to form large 'slug bubbles', identified by Park and Lee[13]. Upon release from the nozzle, the slug bubbles burst into ligaments and then disintegrated into small drops, but large liquid blobs originated from liquid slugs were still observed. The large liquid blobs then broke-up into smaller droplets further downstream.

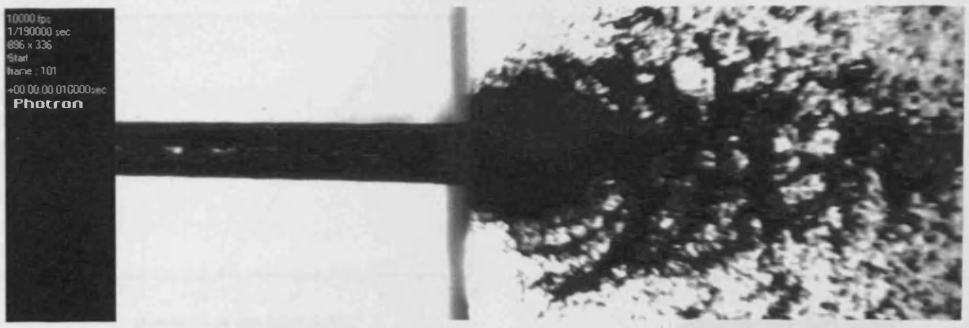

Figure 7.8 External flow conditions at 126.0°C and 2.4bar

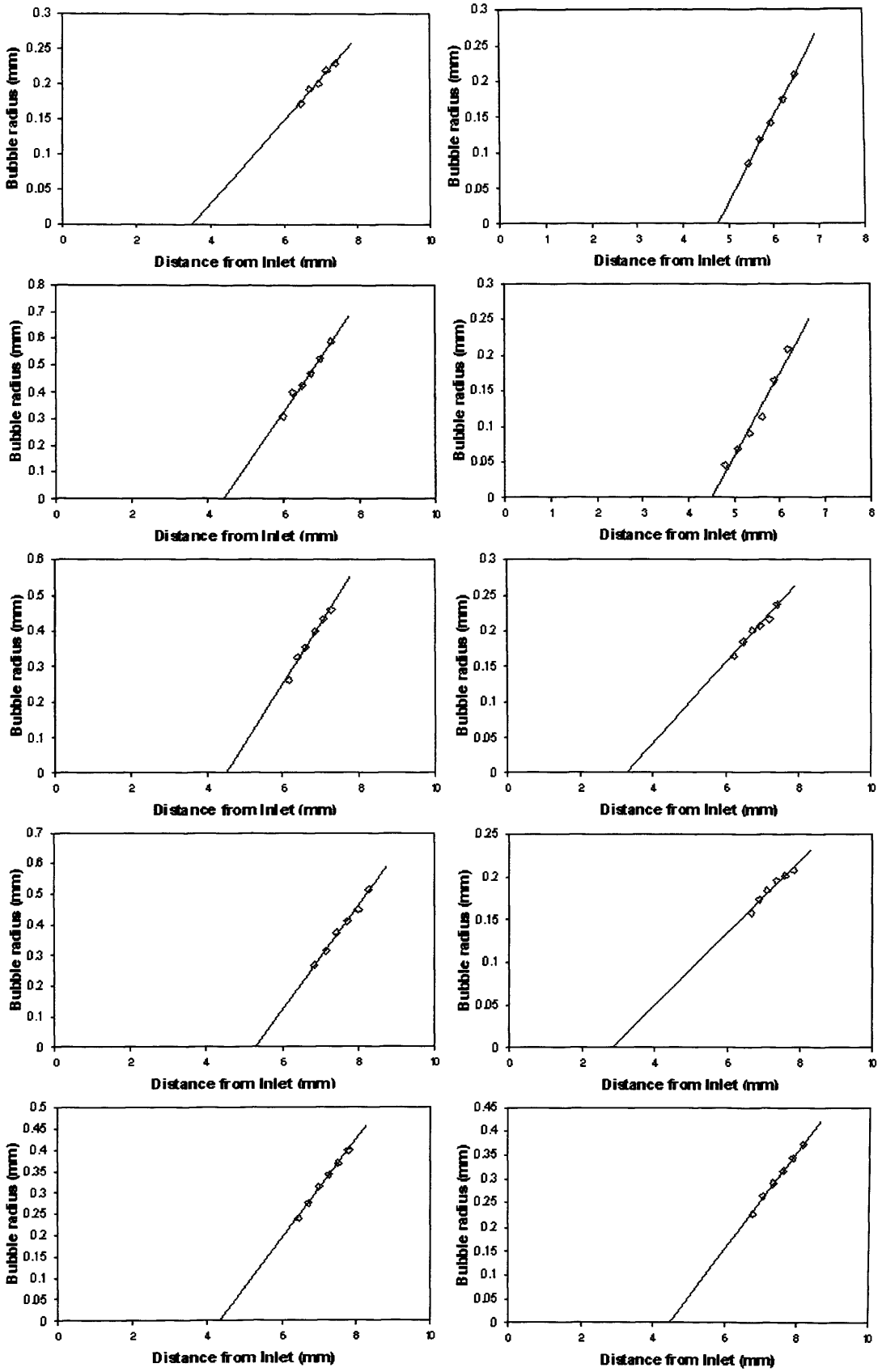

Figure 7.9 Bubble growth rates inside 1mm x 10mm nozzle at 122.2°C and 2.8bar

Figure 7.9 presents the bubble growth rates measured inside the 1x10mm nozzle at 122.2°C and 2.8bar. The bubble radius increased linearly with downstream distance and given that the flow velocity was constant, this indicates that the bubble radius increased linearly with time. The delay time varied between 2.4 – 3.8x10^{-4}s (2.76 – 5.29mm in terms of the delay length). The bubble growth rate varied from 0.8 – 1.9ms^{-1} between cases, which can be explained by the variation in sphericity of the measured bubbles and thermal fluctuations in the liquid.

7.4 1mm x 20mm Orifice

7.4.1 120.0°C jet temperature, 2.5 bar release pressure

Figure 7.10 presents footage taken at 50,000fps of the upstream flow of a superheated jet at 120.0°C and 2.5bar. The upstream bubble frequency was 23.4kHz, which corresponded to a bubble concentration of 8.401x10^{8} bubbles/m^{3}. The bubble growth rate was 0.90ms^{-1}. In this case the high bubble frequency was caused in part by the trumpeted shape of the exit orifice. This created a depressurisation zone, which caused turbulence in the flow and encouraged vapour production. In spite of this, significant bubble nucleation also occurred upstream of this feature.

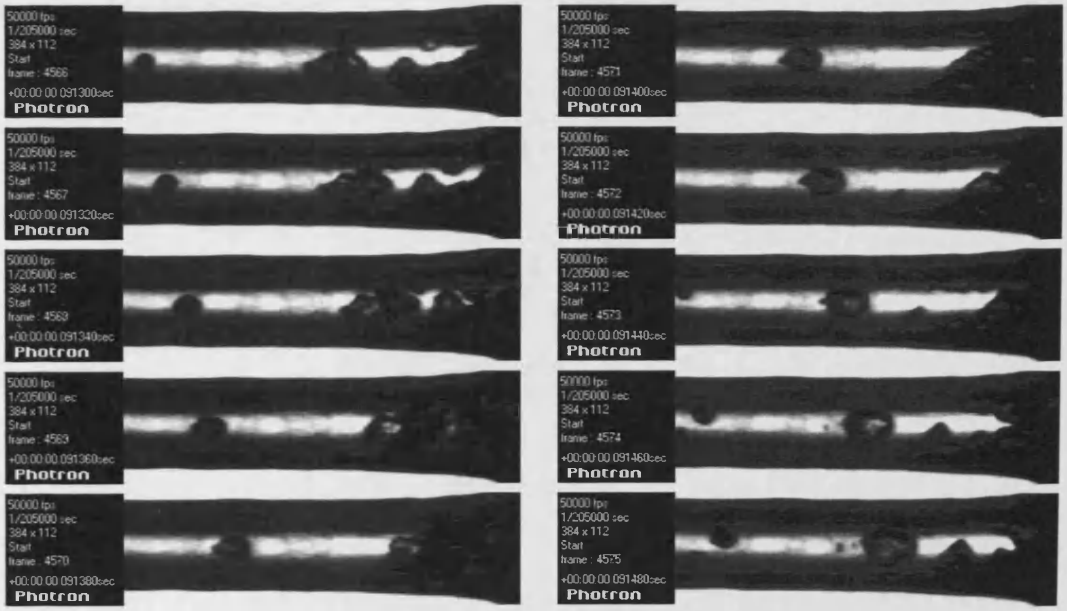

Figure 7.10 Bubble growth inside 1x20mm nozzle at 120.0°C and 2.5bar

Figure 7.11 presents footage taken at 15000fps of the upstream and downstream flow characteristics at conditions of 122.8°C and 2.6bar, where it can be seen that the downstream break-up demonstrated characteristics of an intermediate stage of transition between the onset of and full flashing. Although the flared nozzle outlet contributed to the downstream conditions, the corresponding window for growth of bubbles nucleating upstream of this feature growth was sufficient for 'slug bubbles' to develop close to the nozzle exit. Hence, ligament formation, and large liquid blobs were observed downstream, with a relatively intact liquid core.

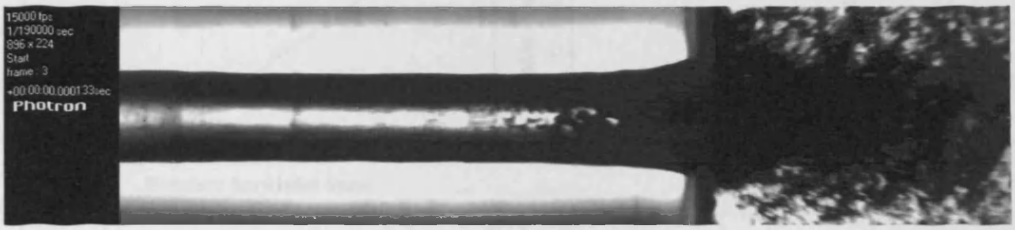

Figure 7.11 Internal and external flow conditions at 122.8°C and 2.6bar

Figure 7.12 presents the bubble growth rates of bubbles nucleating upstream of the flared nozzle outlet at 120.0°C and 2.5bar. The delay time varied between 1.2 -1.6x10^{-3}s (14.4 – 16.0mm in terms of the delay length), giving an average delay length of 15.5mm. Since the nozzle length exceeded the delay length at this superheat, conditions were ideal for advanced upstream bubble development.

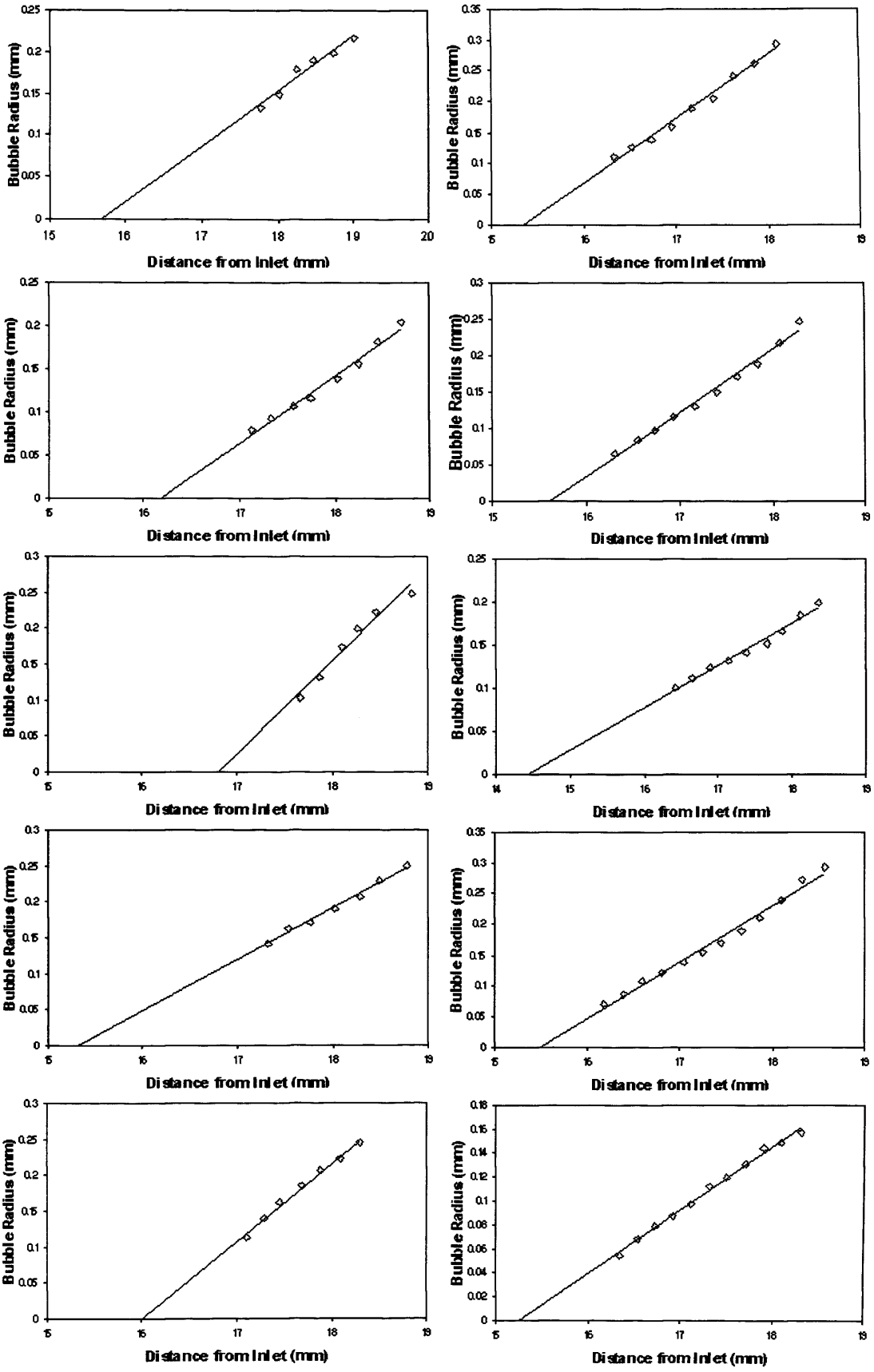

Figure 7.12 Bubble growth rates inside 1 x 20mm nozzle at 120.0°C and 2.5bar

7.5 1mm x 30mm Orifice

7.5.1 115.9°C jet temperature, 2.1 bar release pressure

Figure 7.13 presents footage taken at 15,000fps of an example of upstream bubble growth inside the 1mm x 30mm nozzle at 115.9°C and 2.1bar. The upstream bubble frequency was 15.9kHz, which corresponded to a bubble concentration of 7.393×10^8 bubbles/m^3. The bubble growth rate was $0.42 ms^{-1}$. In this case the combination of bubble frequency and bubble growth rate produced 'bubbly flow' inside the nozzle. There is no footage of the downstream flow characteristics available, however, from the small section of the spray visible in the frames presented it can be seen that despite bubble bursting immediately downstream of the exit orifice the core of the liquid jet had not completely disintegrated. Hence the jet exhibited characteristics of the first stage of transition to flashing.

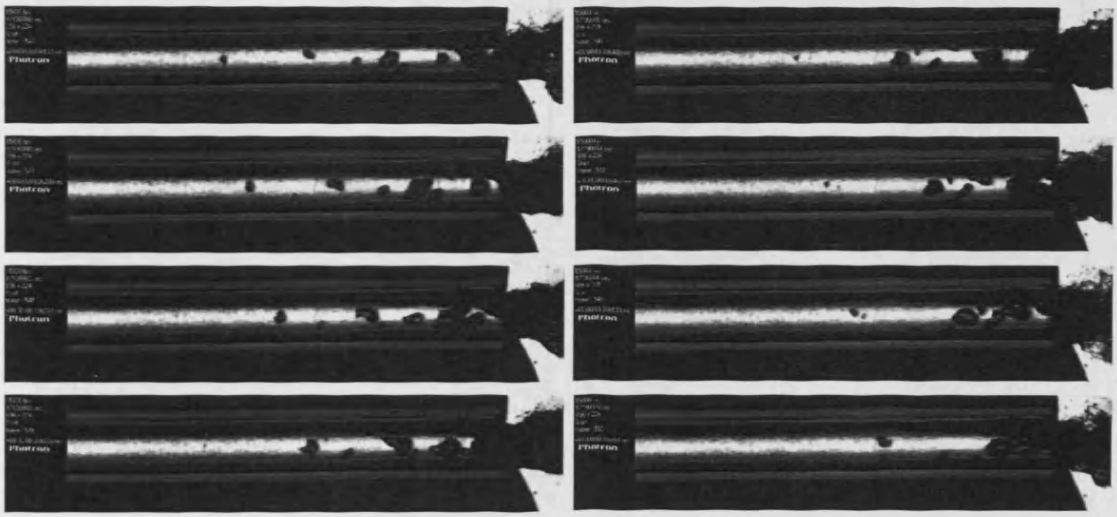

Figure 7.13 Bubble growth inside 1x30mm nozzle at 115.9°C and 2.1bar

Figure 7.14 presents the bubble growth rates measured inside the 1x30mm nozzle at 115.9°C and 2.1bar, which varied from $0.26 - 0.73 ms^{-1}$ between cases. The delay time varied from 2.4 – 2.8×10^{-3}s (21.3 – 25.9mm in terms of the delay length). The nozzle length exceeded the average delay length of 23.3mm, and hence conditions were ideal for upstream bubble nucleation.

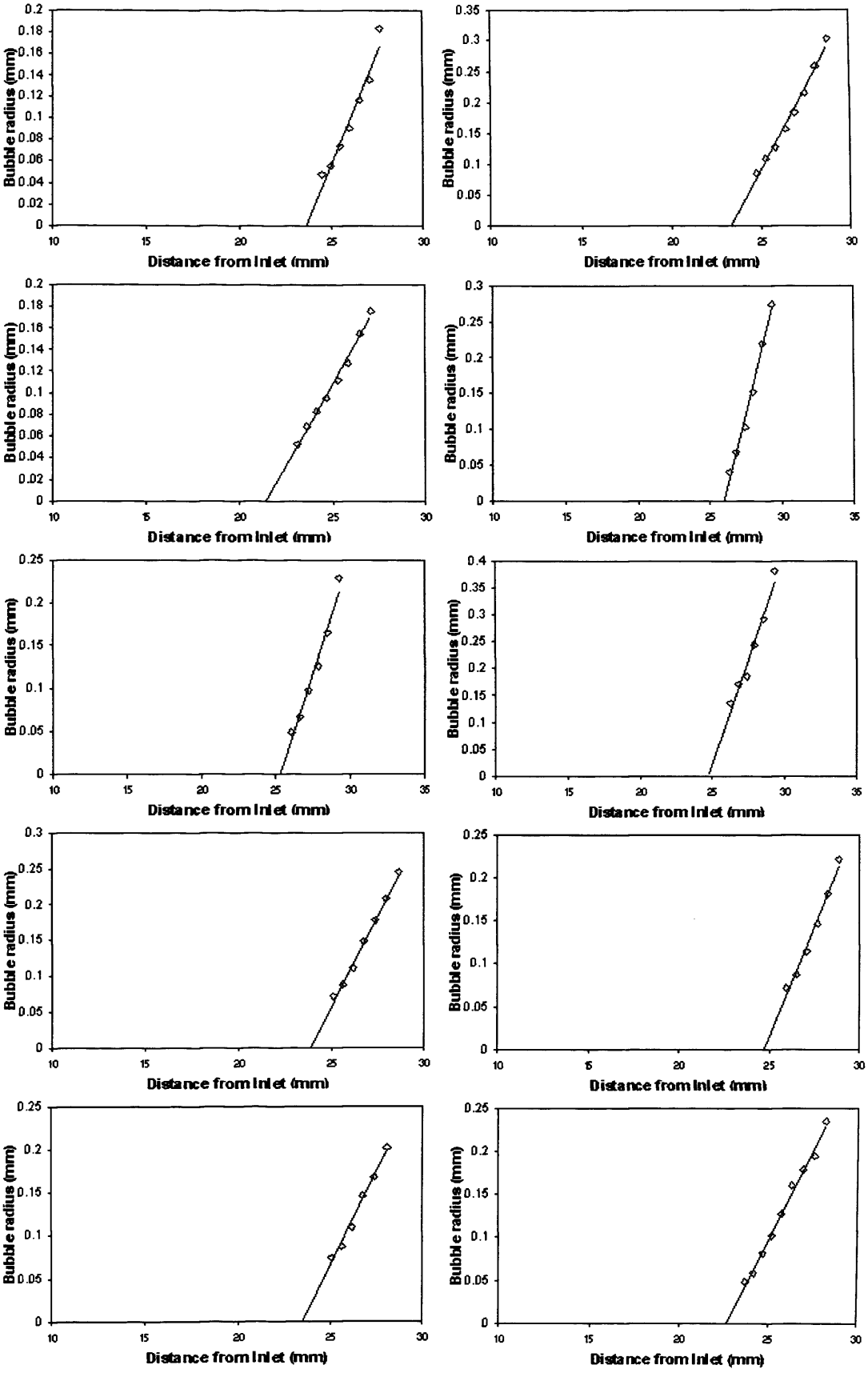

Figure 7.14 Bubble growth rates inside 1 x 30mm nozzle at 115.9°C and 2.1bar

7.6 2mm x 3.4mm Orifice

As in the case of the 1mm x 3.4mm nozzle, inaccuracies in the manufacturing process of the 2mm x 3.4mm orifice caused the diameter of the outlet to be slightly bigger than the inlet. When measuring the droplet diameters a scale factor was applied to the images based on the diameter of the nozzle, which was a 'known' dimension. For this purpose the narrowest section of the nozzle was assumed to be equal to 2mm in diameter.

7.6.1 122.3°C jet temperature, 3.2 bar release pressure

Figure 7.15 presents footage taken at 50,000fps of an example of upstream bubble growth and subsequent downstream shattering at 122.3°C and 3.2bar.

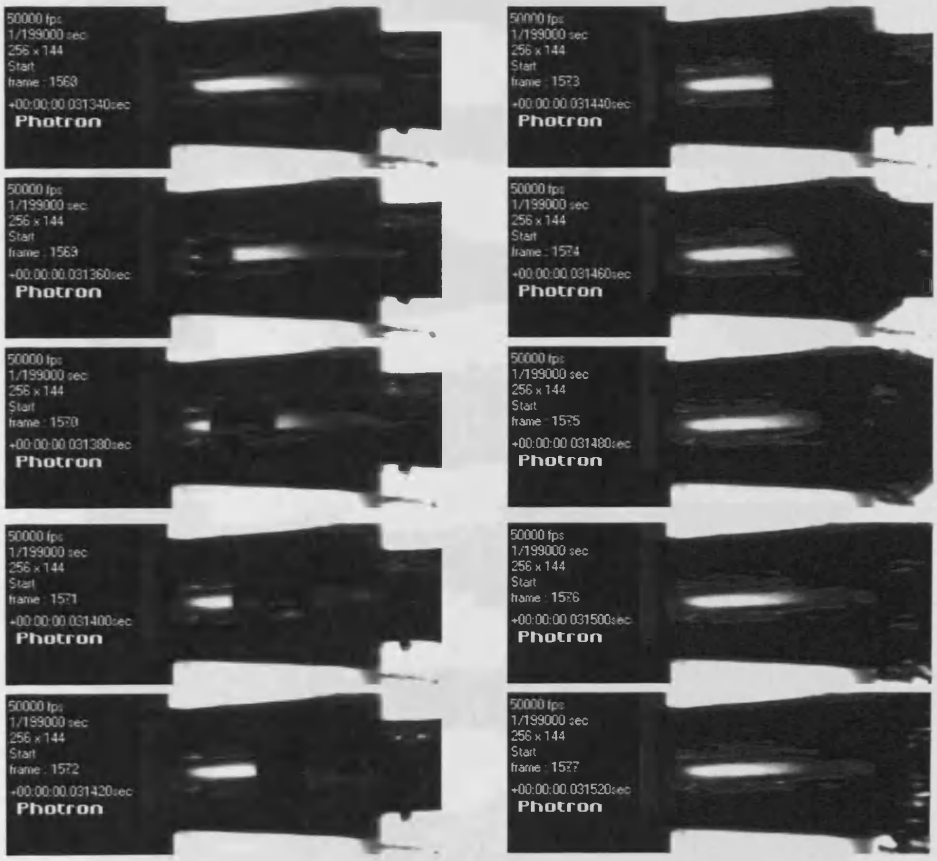

Figure 7.15 Bubble growth inside 2x3.4mm nozzle at 122.3°C and 3.2bar

The upstream bubble frequency was 1.5kHz, which corresponded to a bubble concentration of 7.952×10^6 bubbles/m^3. The bubble growth rate was $6.9 ms^{-1}$. With respect to bubble growth rates measured across the range of conditions investigated this is high and as a result downstream shattering of these bubbles produced fine localised atomisation.

Figure 7.16 presents footage taken at 15,000fps of the internal and external flow characteristics at conditions of 123.1°C and 3.0bar. Clusters of bubbles developing in the jet created complex flow structures downstream of the orifice exit. Nevertheless the liquid core of the jet at the exit orifice remained intact and mechanical processes were still dominant.

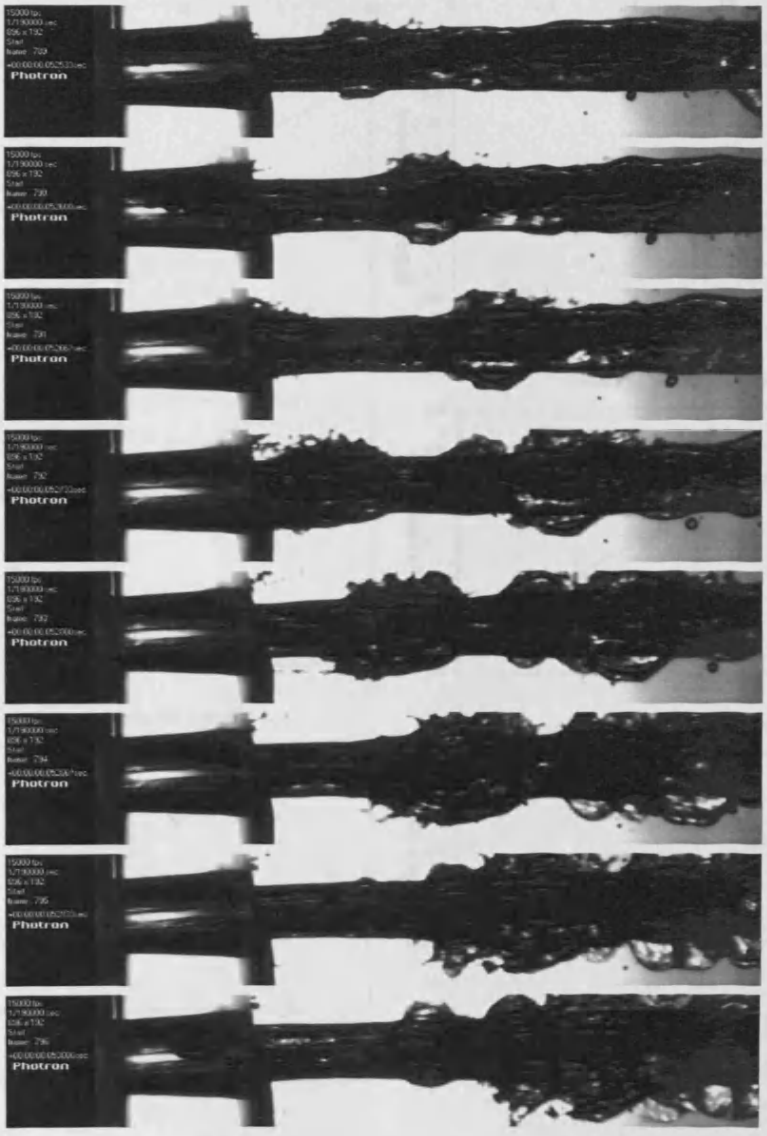

Figure 7.16 Internal and external flow characteristics at 123.1°C and 3.0bar

Figure 7.17 presents the bubble growth rates measured inside the 2x3.4mm nozzle at 122.3°C and 3.2bar. The relationship between the bubble radius and the downstream distance from the nozzle inlet was linear and the overall bubble growth rate varied between 4.4 – 9.2ms^{-1}. Again this variation was caused by variations in bubble sphericity and thermal fluctuations in the liquid.

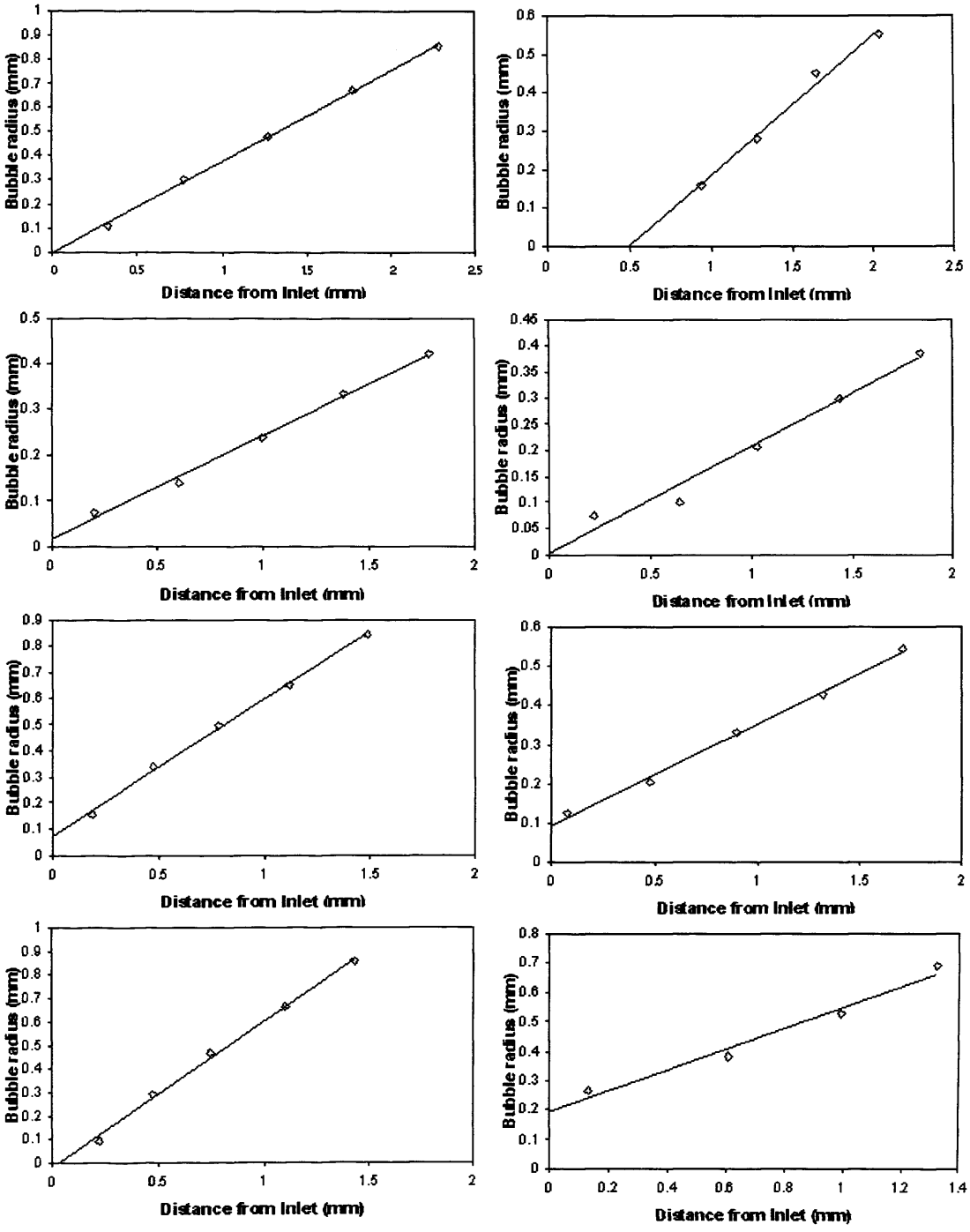

Figure 7.17 Bubble growth rates inside 2x3.4mm nozzle at 122.3°C and 3.2bar

In some cases the delay time was 'negative', which indicates that bubbles were nucleating upstream of the nozzle inlet. Figure 7.18 demonstrates an example of this phenomenon, where the upstream bubble is circled in red. For the sake of simplicity, bubbles nucleating upstream of the nozzle inlet are classed as having zero delay time. This ensures that the average delay time retains a positive value, which is 5.8×10^{-6}s in this case (0.066mm in terms of the delay length).

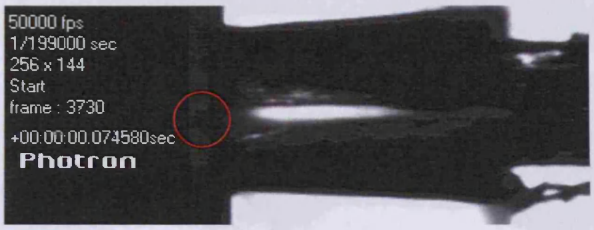

Figure 7.18 Bubble nucleation upstream of the nozzle inlet

7.6.2 131.2°C jet temperature, 4.5 bar release pressure

Figure 7.19 presents footage taken at 50,000fps of an example of upstream bubble growth at 131.2°C and 4.5bar. The upstream bubble frequency was 10.2kHz, which corresponded to a bubble concentration of 4.180×10^{7} bubbles/m^3. The bubble growth rate was 8.2ms^{-1}. With respect to bubble growth rates measured across the range of conditions investigated this was high, causing violent bubble shattering immediately downstream of the exit orifice.

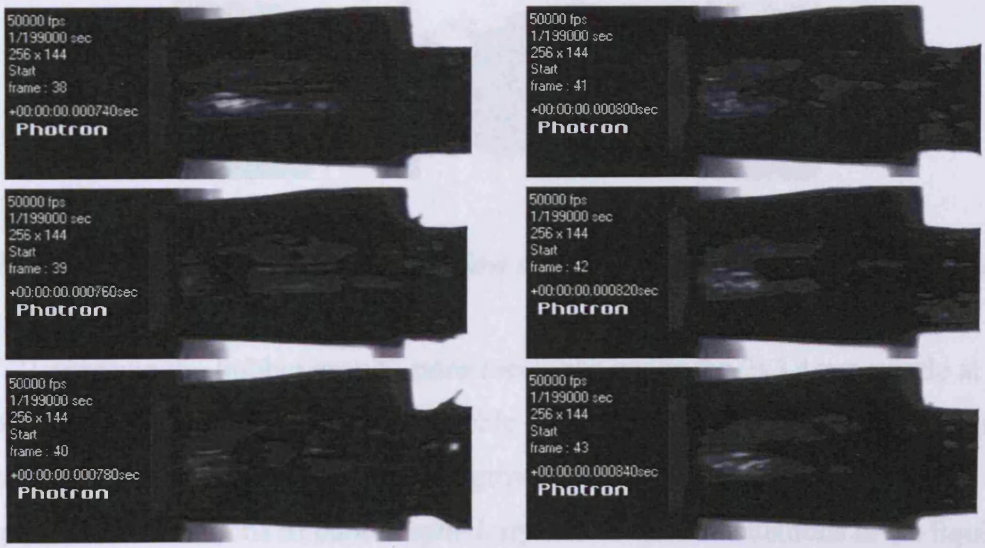

Figure 7.19 Bubble growth inside 2x3.4mm nozzle at 131.2°C and 4.5bar

Figure 7.20 presents footage taken at 15,000fps of the internal and external flow characteristics at 130.2°C and 4.6bar. Downstream break-up exhibited characteristics of the first stage of transition to flashing with mechanical processes no longer dominant.

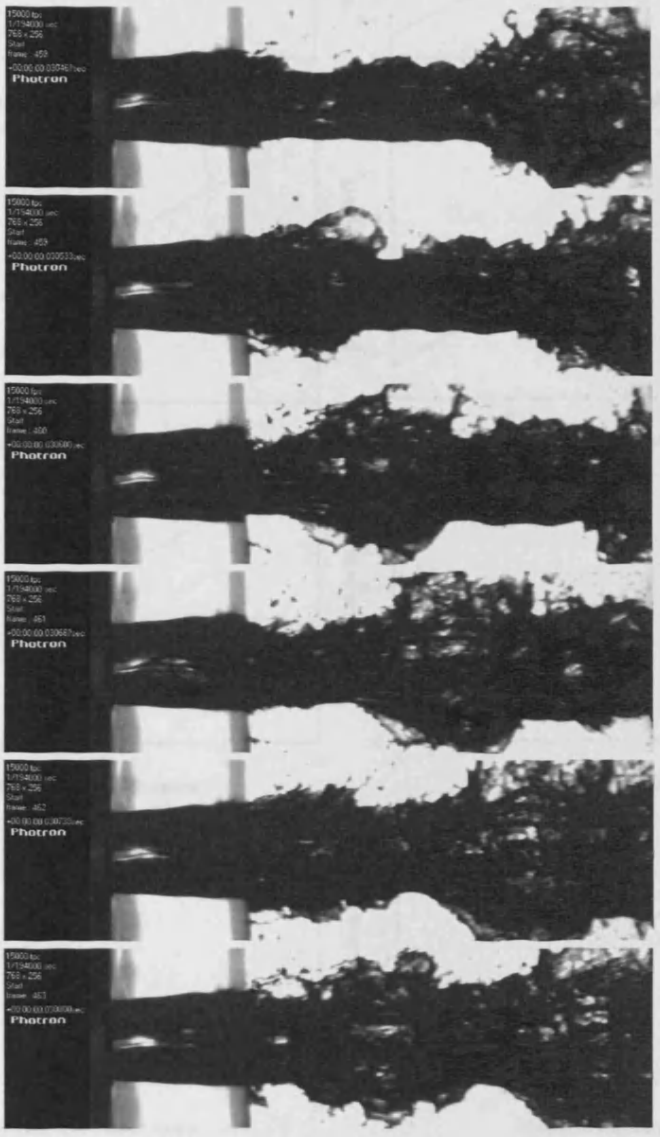

Figure 7.20 Internal and external flow characteristics at 130.2°C and 4.6bar

Figure 7.21 presents the bubble growth rates measured inside the 2x3.4mm nozzle at 131.2°C and 4.5bar. The relationship between the bubble radius and the downstream distance from the nozzle inlet was linear. The overall bubble growth rate varied from 4.9 – 11.4ms^{-1} between cases, again due to variations in bubble sphericity and thermal fluctuations in the liquid.

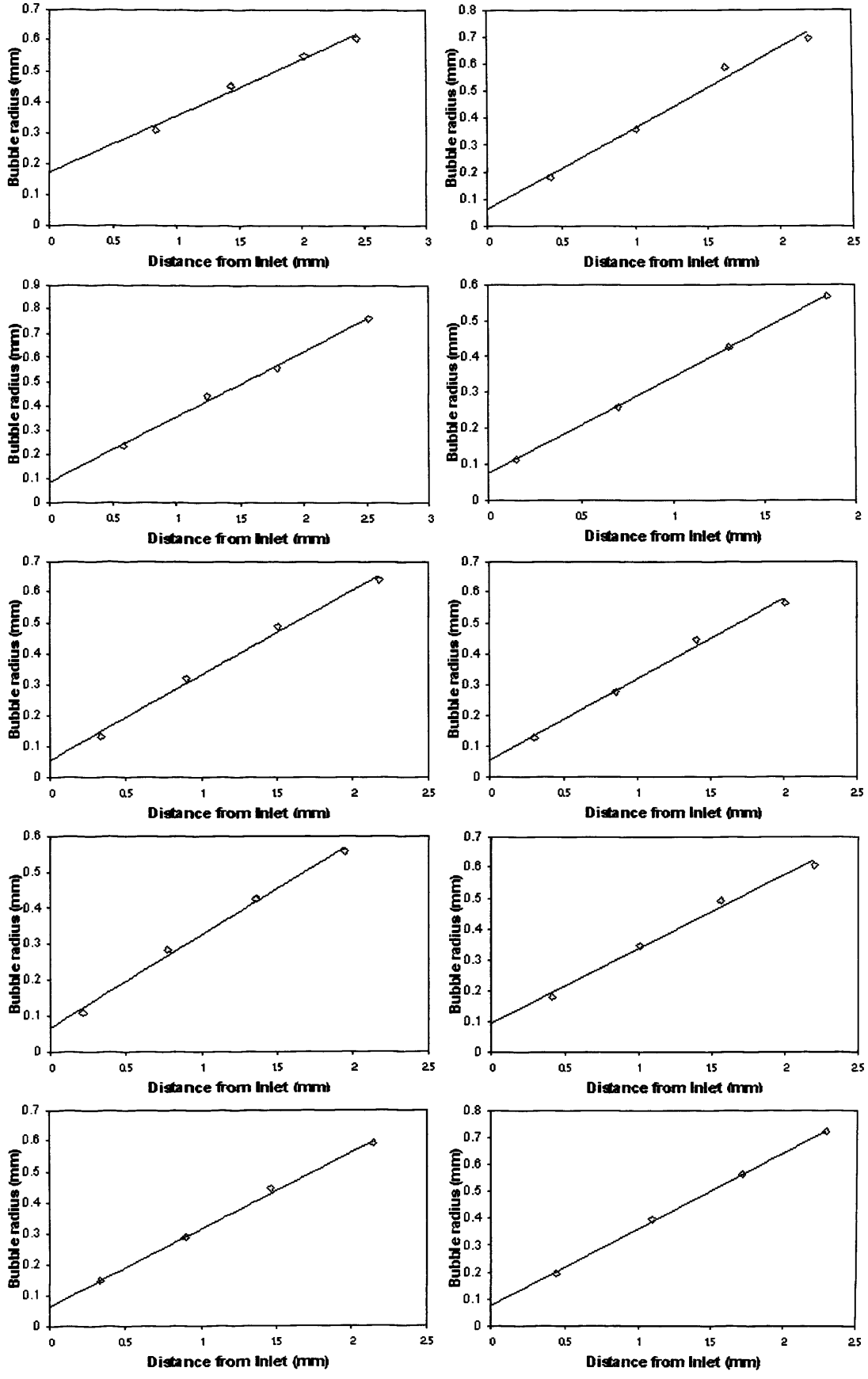

Figure 7.21 Bubble growth rates inside 2x3.4mm nozzle at 131.2°C and 4.5bar

For every bubble analysed the delay time was 'negative', indicating that bubbles were nucleating exclusively upstream of the nozzle inlet. This is significant as it seems to indicate that these conditions represent a critical point at which the bubble delay time effectively equals zero.

7.6.3 137.1°C jet temperature, 5.5 bar release pressure

Figure 7.22 presents footage taken at 15000fps of the upstream and downstream flow characteristics of a superheated jet at 137.1°C and 5.5bar.

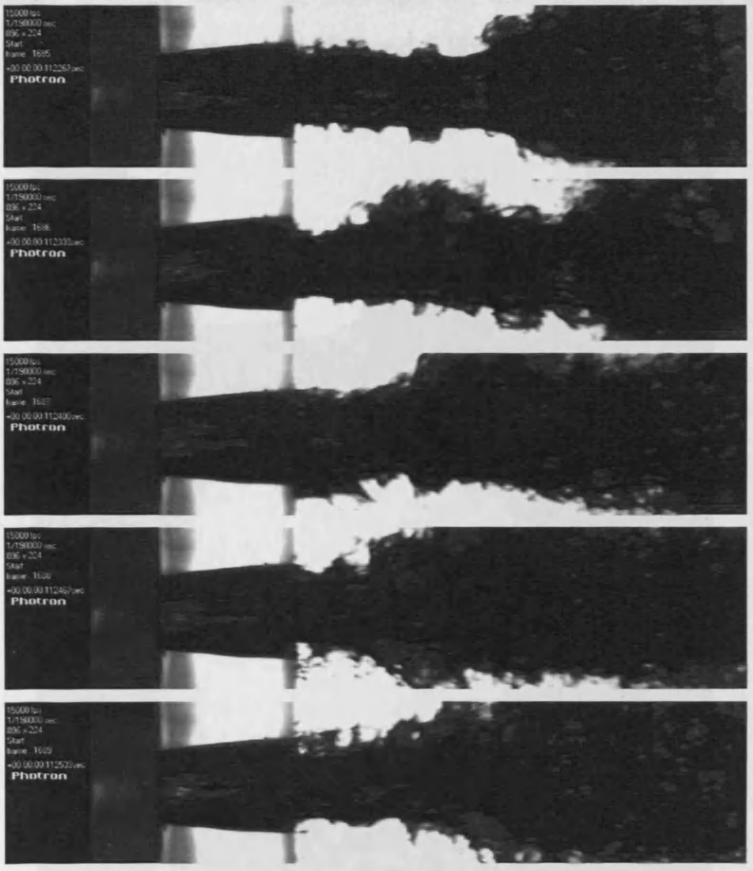

Figure 7.22 Internal and external flow charctaristics at 137.1°C and 5.5bar

The downstream break-up regime exhibited qualities of an intermediate stage of transition. The growth of multiple bubbles in the jet created complex structures downstream of the orifice exit, although the liquid core of the jet remained unbroken immediately downstream

of the nozzle. This was because the combination of high flow velocity, short nozzle length and relatively low bubble growth rate did not produce bubbles of diameter equal to or greater than the nozzle diameter at the orifice exit. Due to the diameter of the jet, and the complex nature of the upstream flow at these conditions, the back-light was insufficient to adequately penetrate the nozzle at higher frame rates and shutter speeds. Hence it was not possible to determine bubble growth rates or bubble frequencies from the images taken at frame rates suitable for this purpose.

7.6.4 150.7°C jet temperature, 6.8 bar release pressure

Figure 7.23 presents footage taken at 5000fps of the upstream and downstream flow characteristics of a superheated jet at 150.7°C and 6.8bar.

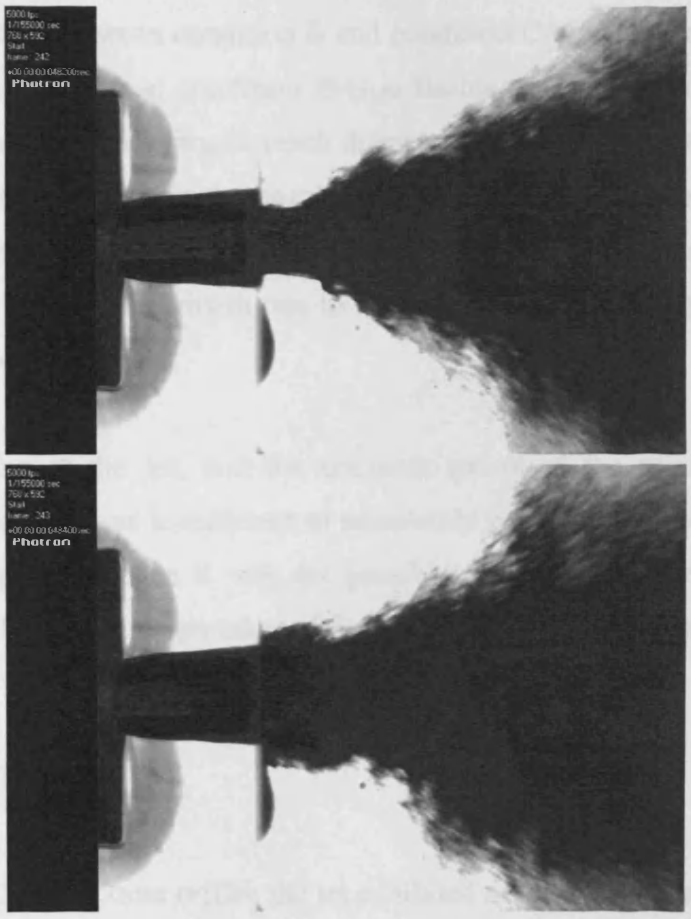

Figure 7.23 Internal and external flow characteristics at 150.7°C and 6.8bar

The downstream break-up regime was on the border between condition B and C outlined in chapter 6. An unbroken liquid core existed immediately downstream of the orifice exit which was punctuated by the intermittent bursting of bubbles at the orifice. The saturated vapour pressure and the pressure inside the nozzle were approximately equal, hence thermal fluctuations in the jet, caused break-up to oscillate between the two highlighted transition regimes. Figure 7.23 presents an example of each occurrence in consecutive frames. Nevertheless, the rate of boiling throughout the jet was so high at this superheat that the bubble growth rates were sufficient to cause the immediate disintegration of the jet irrespective of the nucleation point.

Due to the high flow velocity and short nozzle length in certain instances the growth rate of bubbles nucleating upstream was not sufficient for the bubble diameter to exceed the nozzle diameter prior to release. Hence, it is possible for condition B-type flashing to occur downstream even when the saturated vapour pressure exceeds the pressure in the nozzle. In this way the difference between condition B and condition C-type flashing can be defined in terms of two release scenarios; condition B-type flashing occurs when bubbles nucleating upstream do not have sufficient time to reach diameters in excess of the nozzle diameter prior to release or when the pressure in the nozzle exceeds the saturated vapour pressure, thereby preventing stable upstream bubble nucleation,. However, in both instances the superheat must be high enough for the bubble growth rate to cause the complete disintegration of the jet in spite of the nucleation point.

Due to the diameter of the jet, and the complex nature of the upstream flow at these conditions, the back-light was insufficient to adequately penetrate the nozzle at higher frame rates and shutter speeds. Hence it was not possible to determine bubble growth rates or bubble frequencies from the images taken at frame rates suitable for this purpose.

7.7 2mm x 7mm Orifice

When utilising the 2mm x 7mm orifice the jet exhibited a 'waviness' analogous to Rayleigh-type instabilities for sub-cooled jets at low pressure, as demonstrated by Figure 7.24. This 'waviness' is thought to be a consequence of the slightly divergent nozzle shape, caused by errors in the manufacturing process, because it was a feature of all releases carried out using

this nozzle irrespective of the superheat. This waviness created eddies in the flow, which appeared to be responsible for bubble generation. Hence it was not possible to distinguish whether homogenous bubble nucleation due to molecular processes in the liquid or the turbulent eddies were responsible for bubble nucleation. Nevertheless, the full range of recorded results is presented here in spite of this unconventional behaviour.

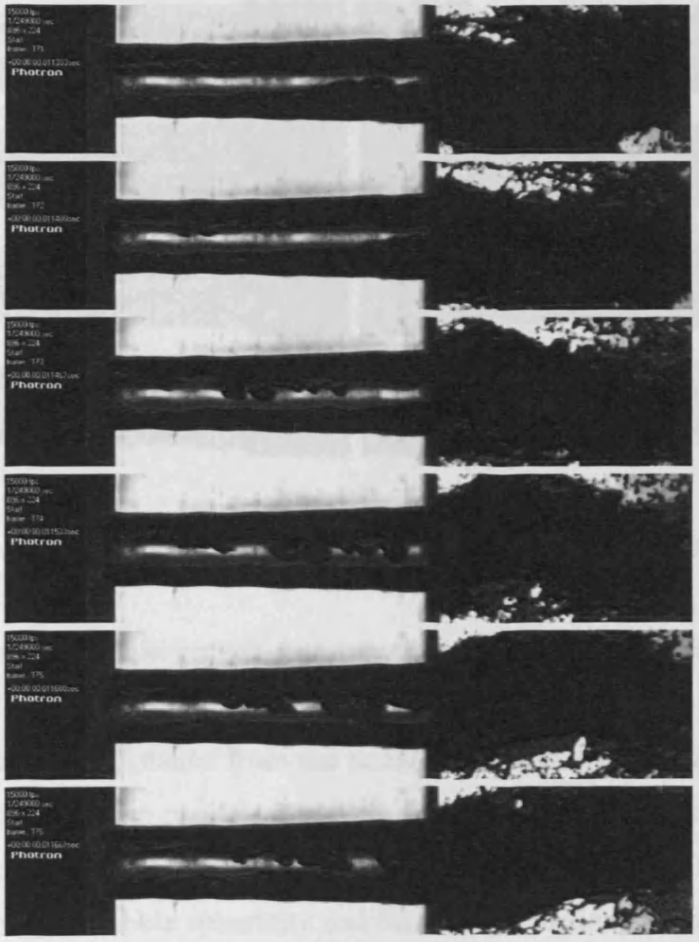

Figure 7.24 Internal and external flow characteristics at 111.1°C and 3.0bar

7.7.1 112.7°C jet temperature, 3.0 bar release pressure

Figure 7.25 presents footage taken at 30,000fps of an example of bubble growth inside the 2x7mm nozzle at 112.7°C and 3.0bar. The upstream bubble frequency was 5.8kHz, which corresponded to a bubble concentration of 3.392×10^7 bubbles/m^3. The bubble growth rate was $1.46 ms^{-1}$. The downstream conditions correspond to those presented in Figure 7.24, where it

can be seen that the jet displayed characteristics of the first stage of transition to flashing, although it is difficult to distinguish between the effect of flashing and the 'waviness' of the jet on the break-up regime. Bubbles were observed to nucleate relatively close to the nozzle inlet and due to the length of the orifice these bubbles were able to grow to relatively large sizes, causing significant fragmentation of the jet downstream of the exit orifice.

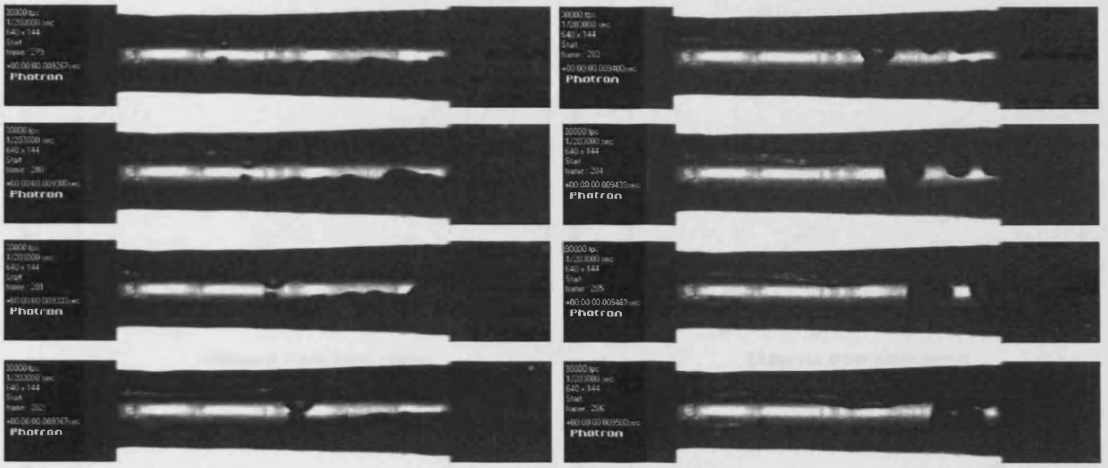

Figure 7.25 Bubble growth inside 2x7mm nozzle at 112.7°C and 3.0bar

Figure 7.26 presents the bubble growth rates measured inside the 2x7mm nozzle at 112.7°C and 3.0bar. In spite of the unusual flow characteristics, the relationship between the bubble radius and the downstream distance from the nozzle inlet was linear. This is significant as it indicates that regardless of the manner in which a bubble nucleates, once nucleation occurs the growth rate is constant. The overall bubble growth rate varied from 1.0 – 2.0ms^{-1} between cases, due to variations in bubble sphericity and thermal fluctuations in the liquid. Despite the low superheat, in some cases the delay time for nucleation appeared to be 'negative'. However, there is no evidence of this occurring at these conditions in any of the footage. Hence it is not clear whether this was an effect of the turbulent eddies associated with the Rayleigh-type instabilities inside the nozzle, or whether bubbles were in fact nucleating upstream of the nozzle. In spite of this peculiarity, the average delay time for bubble nucleation was calculated with the inclusion of these so called 'negative' delay times, where for convenience they were expressed as zero in order to produce a positive number, which in this case was 3.0x10^{-5}s (0.5mm in terms of the delay length).

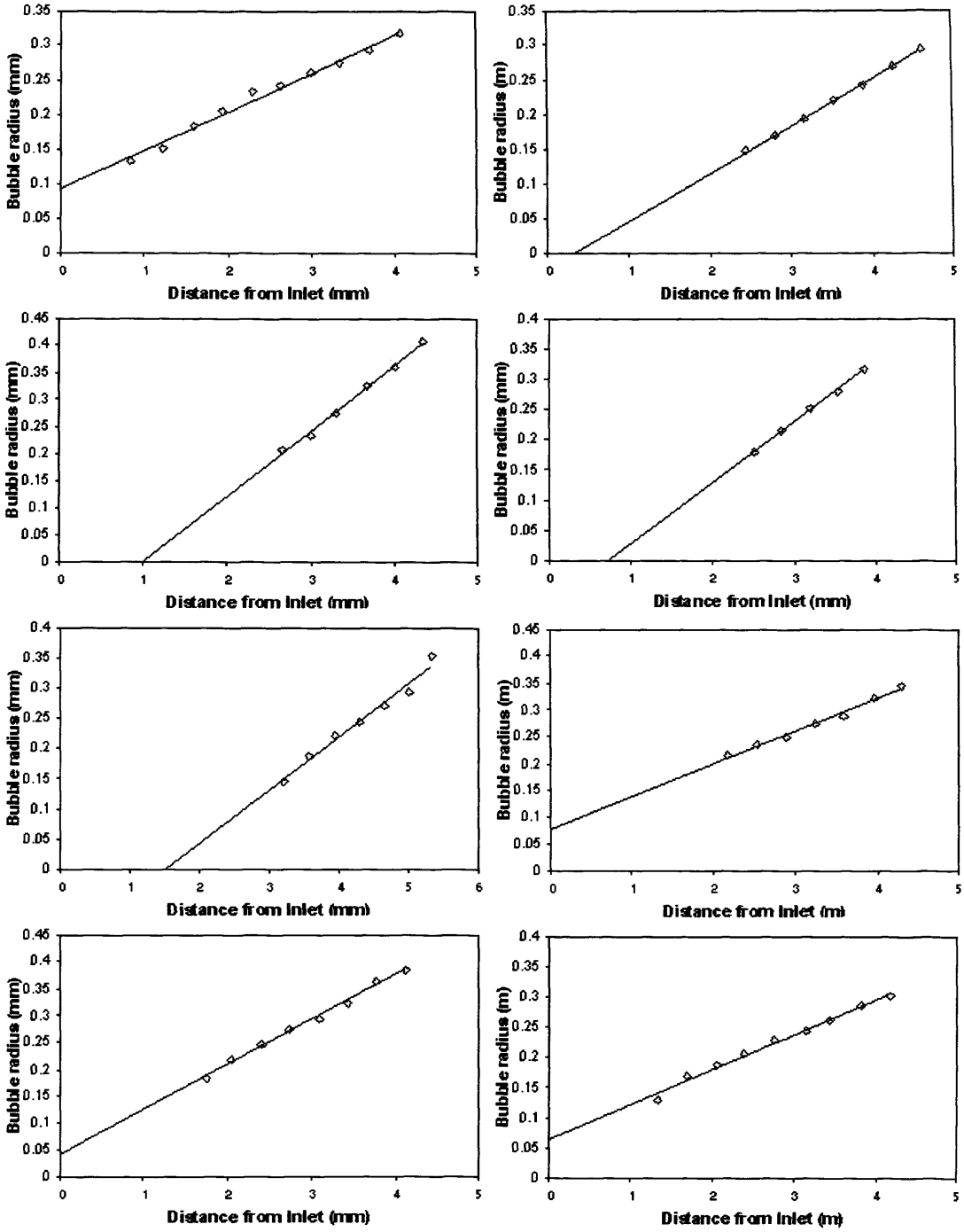

Figure 7.26 Bubble growth rates inside 2x7mm nozzle at 112.7°C and 3.0bar

7.7.2 126.6°C jet temperature, 4.4 bar release pressure

Figure 7.27 presents footage taken at 30,000fps of an example of bubble growth inside the 2mm x 7mm nozzle at 126.6°C and 4.4bar. The upstream bubble frequency was 23.6kHz,

which corresponded to a bubble concentration of 1.148×10^8 bubbles/m^3. The bubble growth rate was $1.46 ms^{-1}$.

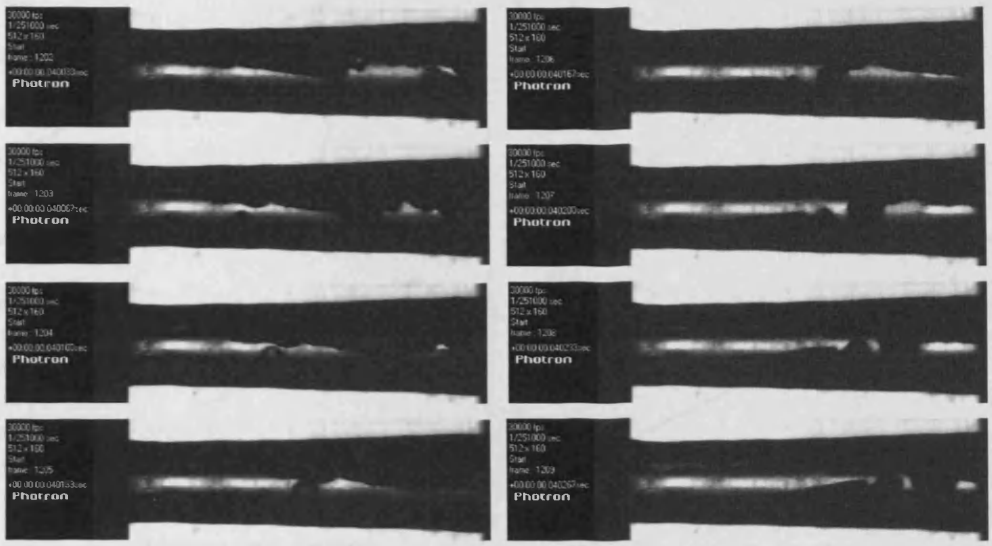

Figure 7.27 Bubble growth inside 2x7mm nozzle at 126.6°C and 4.4bar

In spite of the relatively low superheat the downstream break-up regime demonstrated characteristics of an intermediate stage of transition, although it was closer to full flashing than the first stage of transition. Nevertheless the bursting of 'slug bubbles' downstream produced ligaments which disintegrated into small drops, with large liquid blobs originated from liquid slugs still observed. The core remained relatively intact, although the jet had developed a wide spray angle with small droplets in the outer regions. Figure 7.28 presents the internal and external flow characteristics of a superheated jet at 123.7°C and 4.1bar

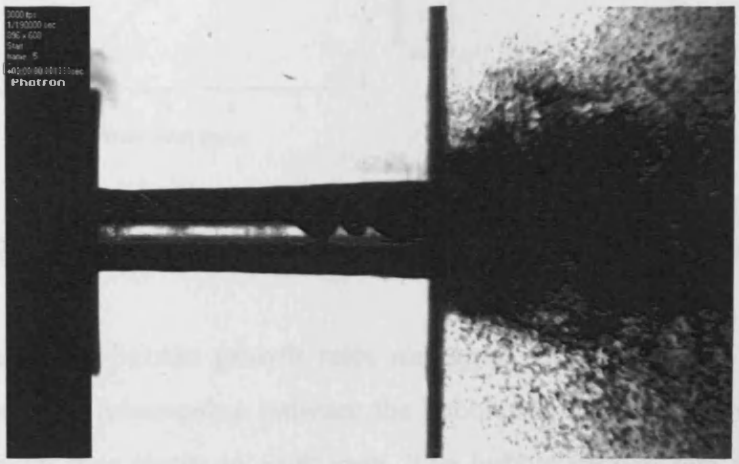

Figure 7.28 Internal and external flow conditions at 123.7°C and 4.1bar

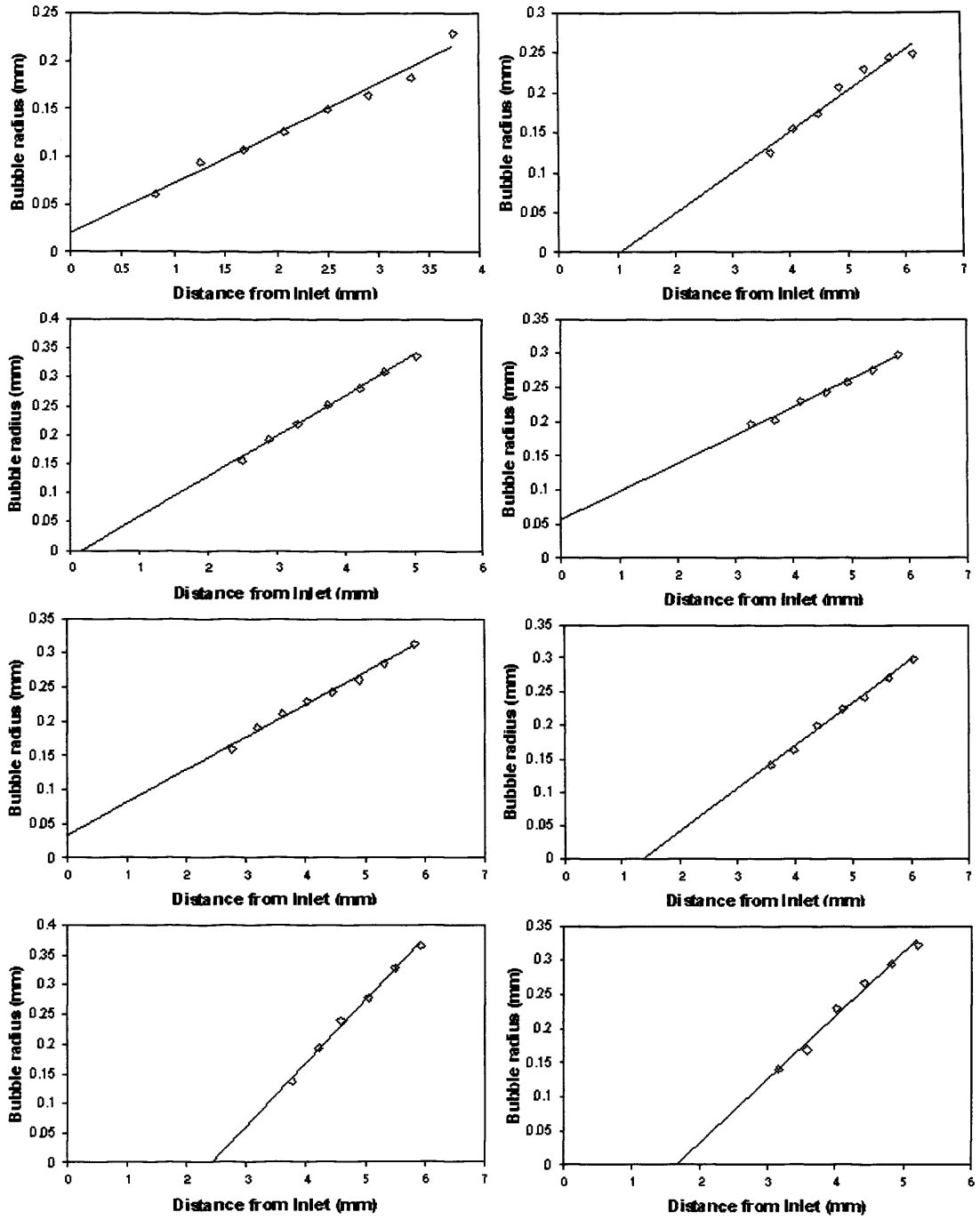

Figure 7.29 Bubble growth rates inside 2x7mm nozzle at 126.6°C and 4.4bar

Figure 7.29 presents the bubble growth rates measured inside the 2mm x 7mm nozzle at 126.6°C and 4.4bar. The relationship between the bubble radius and the downstream distance from the nozzle inlet was linear in each case. The bubble growth rate varied from 1.0 – 2.3ms^{-1} between cases, due to variations in bubble sphericity and thermal fluctuations in the liquid. Again in some cases the delay time for nucleation appeared to be 'negative' and these

times are included as zero when calculating the average, which was $8x10^{-5}$s in this case (1.6mm in terms of the delay length).

7.7.3 132.6°C jet temperature, 4.8 bar release pressure

Figure 7.30 presents footage taken at 50,000fps of an example of bubble growth inside the 2mm x 7mm nozzle at 132.6°C and 4.8bar. The upstream bubble frequency was 49.3kHz, which corresponded to a bubble concentration of $2.413x10^{8}$ bubbles/m^3. The bubble growth rate was $1.31ms^{-1}$.

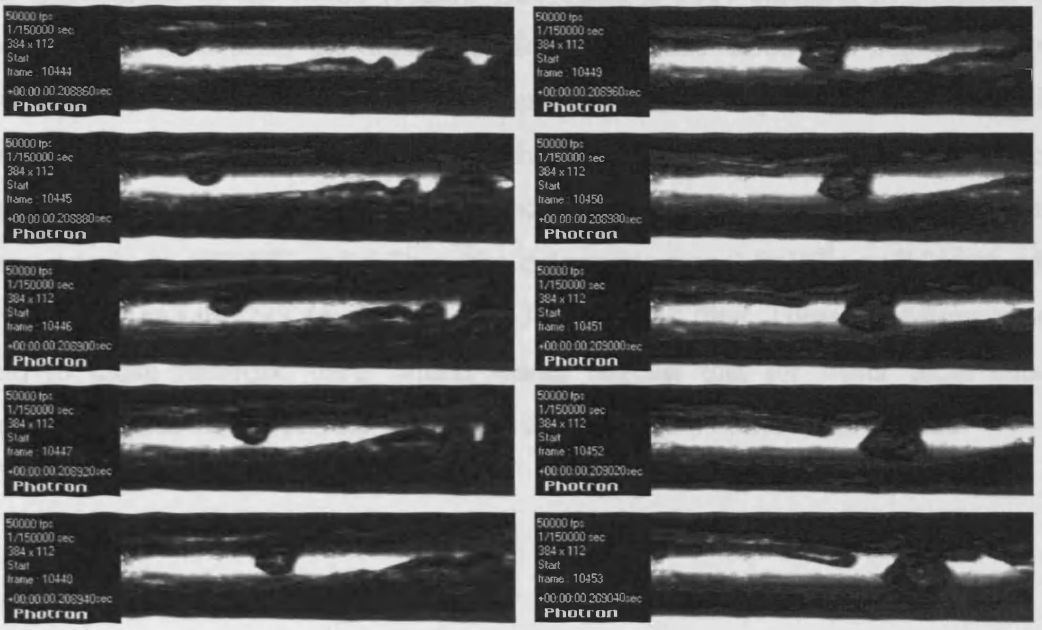

Figure 7.30 Bubble growth inside 2x7mm nozzle at 132.6°C and 4.8bar

Figure 7.31 presents the internal and external flow characteristics of a superheated jet at conditions of 131.2°C and 4.7bar. Although the downstream conditions are not fully visible, the downstream break-up regime demonstrated characteristics of an intermediate stage of transition, although again it was closer to full flashing than the first stage of transition. The liquid core was shorter than the jet produced at 126.6°C and 4.4bar, however, the spray still consisted of ligaments and liquid blobs generated by upstream slug bubbles.

Figure 7.31 Internal and external flow conditions at 131.2°C and 4.7bar

Figure 7.32 presents the bubble growth rates measured inside the 2x7mm nozzle at 132.6°C and 4.8bar. The bubble radius increased linearly with downstream distance from the nozzle inlet, varying from 1 – 1.7ms^{-1} between cases due to variations in bubble sphericity and thermal fluctuations in the liquid (Figure 7.30 being a good example of irregular bubble development). In each case, the delay time for bubble nucleation was negative. However, since the turbulence inside the nozzle appeared to artificially create the impression of upstream bubble nucleation at lower superheats, it is unclear whether this is accurate Interestingly however, the two previous instances of zero delay time were recorded using the 1x3.4mm nozzle at 129.4°C and 5.3bar (the delay time was 2.6x10^{-6}s or 0.06mm which is effectively zero) and the 2x3.4mm nozzle at 131.2°C and 4.5bar. These conditions are almost identical to those recorded here, which would suggest that for water these conditions represent the critical conditions for zero delay time upstream of the nozzle outlet.

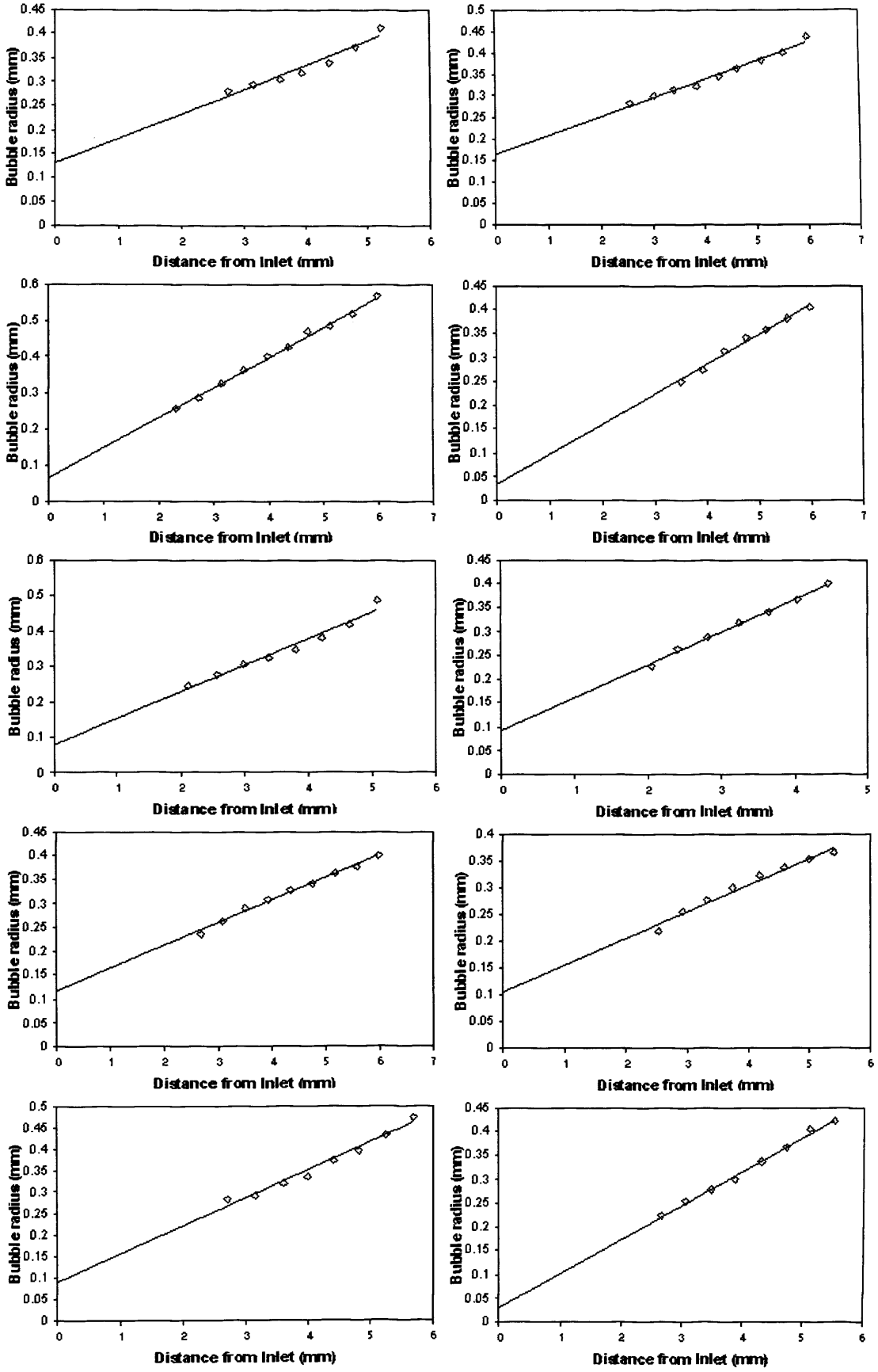

Figure 7.32 Bubble growth rates inside 2x7mm nozzle at 132.6°C and 4.8bar

7.7.4 136.1°C jet temperature, 5.5 bar release pressure

Figure 7.33 presents footage taken at 50,000fps of an example of bubble growth inside the 2x7mm nozzle at 136.1°C and 5.5bar immediately downstream of the nozzle inlet. The upstream bubble frequency was 69.6kHz, which corresponded to a bubble concentration of 3.104×10^8 bubbles/m^3. The bubble growth rate was 1.54ms^{-1}. Bubble nucleation occurred in the flow stream as well as through the effect of the turbulent flow structures associated with this nozzle. Nevertheless, these structures were still responsible for a significant proportion of those bubbles which nucleated upstream.

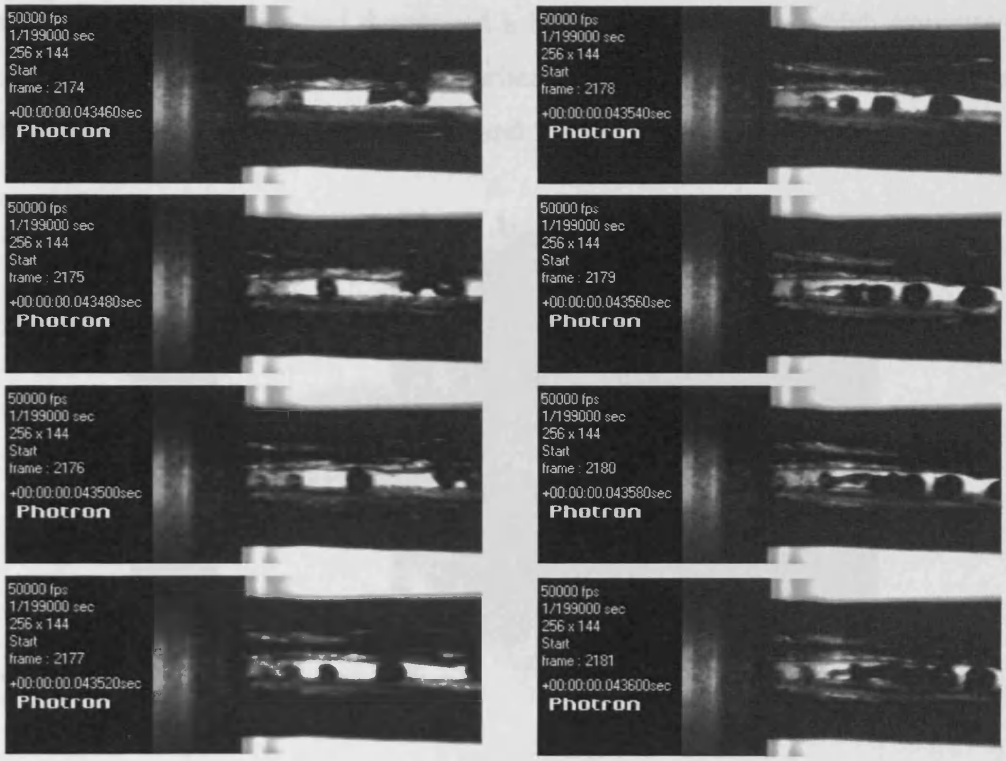

Figure 7.33 Bubble growth inside 2x7mm nozzle at 136.1°C and 5.5bar

At marginally higher superheat and pressure these turbulent structures developed to the extent that they completely dominated the upstream flow structure as demonstrated by Figure 7.34, which presents the internal flow structure at 138.8°C and 5.7bar. As the superheat increased and the turbulent flow structures dominated the upstream conditions, vapour production occurred in the form of continuous streams rather than individual bubbles, which coalesced further downstream to create a highly vaporised flow at the nozzle exit.

Figure 7.34 Internal flow conditions at 138.8°C and 5.7bar

Downstream conditions were still characteristic of an intermediate stage of transition with an intact core of approximately 5 nozzle lengths existing immediately downstream of the orifice exit. Ligaments were observed at the edge of the core which quickly broke up into smaller droplets. Nevertheless the jet had developed a barrel shaped spray, which suggests that the conditions were approaching the transition criteria for full flashing. Figure 7.35 presents the external break-up characteristics at 136.2°C and 5.4bar.

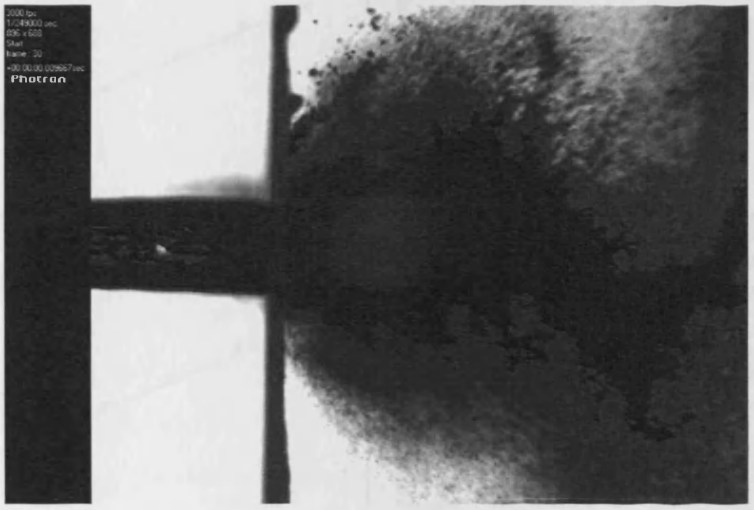

Figure 7.35 External flow conditions at 136.2°C and 5.4bar

Of those bubbles which formed in the flow-stream, nucleation appeared to be instigated by a surface aberration at the nozzle inlet, which effectively gave those bubbles a zero delay time. This is confirmed by the bubble growth rates presented in Figure 7.36, where in each case the delay time was 'negative' or effectively zero.

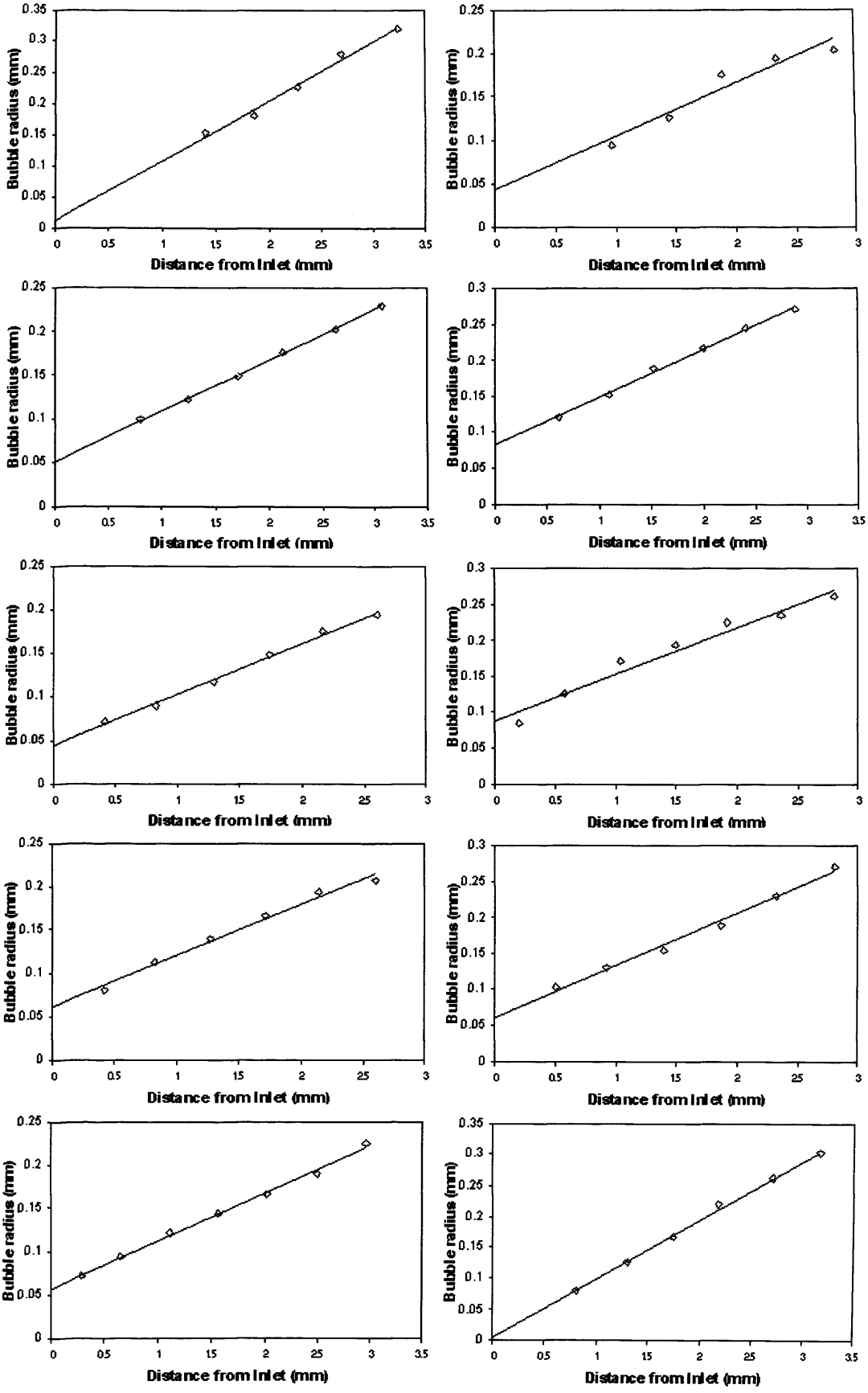

Figure 7.36 Bubble growth rates inside 2x7mm nozzle at 136.1°C and 5.5bar

7.7.5 148.0°C jet temperature, 6.4 bar release pressure

Figure 7.37 presents the upstream and downstream flow characteristics of a superheated jet at 148.0°C and 6.4bar. The downstream conditions are at such an advanced stage of full flashing that even with a shutter speed of $5.3x10^{-6}$s the camera was unable to pick out individual droplets dispersing in the spray.

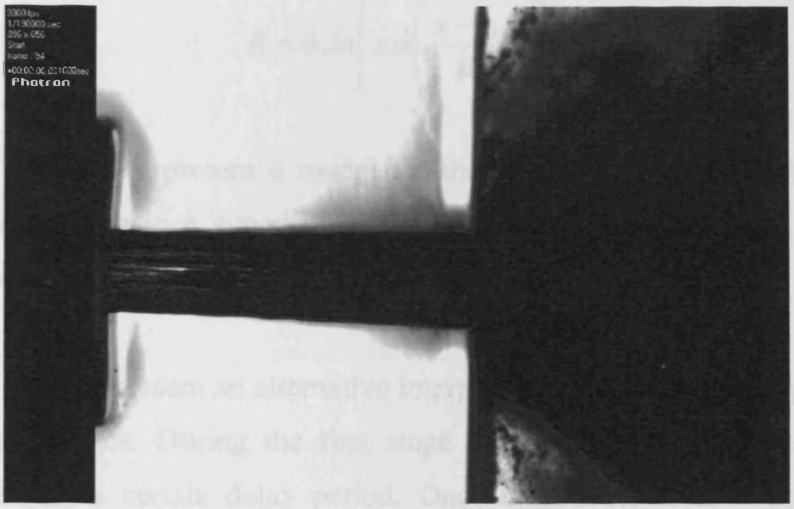

Figure 7.37 Internal and external flow characteristics at 148.0°C and 6.4bar

Vapour production occurred in the form of continuous streams rather than individual bubbles, which coalesced further downstream to create a high void fraction at the nozzle outlet. Hence downstream conditions were characterised by a barrel shaped spray, with violent jet disintegration at the nozzle and no delay time for bubble growth. Little further discernible change in the downstream flow structure would be anticipated with any additional increase in superheat. Due to the lack of individual bubble nucleation upstream of the exit orifice it was not possible to measure bubble growth rate, bubble frequency or bubble concentration at these conditions.

7.8 Bubble Growth Rate

Various models for determining bubble growth rates in uniformly superheated liquids are presented in the literature. Scriven's analysis[99] for bubble growth is presented here in Equation (7.1) and Kitamura's[61] adaptation of this formula is presented in Equation (7.2).

However, both equations are found to considerably under-predict the experimental growth rates measured in the course of this study. However, Scriven's analysis was developed for motionless bubble growth and Kitamura's equation was developed for bubble growth at atmospheric conditions, which both differ from the problem presented here.

$$R = C\,Ja\left[\alpha(t - t_0)\right]^{0.5} \qquad (7.1)$$

$$R = \phi\,Ja\left[\pi\alpha\left(\frac{x - x_0}{u_l}\right)\right]^{0.5} \qquad (7.2)$$

Ivashnyov and Smirnov[155] present a model for the growth of motionless bubbles and the growth of bubbles rising in a superheated liquid. However, this model is again found to under-predict the experimental data.

Various studies[102,103,104] present an alternative interpretation of bubble growth by dividing the process into three stages. During the first stage of growth, surface tension is dominant, impeding growth for a certain delay period. Once the bubble reaches a given size, e.g. doubles its diameter, bubble growth is controlled by the difference between the vapour pressure inside the nozzle and the exterior pressure, balanced by the inertia of the surrounding liquid; i.e. inertial growth. As the bubble grows further, the wall temperature consequently drops, causing an increased temperature difference between the surrounding liquid and the bubble wall. Hence, the final stage of growth is controlled by the rate of energy transfer from the liquid to the liquid-vapour interface to produce vapour and maintain the pressure; i.e. thermal growth. Mikic *et al*[102] developed a model governing bubble growth for the second and third stages of growth. Miyatake and Tanaka[103,104] developed upon this model in an experimentally validated numerical study, to produce an equation which governs complete spherical bubble growth across all three stages. However, both models are again found to under-predict the bubble growth rates measured in the course of this study.

Yuan *et al*[156] adopt the Rayleigh equation[98] in their model governing cavitating flows in injection nozzles, previously presented in Equation (2.24). This equation is based on the difference between the vapour pressure inside a bubble and the exterior pressure, balanced by the inertia of the surrounding liquid. The first phase of inertial growth in the models presented by Mikic *et al* and Miyatake and Tanaka is also described by this formula.

Currently, this equation is also widely used in numerical computation[157]. While Yuan *et al*'s model was developed for sub-cooled sprays, the conditions are similar to those of the problem presented here, where the pressure difference is supplied by the thermodynamic properties of the liquid.

$$\frac{dR}{dt} = \left[\frac{2}{3}\left(\frac{P(v) - P_l}{\rho_l}\right)\right]^{0.5} \qquad (2.24)$$

$P(v)$ is the saturated vapour pressure at the liquid temperature, P_l is the liquid pressure inside the nozzle given by Equation (7.3). P is the absolute pressure upstream of the nozzle inlet, ρ_l is the density of the liquid and u_l is the upstream flow velocity.

$$P_l = P - \frac{1}{2}\rho_l u_l^2 \qquad (7.3)$$

This equation is found to represent the current data relatively well, as demonstrated by Figure 7.38, which presents the measured growth rates versus the theoretical growth rates predicted by the Rayleigh equation

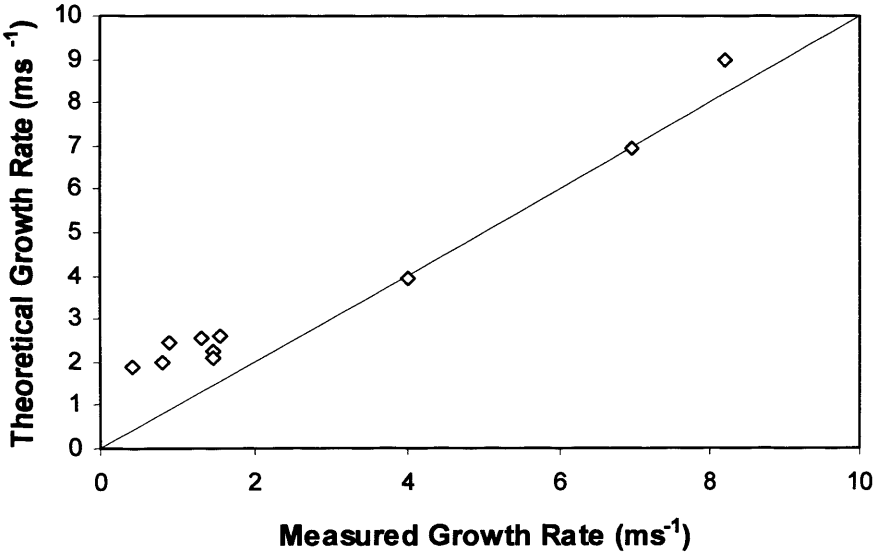

Figure 7.38 Accuracy of Rayleigh equation for predicting experimental growth rates

Equation (7.3) is highly sensitive to the pressure upstream of the nozzle inlet, so a sensitivity analysis was performed in order to examine the reasons for the discrepancy between the theoretical and experimental growth rates when the measured growth rate was below $2ms^{-1}$ the results of which are presented in Table 7.1.

Table 7.1 Sensitivity analysis of Rayleigh equation for bubble growth

Measured pressure Nm-2	Theoretical pressure required to produce measured growth rate Nm-2	Relative error between theoretical and measured pressure	Relative error between theoretical and measured growth rate
530000	529471	0.999	0.988
280000	283177	1.017	2.488
250000	257209	1.029	2.716
205000	209807	1.023	4.528
320000	319663	0.999	0.998
450000	468906	1.042	1.097
295000	299097	1.014	1.532
440000	443159	1.007	1.438
480000	486527	1.014	1.940
550000	556147	1.011	1.700

The figures presented in Table 7.1 show that a small error in the measured pressure is capable of producing a large error in the predicted growth rate. It is conceivable that an error in the synchronisation of the data acquisition system with the recorded footage of the upstream conditions could have produced these errors, especially since the error only needed to be very small. This indicates that the Rayleigh equation for bubble growth seems appropriate for predicting bubble growth rates in superheated jets upstream of the nozzle outlet, which in turn indicates that bubble growth rates measured in this study were controlled by the difference between the vapour pressure inside the nozzle and the exterior pressure, balanced by the inertia of the surrounding liquid

7.9 Delay Time for Bubble Growth

Figure 7.39 plots the average non-dimensionalised delay time ($\bar{t}_d$*) against the non-dimensionalised pressure difference between the vapour pressure inside the nozzle and the exterior pressure (ΔP_0*), where $\bar{t}_d$* *is* given by Equation (7.4) and ΔP_0* is given by Equation (7.5).

$$\bar{t}_d^* = \frac{\bar{t}_d u_l}{L} \qquad (7.4)$$

$$\Delta P_0^* = \frac{P(v) - P_l}{P_l} \qquad (7.5)$$

When calculating the average delay time ($\bar{t}_d$), where the delay time (t_d) was found to be 'negative', it was assumed to be zero. This zero value was then included in the calculations of the average delay time so as not to ignore the existence of this phenomenon and retain some of its influence on the upstream flow conditions.

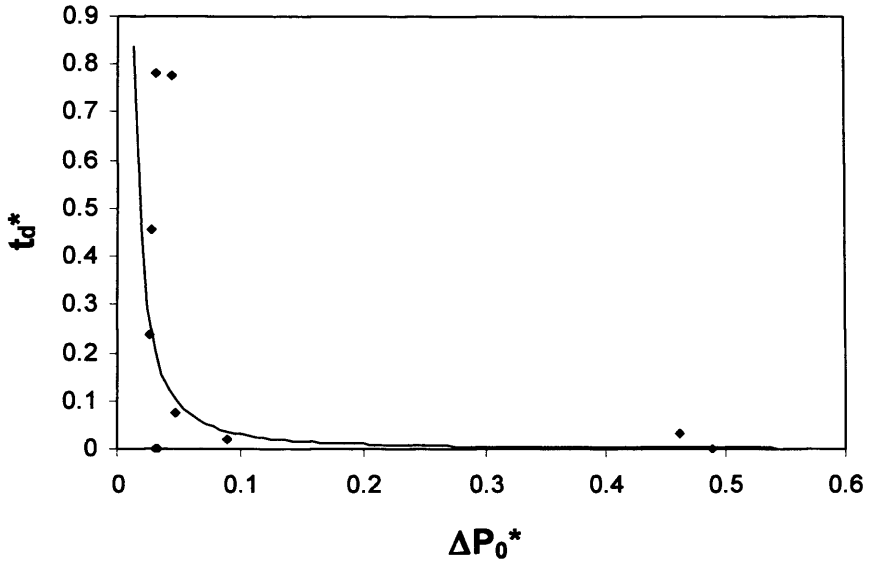

Figure 7.39 Variation of delay time with pressure difference

The relationship between the average non-dimensionalised delay time and the non-dimensionalised pressure difference is described by Equation (7.6).

$$\bar{t}_d^* = 7x10^{-4} \left(\Delta P_0^*\right)^{-1.612} \qquad (7.6)$$

This equation can be used to predict the delay time for the start of inertial growth. According to bubble theory, prior to this stage the bubble nucleus must exceed a critical radius, below which it would collapse due to surface tension. It is widely accepted[102,103,104,158,159] that the critical bubble radius at which a bubble nucleus is sustained as a result of equilibrium between the surface tension and the pressure difference across the bubble wall is reproduced here, having originally been given by Equation (2.13).

$$R_c = \frac{2\sigma}{P(v) - P_l} \qquad (2.13)$$

However, this equation produces critical bubble radii in the order of $1x10^{-6} - 2x10^{-5}$m for the conditions investigated here. These sizes are relatively insignificant with respect to the

measured bubble growth rates. Therefore, for modelling purposes, it is suggested that for the sake of simplicity the critical bubble radius, or the radius at which inertial growth begins can be considered as zero.

7.10 Bubble Concentration

It is well established that two-phase flow is induced via two mechanisms: homogenous nucleation as a result of molecular processes throughout the body of the fluid and heterogeneous nucleation at the liquid/solid surface interface. However, bubble formation by phase change usually occurs in the form of heterogeneous nucleation.

The classical theory for homogenous nucleation, as developed by Volmer and Weber[79] and Becker and Döring[80], predicts a homogenous nucleation temperature of water at atmospheric pressure of 310°C, which is clearly well outside the conditions investigated here. However, in previous experimental studies by Hung *et* al[160], El-Shall[161,162], Peters and Paikert[163] and Strey *et al*[164], where homogenous bubble nucleation was explicitly the subject of investigation, the predicted nucleation rate was found to be too high at high temperatures and too low at low temperatures. Delale *et al*[90] present a re-working of the classical nucleation theory which they demonstrate produces good agreement with experimental data for water over a wide range of liquid pressures. However, this re-working still predicts zero bubble nucleation for the conditions investigated. The non-classical density functional theory of nucleation proposed by Oxtoby and Evans[87] represents a slight improvement on the classical nucleation theory but still significantly under-predicts the current data. This indicates that for the conditions investigated, bubble nucleation was dominated by heterogeneous processes at the liquid/nozzle wall interface.

Heterogeneous nucleation is usually described in terms of the development of trapped vapour nuclei contained in cracks or cavities on container surfaces. Using a classical approach to model the process, it is possible to determine the energy of formation of the critical nucleus for the onset of heterogeneous nucleation, from which one can derive the critical superheat for a given cavity size. Nevertheless, in order to determine the bubble nucleation rate, it is necessary to know the nucleation site density on the active surface and the average cavity diameter. However, experimental and theoretical research into heterogeneous nucleation of

fluids is in its infancy and attempts to predict nucleation site density have met with little success. Recent research by Qi and Klausner[93] found no significant difference between measured nucleation site densities on smooth and rough surfaces, which indicates that vapour trapping cavities are not solely responsible for seeding vapour bubble growth. In addition most current understanding is based on pool boiling of liquid using a submerged heating element, upon the surface of which nucleation takes place. Hence, it is not clear how current theory can be applied to the circumstances investigated here.

Nevertheless, it has been well established that the rate of heat transfer associated with boiling systems is strongly dependent on the nucleation site density. Inconsistencies in the manufacturing process of the nozzles used for investigating the upstream flow characteristics produced varying grades of surface imperfections and aberrations on the nozzle walls. In some cases the cross-sectional area of the nozzle was irregular throughout its length. In the case of the 2x7mm nozzle, this gave rise to Rayleigh-type instabilities, which appeared to be responsible for the augmentation of bubble nucleation inside the nozzle. Hence, there was no means of correlating the primary input parameters with the heterogeneous nucleation rate inside the nozzles investigated and in practice the bubble concentration did not display any correlation with any one input parameter. The influence of the confining walls on phase transition is clearly of strong technological relevance for characterising the upstream conditions of superheated jets and requires detailed investigation in future studies.

7.11 Model Governing Downstream Break-up Conditions

Figure 7.40 presents a model for predicting the downstream break-up regime based on the upstream bubble concentration and bubble growth rate. The model takes the form of a grid which is divided into four shaded sections which represent four stages of downstream break-up. The first stage is mechanical break-up, where despite the presence of upstream bubble nucleation, the bubble concentration is so low that mechanical processes still dominate, irrespective of the bubble growth rate. The next stage is analogous to transition condition A outlined in section 6.1.2, where flashing succeeds mechanical break-up as the dominant break-up mechanism. This regime is characterised by high bubble concentrations but low growth rates or low bubble concentrations but high growth rates. The next stage is an intermediate stage of break-up which essentially represents the transition from condition A to

condition B/C and is characterised by high bubble concentrations but relatively low growth rates or high growth rates but relatively low bubble concentrations. The final stage of break-up is analogous to both transition conditions B and C outlined in section 6.1.2, where the difference between the two break-up regimes can be partly described by the average bubble radius at the nozzle exit. These break-up regimes are characterised by high bubble concentrations and high growth rates.

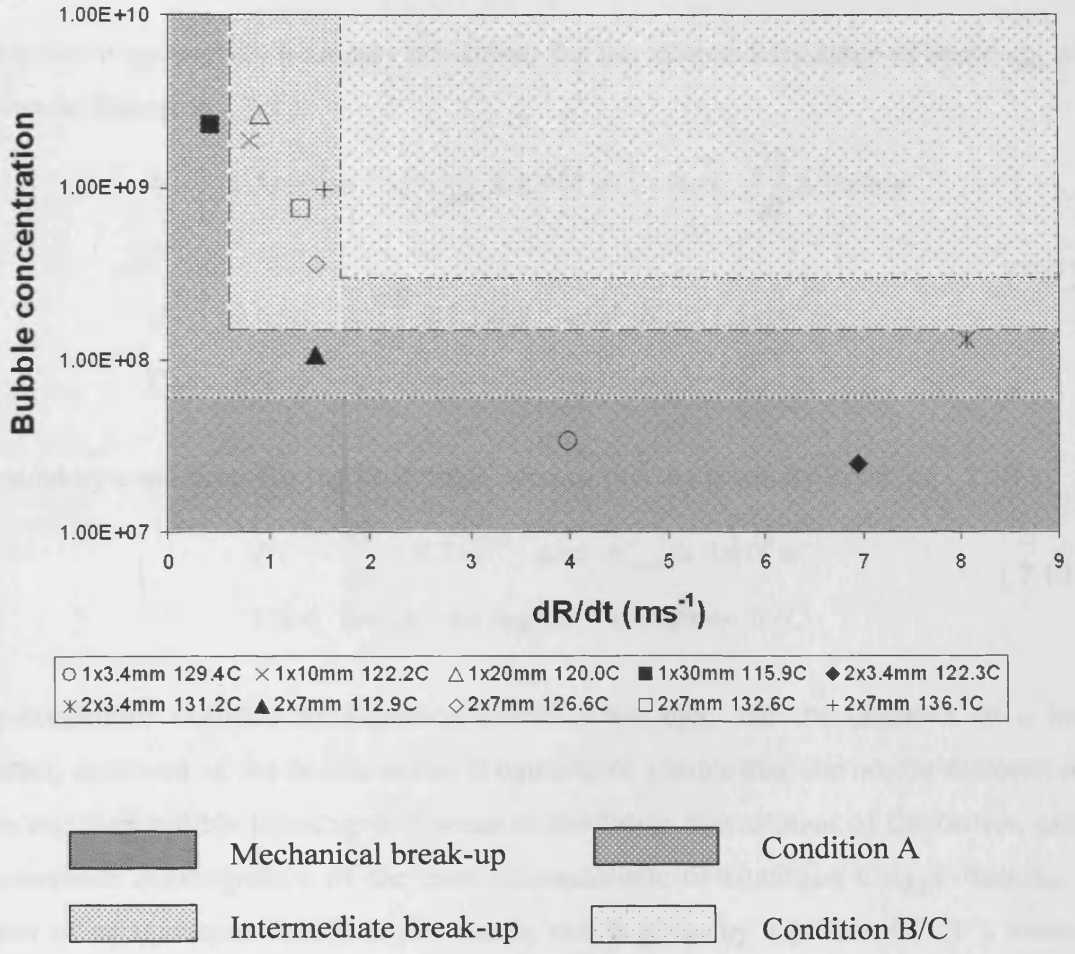

Figure 7.40 Model governing downstream break-up conditions

Mechanical break-up still dominates at low superheats and is described by an upper bubble concentration limit, demonstrated by Equation (7.7)

$$\begin{aligned} &If, \quad N_{conc} \geq 6x10^{7}\, m^{-3} \\ &Then, \quad break-up\ regime = mechanical\ break-up \end{aligned} \qquad (7.7)$$

Two equations govern the boundary conditions for the first stage flashing, which are given by Equation (7.8)

$$\begin{aligned} &If, \quad 6x10^{7}\,m^{-3} < N_{conc} \le 1.5x10^{8}\,m^{-3} \\ &or, \\ &If, \quad \frac{dR}{dt} \le 0.6\,ms^{-1} \;\; and \;\; N_{conc} > 6x10^{7}\,m^{-3} \\ &Then, \;\; break-up\ regime = Condition\ A \end{aligned} \tag{7.8}$$

Two equations govern the boundary conditions for the intermediary stage of break-up, which are given by Equation (7.9).

$$\begin{aligned} &If, \quad 1.5x10^{8}\,m^{-3} < N_{conc} \le 3x10^{8}\,m^{-3} \;\; and \;\; \frac{dR}{dt} > 0.6\,ms^{-1} \\ &or, \\ &If, \quad 0.6\,ms^{-1} < \frac{dR}{dt} \le 1.7\,ms^{-1} \;\; and \;\; N_{B} > 1.5x10^{8}\,m^{-3} \\ &Then, \;\; break-up\ regime = Intermediate\ break-up \end{aligned} \tag{7.9}$$

The boundary conditions for the final stage of transition are given by Equation (7.10)

$$\begin{aligned} &If, \quad \frac{dR}{dt} > 1.7\,ms^{-1} \;\; and \;\; N_{conc} > 3x10^{8}\,m^{-3} \\ &Then, \;\; break-up\ regime = Condition\ B/C \end{aligned} \tag{7.10}$$

If the conditions outlined by Equation (7.10) are met, and the diameter of a bubble nucleating upstream of the nozzle outlet is equal to or greater than the nozzle diameter at the nozzle exit then bubble bursting will occur immediately downstream of the orifice, causing the immediate disintegration of the core, characteristic of condition C type flashing. The diameter of an upstream bubble at the nozzle exit is given by Equation (7.11), where the bubble growth rate dR/dt is given by Equation (2.24), the average delay time $\bar{t}_d$ is derived from Equation (7.6) and t_u is the upper time limit for bubble growth, which is given by L/u_l.

$$d_B = 2\frac{dR}{dt}\left(t_u - \bar{t}_d\right) \tag{7.11}$$

If we assume that the upper bubble diameter limit at the nozzle exit for break-up condition B to occur is $0.9d_0$ then the criteria determining the difference between condition B and C is given by Equation (7.12).

$$
\begin{aligned}
&If, \quad d_B \leq 0.9 d_0 \\
&Then, \quad break-up\ regime = Condition\ B \\
&If, \quad d_B > 0.9 d_0 \\
&Then, \quad break-up\ regime = Condition\ C
\end{aligned}
\qquad (7.12)
$$

If the saturated vapour pressure is less than the pressure in the nozzle, bubble nucleation will not occur upstream of the orifice exit. However, if the saturated vapour pressure exceeds atmospheric pressure, bubble nucleation will occur downstream. Under these conditions, the transition criteria outlined in chapter 6 can be used to determine the downstream break-up conditions.

7.12 Discussion

Superheated jets were observed to flash at lower superheats when the nozzle material was Perspex as opposed to brass. This can be partly explained by the differences in surface roughness and nucleation site density which have been shown to lower the barrier to nucleation and raise the rate of critical bubble nuclei formation. However, the primary reason for this disparity was a difference in the experimental procedure between identifying the downstream transition criteria and the upstream flow characteristics. In the course of establishing the downstream transition criteria, one charge of the superheated atomiser was utilised for each set of initial conditions. However, when investigating the upstream flow structure one charge was used to investigate a given orifice geometry at various frame rates, and sometimes more than one nozzle. In each case filming was started once the temperature of the jet had stabilised. Pressure in the tank was created by the expansion of water, hence the pressure steadily dropped as the tank emptied. Therefore, for a given superheat, downstream break-up criteria were established at the atomiser's maximum operating pressure, while in certain instances upstream flow characteristics were investigated at comparatively low release pressures. Since the bubble growth rate, and delay time have both been shown to be correlated by the difference between the saturated vapour pressure and the pressure in the nozzle, the release pressure is clearly critical to the downstream break-up regime, which explains the apparent discrepancy in the necessary superheat for flashing between the brass and Perspex nozzles.

The proposed model for determining the downstream break-up regime based on the bubble growth rate and bubble concentration has been developed in the absence of conclusive data for fully flashing conditions. Hence the proposed criteria for transition between intermediate flashing and full flashing are intuitive projections based on the data that was available. However, the downstream conditions for the release at 136.1°C and 5.5bar through the 2x7mm nozzle were observed to be at an intermediate stage, which appeared to be approaching full flashing, for which case it was possible to take measurements of bubble growth, bubble concentration and delay time. The downstream conditions for the release at 148.0°C and 6.4bar were observed to be fully flashing, but the upstream conditions precluded the measurement of the bubble properties. The transition criteria for full flashing must therefore lie between these two release conditions. Hence the proposed criteria have been tailored accordingly. Nevertheless, they clearly require validation based on experimental data. Moreover, the model is based on ten data points, hence, all of the boundary conditions outlined require validation and it is recommended at this stage that they be interpreted as guidelines rather than definitive transition criteria.

The lack of understanding in the process of heterogeneous bubble nucleation precludes the prediction of the upstream bubble concentration. Hence for the implementation of the outlined boundary conditions for modelling purposes, this area requires thorough investigation. This is likely to be a highly involved and lengthy process. Nevertheless, qualitatively, the model outlined in Figure 7.40 provides a sound basis for the framework of a model for determining the downstream conditions based on the bubble growth rate and bubble concentration.

7.13 Summary

Results from a high speed photographic study of the upstream flow structure of superheated jets have been presented and discussed. Upstream conditions have been categorised in terms of the bubble growth rate (given as the average measured growth rate), delay time and concentration.

The recorded bubble growth rates have been compared with various previously proposed theories of bubble growth in superheated liquids and the Rayleigh equation has been found to

adequately represent the data. Due to the restrictions applied by the confines of the nozzle geometry, bubble growth did not develop into the thermal growth regime, but was dominated by inertial growth. A sensitivity analysis of the Rayleigh equation highlighted the sensitivity of the predicted bubble growth rate to the upstream pressure. This was used to explain the discrepancies between the theoretical and measured growth rates.

The average delay time for bubble growth has been found to be correlated by the non-dimensionalised difference between the interior bubble pressure and exterior liquid pressure. The correlation effectively determines a critical cut-off point above which the delay time is in effect zero. Given the small size of the theoretical critical bubble radius with respect to the measured bubble radii and bubble growth rates bubble growth rates it is suggested that for modelling purposes it can be assumed to be zero.

Both the classical nucleation theory and the density functional theory for homogenous nucleation grossly under-predict the measured bubble concentrations. Hence, heterogeneous nucleation at the liquid/nozzle wall interface was the dominant mode of bubble production inside the nozzle. Heterogeneous nucleation is poorly understood but it is widely accepted to be a function of the nucleation site density. However, inconsistencies in the manufacturing process of the nozzles used for investigating the upstream flow characteristics produced varying grades of surface imperfections and aberrations on the nozzle walls. Hence, bubble concentration could not be correlated with any of the primary input parameters, and this remains an area for further investigation.

A model based on the upstream bubble concentration and bubble growth has been proposed for predicting transition between four highlighted downstream break-up conditions when the saturated vapour pressure exceeds the pressure in the nozzle. When the pressure in the nozzle exceeds the saturated vapour pressure, it is recommended that the transition criteria outlined in Chapter 6 be applied.

When the saturated vapour pressure exceeds the pressure inside the nozzle, the difference between condition B and condition C-type flashing can be described in terms of the average bubble diameter at the nozzle exit.

7.14 Future Work

The results presented in this chapter are subject to the limitations of quality of manufacture of the nozzles utilised. Hence, the main priority of future studies in this field should be to aim towards eliminating inconsistencies in the manufacturing process of the nozzles utilised and the development of precision engineered orifices representative of idealised conditions. This would also facilitate the investigation of possible homogenous processes occurring in the nozzle. The use of quartz is suggested as an ideal solution to this problem, although it is acknowledged that it may never be possible to completely eliminate surface imperfections from nozzle manufacture.

Heterogeneous nucleation remains poorly understood, yet it is the primary cause of upstream bubble nucleation in superheated liquid jets. It is not only necessary to better understand the influence of the confining nozzle walls on phase transition, but also to recognise the particular nucleation behaviour associated with this application. Hence, the development of experimental methodologies for determining the influence of such input parameters as surface roughness and nucleation site density, as well as temperature and pressure, on the bubble concentration requires considerable attention.

The data presented is limited by the range of initial conditions investigated. A more comprehensive analysis of the upstream flow structure is therefore necessary to validate the current data and potentially develop upon the findings of this study further. Particular attention is required in the investigation of the upstream conditions for fully flashing releases where there still remains a dearth of information. This would facilitate the establishment of validated transition criteria for this mode of break-up.

The technique utilised was limited at high temperature and pressure where the illumination equipment was unable to penetrate both the bubble density upstream and the spray density downstream. High power illumination e.g. by sheet laser may facilitate progress in this area and the feasibility of using such a technique should at least be investigated.

Chapter 8 Conclusions

8.1 Introduction

In this chapter the primary conclusions drawn from all aspects of this experimental study of pressurised liquid releases through simple orifices are collated. Where appropriate, proposed correlations are presented, including recommendations for the use of previously proposed correlations in the literature.

8.2 Mechanical Break-Up

A non-dimensionalised SMD correlation for break-up of sub-cooled sprays has been developed based on PDA data for isothermal water jets in atomisation regime, previously presented by Equation (5.15) and reproduced here.

$$\frac{SMD}{d_0} = 64.73\left(\frac{L}{d_0}\right)^{0.114} \mathrm{Re}^{-0.014} We^{-0.533} \qquad (5.15)$$

The accuracy of the correlation in reproducing the original dataset has been discussed, with predicted results representing a mean relative error of 0.135, and a standard deviation of 0.172 from this error. Sample graphs have been compiled for a range of release scenarios, comparing predictions from 4 different previous models, developed outside the range of conditions investigated in the course of this study. The proposed correlation compares favourably with previously proposed models, demonstrating good agreement for exponents of d_0 and ΔP. Under conditions similar to diesel injection (> 10^8 Pa), SMD values less than 20 microns are predicted by the proposed correlation, which is consistent with data from automotive diesel sprays, providing confidence in using the correlation to extrapolate to conditions outside the current dataset.

Similarity scaling has been performed in terms of the liquid density, shear viscosity and surface tension, in order to evaluate the applicability of the correlation to fluids other than water. The exponents of the primary parameters inherent in the proposed correlation are intuitively sensible and demonstrate good agreement with previously proposed correlations developed outside the domain of this study, which supports the interim use of the correlation in its current form until data from releases of materials other than water becomes available.

The PDA data has been shown to demonstrate significant truncation as a result of inherent inaccuracies in the adopted 1D system and the poor atomisation quality of sprays at low release pressures (< 8bar). The system utilised represented technology at the cutting edge of current diagnostic techniques, which operated at the limit of its capability at all times. Data truncation was therefore an inevitable consequence of the application investigated. Nevertheless the favourable comparison of the proposed correlation with previous droplet size correlations and moreover, with the dataset for low pressure releases (less than 8bar) presented by Buchlin and St.Georges[54], indicates that while errors associated with the measurement process were not insignificant, they do not preclude the use of the correlation as a tool for modelling sub-cooled releases of sub-cooled liquid jets to the atmosphere. On the contrary, it would appear that it is more appropriate than any previously proposed correlation currently available.

A correlation for the droplet size distribution has been proposed based on the common Rossin-Rammler distribution, previously presented by Equation (5.24) and reproduced here. The proposed correlation demonstrates good agreement with the recorded data and represents a significant improvement on previously proposed droplet distributions.

$$1 - v(D) = e^{-1.34\left(\frac{D}{SMD}\right)^{0.5}} \qquad (5.24)$$

8.3 Flashing Atomisation

Analysis of the spray jet-width has been proposed as a simple and unobtrusive method of characterising the transition from mechanical break-up to flashing for superheated sprays. A point of inflection in the relationship between the jet superheat and jet width characterises the point of transition, which is found to exist between 20-30°C for a 2x3.4mm nozzle.

Rainout fraction has been demonstrated to be inversely proportional to the degree of superheat. It is tentatively suggested that the orifice size, height of the orifice above ground level and the length of piping prior to the orifice inlet have no influence on the resultant rainout associated with a release of superheated liquid.

The correlation proposed by De Vaull and King for non-volatile liquids is suggested as a useful tool for providing an estimate of the rainout fraction from releases of non-volatile superheated liqiuids. This correlation is reproduced here.

$$\eta_R = 1 - \frac{C_{pl}}{h_{lg}}(T_0 - T_{as}) \qquad (2.43)$$

A quantitative experimental methodology for identifying transition from mechanical break-up to full flashing has been designed and implemented, allowing comparison of transition data with the correlation previously proposed by Kitamura *et al.* The current dataset has been demonstrated to be consistent with the correlation advocated by Kitamura *et al* for transition to condition B-type flashing identified within the context of this study. The transition criterion is based on the Weber number and Jakob number, modified by a correction factor derived from the difference between theoretical and measured bubble growth rates in superheated jets. Hence, it is proposed that this correlation, reproduced here, is adopted until a broader dataset for a range of materials becomes available.

$$Ja\phi = 100We^{-\frac{1}{7}} \qquad (6.5)$$

Three distinctive stages of transition have been identified for the break-up of superheated jets from the mechanical regime to full flashing. Two equations governing the starting point and end point of transition, identified as condition A and condition C within the context of this study, have been recommended for modelling purposes. These equations are reproduced here.

$$Ja\phi = 55We_v^{-\frac{1}{7}} \qquad (6.6)$$

$$Ja\phi = 150We_v^{-\frac{1}{7}} \qquad (6.7)$$

Traditional laser diffraction based techniques have been shown to be inadequate for investigating large-scale pressurised releases of superheated jets. Although calibration equations exist, the obscuration rates associated with recorded data precluded the application of these equations to the current dataset. Consistent with the recommendations of the literature review, PDA has been shown to be currently the most suitable optical technique for characterisation of flashing jets.

PDA data for fully flashing sprays at two release conditions have been presented and discussed. Close to the orifice exit, the release conditions dominate the droplet size distribution, while aerodynamic influences, coalescence and rainout begin to take over as droplets move further downstream. Hence, post-expansion data was taken at 250mm downstream, at which point it was assumed that dynamic jet break-up was complete and the effect of coalescence and rainout was least significant.

A correlation for the droplet size distribution has been proposed based on the common Rossin-Rammler distribution, reproduced here. The proposed correlation demonstrates good agreement with the recorded data and represents a significant improvement on previously proposed droplet distributions.

$$1 - v(D) = e^{-0.5\left(\frac{D}{SMD}\right)^{3.5}} \qquad (6.9)$$

The SMD correlation for mechanical break-up presented by Equation (5.15), the established transition criteria and the PDA data have been combined to produce an SMD model governing complete transition from mechanical break-up to full flashing, based on Muralidhar's simple model for liquid capture. In the absence of data, a linear relationship has been assumed to exist between droplet SMD and superheat during the intermediary stage of transition. The full model is outlined by Equation (6.10) and is reproduced on the following page.

The model has been validated against experimental data from a range of studies. Since the large majority of the data was generated using water as the model fluid, the lack of data for different materials is considered the most significant deficiency at this stage of understanding Hence, although an improvement on previous models for superheated releases, there is still considerable research and development required to appraise, consolidate and develop some of the assumptions and modelling approaches adopted in this study. Nevertheless, the level of agreement between the model and previous data validates the approach outlined for extending the model for use with fluids other than water until a more comprehensive dataset becomes available.

DNV have integrated this model into their PHAST/ATEX code for modelling large-scale atmospheric dispersion and have found reasonable agreement with a range of materials.

If $Ja\phi \le 55We_v^{-\frac{1}{7}}$

Then $\frac{SMD}{d} = 64.73 \cdot \left(\frac{L}{d}\right)^{0.114} \mathrm{Re}^{-0.014} \cdot We_L^{-0.533}$

If $55We_v^{-\frac{1}{7}} < Ja\phi \le 150We_v^{-\frac{1}{7}}$

Then $SMD = \left(\frac{f_1 - f_2}{x_1 - x_2}\right) \cdot (x - x_1) + f_1$

where $(x_1, f_1) = (\Delta T, SMD)$ when $Ja\phi = 55We_v^{-\frac{1}{7}}$ (6.10)

$(x_2, f_2) = \left(\Delta T, \frac{f_1}{5}\right)$ when $Ja\phi = 150We_v^{-\frac{1}{7}}$

If $Ja\phi > 150We_v^{-\frac{1}{7}}$

Then $SMD = \left(\frac{f_1 - f_2}{x_1 - x_2}\right) \cdot (x - x_1) + f_1$ for $SMD \ge 30\mu m$

Otherwise $SMD = -10^{-7}(x - x_3) + f_3$

Where $(x_3, f_3) = (\Delta T, SMD)$ when $SMD = 30\mu m$

8.4 Upstream Flow Structure

Results from a high speed photographic study of the upstream flow structure of superheated jets have been presented and discussed. Upstream conditions have been categorised in terms of the bubble growth rate (given as the average measured growth rate), delay time and concentration.

The recorded bubble growth rates have been compared with various previously proposed theories of bubble growth in superheated liquids and the Rayleigh equation, reproduced here, has been found to adequately represent the data.

$$\frac{dR}{dt} = \left[\frac{2}{3}\left(\frac{P(v) - P_l}{\rho_l}\right)\right]^{0.5} \quad (2.24)$$

Due to the restrictions applied by the confines of the nozzle geometry, bubble growth did not develop into the thermal growth regime, but was dominated by inertial growth. A sensitivity analysis of the Rayleigh equation highlighted the sensitivity of the predicted bubble growth rate to the upstream pressure. This was used to explain the discrepancies between the theoretical and measured growth rates.

The average delay time for bubble growth has been found to be correlated by the non-dimensionalised difference between the interior bubble pressure and exterior liquid pressure, which is reproduced here.

$$\bar{t}_d^* = 7x10^{-4} \left(\Delta P_0^*\right)^{-1.612} \qquad (7.6)$$

The correlation effectively determines a critical cut-off point above which the delay time is in effect zero. Given the small size of the theoretical critical bubble radius with respect to the measured bubble radii and bubble growth rates bubble growth rates it is suggested that for modelling purposes it can be assumed to be zero.

Both the classical nucleation theory and the density functional theory for homogenous nucleation grossly under-predict the measured bubble concentrations. Hence, heterogeneous nucleation at the liquid/nozzle wall interface was the dominant mode of bubble production inside the nozzle. Heterogeneous nucleation is poorly understood but it is widely accepted to be a function of the nucleation site density. However, inconsistencies in the manufacturing process of the nozzles used for investigating the upstream flow characteristics produced varying grades of surface imperfections and aberrations on the nozzle walls. Hence, bubble concentration could not be correlated with any of the primary input parameters, and this remains an area for further investigation.

A model based on the upstream bubble concentration and bubble growth has been proposed for predicting transition between four highlighted downstream break-up conditions, namely mechanical break-up, intermediate break-up, condition A and condition B/C, when the saturated vapour pressure exceeds the pressure in the nozzle. When the pressure in the nozzle exceeds the saturated vapour pressure, it is recommended that the transition criteria outlined in Equations (6.5) - (6.7) be applied. The boundary conditions of this model are presented by Equations (8.1) - (8.2) and reproduced here.

$$\begin{aligned} &\textit{If,} \quad N_{conc} \geq 6x10^{7} m^{-3} \\ &\textit{Then, break-up regime = mechanical break-up} \end{aligned} \tag{7.7}$$

$$\begin{aligned} &\textit{If,} \quad 6x10^{7} m^{-3} < N_{conc} \leq 1.5x10^{8} m^{-3} \\ &\textit{or,} \\ &\textit{If,} \quad \frac{dR}{dt} \leq 0.6 ms^{-1} \quad \textit{and} \quad N_{conc} > 6x10^{7} m^{-3} \\ &\textit{Then, break-up regime = Condition A} \end{aligned} \tag{7.8}$$

$$\begin{aligned} &\textit{If,} \quad 1.5x10^{8} m^{-3} < N_{conc} \leq 3x10^{8} m^{-3} \quad \textit{and} \quad \frac{dR}{dt} > 0.6 ms^{-1} \\ &\textit{or,} \\ &\textit{If,} \quad 0.6 ms^{-1} < \frac{dR}{dt} \leq 1.7 ms^{-1} \quad \textit{and} \quad N_B > 1.5x10^{8} m^{-3} \\ &\textit{Then, break-up regime = Intermediate break-up} \end{aligned} \tag{7.9}$$

$$\begin{aligned} &\textit{If,} \quad \frac{dR}{dt} > 1.7 ms^{-1} \quad \textit{and} \quad N_{conc} > 3x10^{8} m^{-3} \\ &\textit{Then, break-up regime = Condition B/C} \end{aligned} \tag{7.10}$$

The diameter of an upstream bubble at the nozzle exit is given by Equation (7.11)

$$d_B = 2\frac{dR}{dt}(t_u - \bar{t}_d) \tag{7.11}$$

The criteria determining the difference between flashing condition B and C is given by Equation (7.12).

$$\begin{aligned} &\textit{If,} \quad d_B \leq 0.9 d_0 \\ &\textit{Then, break-up regime = Condition B} \\ &\textit{If,} \quad d_B > 0.9 d_0 \\ &\textit{Then, break-up regime = Condition C} \end{aligned} \tag{7.12}$$

If the saturated vapour pressure is less than the pressure in the nozzle, bubble nucleation will not occur upstream of the orifice exit. However, if the saturated vapour pressure exceeds atmospheric pressure, bubble nucleation will occur downstream. Under these conditions, the transition criteria outlined in chapter 6 can be used to determine the downstream break-up conditions.

Chapter 9 Future Work

9.1 Introduction

The following recommendations concerning future work are made as a result of the findings of this research programme:

9.2 Mechanical Break-Up

The extension of the proposed mechanical break-up correlation to conditions outside the current dataset requires justification. Droplet sizes in sub-cooled releases at pressures above 24bar, and therefore in the 'atomisation' break-up regime should be investigated. The proposed lower and upper cut-off limits for nozzle aspect ratio also require validation.

The influence of fluid properties on the proposed correlation requires assessment, in order to justify its application to fluids other than water. Hence, it is necessary to design and conduct an experimental programme capable of investigating releases of potentially toxic or flammable liquids in a safe and controlled manner.

A more complete understanding of the impact of the nozzle aspect ratio on droplet SMD is required. In addition the impact of realistic surface aberrations, and material of manufacture, on spray characteristics compared with the 'idealised', carefully manufactured orifices utilised in this study requires appraisal.

The dataset for sub-cooled sprays requires validation through the use of a Dual PDA 2D system with particular reference to the impact of the so-called 'trajectory effect'. The development of non-intrusive diagnostic technologies capable of measuring droplet sizes outside the range of the system utilised in the course of this study should be monitored so that the influence of data truncation on the recorded data can be assessed and eliminated when and where such technologies arise.

9.3 Flashing Atomisation

The upper cut-off limit at which the jet width ceases to significantly increase requires investigation. In addition, the use of the jet width as a method of jet characterisation requires validation for a more comprehensive range of initial conditions, with particular reference to the orifice dimensions.

It is necessary to develop towards an improved experimental methodology for the investigation of rainout fraction. The possible effects of inclement ambient conditions need to be eliminated, and a more accurate method of rainout collection requires implementation. The current data requires validation and the precise nature of the influence of superheat on the collected rainout fraction requires investigation.

A feasibility study of the possibility of safely measuring rainout from large scale releases of a range of materials should be conducted, and the results implemented in order to understand the effect of the fluid properties on the rainout fraction.

Given the current structure and relative simplicity of the SMD model for superheated sprays, the main priority for future work should be to provide data representative of conditions between the departure from mechanical break-up and fully flashing conditions

This experimental programme was restricted in terms of scale of release, due to the density of the spray for larger orifice sizes (Reynolds numbers). Further work should aim to utilise new developments in droplet size diagnostics, specifically focussed on dense-spray applications, which allow the measurement of releases for high mass flow-rates to the undertaken.

It is unlikely that a discontinuous linear correlation between the various modes of breakup is appropriate. Methods and models for characterising non-linear effects should be considered. For example, a two-phase model would be more appropriate after fully flashing conditions have been attained, and the presumed 'slow' linear decay of droplet size with superheat after the SMD has reached 30um requires appraisal. In addition the influence of orifice characteristics on droplet SMD in superheated jets needs to be investigated further.

Subject to constraints of the measurement technique, the feasibility of measuring the effect of superheat on droplet SMD in one complete sweep from sub-cooled to fully flashing sprays should be appraised. This would facilitate the direct comparison of the actual correlation function with that presumed (discontinuous linear function) in this study.

This study has only considered water and, as with the results achieved for sub-cooled releases, a similarity scaling approach has been utilised to allow predictions of other materials in lieu of data. Hence, the influence of variation in fluid properties on the proposed correlation needs to be assessed. This could have the affect of modifying the correlation, or require the introduction of additional dimensionless groups.

Whilst the focus of this work has been to develop simplified, semi-empirical models, more detailed modelling approaches for two-phase atomisation would also be beneficial and complementary to this study.

9.4 Upstream Flow Structure

The results of the study of the upstream flow structure of superheated jets are subject to the limitations of quality of manufacture of the nozzles utilised. Hence, the main priority of future studies in this field should be to aim towards eliminating inconsistencies in the manufacturing process of the nozzles utilised and the development of precision engineered orifices representative of idealised conditions. This would also facilitate the investigation of possible homogenous processes occurring in the nozzle. The use of quartz is suggested as an ideal solution to this problem, although it is acknowledged that it may never be possible to completely eliminate surface imperfections from nozzle manufacture.

Heterogeneous nucleation remains poorly understood, yet it is the primary cause of upstream bubble nucleation in superheated liquid jets. It is not only necessary to better understand the influence of the confining nozzle walls on phase transition, but also to recognise the particular nucleation behaviour associated with this application. Hence, the development of experimental methodologies for determining the influence of such input parameters as surface roughness and nucleation site density, as well as temperature and pressure, on the bubble concentration requires considerable attention.

The data presented is limited by the range of initial conditions investigated. A more comprehensive analysis of the upstream flow structure is therefore necessary to validate the current data and potentially develop upon the findings of this study further. Particular attention is required in the investigation of the upstream conditions for fully flashing releases where there still remains a dearth of information. This would facilitate the establishment of validated transition criteria to this mode of break-up.

The technique utilised was limited at high temperature and pressure where the illumination equipment was unable to penetrate both the bubble density upstream and the spray density downstream. High power illumination e.g. by sheet laser may facilitate progress in this area and the feasibility of using such a technique should at least be investigated.

9.5 General Recommendations

In all aspects of the investigation into superheated sprays, the atomiser used was incapable of decoupling the release pressure from the stagnation temperature. Hence, the design and manufacture of a superheated rig capable of decoupling release pressure from the internal stagnation temperature is necessary for a more comprehensive evaluation of the impact of these input variables on the resultant spray characteristics, both upstream and downstream of the nozzle outlet.

References

[1] Hervieu E. and Veneau T., "Experimental Determination of the Droplet Size and Velocity Distributions at the Exit of the Bottom Discharge Pipe of a Liquefied Propane Storage Tank During a Sudden Blowdown" J. Loss Prev. Ind., Vol.9, No 6, pp. 413-455. (1996)

[2] Health and Safety Executive "PEMEX LPG Terminal, Mexico City, Mexico. 19th November 1984" Safety Report Assessment Guidance Contents, www.hse.gov.uk/comah/sragtech/casepemex84.htm

[3] NGT Group Press Release, "National Grid Transco Announces £355 Million Expansion of Isle of Grain LNG Importation Terminal", 31 March 2005

[4] Jones.G., "Park Gives Final Go-Ahead to South Hook", www.pembrokeshiretv.com, 23 February 2006

[5] MacAlister, T., *et al*, "Turning up the Gas – Imports Will Keep UK's Power Plants Running", www.energybulletin.net, 1 April 2005

[6] Ramsdale S.A., "Droplet Formation and Rainout From Two Phase Flashing Jets" AEA Technology. (1998)

[7] Warren, O., "Modelling Liquid Releases for Explosion Mitigation", Dispersion of Toxic/Flammable Materials, Cardiff School of Engineering (2001)

[8] Zhao, F., Lai, M.C., and Harrington, D.L., "Automotive Spark-ignited Direct Injection Gasoline Engines", Progress in Energy and Combustion Science, Vol.25, pp.437-562

[9] Comer, M.A., Bowen, P.J., Bates, C.J., Sapsford, S.M., and Johns, R.J.R., "Transient 3D Analysis of a DI Gasoline Injector Spray", Atomisation and Sprays, No.5, pp.467-482 (1999)

[10] Kay, P.J., Bowen, P.J., Gold, M., and Sapsford, S., "Studies of G-DI Sprays at Elevated Ambient Gas Temperature and Densities", 10th Int. Congress on Liquid Atomisation and Sprays Systems, Kyoto, Japan (2006)

[11] Hewitt, G.F., "Flow Patterns in Two-Phase Flow and Heat Transfer", Eds. Butterworth and Hewitt, Oxford University Press (1977)

[12] Muralidhar R., Jersey , G.R. and Krambeck F.J., "A Two-Phase Model for Sub-Cooled and Superheated Liquid Jets", International Conference and Workshop on Modelling and Mitigating the Accidental Releases of Hazardous Materials, AIChE, CCPS, New Orleans, LA, September Vo.26, No.29, pp.189-224 (1995)

[13] Park B.S. and Lee S.Y., "An Experimental Investigation of the Flash Atomisation Mechanism", Atomisation and Sprays, Vol.4, pp.159-179 (1994)

[14] Rawle, A., "Basic Principles of Particle Size Analysis", www.malvern.co.uk

[15] Johnson, D.W., and Woodward, J.L., "RELEASE. A Model With Data to Predict Aerosol Rainout in Accidental Releases", Center for Chemical Process Safety (CCPS), New York (1999)

[16] Brown R. and York J.L., "Sprays Formed by Flashing Liquid Jets", A.I.Ch.E. Journal, Vol.8, No.2, pp.149-153 (1962)

[17] Kitamura Y., Morimitsu H. and Takahashi T. "Critical Superheat for Flashing of Superheated Liquid Jets" Ind. Eng. Chem Fundamentals, Vol.25, No.2, pp.207-211 (1986)

[18] Lienhard, J.H., and Stephenson, J.M., "Temperature and Scale Effects Upon Cavitation and Flashing in Free and Submerged Jets", Journal of Basic Engineering Vol.88, pp.525-532 (1966)

[19] Peters, E.M., Takimoto, A., and Hayashi, Y., "Flashing and Shattering Phenomena of Superheated Liquid Jets", JSME Int. Journal, Series B, Vol.37, No.2, pp.313-321 (1994)

[20] Reitz, R.D., and Bracco, F.B., "On the Dependence of Spray Angle and Other Spray Parameters on Nozzle Design and Operating Conditions", SAE 790494 (1979)

[21] Zanelli, S., "Behaviour of a Liquid Jet Near The Nozzle", Proceedings of 4th ICLASS, Sendai, Japan (1988)

[22] Lefebvre, A.H., "Atomisation and Sprays", Hemisphere Publishing Corporation (1989)

[23] Lord Rayleigh, "On the Instability of Jets", Proc. London. Math. Soc., Vol.10, pp.4-13 (1878)

[24] Faeth, G.M., 23rd Symposium (International) on Combustion, The Combustion Institute, Pennsylvania, pp. 1345-1352 (1991)

[25] Néda, Z., Bakó, B., and Rees, E., "The Dripping Faucet Revisited", Chaos, Vol.6, No.1 (1996)

[26] Ohnesorge, W., "Formation of Drops by Nozzles and the Break-Up of Liquid Jets", Z. Agnew. Math. Mech., Vol.16, pp.355-358 (1936)

[27] Reitz, R.D., "Atomisation and Other Break-Up Regimes of a Liquid Jet", PhD Thesis, Princeton University (1978)

[28] Giffen, E., and Muraszew, A., "The Atomisation of Liquid Fuels", John Wiley and Sons, New York (1953)

[29] Haenlein, A., "Disintegration of a Liquid Jet", NACA TN 659 (1932)

[30] Merrington A.C., and Richardson E.G., "The Break-Up of Liquid Jets", Proc. Phys. Soc. London, Vol.56, No.33, pp.1-13 (1947)Harmon D.B., "Drop Sizes From Low Speed Jets" Franklin Inst. Journal Vol.259, No.6, pp.519-522 (1955)

[31] Harmon D.B., "Drop Sizes From Low Speed Jets" Franklin Inst. Journal Vol.259, No.6, pp.519-522 (1955)

[32] Tanasawa Y., and Toyoda S., "On The Atomisation of a Liquid Jet Issuing From a Cylindrical Nozzle", Tech. Report of Tohoku University, Japan, Vol.19, No.2, p135 (1955)

[33] Hiroyasu H., and Katoda T., "Fuel Droplet Size Distribution in a Diesel Combustion Chamber", SAE Trans., Paper 74017 (1974)

[34] Elkotb M.M., "Fuel Atomisation for Spray Modelling", Prog. Energy Combust. Sci. Vol.8, No.1, pp.61-91 (1982)

[35] Tilton J.N., and Farley C.W., "Predicting Liquid Jet Break-Up and Aerosol Formation During the Acccidental Release of Pressurised Hydrogen Fluoride", Plant/Operations Progress, Vol.9, No.12, p.120 (1990)

[36] Maragkos, A., and Bowen, P.J., "Combustion Hazards from High-Flashpoint Liquid Fuels: Discharge Coefficients from Sharp-Edged, Plain Orifice Atomisers", Cardiff (2004)

[37] Ohrn, T.R., Senser, D.W., and Lefebvre, A.H., "Geometrical Effects on Discharge Coefficients for Plain Orifice Atomisers", Atomisation and Sprays, Vol.1, No.2, pp.137-153 (1991)

[38] Karasawa, T., Tanaka, M., Abe, K., Shiga, S., and Kurabayashi, T., "Effect of Nozzle Configuration on the Atomisation of a Steady Spray", Atomisation and Sprays, Vol.2, pp.411-426 (1992)

[39] Ramamurti, K., and Nandakumar, K., "Disintegration of Liquid Jets from Sharp-Edged Nozzles", Atomisation and Sprays, Vol.4, pp.551-564 (1994)

[40] Ramamurti, K., and Nandakumar, K., "Characteristics of Flow Through Small Sharp-Edged Cylindrical Orifices" Flow Measurement and Instrumentation, Vol.10, pp.133-143 (1999)

[41] Dumont, N., Simonin, O., and Habchi, C., "Cavitating Flow in Diesel Injectors and Atomisation: a Bibliographical Review", 8th Int. Conference. Liquid Atomisation and Spray Systems, Pasadena, USA, July (2000)

[42] MacCarthy, M.J., PhD Thesis, University of Newcastle, Australia (1972)

[43] Lane, W.R., "Shatter of Drops in Streams of Air", Ind.Eng.Chem., Vol.43, No.6, pp.1312-1317 (1951)

[44] Heinze, J.O., "Fundamentals of the Hydrodynamic Mechanism of Splitting in Dispersion Processes", A.I.Ch.E. Journal, Vol.1, No.3, pp.289-295 (1955)

[45] Haas, F.C., "Stability of Droplets Suddenly Exposed to a High Velocity Gas Stream", A.I.Ch.E,. Journal, Vol.10 pp.920-924 (1964)

[46] Hanson, A.R., Domich, E.G. and Adams, H.S., "Shock Tube Investigation of the Breakup of Drops by Air Blasts", Phys. Fluids, Vol.6, pp.1070-1080 (1963)

[47] Witlox, H.W.M., and Holt, A., "Unified Dispersion Model", Technical Reference Manual, Version 6.0, DNV, London (2000)

[48] Van den Bosch, C.J.H., and Duijm, N.J., "Methods for Calculating Physical Effects", TNO Yellow Book, Ch.2, pp.2.105-2.112 (1997)

[49] Wheatley, C.J., "Discharge of Liquid Ammonia to Moist Atmospheres – Survey of Experimental Data and Model for Estimating Initial Conditions for Dispersion Calculations", SRD, Culceth, Cheshire, UK, report SRD/HSE/R410 (1987)

[50] Appleton, P.R., "A Study of Two-Phase Flashing Jets", SRD report R303, UK AEA, Culceth, Cheshire, UK (1984)

[51] Tropea, C., and Roisman, I.V., "Modelling of Spray Impact on Solid Surfaces", Special Issue of Atomisation and Sprays, Vol.10 Nos. 3-4 (2000)

[52] Reitz, R.D., and Diwakar, R., "Effect of Drop Break-Up on Fuel Sprays", SAE Paper 860469 (1986)

[53] Reitz, R.D., "Modelling Atomisation Processes in High-Pressure Vaporising Sprays", Atomisation and Spray Technology, Vol.3 No.309 (1987)

[54] St.Georges, M., and Buchlin, J.M., "Detailed Single Spray Experimental Measurements and One-Dimensional Modelling", Int. J. Multiphase Flow, Vol.20, No.6, pp.979-992 (1994)

[55] Rosin, P., and Rammler, E., "The Laws Governing the Fineness of Powdered Coal" J. Inst. Fuel, Vol.7, No.29 (1933)

[56] Lienhard, J.H., and Day, J.B., "The Break-Up of Superheated Liquid Jets", ASME Paper No.69-WA/FE-19 (1969)

[57] Sher, E., and Elata, C., "Spray Formation from Pressure Cans by Flashing", Ind. Eng. Chem., Process Des. Dev., Vol.16, No.2, pp.237-242 (1977)

[58] Suzuki, M., Yamamoto, T., Futaganii, N., and Maeda, S., "Atomisation of Superheated Liquid Jets", ICLASS-78, Tokyo, Japan, (1978)

[59] Aquino, C., Plensdort, W., Lavoie, G., and Curtis, E., SAE Paper 982522 (1998)

[60] Lantzy, R.J., Myers, R.D., Pfenning, D.B., and Millsap, S.B., "Atmospheric Release Tests of Monomethylamine", J. Loss Prev. Process Ind., Vol.3 (1990)

[61] Kitamura Y., Morimitsu H. and Takahashi T. "Critical Superheat for Flashing of Superheated Liquid Jets" Ind. Eng. Chem Fundamentals, Vol.25, No.2, pp.207-211 (1986)

[62] Oza, R.D., and Sinnamon, J.F., "An Experimental Investigation of Flash Boiling Fuel Injection", SAE paper 830590 (1985)

[63] Razzaghi, M., "Droplet Size Estimation of Two-Phase Flashing Jets", Nuclear Engineering Design, Vol.114, pp.115-124 (1989)

[64] Shepherd, J.E., and Sturtevant, B., "Rapid Evaporation at the Superheat Limit", J. Fluid Mech. Vol.121 (1982)

[65] Zeng, Y., and Lee, C.F., "Modelling Atomisation for Hollow-Cone Sprays Under Flash Boiling Conditions", 8th International Conference on Liquid Atomisation and Spray Systems, Pasadena, CA, July (200)

[66] Bates, C.J., Bowen, P.J., Teixeira, J.C.F., "Influence of Orifice Characteristics on Transition Between Flow Regimes in Effervescent Atomisers" 8th Int. Conf. on Liquid Atomisation and Spray Systems, Pasadea CA, July (2000)

[67] Panchagnula, M.V., and Sojka, P.E., "Spatial Droplet Velocity and Size Profiles in Effervescent Atomiser-Produced Sprays", Fuel Vol.78 pp.729-741 (1999)

[68] Lefebvre, A.H., Wang, X.F., Martin, C.A., "Spray Characteristics of Aerated-Liquid Pressure Atomisers", AIAA J. Prop. Power., Vol.4, No.4, pp293-298 (1988)

[69] Wang, X.F., Chin, J.S., Lefebvre, A.H., "Influence of Gas Injector Geometry on Atomisation Performance of Aerated-Liquid Nozzles", Int. J. Turbo Jet Engines Vol.6, pp.271-280 (1989)

[70] Whitlow, J.D., Lefebvre, A.H., "Effervescent Atomiser Operation and Spray Characteristics", Atomisation & Sprays, Vol.3, pp.137-156 (1993)

[71] Chen, S.K., Lefebvre, A.H., Rollbuhler, J.R., "Influence of Ambient Air Pressure on Effervescent Atomisation", J. Propulsion Power, Vol.9, No.1, pp.10-15 (1993)

[72] Wade, R.A., Sojka, P.E., Gore, J.P., "Effervescent Atomisation Using High Supply Pressures", Proceedings of the 9th Annual Conference on Liquid Atomisation and Spray Systems", San Francisco, CA, PP.263-270 (1996)

[73] Wade, R.A., Weerts, J.M., Sojka, P.E., Gore, J.P., Eckerle, W.A., "Effervescent Atomisation at Injection Pressures in MPa Range", Atomisation & Sprays, Vol.9, No.6, pp.651-667 (1999)

[74] Shin, T.S., and Jones, O.C., "An Active Cavity Model for Flashing", Nuclear Eng. And Design, Vol.95, pp.185-196 (1986)

[75] Blinkov, V.N., Jones, O.C., and Nigmatulin, "Nucleation and Flashing in Nozzles 2 – Comparison with Experiments Using Five-Equation Model for Vapor Void Development" Int. J. Multiphase Flow, Vol.19, No.6, pp.965-986 (1994)

[76] Saha P., Abuaf N., and Wu, B.J.C., "A Non-Equilibrium Vapor Generation Model for Flashing Flow", Trans. ASME., Jnl. Heat Transfer, Vol.106, pp.199-203 (1984)

[77] Ishtii, M., and Mishima, K., "Flow Regime Transition Criteria Consistent with a Two-Fluid Model for Vertical Two-Phase Flow", Reports NUREG/CR-3338 and ANL-83-42 (1983)

[78] Fujimoto, H., Nishikori, T., Hojyo, Y., Tsukamoto, T., and Senda, J., "Modelling of Atomisationand Vaporisation Process in Flash Boiling Spray", The International Conference on Liquid Atomisation and Spray Systems, Paper VI-13, Rouen, July (1994)

[79] Volmer, M., and Weber, A., "Nuclei Formation in Supersaturated States", Z.Phys.Chem, Vol.119, pp.277-301 (1925)

[80] Becker, R., and Döring, W., Ann.Phys (Leipzig) Vol.24,p.719 (1935)

[81] Otoxby, D.W., J. Phys. Condens. Matter Vol.4, pp.7627-7650 (1992)

[82] Blander, M. and Koltz, J.L., "Bubble Nucleation in Liquids", AIChE Journal, Vol.21, No.5, p.833 (1975)

[83] Skirpov, V.P., Pavlov, P.A., Teplo. Vsyo. Temp., Vol.8, No.4, p.833 (1970)

[84] Iwamatsu, M., "Homogenous Nucleation of Spherical Droplets and Bubbles: An Analysis Using the Density Functional Method", Chinese. J. Phys., Vol.33, No.2, pp.139-152 (1995)

[85] Talanquer, V., "Nucleation in Gas-Liquid Transitions", J. Chemical Education, Vol.79, No.7 (2002)

[86] Cahn, J.W., and Hilliard, J.E., "Free Energy of Nonuniform System.I.Interfacial Free Energy", Vol.28, pp.258-267 (1958)

[87] Oxtoby, D.W., and Evans, R., "Nonclassical Nucleation Theory for the Gas-Liquid Transition", J.Chem.Phys., Vol.89, pp.7521-7530 (1988)

[88] Laaksonen, A., Talanquer, V., Oxtoby, D.W., "Nucleation: Measurements Theory and Atmospheric Applications", Ann. Rev. Phys. Chem., Vol.46, pp.489-524 (1995)

[89] Oxtoby, D.W., "Homogenous Nucleation: Theory and Experiment", J. Phys. Condens. Matter, Vol.4, pp.7627-7650 (1992)

[90] Delale, C.F., Hruby, J., and Marsik, F., "The Classical Theory of Homogenous Bubble Nucleation Revisted", 5th Int. Symp. Cavitation, Osaka, Japan (2003)

[91] Turnbull, D., Kinetics of Heterogeneous Nucleation", J.Chem.Phys., Vol.18, pp.198-203 (1950)

[92] Kolev, N.K., "Uniqueness of the Elementary Physics Driving Heterogeneous Nucleate Boiling and Flashing", Nuclear Eng. and Tech., Vol.38, No.2, pp.175-184 (2006)

[93] Qi, Y., and Klausner, J.F., "Comparison of Nucleation Site Density for Pool Boiling and Gas Nucleation", J.Heat.Transfer, Vol.128, No.1, pp.13-20 (2006)

[94] Corradini, M.L., "Fundamentals of Multiphase Flow", University of Wisconsin, http://wins.engr.wisc.edu/teaching/mpfBook/main.html, (1997)

[95] Cornwell, K., and Brown, R.D., "Boiling Surface Topology", Proc. 6th Int. Heat Transfer Conf. Toronto, Vol.1, pp.157-161 (1978)

[96] Kocamustafaogullari, G. and Ishii, M., "Interfacial Area and Nucleation Site Density in Boiling Systems", Int. J. Heat Mass Transfer, Vol.26, pp.1377-1389 (1983)

[97] Wang, C.H. and Dhir, V.K., "Effect of Surface Wettability on Active Nucleation Site Density During Pool Boiling of Water on a Vertical Surface", ASME J. Heat Transfer, Vol.115, pp.659-669 (1993)

[98] Rayleigh, L., "On the Pressure Developed During the Collapse of a Spherical Cavity" Phil. Mag. S. Vol.6 No.34 (200) pp.94-98 (1917)

[99] Scriven, L.E., "On the Dynamics of Phase Growth", Chem. Eng. Sci. Vol.10. pp.1-13 (1959)

[100] Plesset, M.S., and Zwick, S.A., "The Growth of Vapour Bubbles in Superheated Liquids", J. Appl. Phys. Vol.25. pp. 493-500 (1954)

[101] Forster, H.K., and Zuber, N., J., "Growth of a Vapour Bubble in a Superheated Liquid", Appl. Phys. Vol. 25. pp. 474-478 (1954)

[102] Mikic, B.B., Rohsenow, W.M., and Griffith, P., "On Bubble Growth Rates" Int. Journal of Heat and Mass Transfer, Vol.13, pp. 657-666 (1970)

[103] Miyatake, O., and Tanaka, I., "Bubble Growth in Uniformly Superheated Water at Reduced Pressures, Part 1: Numerical Analysis and Derivation of a Simplified Expression" Transactions JSME, Series B, Vol.48, pp.355-363 (1982)

[104] Miyatake, O., and Tanaka, I., "Bubble Growth in Uniformly Superheated Water at Reduced Pressures, Part 2:Experimental Results and Comparison with Numerical Results and with Simplified Expression" Transactions JSME, Series B, Vol.48, pp.364-372 (1982)

[105] Lee, H.S. and Merte, H., "Spherical Vapour Bubble Growth in Uniformly Superheated Liquids", Int. J. Heat Mass Transfer, Vol.39, No.12, pp.2427-2447 (1995)

[106] Chang, D.L., and Lee, C.F.F., Development of a Simplified Bubble Growth Model for Flash Boiling Sprays in Direct Injection Spark Engines", Proceedings of the Combustion Institute, Vol.30, pp.2737-2744 (2005)

[107] Solomon, A.S.P., Rupprecht, S.D., Chen, L.D., and Faeth, G.M., "Flow and Atomisation in Flashing Injectors", Atomisation and Spray Technology, Vol.1, pp.53-76 (1985)

[108] Mayer, E., "Theory of Liquid Atomisation in High Velocity Gas Streams", ARS J., Vol.31, pp.1783-1785 (1961)

[109] Adelberg, M., "Mean Drop Size Resulting from the Injection of a Liquid Jet into a High-speed Gas Stream", AIAA J., Vol.6, pp.1143-1147 (1968)

[110] Lefebvre, A., "Airblast Atomisation", Prog. Energy Combust. Sci., Vol.6, pp.233-261 (1980)

[111] Senda, J., Yanmaguchi, M., Tsukamoto, T., and Fujimoto, H., "Characteristics of Spray Injected From Gasoline Injectors" JSME Int. Jnl., Series B, Vol.38, No.4, pp.931-936 (1994)

[112] Crowe, C.T., and Comfort, W.J., "Atomisation Mechanisms in Single-Component, Two-Phase Nozzle Flows", Proceedings of the First International Conference on Liquid Atomisation and Spray Systems, Tokyo, August (1978)

[113] Nagai, N., Sato, K., and Lee, C.W., "Atomisation Characteristics of Superheated Liquid Jets", International Conference on Liquid Atomisation and Spray Systems, Tokyo, August (1978)

[114] Vesala, T., "Binary Droplet Evaporation and Condensation as Phenomenological Process", Commentationes Physico-Mathematicae, Dissertationes No. 127/1991, The Finnish Society of Science and Letters (1991)

[115] Kukkonen, J., "Modelling Source Terms for the Atmospheric Dispersion of Hazardous Substances", Commentationes Physico-Mathematicae, Dissertationes No.34, 115/1990, The Finnish Society of Science and Letters (1990)

[116] Vasela, T., Kukkonen, J., and Kumula, M., "A Model for Evaporation of Freely Falling Droplets", Publications of Air Qualty, No.6, Finnish Meteorological Institute (1989)

[117] Kletz, T., "Unconfined Vapour Cloud Explosions", AIChE Loss Prevention. (1977)

[118] De Vaull, G.E., and King, J.A., "Similarity Scaling of Droplet Evaporation and Liquid Rainout Following the Release of Superheated Flashing Liquid to the Environment", presented at 85th Annual Meeting , Air and Waste Management Assoc., Kansas (1992)

[119] Allen, J.T., "Development of a Fluorescent-Based Temperature Measurement Technique for Two-Phase Flashing Propane Jets", HSL Report Number IR/L/FR/96/6 (1996)

[120] Allen, J.T., "Laser-Based Measurements in Two-Phase Flashing Propane Jets. Part One: Velocity Profiles", Journal of Loss Prevention in Process Ind, Vol.11, pp.291-297 (1998)

[121] Allen, J.T., "Laser-Based Measurements in Two-Phase Flashing Propane Jets. Part Two: Droplet Size Distribution", Journal of Loss Prevention in Process Ind, Vol.11, pp.299-306 (1998)

[122] Vandroux-Koenig, S., and Berthoud, G., "Modelling of a Two-Phase Momentum Jet Close to The Breach in the Containment Vessel of a Liquefied Gas", J. Loss Prev. Ind., Vol.10, No.1, pp.17-29 (1997)

[123] Yildiz, D, Rambaud, P., van Beeck, J. "Break-up, Droplet Size and Velocity Characterisations of a Two-Phase Flashing R134A Jet", 5th International Conference on Multiphase Flow (ICMF'04), Yokohama, Japan, May 30- June 4, Paper No. 408 (2004)

[124] Yildiz, D., Rambaud, P., van Beeck., J.P.A.J., and Buchlin, J.M., "Effect of the Initial Flow Conditions on the Evolution of the Droplet Size and Velocity in Superheated Liquid Jet Atomization", National Congress on Theoretical and Applied Mechanics, May 29-30, Mons, Belgium (2006)

[125] Yildiz, D, Rambaud, P., van Beeck, J., and Buchlin, J.M., "Characterization of Superheated Liquid Jet Atomisation with Phase Doppler Anemometer (PDA) and High-Speed Imaging", Proceedings of ASME Joint U.S. – European Fluids Engineering Summer Meeting, July 17-18, Miami, USA (2006)

[126] Witlox, H.W.M., and Holt, A., "A Unified Model For Jet, Heavy and Passive Dispersion Including Droplet Rainout and Re-Evaporation", International Conference and Workshop on Modelling the Consequences of Accidental Releases of Hazardous Materials, CCPS, San Francisco, California, pp.315-344 (1999)

[127] Witlox, H.W.M., and Holt, A., "Unified Dispersion Model", Technical Reference Manual, Version 6.0, DNV, London (2000)

[128] van den Bosch, C.J.H., and Duijm, N.J., "Methods for the Calculation of Physical Effects – TNO Yellow Book", CPR14E, Third Edition, Committee for the Prevention of Disasters, SDU, The Hague (1997)

[129]Oxford University - Physical and Theoretical Chemistry Laboratory. website link http://physchem.ox.ac.uk/MSDS/TE/1,1,1,2-tetrafluoroethane.html, database of MSDS information

[130] Comer, M.A., Bowen, P.J., Bates, C.J., Sapsford, S.M., and Johns, R.J.R., "Transient 3D Analysis of a DI Gasoline Engine Injector Spray", Atomisation and Sprays, Vol.9, No.5, pp.467-482 (1999)

[131] Swithenbank, J., Beer, J.M., Taylor, D.S., Abbot, D., and McCreath, G.C., "A Laser Diagnostic Technique for the Measurement of Droplet Particle Size and Distribution", Prog. Astro and Aero., Vol.53, pp.421-447 (1977)

[132] Dodge, L.G., "Change of Calibration of Diffraction-Based Particle Sizing in Dense Sprays", Optical Engineering, Vol.23, No.5, pp.626-630 (1984)

[133] Durst, F., and Zaré, M., "Laser Doppler Measurements in Two Phase Flows", Proc. LDA Symp., pp.403-429 (1975)

[134] Ohrn T.R., Senser D.W. and Lefebvre A.H., "Geometrical Effects on Discharge Coefficients for Plain Orifice Atomisers", Atomisation and Sprays, v.1, No.2, pp.137-153 (1991)

[135] Brown R. and York J.L., "Sprays Formed by Flashing Liquid Jets", A.I.Ch.E. Journal, v.8, No.2, pp.149-153 (1962)

[136] Hamidi, A.A., and Swithenbank, J., "Treatment of Multiple Scattering of Light in laser Diffraction Measurement Techniques in Dense Sprays and Particle Fields", J. Institute. Energy

[137] Bowen, P.J., Bull, D.C., Prothero, A., Rowson, J.J., "Deflagration of Hydrocarbon Aerosol Fuels", Combust. Sci and Tech., Vol.130, pp.25-47 (1997)

[138]Cooper, J., "Particle Size Analysis - The Laser Diffraction Technique", Materials World, Vol.6, No.1, pp.5-7 (1998)

[139] Cleary, V.M., Bowen, P.J., and Maragkos, A., "Jet Transition and Rainout from Large Superheated Spray Releases" 9th International Conference of Liquid Atomization and Spray Systems, Sorrento, Italy (2003)

[140] Rosin, P., and Rammler, E., "The Laws Governing the Fineness of Powdered Coal", J.Inst.Fuel., Vol.7, No.29 (1933)

[141] Maragkos A., "Combustion Hazard Quantification of Accidental Releases of High-Flashpoint Liquid Fuels", PhD Thesis, University of Wales, Cardff (2000)

[142] "Principles of Phase Doppler Anemometry" DANTEC Dynamics, www.dantecmt.com

[143] Dergarabedian, P., "The Rate of Growth of Vapor Bubbles in Superheated Water", Journal Appl. Mech. Vol.20 pp.537-545 (1953)

[144] Hooper F.C., and Abdelmessih A.H., "Proceedings of the 3rd International Heat Transfer Conference, Chicago, 1966" Vol.44 No.50 A.I.Chem.E, New York, (1966)

[145] Cole R. and Shulman H.L., "Bubble Growth Rates at High Jakob Numbers", Int. Journal. Heat Mass Transfer, Vol.9. pp.1377-1390 (1966)

[146] Kosky, P.G., "Bubble Growth Measurement in Uniformly Superheated Liquids", Chem. Eng. Sci. Vol.23 pp.695-706 (1968)

[147] Witlox, H., Harper, M., Cleary, V., and Bowen, P., "Flashing Liquid Jets and Two-Phase Droplet Disprsion", Conference Proceedings of Major Hazards Onshore and Offshore, ERA Technology, ISBN 0700807845 (2004)

[148] Witlox, H.W.M., Harper M., Bowen, P. and Cleary, V., "Flashing Liquid Jets and Two-Phase Dispersion", ASSE-MEC 7th Professional Development Conference, Bahrain, pp. 123-134, March (2006)

[149] Cleary, V., Bowen, P.J., and Witlox, H., "Flashing Liquid Jets and Two-Phase Droplet Dispersion II. Experiments for Derivation of Droplet Atomisation Correlations", 8th Ann. Symp. Mary Kay O'Connor Process Safety Center, Texas (2005)

[150] Cleary, V., Bowen, P.J., and Witlox, H., "Flashing Liquid Jets and Two-Phase Droplet Dispersion I. Experiments for Derivation of Droplet Atomisation Correlations", J. Hazardous Materials (accepted for publication 2006)

[151] Touil, A., Bigot, J.P., Bonnet, P., Lacome, J.M., and Duplantier, S, "Rainout Prediction: Initial Droplet Diameter Experimental Determination", Loss Prevention and Safety Promotion in the Process Industries, 11th International Symposium, pp.3201-3309, Prague (2004)

[152] Witlox, H., Harper, M., Bowen, P.J., and Cleary, V.M., "Flashing Liquid Jets and Two-Phase Droplet Dispersion I. Overview (Literature Survey, Experiments and Model Implementation/Validation)", 8th Ann. Symp. Mary Kay O'Connor Process Safety Center, Texas (2005)

[153] Witlox, H., Harper, M., Bowen, P.J., and Cleary, V.M., "Flashing Liquid Jets and Two-Phase Droplet Dispersion II. Comparison and Validation of Droplet Size and Rainout Formulations", J. Hazardous Materials (accepted for publication 2006)

[154]Oxford University - Physical and Theoretical Chemistry Laboratory. website link http://physchem.ox.ac.uk/MSDS/TE/1,1,1,2-tetrafluoroethane.html, database of MSDS information

[155] Ivashnyov, O.E., and Smirnov, N.N., "Thermal Growth of a Vapour Bubble Moving in Superheated Liquid", Jrnl. Phys. Fluids., Vol.16, No.3 pp.809-823 (2004)

[156] Yuan, W., Sauer, J. and Schnerr, G.H., "Modelling and Computation of Unsteady Cavitation Flows in Injection Nozzles", Jurnal Mec. Ind Vol.2 pp383-394 (2001)

[157] FLUENT 5: User's Guide Volume 3 (1999)

[158] Askovic, R., "Drag of a Bubble at Rectilinear Accelerated Ascension in Pure Liquids and Binary Solutions", Jrnl. Theoret. Appl. Mech. Vol.30, No.3, pp.171-191 (2003)

[159] Chang, D.L., and Lee, C.F.F., "Development of a Simplified Bubble Growth Model for Flash Boiling Sprays in Direct Injection Spark Engines", Proceedings of Combust. Inst. Vol.30, pp.2737-2744 (2005)

[160] Hung, C.H., Krasnopoler, M.J., and Katz, J.L., "Condensation of a Supersaturated Vapour. VIII. The Homogenous Nucleation of N-Nonane", J.Chem.Phys., Vol.90, No.3, pp.1856-1865 (1989)

[161] El-Shall, M.S., "Homogenous Nucleation in Metal Tetrachloride Vapours: Tin and Titanium Tetrachlorides", J.Chem.Phys., Vol.90, No.11, pp.6533-6540 (1989)

[162] El-Shall, M.S., "Homogenous Nucleation of Iron Pentacarbonyl: Experiment and Prediction of Scaled Nucleation Models", Vol.93, No.25, pp.8253-8257 (1989)

[163] Peters, F., and Paikert, B., "Experimental Results on the Role of Nucleation in Supersaturated N-Propanaol, Ethanol and Methanol Vapours", J.Chem.Phys., Vol.91, No.9, pp.5672-5678 (1989)

[164] Strey, R., Wagner, P.E., and Schmeling, T., "Homogenous Nucleation Rates for the N-Alcohols From a Two Piston Expansion Chamber", J.Chem.Phys., Vol.84, No.4, pp.2325-2335